AA283

Course Reader

Aircraft and Rocket Propulsion

by

Brian J. Cantwell

Department of Aeronautics and Astronautics
Stanford University, Stanford, California 94305

January 18, 2021

Contents

1 Propulsion Thermodynamics **1-1**
- 1.1 Introduction . . . 1-1
- 1.2 Thermodynamic cycles . . . 1-8
  - 1.2.1 The Carnot cycle . . . 1-8
  - 1.2.2 The Brayton cycle . . . 1-11
- 1.3 The standard atmosphere . . . 1-14
- 1.4 Problems . . . 1-14

2 Engine performance parameters **2-1**
- 2.1 The definition of thrust . . . 2-1
- 2.2 Energy balance . . . 2-6
- 2.3 Capture area . . . 2-8
- 2.4 Overall efficiency . . . 2-9
- 2.5 Breguet aircraft range equation . . . 2-10
- 2.6 Propulsive efficiency . . . 2-11
- 2.7 Thermal efficiency . . . 2-12
- 2.8 Specific impulse, specific fuel consumption . . . 2-14
- 2.9 Dimensionless forms . . . 2-14
- 2.10 Engine notation . . . 2-15
- 2.11 Problems . . . 2-21

3 The ramjet cycle **3-1**
- 3.1 Ramjet flow field . . . 3-1
- 3.2 The role of the nozzle . . . 3-9
- 3.3 The ideal ramjet cycle . . . 3-11
- 3.4 Optimization of the ideal ramjet cycle . . . 3-14
- 3.5 The non-ideal ramjet . . . 3-16
- 3.6 Ramjet control . . . 3-17
- 3.7 Example - Ramjet with un-started inlet . . . 3-18
- 3.8 Very high speed flight - scramjets . . . 3-29

3.8.1 Real chemistry effects . . . 3-32
3.8.2 Scramjet operating envelope . . . 3-33
3.9 Problems . . . 3-35

4 The Turbojet cycle 4-1
4.1 Thermal efficiency of the ideal turbojet . . . 4-1
4.2 Thrust of an ideal turbojet engine . . . 4-6
4.3 Maximum thrust ideal turbojet . . . 4-9
4.4 Turbine-nozzle mass flow matching . . . 4-12
4.5 Free-stream-compressor inlet flow matching . . . 4-13
4.6 Compressor-turbine mass flow matching . . . 4-13
4.7 Summary - engine matching conditions . . . 4-14
4.7.1 Example - turbojet in supersonic flow with an inlet shock . . . 4-15
4.8 How does a turbojet work? . . . 4-19
4.8.1 The compressor operating line . . . 4-20
4.8.2 The gas generator . . . 4-20
4.8.3 Corrected weight flow is related to $f(M_2)$. . . . 4-22
4.8.4 A simple model of compressor blade aerodynamics . . . 4-24
4.8.5 Turbojet engine control . . . 4-29
4.8.6 Inlet operation . . . 4-30
4.9 The non-ideal turbojet cycle . . . 4-33
4.9.1 The polytropic efficiency of compression . . . 4-35
4.10 The polytropic efficiency of expansion . . . 4-38
4.11 The effect of afterburning . . . 4-39
4.12 Nozzle operation . . . 4-40
4.13 Problems . . . 4-41

5 The Turbofan cycle 5-1
5.1 Turbofan thrust . . . 5-1
5.2 The ideal turbofan cycle . . . 5-3
5.2.1 The fan bypass stream . . . 5-4
5.2.2 The core stream . . . 5-5
5.2.3 Turbine-compressor-fan matching . . . 5-6
5.2.4 The fuel/air ratio . . . 5-7
5.3 Maximum specific impulse ideal turbofan . . . 5-7
5.4 Turbofan thermal efficiency . . . 5-10
5.4.1 Thermal efficiency of the ideal turbofan . . . 5-12
5.5 The non-ideal turbofan . . . 5-12
5.5.1 Non-ideal fan stream . . . 5-13
5.5.2 Non-ideal core stream . . . 5-14
5.5.3 Maximum specific impulse non-ideal cycle . . . 5-15

5.6 Problems 5-16

6 The Turboprop cycle **6-1**
6.1 Propellor efficiency 6-1
6.2 Work output coefficient 6-7
6.3 Power balance 6-8
6.4 The ideal turboprop 6-8
6.4.1 Optimization of the ideal turboprop cycle 6-10
6.4.2 Compression for maximum thrust of an ideal turboprop 6-11
6.5 Turbine sizing for the non-ideal turboprop 6-12
6.6 Problems 6-13

7 Rocket performance **7-1**
7.1 Thrust 7-1
7.2 Momentum balance in center-of-mass coordinates 7-4
7.3 Effective exhaust velocity 7-9
7.4 C^* efficiency 7-11
7.5 Specific impulse 7-11
7.6 Chamber pressure 7-12
7.7 Combustion chamber stagnation pressure drop 7-14
7.8 The Tsiolkovsky rocket equation 7-15
7.9 Reaching orbit 7-17
7.10 The thrust coefficient 7-18
7.11 Problems 7-20

8 Multistage Rockets **8-1**
8.1 Notation 8-1
8.2 The variational problem 8-3
8.3 Example - exhaust velocity and structural coefficient the same for all stages 8-6
8.4 Problems 8-7

9 Thermodynamics of reacting mixtures **9-1**
9.1 Introduction 9-1
9.2 Ideal mixtures 9-2
9.3 Criterion for equilibrium 9-5
9.4 The entropy of mixing 9-5
9.5 Entropy of an ideal mixture of condensed species 9-10
9.6 Thermodynamics of incompressible liquids and solids 9-12
9.7 Enthalpy 9-14
9.7.1 Enthalpy of formation and the reference reaction 9-15
9.8 Condensed phase equilibrium 9-17

9.9 Chemical equilibrium, the method of element potentials 9-23
9.9.1 Rescaled equations 9-29
9.10 Example - combustion of carbon monoxide 9-32
9.10.1 CO Combustion at $2975.34K$ using Gibbs free energy of formation. 9-37
9.10.2 Adiabatic flame temperature 9-40
9.10.3 Isentropic expansion 9-42
9.10.4 Nozzle expansion 9-43
9.10.5 Fuel-rich combustion, multiple phases 9-44
9.11 Rocket performance using CEA 9-46
9.12 Problems 9-47

10 Solid Rockets **10-1**
10.1 Introduction 10-1
10.2 Combustion chamber pressure 10-2
10.3 Dynamic analysis 10-4
10.3.1 Exact solution 10-6
10.3.2 Chamber pressure history 10-8
10.4 Problems 10-9

11 Hybrid Rockets **11-1**
11.1 Conventional bi-propellant systems 11-1
11.2 The hybrid rocket idea 11-3
11.2.1 The fuel regression rate law 11-4
11.2.2 Specific impulse 11-7
11.2.3 The problem of low regression rate 11-7
11.3 Historical perspective 11-9
11.4 High regression rate fuels 11-12
11.5 The O/F shift 11-15
11.6 Scale-up tests 11-16
11.7 Regression rate analysis 11-17
11.7.1 Regression rate with the effect of fuel mass flow neglected. 11-17
11.7.2 Exact solution of the coupled space-time problem for $n = 1/2$. . . . 11-18
11.7.3 Similarity solution of the coupled space-time problem for general n and m. 11-19
11.7.4 Numerical solution for the coupled space-time problem, for general n and m and variable oxidizer flow rate. 11-20
11.7.5 Example - Numerical solution of the coupled problem for a long burning, midsize motor as presented in reference [1]. 11-23
11.7.6 Sensitivity of the coupled space-time problem to small changes in a, n, and m. 11-25
11.8 Problems 11-27

A Thermochemistry **A-1**
A.1 Thermochemical tables . . . A-1
A.2 Standard pressure . . . A-2
A.2.1 What about pressures other than standard? . . . A-4
A.2.2 Equilibrium between phases . . . A-5
A.2.3 Reference temperature . . . A-7
A.3 Reference reaction and reference state for elements . . . A-7
A.4 The heat of formation . . . A-8
A.4.1 Example - heat of formation of monatomic hydrogen at 298.15 K and at 1000 K. . . . A-9
A.4.2 Example - heat of formation of gaseous and liquid water . . . A-11
A.4.3 Example - combustion of hydrogen and oxygen diluted by nitrogen . A-13
A.4.4 Example - combustion of methane . . . A-14
A.4.5 Example - the heating value of JP-4 . . . A-16
A.5 Heat capacity . . . A-17
A.6 Chemical bonds and the heat of formation . . . A-20
A.6.1 Potential energy of two hydrogen atoms . . . A-20
A.6.2 Atomic hydrogen . . . A-22
A.6.3 Diatomic hydrogen . . . A-23
A.7 Heats of formation computed from bond energies . . . A-26
A.8 References . . . A-28

B Selected JANAF data **B-1**

Chapter 1

Propulsion Thermodynamics

1.1 Introduction

The Figure below shows a cross-section of a Pratt and Whitney JT9D-7 high bypass ratio turbofan engine. The engine is depicted without any inlet, nacelle or nozzle.

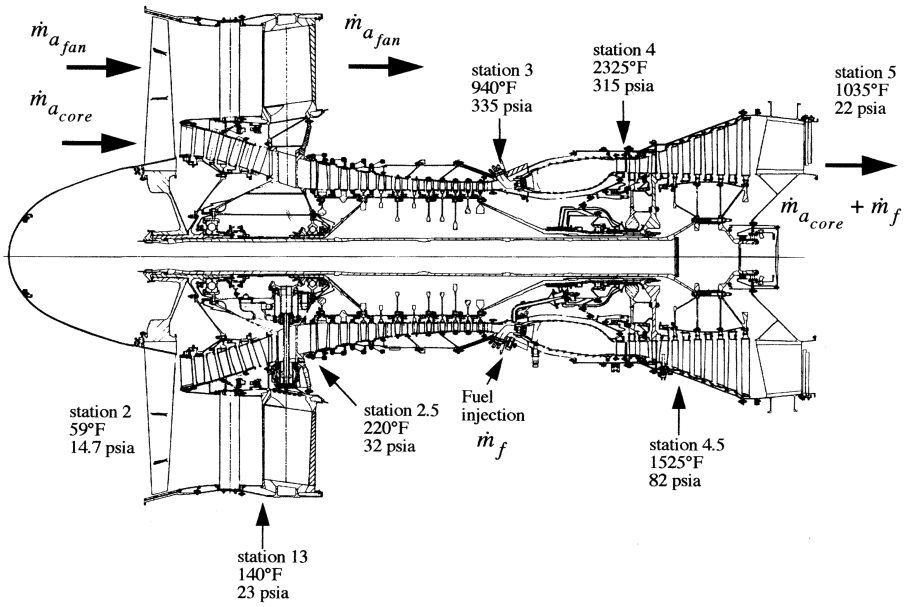

Figure 1.1: *Cross-section of the Pratt and Whitney JT9D-7 turbofan engine*

Two gas streams are indicated in the Figure. The air mass flow rate of the bypass stream

is $\dot{m}_{a_{fan}}$ and that of the engine core stream is $\dot{m}_{a_{core}}$. The bypass ratio of the engine is defined as

$$\beta = \frac{\dot{m}_{a_{fan}}}{\dot{m}_{a_{core}}}. \tag{1.1}$$

The fuel is injected as a liquid; atomized, mixed, and burned with the core air. The exhaust mass flow rate of the core is equal to the sum of core air mass flow rate and fuel mass flow rate $\dot{m}_{a_{core}} + \dot{m}_f$.

This engine was among the first generation of high thrust jet engines designed in the 1960's to power a new class of wide body aircraft. It was the engine that powered the Boeing 747 when it was introduced into service in 1968. This engine is capable of generating 46,500 pounds of thrust at sea level static conditions typical of the initiation of aircraft takeoff roll. Derivatives of this engine as well as competitors offered by General Electric and Rolls Royce continue to power the 747 today as well as the 767, A300, A310 and DC10. At cruise the engine generates about 10,000 pounds of thrust.

Figure 1.1 is particularly useful in that it shows the pressures and temperatures at various stations in the engine and it presents a powerful reminder that to understand modern propulsion systems we will need to employ the full range of thermodynamic and gas-dynamic tools available to us. The total air weight flow at take-off is 1508 pounds per second (685.5 kg/sec) and the bypass ratio is 4.8 with 260 pounds of air per second (118.2 kg/sec) passing through the core of the engine. The thrust to weight ratio of the engine at takeoff thrust is 5.15.

You will notice that I used English units to describe the mass flow. It is an unfortunate fact that in spite of the now generally accepted use of the metric system by the vast majority of the scientific and engineering community, US propulsion companies are still stuck on English units to a large extent (although the British are not). That does not mean that we have to slavishly accept this use and in fact we will generally use metric units throughout this text although quite often the English equivalent will be quoted as well.

The ability of this sort of engine to generate power is remarkable. In metric units the heat capacity of air at room temperature is $C_p = 1005\, m^2/\left(\sec^2 - K\right)$. The stagnation temperature change of the gas that passes through the core is $T_{t5} - T_{t2} = (5/9)\,(1035 - 59) = 542\, K$ and that across the fan is $T_{t13} - T_{t2} = (5/9)\,(140 - 59) = 45\, K$. The total power generated is the enthalpy change of the gas times the mass flow.

$$\begin{aligned} &W = \dot{m}_{a_{core}} C_p\,(T_{t5} - T_{t2}) + \dot{m}_{a_{fan}} C_p\,(T_{t13} - T_{t2}) = \\ &118.2 \times 1005 \times 542 + 567.3 \times 1005 \times 45 = 9 \times 10^7 J/\sec \end{aligned} \tag{1.2}$$

In English units this is equivalent to approximately 120,000 horsepower (1 horsepower=746 Watts, 1 Watt = 1 Joule/sec). Note that the engine is designed so that the static pressure of the core exhaust flow is nearly equal to the static pressure of the fan exhaust to avoid large changes in flow direction where the two streams meet. The overall engine stagnation pressure ratio is approximately 1.5.

Now let's examine the work done per second across some of the components. The work done by the gas on the high pressure turbine is

$$W_{hpt} = 118.2 \times 1005 \times (5/9) \times (2325 - 1525) = 5.28 \times 10^7 \, J/\sec \tag{1.3}$$

where the added fuel mass flow is neglected. The high pressure turbine drives the high pressure compressor through a shaft that connects the two components. The work per second done by the high pressure compressor on the core air is

$$W_{hpc} = 118.2 \times 1005 \times (5/9) \times (940 - 220) = 4.75 \times 10^7 \, J/\sec \, . \tag{1.4}$$

Note that the work per second done by the gas on the turbine is very close to but slightly larger than that done by the compressor on the gas. If the shaft connecting the compressor and turbine has no frictional losses and if the mass flow through both components is indeed the same and if both components are adiabatic then the work terms would be identical. The system is not quite adiabatic due to heat loss to the surroundings. The mass flow is not precisely the same because of the added fuel and because some of the relatively cooler compressor flow is bled off to be used for power generation and to internally cool the high temperature components of the turbine.

Since the work output of the turbine and compressor is practically the same across both components why does the compressor have so many more stages than the turbine? The answer comes from the viscous nature of fluid flow. In the compressor, the flow is in the direction of increasing pressure and so the boundary layers on the compressor blades and in the compressor passages encounter an adverse pressure gradient that increases the tendency for flow separation and blade stall. The pressure rise achievable in a single compressor stage is limited by this effect. In the turbine the opposite is the case, the flow is in the direction of decreasing pressure which tends to stabilize the boundary layers on the turbine airfoils reducing the tendency for blade stall. As a result the work output of a single turbine stage is several times larger than that possible in a single compressor stage. If there was no such thing as flow separation all compressors and turbines would have the same number of stages. At the level of an individual blade, turbine blades are much more highly loaded (have much higher lift) than compressor blades. The difference in lift and the requirement that the turbine blades be cooled is reflected in significant differences in the blade profiles as illustrated in Figure 1.2. Cooling of the turbine blades is required because of the very

high temperature of the gas entering the turbine from the combustor. In modern engines the turbine inlet temperature may be several hundred degrees higher than the melting temperature of the turbine blade material and complex cooling schemes are needed to enable the turbine to operate for tens of thousands of hours before overhaul.

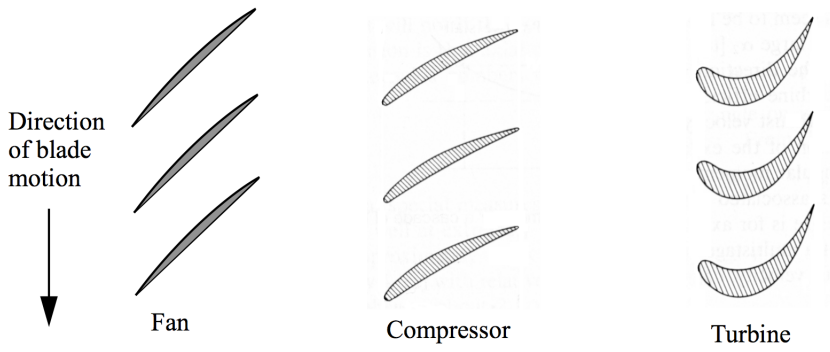

Figure 1.2: *Generic fan, compressor and turbine blade profiles.*

In general turbine blades are thicker and have much more camber than compressor blades. The extra thickness allows the turbine blades to be fabricated with internal cooling air passages and the combination of thickness and camber is responsible for the high lift generated by a turbine blade. In a modern turbofan engine the fan operates at blade tip Mach numbers approaching, or slightly above, one. As a result the profile of a typical fan blade tends to be quite slender with a relatively sharp leading edge as illustrated in Figure 1.2.

Let's take a look at the entropy change per unit mass of the gas as it passes from one engine component to another. The Gibbs equation for an ideal gas is

$$\frac{ds}{C_p} = \frac{dT}{T} - \left(\frac{\gamma - 1}{\gamma}\right)\frac{dP}{P}. \tag{1.5}$$

For air $\gamma = 1.4$. Throughout our study of air breathing propulsion systems we will assume the gas to be calorically perfect (heat capacities are assumed constant). From a pedagogical standpoint this is the most appropriate approach for learning how air breathing engines work and for a preliminary analysis of engine performance. A designer would use aero-thermodynamic software that would incorporate the temperature dependence of the heat capacities as well as detailed semi-empirical flow models of the various engine components. Occasionally, it may be useful to use different values of the heat capacities in the cold and hot sections of the engine.

Between any two points a and b the Gibbs equation integrates to

$$\frac{s_b - s_a}{C_p} = Ln\left(\frac{T_b}{T_a}\right) - \left(\frac{\gamma - 1}{\gamma}\right) Ln\left(\frac{P_b}{P_a}\right). \tag{1.6}$$

Integrating between the various stations of the engine shown in Figure 1.1 leads to the following. Note that station 0 is in the free stream and station 1 is at the entrance to the inlet. Neither station is shown in Figure 1.1.

Station 2 - Sea level static conditions from Figure 1.1 are

$$\begin{aligned} P_{t2} &= 14.7\, psia \\ T_{t2} &= 519\, R \end{aligned} \tag{1.7}$$

where the inlet (not shown) is assumed to be adiabatic and isentropic.

Station 3 - At the outlet of the high pressure compressor

$$\begin{aligned} P_{t3} &= 335\, psia \\ T_{t3} &= 1400\, R. \end{aligned} \tag{1.8}$$

The non-dimensional entropy change per unit mass across the inlet compression system is

$$\frac{s_b - s_a}{C_p} = Ln\left(\frac{1400}{519}\right) - \left(\frac{0.4}{1.4}\right) Ln\left(\frac{335}{14.7}\right) = 0.992 - 0.893 = 0.099. \tag{1.9}$$

Station 4 - The heat put into the cycle is equal to the stagnation enthalpy change across the burner.

$$\dot{m}_f h_f = \left(\dot{m}_{a_{core}} + \dot{m}_f\right) h_{t4} - \dot{m}_{a_{core}} h_{t3} \tag{1.10}$$

The thermodynamic heat of combustion of a fuel is calculated as the heat that must be removed to bring all the products of combustion back to the original pre-combustion temperature. The enthalpy of combustion for fuels is usually expressed as a higher or lower heating value. The higher heating value is realized if the original temperature is below the condensation temperature of water and any water vapor is condensed giving up its vaporization energy as heat. The lower heating value is calculated by subtracting the

heat of vaporization of the water in the combustion products from the higher heating value. In this case any water formed is treated as a gas.

The enthalpy of combustion of a typical jet fuel such as JP-4 is generally taken to be the lower heating value since the water vapor in the combustion products does not condense before leaving the nozzle. The value we will use is

$$h_f|_{JP-4} = 4.28 \times 10^7 \, J/\sec . \tag{1.11}$$

The higher heating value of JP-4 is about $4.6 \times 10^7 \, J/kg$ and can be calculated from a knowledge of the water vapor content in the combustion products. The higher and lower heating values of most other hydrocarbon fuels are within about 10% of these values. At the outlet of the burner

$$\begin{aligned} P_{t4} &= 315 \, psia \\ T_{t4} &= 2785 \, R. \end{aligned} \tag{1.12}$$

Note the very small stagnation pressure loss across the burner. The stagnation pressure drop across any segment of a channel flow is proportional to the Mach number squared.

$$\frac{dP_t}{P_t} = -\frac{\gamma M^2}{2}\left(\frac{dT_t}{T_t} + 4C_f \frac{dx}{D}\right) \tag{1.13}$$

A key feature of virtually all propulsion systems is that the heat addition is carried out at very low Mach number in part to keep stagnation pressure losses across the burner as small as possible. The exception to this is the scramjet concept used in hypersonic flight where the heat addition inside the engine occurs at supersonic Mach numbers that are well below the flight Mach number.

The non-dimensional entropy change per unit mass across the burner of the JT9D-7 is

$$\frac{s_4 - s_3}{C_p} = Ln\left(\frac{2785}{1400}\right) - \left(\frac{0.4}{1.4}\right) Ln\left(\frac{315}{335}\right) = 0.688 + 0.0176 = 0.706. \tag{1.14}$$

Station 5 - At the outlet of the turbine

$$\begin{aligned} P_{t5} &= 22 \, psia \\ T_{t5} &= 1495 \, R. \end{aligned} \tag{1.15}$$

The non-dimensional entropy change per unit mass across the turbine is

$$\frac{s_5 - s_4}{C_p} = Ln\left(\frac{1495}{2785}\right) - \left(\frac{0.4}{1.4}\right) Ln\left(\frac{22}{315}\right) = -0.622 + 0.760 = 0.138. \tag{1.16}$$

Station 0 - The exhaust gas returns to the reference state through nozzle expansion to ambient pressure and thermal mixing with the surrounding atmosphere.

$$\begin{aligned} P_{t0} &= 14.7\, psia \\ T_{t0} &= 519\, R \end{aligned} \tag{1.17}$$

The non-dimensional entropy change back to the reference state is

$$\frac{s_0 - s_5}{C_p} = Ln\left(\frac{519}{1495}\right) - \left(\frac{0.4}{1.4}\right) Ln\left(\frac{14.7}{22}\right) = -1.058 + 0.115 = -0.943. \tag{1.18}$$

The net change in entropy around the cycle is zero as would be expected. That is $\Delta s = 0.099 + 0.706 + 0.138 - 0.943 = 0$.

Note that the entropy changes across the compressor and turbine are much smaller than across the burner where substantial heat is added with only a very small change in pressure. Similarly there is a large temperature and entropy decrease of the exhaust gases as they mix with the surrounding air. Figure 1.3 shows the fully expanded exhaust from an engine. As the exhaust gas emerges from the nozzle and mixes with the surroundings, heat is conducted from the hot gases to the ambient air.

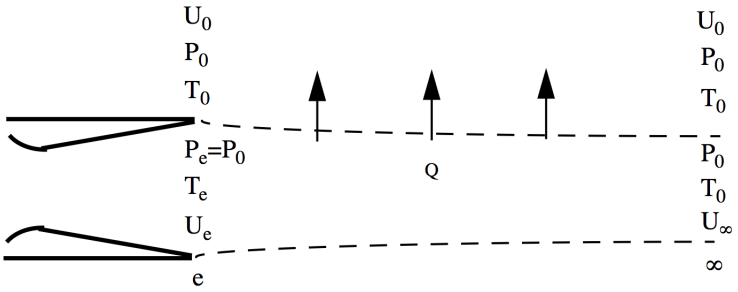

Figure 1.3: *Constant pressure heat transfer from the engine exhaust to the surroundings.*

Through mixing, the exhaust gas eventually returns to the temperature and pressure of the reference state entering the engine. One can think of this as a two step process. In the first step viscosity is neglected and the exhaust flow is treated using the 1-D equations

of motion. In this approximation, the flow in the stream-tube within the dashed lines in Figure 1.3 is governed by the 1-D momentum equation (the Euler equation).

$$dP + \rho U dU = 0 \tag{1.19}$$

According to (1.19) since the pressure is constant along this stream-tube, the velocity must also be constant ($dP = 0, dU = 0$) and the flow velocity at the end of the stream-tube must be the same as at the nozzle exit $U_\infty = U_e$. The 1-D energy equation for the flow in the stream tube is

$$\delta q = dh_t \tag{1.20}$$

and so the heat rejected to the surroundings per unit mass flow is given by

$$q = h_{te} - h_{t\infty} = h_e + \frac{1}{2}{U_e}^2 - h_\infty - \frac{1}{2}{U_\infty}^2 = h_e - h_\infty. \tag{1.21}$$

The heat rejected through conduction to the surrounding air in the wake of the engine is equal to the change in static enthalpy of the exhaust gas as it returns to the initial state. At this point the cycle is complete.

In the second step, viscosity is turned on and the kinetic energy of the exhaust gas is eventually lost through viscous dissipation. The temperature of the atmosphere is raised by an infinitesimal amount in the process. In actual fact both processes occur simultaneously through a complex process of nearly constant pressure heat transfer and turbulent mixing in the engine wake.

The process of constant pressure heat addition and rejection illustrated by this example is known as the Brayton cycle.

1.2 Thermodynamic cycles

1.2.1 The Carnot cycle

Using the Second Law one can show that heat and work, are not equivalent though each is a form of energy. All work can be converted to heat but not all heat can be converted to work. The most efficient thermodynamic cycle, the Carnot cycle which involves heat interaction at constant temperature, can be used to illustrate this point. Consider the piston cylinder combination shown in Figure 1.4 and the sequence of piston strokes representing the four basic states in the Carnot cycle.

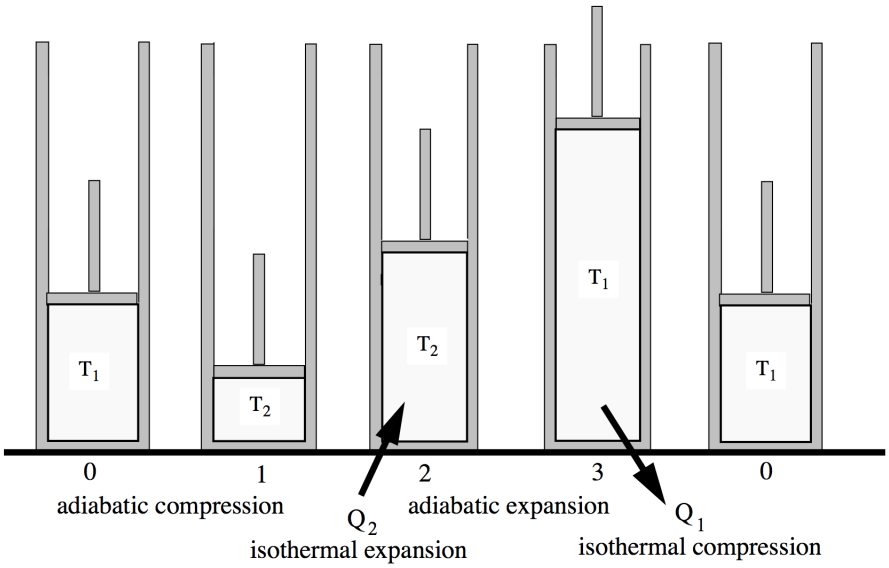

Figure 1.4: *The Carnot cycle heat engine.*

In the ideal Carnot cycle the adiabatic compression and expansion strokes are carried out isentropically. A concrete example in the P-V plane and T-S plane is shown in Figure 1.5 and Figure 1.6. The working fluid is Nitrogen cycling between the temperatures of 300 and 500 Kelvin with the compression stroke moving between one and six atmospheres. The entropy of the compression leg comes from tabulated data for nitrogen. The entropy of the expansion leg is specified to be $7300\,\mathrm{J/(kg-K)}$.

The thermodynamic efficiency of the cycle is

$$\eta = \frac{work\ output\ during\ the\ cycle}{heat\ added\ to\ the\ system\ during\ the\ cycle} = \frac{W}{Q_2}. \tag{1.22}$$

According to the first law of thermodynamics

$$\delta Q = dE + \delta W. \tag{1.23}$$

Over the cycle, the change in internal energy which is a state variable is zero and the work done is

$$W = Q_2 - Q_1 \tag{1.24}$$

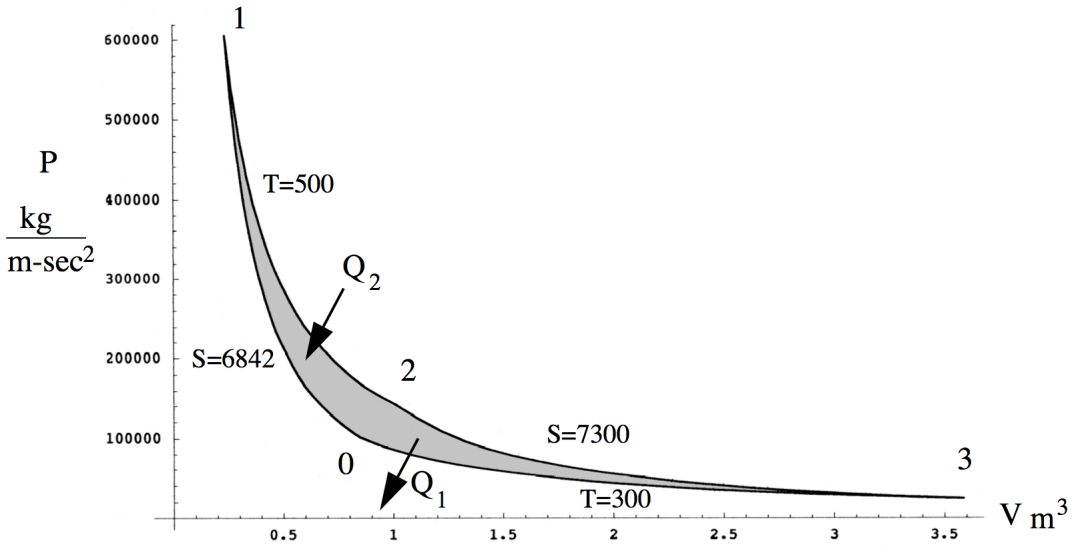

Figure 1.5: *P-V diagram of a Carnot cycle working between the temperatures of 300K and 500K. The working fluid is nitrogen.*

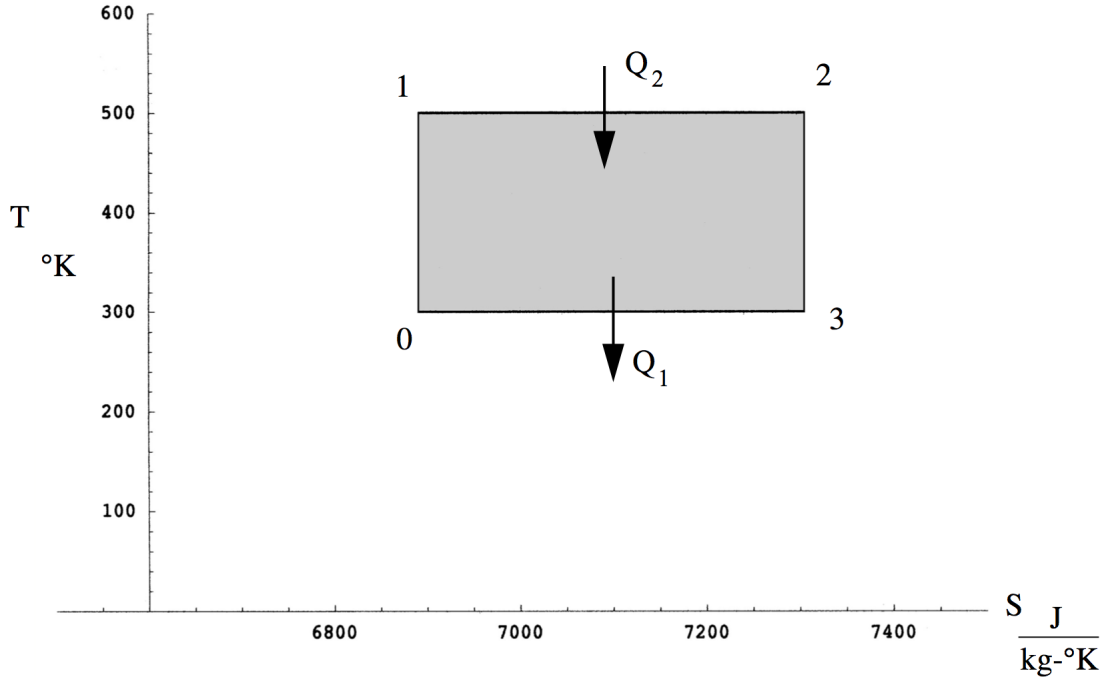

Figure 1.6: *T-S diagram for the Carnot cycle shown above.*

and so the efficiency is

$$\eta = 1 - \frac{Q_1}{Q_2}. \tag{1.25}$$

The change in entropy over the cycle is also zero and so from the Second Law

$$\oint ds = \oint \frac{\delta Q}{T} = 0. \tag{1.26}$$

Since the temperature is constant during the heat interaction we can use this result to write

$$\frac{Q_1}{T_1} = \frac{Q_2}{T_2}. \tag{1.27}$$

Thus the efficiency of the Carnot cycle is

$$\eta_C = 1 - \frac{T_1}{T_2} < 1. \tag{1.28}$$

For the example shown$\eta_C = 0.4$. At most only 40% of the heat added to the system can be converted to work. The maximum work that can be generated by a heat engine working between two finite temperatures is limited by the temperature ratio of the system and is always less than the heat put into the system.

1.2.2 The Brayton cycle

As illustrated by the JT9D example, the Brayton cycle involves heat interaction at constant pressure. Now consider the piston cylinder combination shown below and the sequence of piston strokes representing the four basic states of the Brayton cycle. The piston motion is similar to the Carnot cycle except that the heat interaction occurs at constant pressure.

In the ideal Brayton cycle the adiabatic compression and expansion strokes are carried out isentropically. The corresponding behavior of the ideal Brayton cycle in the P-V plane and T-S plane is shown in Figures 1.8 and 1.9.

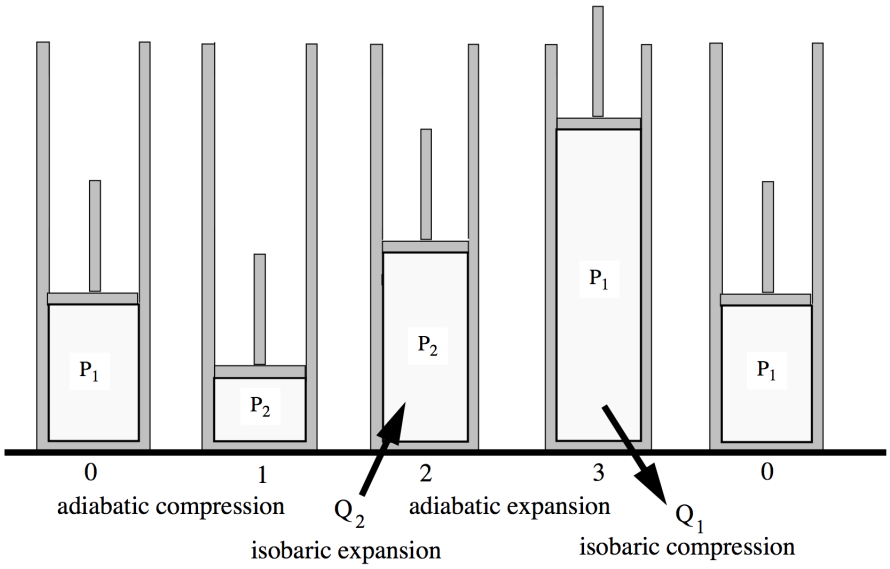

Figure 1.7: *The Brayton cycle heat engine*

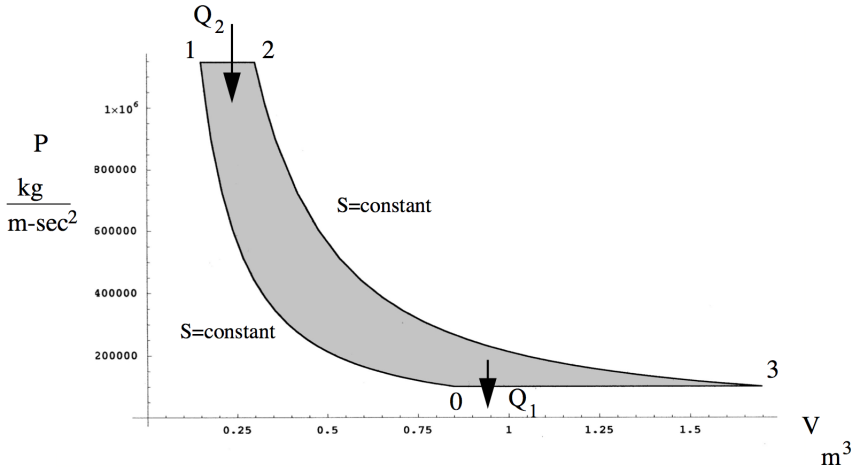

Figure 1.8: *P-V diagram of a Brayton cycle working between the pressures of one and six atmospheres. Nitrogen is the working fluid.*

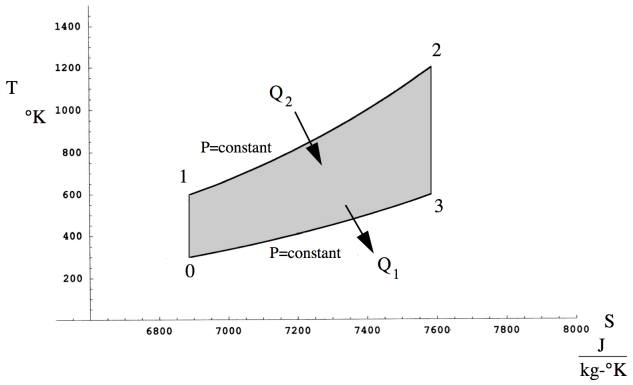

Figure 1.9: *T-S diagram of the Brayton cycle shown above.*

In the case of the Brayton cycle the work done is still $W = Q_2 - Q_1$. The first law can be written

$$\delta Q = dE + PdV = dH - VdP. \tag{1.29}$$

The heat interaction occurs at constant pressure, $dP = 0$ and so the heat added and removed is equal to the enthalpy change.

$$\begin{aligned} Q_2 &= H_2 - H_1 \\ Q_1 &= H_3 - H_0 \end{aligned} \tag{1.30}$$

The efficiency of the Brayton cycle is

$$\eta_B = 1 - \frac{H_3 - H_0}{H_2 - H_1}. \tag{1.31}$$

If the working fluid is an ideal gas with constant heat capacity then we can write for the ideal Brayton cycle

$$\frac{H_0}{H_1} = \frac{T_0}{T_1} = \left(\frac{P_0}{P_1}\right)^{\frac{\gamma-1}{\gamma}} = \left(\frac{P_3}{P_2}\right)^{\frac{\gamma-1}{\gamma}} = \frac{T_3}{T_2} = \frac{H_3}{H_2}. \tag{1.32}$$

Using (1.32) the Brayton efficiency can be written

$$\eta_B = 1 - \frac{T_0}{T_1}\left(\frac{\frac{T_3}{T_0} - 1}{\frac{T_2}{T_1} - 1}\right). \tag{1.33}$$

From (1.32) the term in parentheses is one and so the efficiency of the ideal Brayton cycle is finally

$$\eta_B = 1 - \frac{T_0}{T_1}. \tag{1.34}$$

The important point to realize here is that the efficiency of a Brayton process is determined entirely by the temperature increase during the compression step of the cycle (or equivalently the temperature decrease during the expansion step.

1.3 The standard atmosphere

Figure 1.10 below shows the distribution of temperature and density in the atmosphere with comparisons with isothermal and isentropic models of the atmosphere. The scale height of the atmosphere is

$$H = \frac{{a_0}^2}{\gamma g} = \frac{RT_0}{g}. \tag{1.35}$$

The speed of sound, temperature, and gravitational acceleration in (1.35) are evaluated at zero altitude. For air at $288.15\,K$ the scale height is 8,435 meters (27,674 feet). At this altitude the thermal and potential energy of the atmosphere are of the same order. Below a scale height of one the atmosphere is approximately isentropic and the temperature falls off almost linearly. Above a scale height of about 1.5 the temperature is almost constant. In order to standardize aircraft performance calculations Diehl (Ref. W. S. Diehl, *Some Approximate Equations for the Standard Atmosphere* N.A.C.A. Technical Report No. 375, 1930) defined a standard atmosphere which was widely adopted by the aeronautics community. According to this standard the atmospheric values at sea level in Figure 1.11 are assumed.

1.4 Problems

Problem 1 - Consider the JT9D-7 turbofan cross-section discussed above. Plot the state

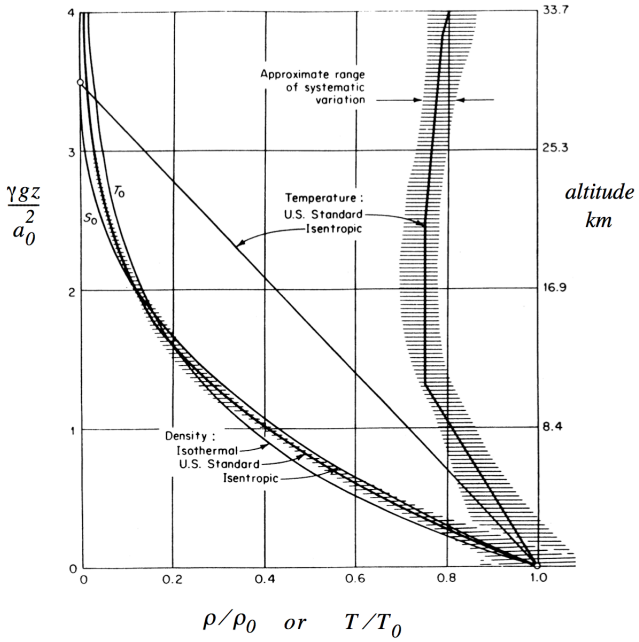

Figure 1.10: *Isothermal and isentropic models of the standard atmosphere.*

$T_{SL} = 518.67°R\ (59\ °F)$	$T_{SL} = 288.15°K\ (15\ °C)$
$P_{SL} = 2116.22\ pounds/ft^2$	$P_{SL} = 1.013250 \times 10^5\ newtons/m^2$
$\rho_{SL} = 0.0023769\ slug/ft^3$	$\rho_{SL} = 1.2250\ kilograms/m^3$
$g = 32.1741\ ft/sec^2$	$g = 9.80665\ m/sec^2$
$a_0 = 1116.45\ ft/sec$	$a_0 = 340.294\ m/sec$
$H = 27,672\ ft$	$H = 8434.5\ m$
$R_{air} = 1710.2\ ft^2/(sec^2 - °R)$	$R_{air} = 287.06\ m^2/(sec^2 - °K)$

Figure 1.11: *Standard atmospheric values at sea level in English and metric units*

of the gas which passes through the core of the engine on a temperature versus entropy diagram and on a pressure versus specific volume diagram. Assume constant specific heat throughout the engine with $\gamma = 1.4$. Do the same for the gas which passes through the fan. Determine the efficiency of the cycle. Assume the fan, compressor and turbine are adiabatic, the inlet is isentropic and the exhaust gas of the JT9D passes through an isentropic nozzle where it is expanded to atmospheric pressure before mixing with the surrounding air. Assume pressures and temperatures within the engine are stagnation values.

Problem 2 - An accurate approximation to the specific heat of air as a function of temperature is

$$\frac{C_p}{R} = \frac{7}{2} + \left(\frac{\frac{\theta_v}{2T}}{Sinh\left(\frac{\theta_v}{2T}\right)} \right)^2 \tag{1.36}$$

where the vibrational reference temperature for air, $\theta_v = 3060\,K$. Plot C_p, C_v, γ and the enthalpy, h , of air as a function of T/θ_v over the range $300\,K$ to $4000\,K$.

Problem 3 - Review quasi-one-dimensional gas dynamics. Carefully derive the mass, momentum and energy equations for stationary 1-D flow

$$\begin{aligned}
&d\left(\rho U A\right) = \delta\dot{m} \\
&d\left(P - \tau_{xx}\right) + \rho U dU = -\tau_w \left(\frac{\pi D dx}{A}\right) + \frac{\left(U_{xm} - U\right)\delta\dot{m}}{A} - \frac{\delta F_x}{A} \\
&d\left(h_t - \frac{\tau_{xx}}{\rho} + \frac{Q_x}{\rho U}\right) = \frac{\delta Q}{\rho U A} - \frac{\delta W}{\rho U A} + \left(h_{tm} - (h_t - \frac{\tau_{xx}}{\rho} + \frac{Q_x}{\rho U})\right)\delta\dot{m}
\end{aligned} \tag{1.37}$$

where U_{mx} is the stream-wise component of the velocity and h_{tm} is the enthalpy of the injected mass $\delta\dot{m}$. Explain the assumptions used to get from the full equations of motion to (1.37).

Chapter 2

Engine performance parameters

2.1 The definition of thrust

One might be surprised to learn that there is no direct way to determine the thrust generated by a propulsion system. The reason for this is that the flow over and through an installed engine on an aircraft or an engine attached to a test stand is responsible for the total force on the engine and its nacelle. On any part of the propulsion surface the combination of pressure and viscous stress forces produced by the flow may contribute to the thrust or to the drag and there is no practical way to extricate one force component from the other. Even the most sophisticated test facility can measure the thrust produced by an engine only up to an accuracy of about 0.5%. Wind and weather conditions during the test, inaccuracies in measurement, poorly known flow characteristics in the entrance flow and exhaust and a variety of minor effects limit the ability of a test engineer to precisely measure or predict the thrust of an engine. Thus as a practical matter we must be satisfied with a thrust formula that is purely a definition. Such a definition is only useful to the extent that it reflects the actual thrust force produced by an engine up to some reasonable level of accuracy. In the following, we will use mass and momentum conservation over an Eulerian control volume surrounding a ramjet to motivate a definition of thrust. The control volume is indicated as the dashed line shown in Figure 2.1.

The control volume is in the shape of a cylinder centered about the ramjet.Note that the control volume is simply connected. That is, by suitable distortions without tearing, it is developable into a sphere. The surface of the control volume runs along the entire wetted surface of the ramjet and encloses the inside of the engine. The upstream surface is far enough upstream so that flow variables there correspond to free-stream values. The downstream surface of the control volume coincides with the nozzle exit. The reason for positioning the downstream surface this way is that we need a definition of thrust that

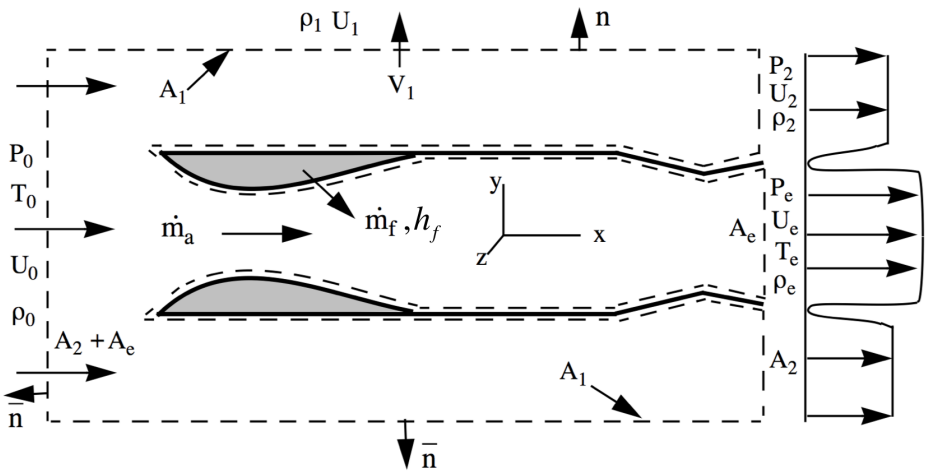

Figure 2.1: *Ramjet control volume for developing a definition of thrust*

is expressed in terms of flow variables that can be determined relatively easily in terms of the thermodynamic and geometrical properties of the engine internal gas flow. Note that the velocity profile in the wake cannot be used to determine thrust since the profile is momentum-less. An integral over the wake profile is proportional to the sum of thrust plus drag and since the engine is not accelerating this sum is zero. We will assume that within the engine all flow variables are area averaged (averaged in the y-z plane) and that the flow is steady. Fuel from an onboard tank is injected through the control volume surface. The mass flows through the engine are

$$\begin{aligned} \dot{m}_a &= air\ mass\ flow\ rate \\ \dot{m}_f &= fuel\ mass\ flow\ rate. \end{aligned} \tag{2.1}$$

The fuel mixes and reacts with the incoming air flow releasing heat and the heat is assumed to be uniformly distributed over the engine cross section downstream of the region of combustion. The integrated form of the conservation equations for steady flow with no

body forces on an Eulerian control volume is

$$\begin{aligned}
&\int_A \rho\bar{U}\cdot\bar{n}dA = 0 \\
&\int_A \left(\rho\bar{U}\bar{U} + P\bar{\bar{I}} - \bar{\bar{\tau}}\right)\cdot\bar{n}dA = 0 \\
&\int_A \left(\rho h_t\bar{U} - \bar{\bar{\tau}}\cdot\bar{U} + \bar{Q}\right)\cdot\bar{n}dA = 0.
\end{aligned} \tag{2.2}$$

where h_t is the stagnation enthalpy of the gas flow.

$$h_t = e + Pv + k \tag{2.3}$$

Mass Balance

The continuity equation integrated over the control volume leads to

$$\begin{aligned}
&\int_A \rho\bar{U}\cdot\bar{n}dA = \\
&\int_{A_2} \rho_2 U_2 dA + \rho_e U_e A_e - \rho_0 U_0 \left(A_2 + A_e\right) - \dot{m}_f + \int_{A_1} \rho_1 V_1 dA = 0.
\end{aligned} \tag{2.4}$$

The first integral in (2.4) involving a flux of mass out of the control volume is carried out over the annular area labeled A_2 in Figure 2.1. It is a complicated integral in that it involves the wake velocity profile which is not accurately known without a direct measurement. In fact the nozzle exit flow is assumed to be an area averaged plug flow and so all the complexity of the wake profile is thrown into this integral. The last integral in (2.4) is carried out over the outer surrounding surface of the control volume and involves a flux of mass leaving the control volume due to the outward displacement of air produced by the blockage effect of the engine. It too is a complicated integral but one we will be able to easily approximate. Note that this part of the control volume is taken to be straight. It does not follow a streamline. Thus the area of the upstream face of the control volume is equal to $A_2 + A_e$.

Momentum Balance

Now integrate the x-momentum equation over the control volume.

$$\int_A \left(\rho \bar{U}\bar{U} + P\bar{\bar{I}} - \bar{\bar{\tau}}\right) \cdot \bar{n} dA \Big|_x =$$

$$\int_{A_2} \left(\rho_2 {U_2}^2 + P_2\right) dA + \left(\rho_e {U_e}^2 A_e + P_e A_e\right) - \left(\rho_0 {U_0}^2 + P_0\right)(A_2 + A_e) + \tag{2.5}$$

$$\int_{A_1} \rho_1 U_1 V_1 dA + \int_{A_w} \left(P\bar{\bar{I}} - \bar{\bar{\tau}}\right) \cdot \bar{n} dA \Big|_x = 0$$

Note that the x-momentum of the injected fuel mass has been neglected. The first integral involves a complicated distribution of pressure and momentum over the area A_2 and there is little we can do with it. The last integral involves the pressure and stress forces acting over the entire wetted surface of the engine and although the kernel of this integral may be an incredibly complicated function, the integral itself must be zero since the engine is not accelerating or decelerating (the free stream speed is not a function of time).

$$\int_{A_w} \left(P\bar{\bar{I}} - \bar{\bar{\tau}}\right) \cdot \bar{n} dA \Big|_x = Thrust - Drag = 0 \tag{2.6}$$

The second to last integral in (2.5) can be approximated as follows.

$$\int_{A_1} \rho_1 U_1 V_1 dA \cong \int_{A_1} \rho_1 U_0 V_1 dA \tag{2.7}$$

The argument for this approximation is that at the outside surface of the control volume the x-component of the fluid velocity is very close to the free stream value. This is a good approximation as long as the control volume surface is reasonably far away from the engine. This approximation allows us to use the mass balance to get rid of this integral. Multiply (2.4) by U_0. and subtract from (2.5). The result is

$$\rho_e U_e \left(U_e - U_0\right) A_e + \left(P_e - P_0\right) A_e + \dot{m}_f U_0 + \int_{A_2} \left(\rho_2 U_2 \left(U_2 - U_0\right) + \left(P_2 - P_0\right)\right) dA = 0. \tag{2.8}$$

This is as far as we can go with our analysis and at this point we have to make an arbitrary choice. We will define the drag of the engine as

$$Drag = \int_{A_2} \left(\rho_2 U_2 \left(U_0 - U_2\right) + \left(P_0 - P_2\right)\right) dA \tag{2.9}$$

and the thrust as

$$Thrust = \rho_e U_e \left(U_e - U_0\right) A_e + \left(P_e - P_0\right) A_e + \dot{m}_f U_0. \tag{2.10}$$

This is a purely practical choice where the thrust is defined in terms of flow variables that can be determined from a thermo-gas-dynamic analysis of the area-averaged engine internal flow. All the complexity of the flow over the engine has been thrown into the drag integral (2.9) which of course could very well have contributions that could be negative. This would be the case, for example, if some part of the pressure profile had $P_2 - P_0 > 0$. The exit mass flow is the sum of the air mass flow plus the fuel mass flow.

$$\rho_e U_e A_e = \dot{m}_a + \dot{m}_f \tag{2.11}$$

Using (2.11) the thrust definition (2.10) can be written in the form

$$T = \dot{m}_a \left(U_e - U_0\right) + \left(P_e - P_0\right) A_e + \dot{m}_f U_e. \tag{2.12}$$

In this form the thrust definition can be interpreted as the momentum change of the air mass flow across the engine plus the momentum change of the fuel mass flow. The pressure term reflects the acceleration of the exit flow that occurs as the jet exhaust eventually matches the free stream pressure in the far wake. Keep in mind that the fuel is carried on board the aircraft, and in the frame of reference attached to the engine, the fuel has zero velocity before it is injected and mixed with the air.

The thrust definition (2.12) is very general and applies to much more complex systems. If the selected engine was a turbojet the control volume would look like that shown in Figure 2.2.

The surface of the control volume covers the entire wetted surface of the engine including the struts that hold the rotating components in place as well as the rotating compressor, shaft and turbine. In this case the control volume is of mixed Eulerian-Lagrangian type with part of the control volume surface attached to and moving with the rotating parts. The cut on the engine centerline comes from the wrapping of the control volume about the supports and rotating components. All fluxes cancel on the surface of the cut, which is

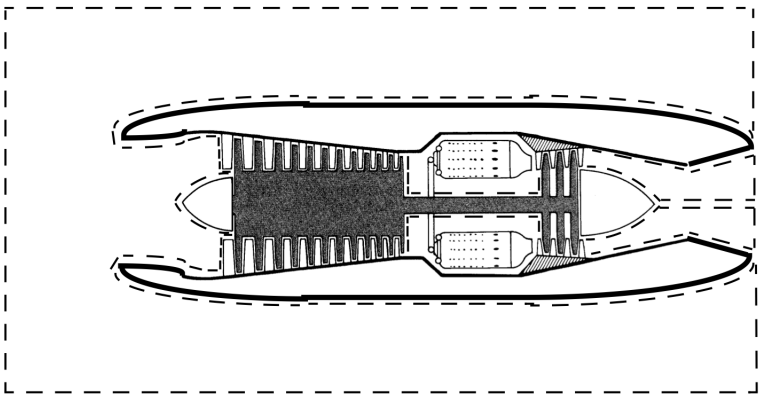

Figure 2.2: *Turbojet control volume.*

really a line on the engine axis. The terms arising from the pressure-viscous stress forces on the rotating components are just part of the total surface force integral (2.6) that is still zero. A mass and momentum balance over the control volume shown in Figure 2.2 would lead to the same result (2.12).

2.2 Energy balance

The energy balance across the engine is very simple. The energy equation integrates to

$$\begin{aligned} &\int_A \left(\rho h_t \bar{U} - \bar{\bar{\tau}} \cdot \bar{U} + \bar{Q}\right) \cdot \bar{n} dA = 0 \\ &\int_{A_2} \left(\rho_2 h_{t2} U_2\right) dA + \rho_e h_{te} U_e A_e - \rho_0 h_{t0} U_0 \left(A_2 + A_e\right) - \dot{m}_f h_f + \int_{A_1} \rho_1 h_{t1} V_1 dA = 0. \end{aligned} \tag{2.13}$$

Here the viscous and heat conduction terms across the boundaries of the control volume have been neglected and the flow over the inside and outside surface of the ramjet is assumed to be adiabatic (or at least the temperature of the engine is assumed to be at steady state where any heat conducted into the engine is conducted out elsewhere). This is a very reasonable though not an exact assumption. Some heat is always lost through the engine nacelle but this is a tiny fraction of the enthalpy flow in the exhaust. The viscous power term on the wetted surface is zero due to the no-slip condition. The only

contribution over the wetted surface is from the flux of fuel which carries with it its fuel enthalpy h_f.

A typical value of fuel enthalpy for JP-4 jet fuel is

$$h_f|_{JP-4} = 4.28 \times 10^7 \, J/kg. \tag{2.14}$$

As a comparison, the enthalpy of Air at sea level static conditions is

$$h|_{Airat288.15K} = C_p T_{SL} = 1005 \times 288.15 = 2.896 \times 10^5 \, J/kg. \tag{2.15}$$

The ratio is

$$\frac{h_f|_{JP-4}}{h|_{Airat288.15K}} = 148. \tag{2.16}$$

The energy content of a kilogram of hydrocarbon fuel is remarkably large and constitutes one of the important facts of nature that makes extended powered flight possible.

If the flow over the outside of the engine is adiabatic then the stagnation enthalpy of flow over the outside control volume surfaces is equal to the free-stream value and we can write the energy balance as

$$\int_{A_2} (\rho_2 h_{t0} U_2) \, dA + \rho_e h_{te} U_e A_e - \rho_0 h_{t0} U_0 \, (A_2 + A_e) - \dot{m}_f h_f + \int_{A_1} \rho_1 h_{t0} V_1 dA = 0. \tag{2.17}$$

Now multiply the continuity equation (2.4) by h_{t0} and subtract from (2.17). The result is

$$\rho_e h_{te} U_e A_e - \rho_e h_{t0} U_e A_e - \dot{m}_f \, (h_f - h_{t0}) = 0. \tag{2.18}$$

Using (2.11) the energy balance across the engine can be written as

$$(\dot{m}_a + \dot{m}_f) \, h_{te} = \dot{m}_a h_{t0} + \dot{m}_f h_f. \tag{2.19}$$

The energy balance boils down to a simple algebraic relationship that states that the change in the stagnation enthalpy per second of the gas flow between the exit and entrance of the engine is equal to the added chemical enthalpy per second of the injected fuel flow.

2.3 Capture area

As the operating point of an engine changes, the amount of air passing through the engine may also vary. This is typically the case for an engine operating at subsonic Mach numbers. The capture area of the engine A_0 is defined in terms of the air mass flow rate.

$$\dot{m}_a = \rho_0 U_0 A_0 \tag{2.20}$$

The sketches below depict the variation in capture area that can occur as the engine flight Mach number changes from low subsonic to near sonic flight. The geometric entrance area of the engine is A_1. Similar changes can occur at a fixed flight Mach number, for example as the engine throttle is changed leading to changes in the demand of the engine for air. More will be said on this topic in a later chapter when we examine how a jet engine operates.

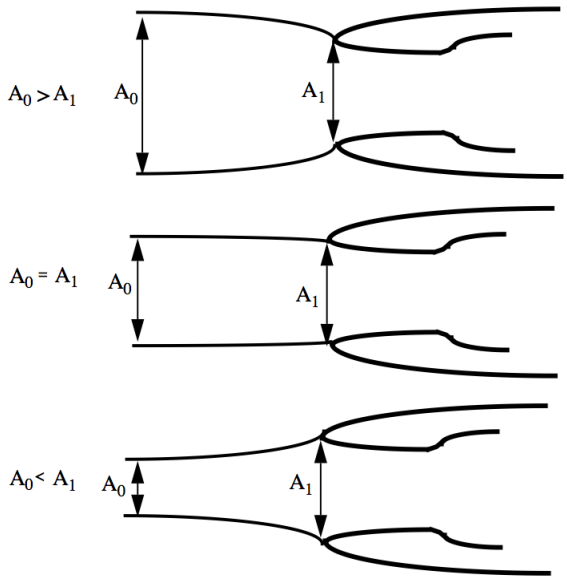

Figure 2.3: *Variation of inlet capture area with engine operating point.*

2.4 Overall efficiency

The overall efficiency of a propulsion system is defined as

$$\eta_{ov} = \frac{\textit{The power delivered to the vehicle}}{\textit{The total energy released per second through combustion}}. \tag{2.21}$$

That is

$$\eta_{ov} = \frac{TU_0}{\dot{m}_f h_f}. \tag{2.22}$$

It may not be so obvious but the definition of overall efficiency embodies a certain choice of the frame of reference in which the engine is viewed. In particular we have selected a frame in which the thrust generated by the engine T acts at a speed U_0. This is a frame in which the surrounding air is at rest and the engine moves to the left at the given speed. This idea is illustrated in Figure 2.4.

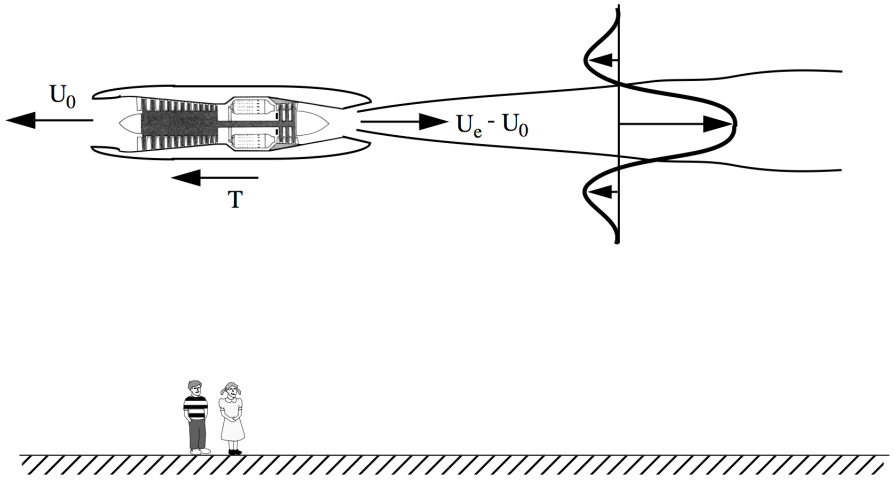

Figure 2.4: *Frame of reference used to define efficiencies.*

Note that in the frame of reference depicted in Figure 2.1 and Figure 2.2 the power generated by the engine thrust is zero.

To the children observing the engine from the ground in Figure 2.4 a parcel of still air is engulfed by the engine moving to the left and exits the engine as a mixture of air and combustion products with a speed to the right equal to $U_e - U_0$.

2.5 Breguet aircraft range equation

There are a number of models of aircraft range. The simplest assumes that the aircraft flies at a constant value of lift to drag ratio and constant engine overall efficiency. The range is

$$R = \int U_0 dt = \int \frac{\dot{m}_f h_f \eta_{ov}}{T} dt. \tag{2.23}$$

The fuel mass flow is directly related to the change in aircraft weight, w , per second.

$$\dot{m}_f = -\frac{1}{g}\frac{dw}{dt} \tag{2.24}$$

Since thrust equals drag and aircraft weight equals lift we can write

$$T = D = \left(\frac{D}{L}\right) L = \left(\frac{D}{L}\right) w. \tag{2.25}$$

Now the range integral becomes

$$R = -\eta_{ov}\frac{h_f}{g}\left(\frac{L}{D}\right)\int_{w_{initial}}^{w_{final}} \frac{dw}{w}. \tag{2.26}$$

The result is

$$R = \eta_{ov}\frac{h_f}{g}\left(\frac{L}{D}\right) Ln\left(\frac{w_{initial}}{w_{final}}\right). \tag{2.27}$$

The range formula (2.27) is generally attributed to the great French aircraft pioneer Louis Charles Breguet who in 1919 founded a commercial airline company that would eventually become Air France. This result highlights the key role played by the engine overall efficiency in determining aircraft range. Note that as the aircraft burns fuel it must increase altitude to maintain constant L/D . and the required thrust decreases. The small, time dependent effects due to the upward acceleration are neglected.

2.6 Propulsive efficiency

It is instructive to decompose the overall efficiency into an aerodynamic factor and a thermal factor. To accomplish this, the overall efficiency is written as the product of a propulsive and thermal efficiency.

$$\eta_{ov} = \eta_{pr} \times \eta_{th} \tag{2.28}$$

The propulsive efficiency is

$$\eta_{pr} = \frac{Power\ delivered\ to\ the\ vehicle}{Power\ delivered\ to\ the\ vehicle\ +\ \frac{\Delta\ kinetic\ energy\ of\ air}{second} + \frac{\Delta\ kinetic\ energy\ of\ fuel}{second}} \tag{2.29}$$

or

$$\eta_{pr} = \frac{TU_0}{TU_0 + \left(\frac{\dot{m}_a(U_e - U_0)^2}{2} - \frac{\dot{m}_a(0)^2}{2}\right) + \left(\frac{\dot{m}_f(U_e - U_0)^2}{2} - \frac{\dot{m}_f(U_0)^2}{2}\right)}. \tag{2.30}$$

If the exhaust is fully expanded so that $P_e = P_0$ and the fuel mass flow is much less than the air mass flow $\dot{m}_f \ll \dot{m}_a$, the propulsive efficiency reduces to

$$\eta_{pr} = \frac{2U_0}{U_e + U_0}. \tag{2.31}$$

This is quite a general result and shows the fundamentally aerodynamic nature of the propulsive efficiency. It indicates that for maximum propulsive efficiency we want to generate thrust by moving as much air as possible with as little a change in velocity across the engine as possible. We shall see later that this is the basis for the increased efficiency of a turbofan over a turbojet with the same thrust. This is also the basis for comparison of a wide variety of thrusters. For example, the larger the area of a helicopter rotor the more efficient the lift system tends to be.

2.7 Thermal efficiency

The thermal efficiency is defined as

$$\eta_{th} = \frac{Power\ delivered\ to\ the\ vehicle\ +\ \frac{\Delta\ kinetic\ energy\ of\ air}{second} + \frac{\Delta\ kinetic\ energy\ of\ fuel}{second}}{\dot{m}_f h_f} \tag{2.32}$$

or

$$\eta_{th} = \frac{TU_0\ +\ \left(\frac{\dot{m}_a(U_e-U_0)^2}{2} - \frac{\dot{m}_a(0)^2}{2}\right) + \left(\frac{\dot{m}_f(U_e-U_0)^2}{2} - \frac{\dot{m}_f(U_0)^2}{2}\right)}{\dot{m}_f h_f}. \tag{2.33}$$

If the exhaust is fully expanded so that $P_e = P_0$ the thermal efficiency reduces to

$$\eta_{th} = \frac{(\dot{m}_a + \dot{m}_f)\,\frac{{U_e}^2}{2} - \dot{m}_a\frac{{U_0}^2}{2}}{\dot{m}_f h_f}. \tag{2.34}$$

The thermal efficiency directly compares the change in gas kinetic energy across the engine to the energy released through combustion.

The thermal efficiency of a thermodynamic cycle compares the work out of the cycle to the heat added to the cycle.

$$\eta_{th} = \frac{W}{Q_{input\ during\ the\ cycle}} = \frac{Q_{input\ during\ the\ cycle} - Q_{rejected\ during\ the\ cycle}}{Q_{input\ during\ the\ cycle}} = 1 - \frac{Q_{rejected\ during\ the\ cycle}}{Q_{input\ during\ the\ cycle}} \tag{2.35}$$

We can compare (2.34) and (2.35) by rewriting (2.34) as

$$\eta_{th} = 1 - \left(\frac{\dot{m}_f h_f + \dot{m}_a\frac{{U_0}^2}{2} - (\dot{m}_a + \dot{m}_f)\,\frac{{U_e}^2}{2}}{\dot{m}_f h_f}\right). \tag{2.36}$$

This equation for the thermal efficiency can also be expressed in terms of the gas enthalpies. Recall that

$$\begin{aligned} h_{te} &= h_e + \frac{{U_e}^2}{2} \\ h_{t0} &= h_0 + \frac{{U_0}^2}{2}. \end{aligned} \tag{2.37}$$

Replace the velocities in (2.36).

$$\eta_{th} = 1 - \left(\frac{\dot{m}_f h_f + \dot{m}_a \left(h_{t0} - h_0 \right) - \left(\dot{m}_a + \dot{m}_f \right) \left(h_{te} - h_e \right)}{\dot{m}_f h_f} \right) \tag{2.38}$$

Use (2.19) to replace $\dot{m}_f h_f$ in (2.38). The result is

$$\eta_{th} = 1 - \frac{Q_{rejected\ during\ the\ cycle}}{Q_{input\ during\ the\ cycle}} = 1 - \left(\frac{\left(\dot{m}_a + \dot{m}_f \right) \left(h_e - h_0 \right) + \dot{m}_f h_0}{\dot{m}_f h_f} \right). \tag{2.39}$$

According to (2.39) the heat rejected during the cycle is

$$Q_{rejected\ during\ the\ cycle} = \left(\dot{m}_a + \dot{m}_f \right) \left(h_e - h_0 \right) + \dot{m}_f h_0. \tag{2.40}$$

This expression deserves some discussion. Strictly speaking the engine is not a closed system because of the fuel mass addition across the burner. So the question is; How does the definition of thermal efficiency account for this mass exchange within the concept of the thermodynamic cycle? The answer is that the heat rejected from the exhaust is comprised of two distinct parts. There is the heat rejected by conduction from the nozzle flow to the surrounding atmosphere plus physical removal from the thermally equilibrated nozzle flow of a portion equal to the added fuel mass flow. From this perspective, the fuel mass flow carries its fuel enthalpy into the system by injection in the burner and the exhaust fuel mass flow carries its ambient enthalpy out of the system by mixing with the surroundings. There is no net mass increase or decrease to the system.

Note that there is no assumption that the compression or expansion process operates isentropically, only that the exhaust is fully expanded.

2.8 Specific impulse, specific fuel consumption

An important measure of engine performance is the amount of thrust produced for a given amount of fuel burned. This leads to the definition of specific impulse

$$I_{sp} = \frac{Thrust\ force}{Weight\ flow\ of\ fuel\ burned} = \frac{T}{\dot{m}_f g} \tag{2.41}$$

with units of seconds. The specific fuel consumption is essentially the inverse of the specific impulse.

$$SFC = \frac{Pounds\ of\ fuel\ burned\ per\ hour}{Pounds\ of\ thrust} = \frac{3600}{I_{sp}} \tag{2.42}$$

The specific fuel consumption is a relatively easy to remember number of order one. Some typical values are

$$\begin{aligned} SFC|_{JT9D-takeoff} &\cong 0.35 \\ SFC|_{JT9D-cruise} &\cong 0.6 \\ SFC|_{militaryengine} &\cong 0.9 to 1.2 \\ SFC|_{militaryenginewithafterburning} &\cong 2. \end{aligned} \tag{2.43}$$

The SFC generally goes up as an engine moves from takeoff to cruise, as the energy required to produce a pound of thrust goes up with increased percentage of stagnation pressure losses and with the increased momentum of the incoming air.

2.9 Dimensionless forms

We have already noted the tendency to use both Metric and English units in dealing with propulsion systems. Unfortunately, despite great effort, the US propulsion industry has been unable to move away from the clumsy system of English units. Whereas the rest of the world, including the British, has gone fully metric. This is a real headache and something we will just have to live with, but the problem is vastly reduced by expressing all of our equations in dimensionless form.

Dimensionless forms of the Thrust.

$$\begin{aligned}\frac{T}{P_0 A_0} &= \gamma {M_0}^2 \left((1+f)\frac{U_e}{U_0} - 1 \right) + \frac{A_e}{A_0}\left(\frac{P_e}{P_0} - 1\right) \\ \frac{T}{\dot{m}_a a_0} &= \left(\frac{1}{\gamma M_0}\right)\frac{T}{P_0 A_0}\end{aligned} \tag{2.44}$$

Normalizing the thrust by $P_0 A_0$ produces a number that compares the thrust to a force equal to the ambient pressure multiplied by the capture area. In order to overcome drag it is essential that this be a number considerably larger than one.

Dimensionless Specific impulse.

$$\frac{I_{sp} g}{a_0} = \left(\frac{1}{f}\right)\frac{T}{\dot{m}_a a_0} \tag{2.45}$$

The quantity f is the fuel/air ratio defined as

$$f = \frac{\dot{m}_f}{\dot{m}_a}. \tag{2.46}$$

Overall efficiency.

$$\eta_{ov} = \left(\frac{\gamma - 1}{\gamma}\right)\left(\frac{1}{f\tau_f}\right)\left(\frac{T}{P_0 A_0}\right) \tag{2.47}$$

The ratio of fuel to ambient enthalpy appears in this definition.

$$\tau_f = \frac{h_f}{C_p T_0} \tag{2.48}$$

And T_0 is the temperature of the ambient air. Note that the fuel/air ratio is relatively small whereas τ_f is rather large (See (2.16)). Thus $1/(f\tau_f)$ is generally a fraction somewhat less than one.

2.10 Engine notation

An important part of analyzing the performance of a propulsion system has to do with being able to determine how each component of the engine contributes to the overall thrust

and specific impulse. To accomplish this, we will use a standard notation widely used in industry for characterizing the pressure and temperature change across each component. First we need to adopt a standard system for numbering the engine components. Consider the generic engine cross sections shown in Figure 2.5.

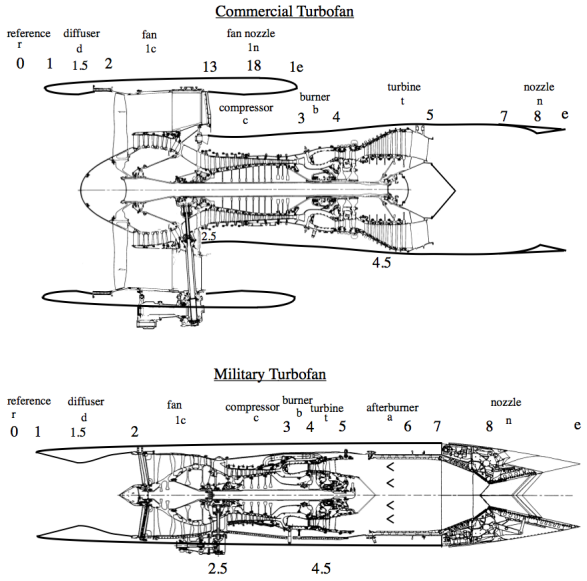

Figure 2.5: *Engine numbering and component notation*

The performance of each component is defined in terms of the stagnation pressure and temperature entering and leaving the component. A widely accepted notation is

$$\tau = \frac{\textit{The stagnation temperature leaving the component}}{\textit{The stagnation temperature entering the component}}$$
$$\pi = \frac{\textit{The stagnation pressure leaving the component}}{\textit{The stagnation pressure entering the component}}. \tag{2.49}$$

The various stations are defined as follows.

Station 0 - This is the reference state of the gas well upstream of the engine entrance. The

temperature/pressure parameters are

$$\begin{aligned} \tau_r &= \frac{\mathrm{T}_{t0}}{\mathrm{T}_0} = 1 + \left(\frac{\gamma - 1}{2}\right) {M_0}^2 \\ \pi_r &= \frac{P_{t0}}{P_0} = \left(1 + \left(\frac{\gamma - 1}{2}\right) {M_0}^2\right)^{\frac{\gamma}{\gamma - 1}}. \end{aligned} \tag{2.50}$$

Note that these definitions are exceptional in that the denominator is the static temperature and pressure of the free stream.

Station 1 - Entrance to the engine inlet. The purpose of the inlet is to reduce the Mach number of the incoming flow to a low subsonic value with as small a stagnation pressure loss as possible. From the entrance to the end of the inlet there is always an increase in area and so the component is appropriately called a diffuser.

Station 1.5 - The inlet throat.

Station 2 - The fan or compressor face. The temperature/pressure parameters across the diffuser are

$$\begin{aligned} \tau_d &= \frac{\mathrm{T}_{t2}}{\mathrm{T}_{t1}} \\ \pi_d &= \frac{P_{t2}}{P_{t1}}. \end{aligned} \tag{2.51}$$

In the absence of an upstream shock wave the flow from the reference state is regarded as adiabatic and isentropic so that

$$\begin{aligned} \mathrm{T}_{t1} &= \mathrm{T}_{t0} \\ P_{t1} &= P_{t0}. \end{aligned} \tag{2.52}$$

The inlet is usually modeled as an adiabatic flow so the stagnation temperature is approximately constant, however the stagnation pressure decreases due to the presence of viscous boundary layers and possibly shock waves.

Station 2.5 - All turbofan engines comprise at least two spools. The fan is usually accompanied by a low pressure compressor driven by a low pressure turbine through a shaft along the centerline of the engine. A concentric shaft connects the high pressure turbine and high pressure compressor. Station 2.5 is generally taken at the interface between the

low and high pressure compressor. Roll Royce turbofans commonly employ three spools with the high pressure compressor broken into two spools.

Station 13 - This is a station in the bypass stream corresponding to the fan exit ahead of the entrance to the fan exhaust nozzle. The temperature/pressure parameters across the fan are

$$\begin{aligned} \tau_{1c} &= \frac{\mathrm{T}_{t13}}{\mathrm{T}_{t2}} \\ \pi_{1c} &= \frac{P_{t13}}{P_{t2}}. \end{aligned} \tag{2.53}$$

Station 18 - The fan nozzle throat.

Station 1e - The fan nozzle exit. The temperature/pressure parameters across the fan nozzle are

$$\begin{aligned} \tau_{1n} &= \frac{\mathrm{T}_{t1e}}{\mathrm{T}_{t13}} \\ \pi_{1n} &= \frac{P_{t1e}}{P_{t13}}. \end{aligned} \tag{2.54}$$

Station 3 - The exit of the high pressure compressor. The temperature/pressure parameters across the compressor are

$$\begin{aligned} \tau_{c} &= \frac{\mathrm{T}_{t3}}{\mathrm{T}_{t2}} \\ \pi_{c} &= \frac{P_{t3}}{P_{t2}}. \end{aligned} \tag{2.55}$$

Note that the compression includes that due to the fan. From a cycle perspective it is usually not necessary to distinguish the high and low pressure sections of the compressor. The goal of the designer is to produce a compression system that is as near to isentropic as possible.

Station 4 - The exit of the burner. The temperature/pressure parameters across the burner

are

$$\begin{aligned} \tau_b &= \frac{\mathrm{T}_{t4}}{\mathrm{T}_{t3}} \\ \pi_b &= \frac{P_{t4}}{P_{t3}}. \end{aligned} \tag{2.56}$$

The temperature at the exit of the burner is regarded as the highest temperature in the Brayton cycle although generally higher temperatures do occur at the upstream end of the burner where combustion takes place. The burner is designed to allow an influx of cooler compressor air to mix with the combustion gases bringing the temperature down to a level that the high pressure turbine structure can tolerate. Modern engines use sophisticated cooling methods to enable operation at values of T_{t4} that approach $3700R(2050\mathrm{K})$, well above the melting temperature of the turbine materials.

Station 4.5 - This station is at the interface of the high and low pressure turbines.

Station 5 - The exit of the turbine. The temperature/pressure parameters across the turbine are

$$\begin{aligned} \tau_t &= \frac{\mathrm{T}_{t5}}{\mathrm{T}_{t4}} \\ \pi_t &= \frac{P_{t5}}{P_{t4}}. \end{aligned} \tag{2.57}$$

As with the compressor the goal of the designer is to produce a turbine system that operates as isentropically as possible.

Station 6 - The exit of the afterburner if there is one. The temperature/pressure parameters across the afterburner are

$$\begin{aligned} \tau_a &= \frac{\mathrm{T}_{t6}}{\mathrm{T}_{t5}} \\ \pi_a &= \frac{P_{t6}}{P_{t5}}. \end{aligned} \tag{2.58}$$

The Mach number entering the afterburner is fairly low and so the stagnation pressure ratio of the afterburner is fairly close to, and always less than, one.

Station 7 - The entrance to the nozzle.

Station 8 - The nozzle throat. Over the vast range of operating conditions of modern engines the nozzle throat is choked or very nearly so.

Station e - The nozzle exit. The temperature/pressure component parameters across the nozzle are

$$\begin{aligned} \tau_n &= \frac{\mathrm{T}_{te}}{\mathrm{T}_{t7}} \\ \pi_n &= \frac{P_{te}}{P_{t7}}. \end{aligned} \tag{2.59}$$

In the absence of the afterburner, the nozzle parameters are generally referenced to the turbine exit condition so that

$$\begin{aligned} \tau_n &= \frac{\mathrm{T}_{te}}{\mathrm{T}_{t5}} \\ \pi_n &= \frac{P_{te}}{P_{t5}}. \end{aligned} \tag{2.60}$$

In general the goal of the designer is to minimize heat loss and stagnation pressure loss through the inlet, burner and nozzle.

There are two more very important parameters that need to be defined. The first is one we encountered before when we compared the fuel enthalpy to the ambient air enthalpy.

$$\tau_f = \frac{h_f}{C_p \mathrm{T}_0} \tag{2.61}$$

The second parameter is, in a sense, the most important quantity needed to characterize the performance of an engine.

$$\tau_\lambda = \frac{T_{t4}}{\mathrm{T}_0} \tag{2.62}$$

In general every performance measure of the engine gets better as τ_λ is increased and a tremendous investment has been made over the years to devise turbine cooling and ceramic coating schemes that permit ever higher turbine inlet temperatures, T_{t4}.

2.11 Problems

Problem 1 - Suppose 10% of the heat generated in a ramjet combustor is lost through conduction to the surroundings. How would this change the energy balance (2.19)? How would it affect the thrust?

Problem 2 - Write down the appropriate form of the thrust definition (2.12) for a turbofan engine with two independent streams. Suppose 5% of the air from the high pressure compressor is to be used to power aircraft systems. What would be the appropriate thrust formula?

Problem 3 - Consider the flow through a turbojet. The energy balance across the burner is

$$(\dot{m}_a + \dot{m}_f)\, h_{t4} = \dot{m}_a h_{t3} + \dot{m}_f h_f. \tag{2.63}$$

The enthalpy rise across the compressor is equal to the enthalpy decrease across the turbine. Show that the energy balance (2.63) can also be written

$$(\dot{m}_a + \dot{m}_f)\, h_{t5} = \dot{m}_a h_{t2} + \dot{m}_f h_f. \tag{2.64}$$

The inlet and nozzle are usually assumed to operate adiabatically. Show that (2.64) can be expressed as

$$(\dot{m}_a + \dot{m}_f)\, h_{te} = \dot{m}_a h_{t0} + \dot{m}_f h_f \tag{2.65}$$

which is the same as the overall enthalpy balance for a ramjet (2.19).

Problem 4 - Work out the dimensionless forms in Section 2.9.

Chapter 3

The ramjet cycle

3.1 Ramjet flow field

Before we begin to analyze the ramjet cycle we will consider an example that can help us understand how the flow through a ramjet comes about. The key to understanding the flow field is the intelligent use of the relationship for mass flow conservation. In this connection there are two equations that we will rely upon. The first is the expression for 1-D mass flow in terms of the stagnation pressure and temperature.

$$\dot{m} = \rho U A = \frac{\gamma}{\left(\frac{\gamma+1}{2}\right)^{\frac{\gamma+1}{2(\gamma-1)}}} \left(\frac{P_t A}{\sqrt{\gamma R T_t}}\right) f(M) \tag{3.1}$$

The second is the all-important area-Mach number function.

$$f(M) = \frac{A^*}{A} = \left(\frac{\gamma+1}{2}\right)^{\frac{\gamma+1}{2(\gamma-1)}} \frac{M}{\left(1+\frac{\gamma-1}{2}M^2\right)^{\frac{\gamma+1}{2(\gamma-1)}}} \tag{3.2}$$

This function is plotted in Figure 3.1 for three values of γ.

For adiabatic, isentropic flow of a calorically perfect gas along a channel Equation (3.1) provides a direct connection between the local channel cross sectional area and Mach number.

In addition to the mass flow relations there are two relationships from Rayleigh line theory that are also very helpful in guiding our understanding of the effect of heat addition on

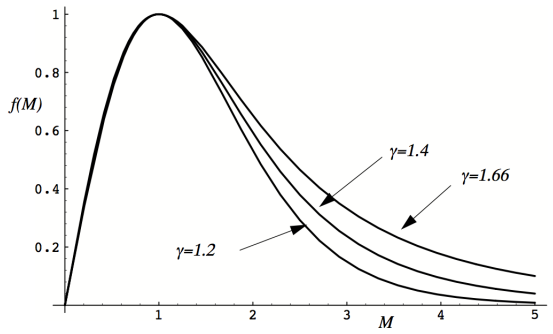

Figure 3.1: *Area - Mach number relation.*

the flow in the ramjet. These are the equations that describe the effect of heat addition on the Mach number and stagnation pressure of the flow.

$$\begin{aligned} \frac{T_t^*}{T_t} &= \frac{\left(1+\gamma M^2\right)^2}{2\left(1+\gamma\right)M^2\left(1+\frac{\gamma-1}{2}M^2\right)} \\ \frac{P_t^*}{P_t} &= \left(\frac{1+\gamma M^2}{1+\gamma}\right)\left(\frac{\frac{\gamma+1}{2}}{1+\frac{\gamma-1}{2}M^2}\right)^{\frac{\gamma}{\gamma-1}} \end{aligned} \tag{3.3}$$

These equations are plotted in Figure 3.2.

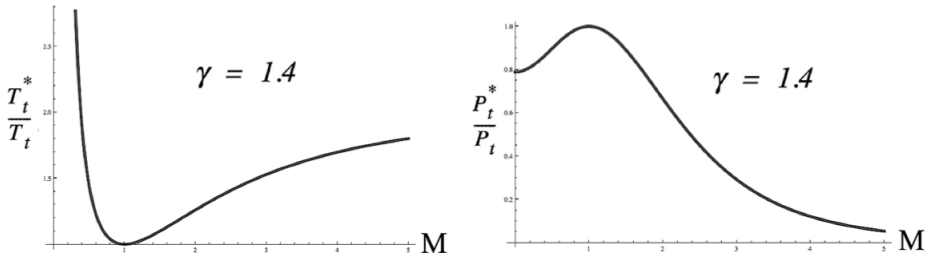

Figure 3.2: *Effects of heat exchange on Mach number and stagnation pressure.*

There are several features shown in these plots that have important implications for the ramjet flow. The first is that much more heat can be added to a subsonic flow than to a supersonic flow before thermal choking occurs; that is, before the flow is brought to Mach one. The second is that stagnation pressure losses due to heat addition in subsonic flow are relatively small and cannot exceed about 20% of the stagnation pressure of the flow

entering the region of heat addition. In contrast stagnation pressure losses due to heat addition can be quite large in a supersonic flow.

With this background we will now construct a ramjet flow field beginning with supersonic flow through a straight, infinitely thin tube. For definiteness let the free stream Mach number be three and the ambient temperature $T_0 = 216\,K$. Throughout this example we will assume that the friction along the channel wall is negligible.

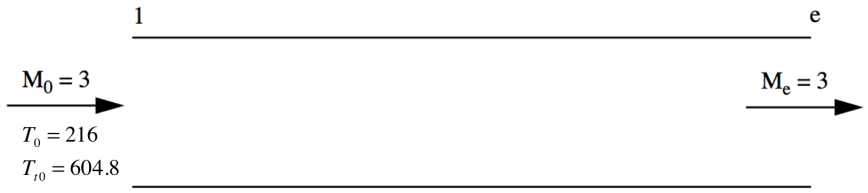

Figure 3.3: *Step 1 - Initially uniform Mach three flow.*

Add an inlet convergence and divergence.

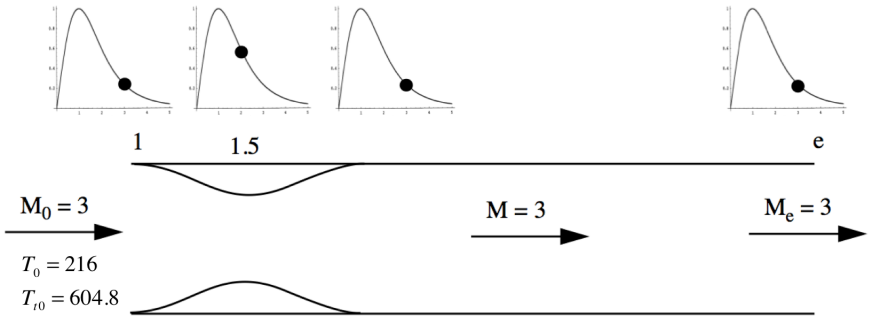

Figure 3.4: *Step 2 - Inlet convergence and divergence with $f(M)$ shown.*

Let the throat Mach number be two ($M_{1.5} = 2.0$). In Figure 3.4 the Mach number decreases to the inlet throat ($f(M)$ increases), then increases again to the inlet value of three, ($f(M) = 0.236$). The thrust of this system is clearly zero since the x-directed component of the pressure force on the inlet is exactly balanced on the upstream and downstream sides of the inlet.

In Figure 3.5 heat is added to the supersonic flow inside the engine. Neglect the mass flow of fuel added compared to the air mass flow. As the heat is added the mass flow is conserved. Thus, neglecting the fuel added, the mass balance is

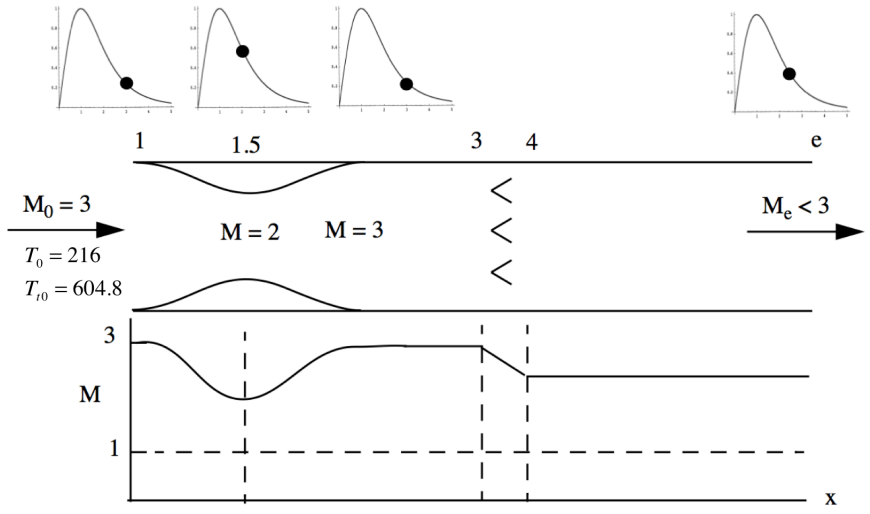

Figure 3.5: *Step 2 - Introduce a burner and add heat to the flow.*

$$\dot{m} = \frac{\gamma}{\left(\frac{\gamma+1}{2}\right)^{\frac{\gamma+1}{2(\gamma-1)}}} \frac{P_{t0}A_3}{\sqrt{\gamma RT_{t0}}} f(3) = \frac{\gamma}{\left(\frac{\gamma+1}{2}\right)^{\frac{\gamma+1}{2(\gamma-1)}}} \frac{P_{t4}A_4}{\sqrt{\gamma RT_{t4}}} f(M_4). \tag{3.4}$$

As the heat is added, T_{t4} goes up and P_{t4} goes down while the following equality must be maintained

$$\frac{P_{t0}}{\sqrt{T_{t0}}} f(3) = \frac{P_{t4}}{\sqrt{T_{t4}}} f(M_4). \tag{3.5}$$

Conservation of mass (3.5) implies that $f(M_4)$ must increase and the Mach number downstream of the burner decreases. There is a limit to the amount of heat that can be added to this flow and the limit occurs when $f(M_4)$ attains its maximum value of one. At this point the flow looks like Figure 3.6.

The Rayleigh line relations tell us that the temperature rise across the burner that produces this flow is

$$\left.\frac{T_{t4}}{T_{t3}}\right|_{M_4=1} = 1.53. \tag{3.6}$$

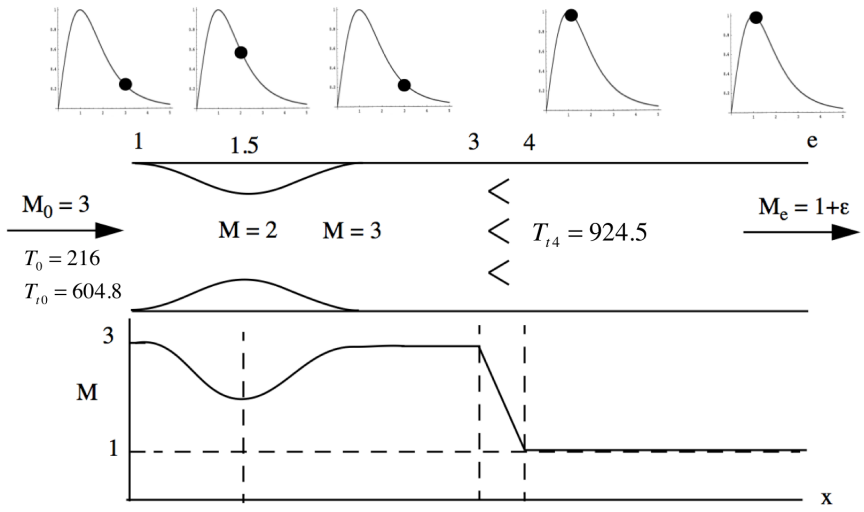

Figure 3.6: *Step 3 - Introduce sufficient heat to bring the exit Mach number to a value slightly greater than one.*

The corresponding stagnation pressure ratio across the system is

$$\left(\frac{P_{t4}}{P_{t3}}\bigg|_{M_4=1} \right)_{before\ unstart} = 0.292. \tag{3.7}$$

Now, suppose the temperature at station 4 is increased very slightly. We have a problem; T_{t4} is up slightly, P_{t4} is down slightly but $f(M_4)$ cannot increase. To preserve the mass flow rate imposed at the inlet, the supersonic flow in the interior of the engine must undergo an un-start. The flow must switch to the configuration shown in Figure 3.7. The mass flow equation (3.5) can only be satisfied by a flow between the inlet throat and the burner that achieves the same stagnation pressure loss (3.7), since $f(M_4)$ cannot exceed one and the stagnation temperature ratio is essentially the same.

As a result of the un-start, a shock wave now sits at the end of the diffuser section of the inlet. Notice that the engine internal pressure is still very large and the exit Mach number must remain one. The stagnation temperature has not changed and so, as was just pointed out, the mass balance tells us that the stagnation pressure of the exit flow must be the same as before the un-start. Thus

$$\left(\frac{P_{t4}}{P_{t0}}\bigg|_{M_4=1} \right)_{after\ unstart} = 0.292. \tag{3.8}$$

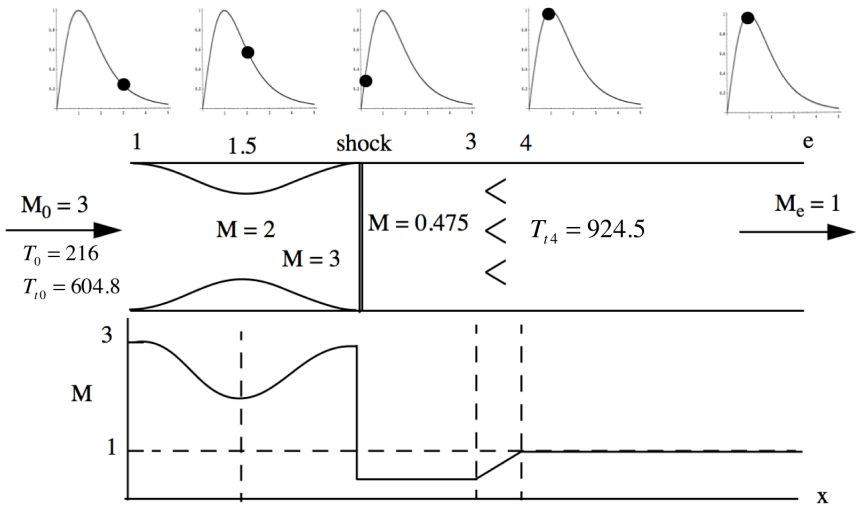

Figure 3.7: *Step 4 - Increase the heat added very slightly to unstart the flow.*

Now, the stagnation pressure loss is divided between two mechanisms, the loss across the shock wave, and the loss due to heat addition across the burner. The stagnation pressure ratio across a Mach three shock wave is

$$\left.\frac{P_{t3}}{P_{t0}}\right|_{M=3} = 0.3285. \tag{3.9}$$

The burner inlet Mach number is $M_3 = 0.475$, and the stagnation loss due to thermal choking across the burner is

$$\left.\frac{P_{t4}}{P_{t3}}\right|_{M=0.475} = 0.889. \tag{3.10}$$

The product of (3.9), and (3.10) is 0.292.

Now let's look at the thrust generated by the flow depicted in Figure 3.7. The thrust definition, neglecting the fuel/air ratio, is

$$\frac{T}{P_0 A_0} = \gamma {M_0}^2 \left(\frac{U_e}{U_0} - 1\right) + \frac{A_e}{A_0}\left(\frac{P_e}{P_0} - 1\right). \tag{3.11}$$

The pressure ratio across the engine is

$$\frac{P_e}{P_0} = \frac{P_{te}}{P_{t0}} \left(\frac{1 + \frac{\gamma-1}{2} {M_0}^2}{1 + \frac{\gamma-1}{2} {M_e}^2} \right)^{\frac{\gamma}{\gamma-1}} = 0.292 \left(\frac{2.8}{1.2} \right)^{3.5} = 5.66 \tag{3.12}$$

and the temperature ratio is

$$\frac{T_e}{T_0} = \frac{T_{te}}{T_{t0}} \left(\frac{1 + \frac{\gamma-1}{2} {M_0}^2}{1 + \frac{\gamma-1}{2} {M_e}^2} \right) = 1.53 \left(\frac{2.8}{1.2} \right) = 3.5667. \tag{3.13}$$

This produces the velocity ratio

$$\frac{U_e}{U_0} = \frac{M_e}{M_0} \sqrt{\frac{T_e}{T_0}} = 0.6295. \tag{3.14}$$

Now substitute into (3.11).

$$\frac{T}{P_0 A_0} = 1.4 \times 9 \times (0.6295 - 1) + 1 \times (5.66 - 1) = -4.66 + 4.66 = 0 \tag{3.15}$$

The thrust is zero. We would expect this from the symmetry of the upstream and downstream distribution of pressure on the inlet. Now let's see if we can produce some thrust. First adjust the inlet so that the throat area is reduced until the throat Mach number is just slightly larger than one. This will only effect the flow in the inlet and all flow variables in the rest of the engine will remain the same.

With the flow in the engine subsonic, and the shock positioned at the end of the diffuser, we have a great deal of margin for further heat addition. If we increase the heat addition across the burner the mass balance (3.5) is still preserved and the exit Mach number remains one. Let the burner outlet temperature be increased to $T_{t4} = 1814.4K$. The flow now looks something like Figure 3.8.

The stagnation temperature at the exit is up, the stagnation pressure is up, and the shock has moved to the left to a lower upstream Mach number (higher $f(M)$), while the mass flow (3.5) is preserved. Note that we now have some thrust arising from the x-component of the high pressure force behind the shock that acts to the left on an outer portion of the inlet surface. This pressure exceeds the inlet pressure on the corresponding upstream

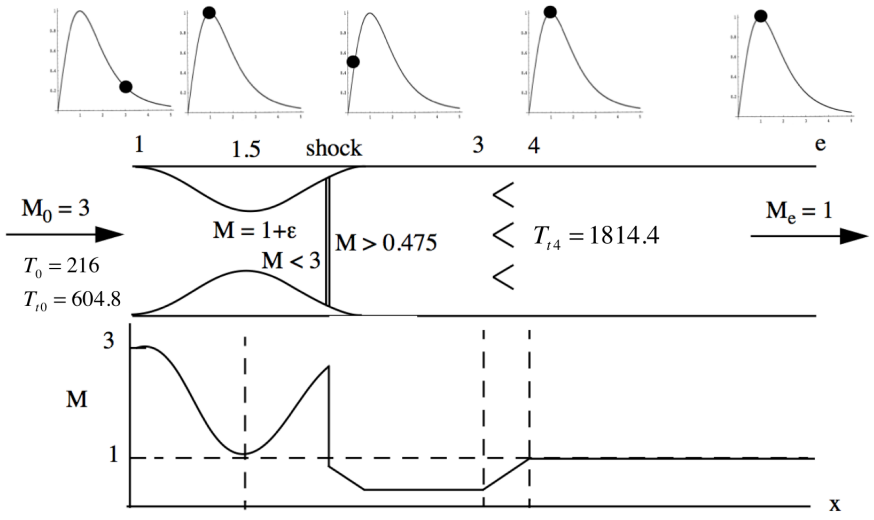

Figure 3.8: *Step 5 - Increase the heat addition to produce some thrust.*

portion of the inlet surface. The stagnation pressure ratio across the engine is determined from the mass balance (3.5).

$$\frac{P_{te}}{P_{t0}} = f\,(3)\sqrt{\frac{T_{te}}{T_{t0}}} = 0.263\sqrt{3} = 0.409 \tag{3.16}$$

Let's check the thrust. The pressure ratio across the engine is

$$\frac{P_e}{P_0} = 0.409\left(\frac{2.8}{1.2}\right)^{3.5} = 7.94. \tag{3.17}$$

The temperature ratio is

$$\frac{T_e}{T_0} = \frac{T_{te}}{T_{t0}}\left(\frac{1+\frac{\gamma-1}{2}M_0{}^2}{1+\frac{\gamma-1}{2}M_e{}^2}\right) = 3\left(\frac{2.8}{1.2}\right) = 7 \tag{3.18}$$

and the velocity ratio is now

$$\frac{U_e}{U_0} = \frac{M_e}{M_0}\sqrt{\frac{T_e}{T_0}} = \frac{\sqrt{7}}{3} = 0.882. \tag{3.19}$$

The thrust is

$$\frac{T}{P_0 A_0} = 1.4 \times 9 \times (0.882 - 1) + 1 \times (7.94 - 1) = -1.49 + 6.94 = 5.45. \tag{3.20}$$

This is a pretty substantial amount of thrust. Note that, so far, the pressure term in the thrust definition is the important thrust component in this design.

3.2 The role of the nozzle

Let's see if we can improve the design. Add a convergent nozzle to the engine as shown in Figure 3.9. The mass balance is

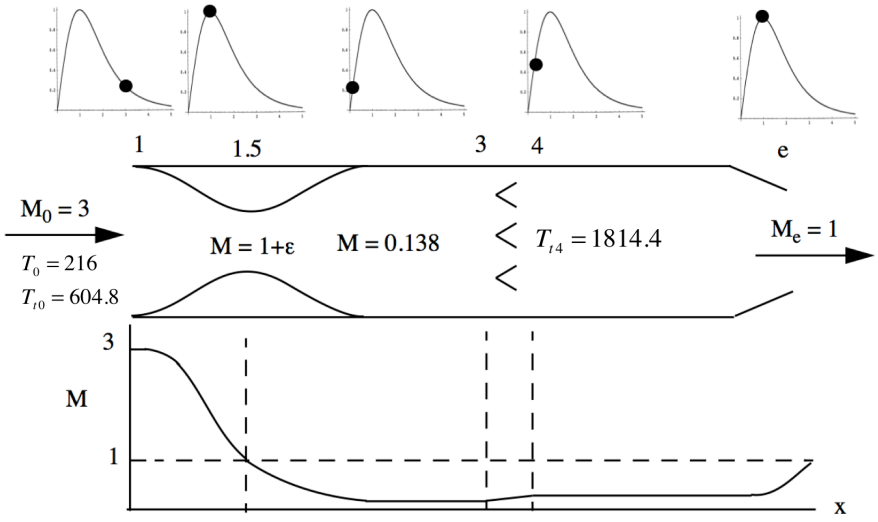

Figure 3.9: *Step 6 - Add a convergent nozzle.*

$$\frac{P_{t0} A_{1.5}}{\sqrt{604.8}} = \frac{P_{te} A_e}{\sqrt{1814.4}}. \tag{3.21}$$

How much can we decrease A_e? Begin with Figure 3.8. As the exit area is decreased the exit Mach number remains one due to the high internal pressure in the engine. The shock moves upstream toward the inlet throat, the exit stagnation pressure increases and the product $P_{te} A_e$ remains constant. The minimum exit area that can be reached without un-starting the inlet flow is when the inlet shock is very close to the throat, becoming vanishingly weak. At this condition, the only mechanism for stagnation pressure loss is the

heat addition across the burner. The Mach number entering the burner is $M_3 = 0.138$ as shown in Figure 3.9. The stagnation pressure loss across the burner is proportional to the square of the entering Mach number.

$$\frac{dP_t}{P_t} = -\gamma M^2 \frac{dT_t}{T_t} \tag{3.22}$$

To a reasonable approximation the stagnation loss across the burner can be neglected and we can take $P_{te} \cong P_{t0}$. In this approximation, the area ratio that leads to the flow depicted in Figure 3.9 is

$$\left.\frac{A_e}{A_{1.5}}\right|_{ideal} = \sqrt{\frac{1814.4}{604.8}} = 1.732. \tag{3.23}$$

This relatively large area ratio is expected considering the greatly increased temperature and lower density of the exhaust gases compared to the gas that passes through the upstream throat. What about the thrust? Now the static pressure ratio across the engine is

$$\frac{P_e}{P_0} = \left(\frac{2.8}{1.2}\right)^{3.5} = 19.41. \tag{3.24}$$

The temperatures and Mach numbers at the nozzle exit are the same as before so the velocity ratio does not change between Figure 3.8 and Figure 3.9. The dimensionless thrust is

$$\frac{T}{P_0 A_0} = 1.4 \times 9 \times (0.882 - 1) + 1.732 \times 0.236 \times (19.41 - 1) = -1.49 + 7.53 = 6.034. \tag{3.25}$$

That's pretty good; just by adding a convergent nozzle and reducing the shock strength we have increased the thrust by about 20%. Where does the thrust come from in this ramjet design? The figure below schematically shows the pressure distribution through the engine. The pressure forces on the inlet and nozzle surfaces marked "a" roughly balance, although the forward pressure is slightly larger compared to the rearward pressure on the nozzle due to the heat addition. But the pressure on the inlet surfaces marked "b" are not balanced by any force on the nozzle. These pressures substantially exceed the pressure on the upstream face of the inlet and so net thrust is produced.

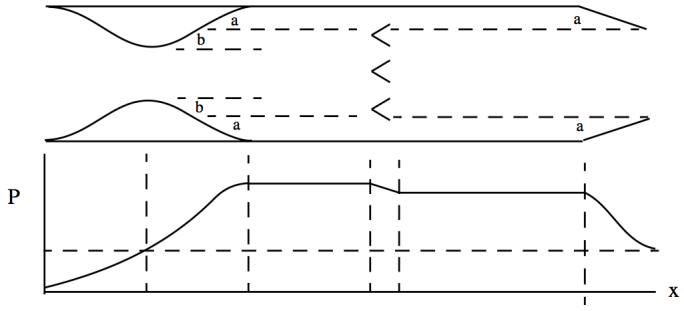

Figure 3.10: *Imbalance of pressure forces leading to net thrust.*

3.3 The ideal ramjet cycle

But we can do better still! The gas that exits the engine is at a very high pressure compared to the ambient and it should be possible to gain thrust from this by adding a divergent section to the nozzle as shown below.

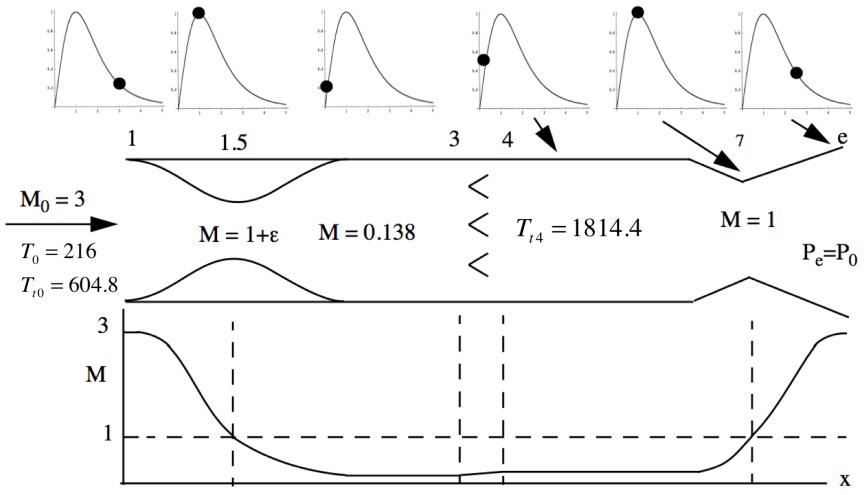

Figure 3.11: *Ideal ramjet with a fully expanded nozzle.*

The area ratio of the nozzle is chosen so that the flow is fully expanded, $P_e = P_0$. The

stagnation pressure is constant through the engine and so we can conclude from

$$\begin{aligned} \frac{P_e}{P_0} &= \frac{P_{te}}{P_{t0}} \left(\frac{1 + \frac{\gamma-1}{2} {M_0}^2}{1 + \frac{\gamma-1}{2} {M_e}^2} \right)^{\frac{\gamma}{\gamma-1}} \\ 1 &= 1 \times \left(\frac{1 + \frac{\gamma-1}{2} {M_0}^2}{1 + \frac{\gamma-1}{2} {M_e}^2} \right)^{\frac{\gamma}{\gamma-1}} \end{aligned} \tag{3.26}$$

that $M_e = M_0$. The temperature ratio is

$$\frac{T_e}{T_0} = \frac{T_{te}}{T_{t0}} \left(\frac{1 + \frac{\gamma-1}{2} {M_0}^2}{1 + \frac{\gamma-1}{2} {M_e}^2} \right) = \frac{T_{te}}{T_{t0}} = 3. \tag{3.27}$$

Finally, the dimensionless thrust is

$$\frac{T}{P_0 A_0} = \gamma {M_0}^2 \left(\frac{M_e}{M_0} \sqrt{\frac{T_e}{T_0}} - 1 \right) = 1.4 \times 9 \times \left(\sqrt{3} - 1 \right) = 9.22. \tag{3.28}$$

Adding a divergent section to the nozzle at this relatively high Mach number increases the thrust by 50%.

Now work out the other engine parameters. The fuel/air ratio is determined from

$$\dot{m}_f h_f = \left(\dot{m}_a + \dot{m}_f \right) h_{t4} - \dot{m}_a h_{t3}. \tag{3.29}$$

Assume the fuel added is JP-4 with $h_f = 4.28 \times 10^7 J/kg$. Equation (3.29) becomes

$$f = \frac{\frac{T_{t4}}{T_{t3}} - 1}{\frac{h_f}{C_p T_{t3}} - \frac{T_{t4}}{T_{t3}}} = \frac{\frac{1814.4}{604.8} - 1}{70.41 - \frac{1814.4}{604.8}} = 0.0297. \tag{3.30}$$

The relatively small value of fuel/air ratio is the *a posteriori* justification of our earlier neglect of the fuel mass flow compared to the air mass flow. If we include the fuel/air ratio in the thrust calculation (but still ignore the effect of mass addition on the stagnation pressure change across the burner) the result is

$$\frac{T}{P_0 A_0} = \gamma {M_0}^2 \left((1 + f) \frac{M_e}{M_0} \sqrt{\frac{T_e}{T_0}} - 1 \right) = 1.4 \times 9 \times \left(1.0297 \times \sqrt{3} - 1 \right) = 9.872. \tag{3.31}$$

The error in the thrust is about 7% when the fuel contribution is neglected. The dimensionless specific impulse is

$$\frac{I_{sp}g}{a_0} = \left(\frac{1}{f}\right)\left(\frac{1}{\gamma M_0}\right)\frac{T}{P_0 A_0} = \frac{9.872}{0.0297 \times 1.4 \times 3} = 79.14 \tag{3.32}$$

and the overall efficiency is, ($\tau_f = h_f/C_p T_0 = 197.2$),

$$\eta_{ov} = \left(\frac{\gamma - 1}{\gamma}\right)\left(\frac{1}{f\tau_f}\right)\frac{T}{P_0 A_0} = \left(\frac{0.4}{1.4}\right)\left(\frac{9.872}{0.0297 \times 197.2}\right) = 0.482. \tag{3.33}$$

The propulsive efficiency is

$$\eta_{pr} = \frac{2U_0}{U_e + U_0} = \frac{2}{1 + \sqrt{3}} = 0.732. \tag{3.34}$$

The thermal efficiency of the engine shown in Figure 3.11 can be expressed as follows

$$\begin{aligned}
\eta_{th} &= \frac{(\dot{m}_a + \dot{m}_f)\frac{{U_e}^2}{2} - \dot{m}_a\frac{{U_0}^2}{2}}{\dot{m}_f h_f} = \frac{(\dot{m}_a + \dot{m}_f)(h_{te} - h_e) - \dot{m}_a(h_{t0} - h_0)}{(\dot{m}_a + \dot{m}_f)h_{te} - \dot{m}_a h_{t0}} \\
\eta_{th} &= 1 - \frac{Q_{rejected\,during\,the\,cycle}}{Q_{input\,during\,the\,cycle}} = 1 - \frac{(\dot{m}_a + \dot{m}_f)h_e - \dot{m}_a h_0}{(\dot{m}_a + \dot{m}_f)h_{te} - \dot{m}_a h_{t0}} \\
\eta_{th} &= 1 - \frac{T_0}{T_{t0}}\left(\frac{(1+f)\frac{T_e}{T_0} - 1}{(1+f)\frac{T_{te}}{T_{t0}} - 1}\right).
\end{aligned} \tag{3.35}$$

The heat rejection is accomplished by mixing of the hot exhaust stream with surrounding air at constant pressure. Noting (3.27) for the ideal ramjet, the last term in brackets is one and the thermal efficiency becomes

$$\eta_{th\,ideal\,ramjet} = 1 - \frac{T_0}{T_{t0}}. \tag{3.36}$$

For the ramjet conditions of this example the thermal efficiency is 2/3 . The Brayton cycle efficiency is

$$\eta_B = 1 - \frac{T_0}{T_3}. \tag{3.37}$$

In the ideal cycle approximation, the Mach number at station 3 is very small thus $T_3 \cong T_{t0}$ and the thermal and Brayton efficiencies are identical. Note that, characteristically for a Brayton process, the thermal efficiency is determined entirely by the inlet compression process. The ramjet design shown in Figure 3.11 represents the best we can do at this Mach number. In fact the final design is what we would call the ideal ramjet. The ideal cycle will be the basis for comparison with other engine cycles but it is not a practically useful design. The problem is that the inlet is extremely sensitive to small disturbances in the engine. A slight increase in burner exit temperature or decrease in nozzle exit area or a slight decrease in the flight Mach number will cause the inlet to un-start. This would produce a strong normal shock in front of the engine, a large decrease in air mass flow through the engine and a consequent decrease in thrust. *A practical ramjet design for supersonic flight requires the presence of a finite amplitude inlet shock for stable operation.*

3.4 Optimization of the ideal ramjet cycle

For a fully expanded nozzle the thrust equation reduces to

$$\frac{T}{P_0 A_0} = \gamma {M_0}^2 \left((1+f) \frac{M_e}{M_0} \sqrt{\frac{T_e}{T_0}} - 1 \right). \tag{3.38}$$

For the ideal cycle, where $P_{te} = P_{t0}$, $M_e = M_0$ and $T_{te}/T_{t0} = T_e/T_0$, the thrust equation using $(1+f) = (\tau_f - \tau_r)\,/\,(\tau_f - \tau_\lambda)$ becomes

$$\frac{T}{P_0 A_0} = \frac{2\gamma}{\gamma - 1} (\tau_r - 1) \left(\frac{\tau_f - \tau_r}{\tau_f - \tau_\lambda} \sqrt{\frac{\tau_\lambda}{\tau_r}} - 1 \right). \tag{3.39}$$

This form of the thrust equation is useful because it expresses the thrust in terms of cycle parameters that we can rationalize. The parameter τ_r is fixed by the flight Mach number. At a given altitude τ_λ is determined by maximum temperature constraints on the hot section materials of the engine, as well as fuel chemistry, and gas dissociation. If the flight Mach number goes to zero the thrust also goes to zero. As the flight Mach number increases for fixed τ_λ the fuel flow must decrease until $\tau_\lambda = \tau_r$ when fuel shut-off occurs and the thrust is again zero. A typical thrust plot is shown below.

The optimization question is; at what Mach number should the ramjet operate for maximum thrust at a fixed τ_λ? Differentiate (3.39) with respect to τ_r and set the result to

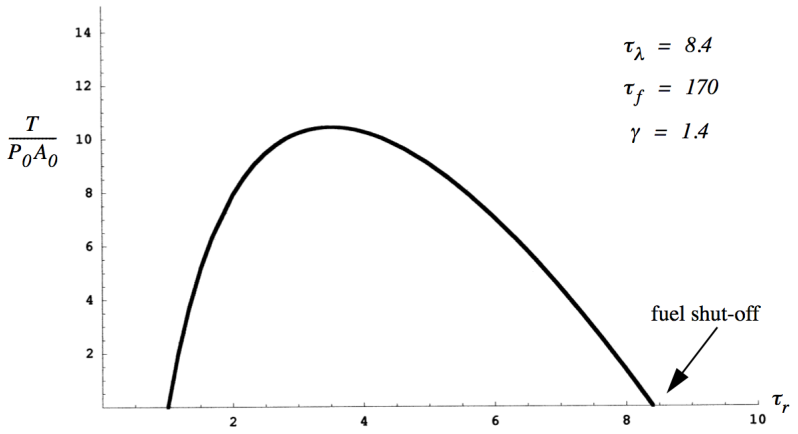

Figure 3.12: *Ramjet thrust*

zero.

$$\frac{\partial}{\partial \tau_r}\left(\frac{T}{P_0 A_0}\right) = \frac{2\gamma}{\gamma - 1}\left(\frac{\tau_\lambda \tau_r\left(1 - 3\tau_r + 2\tau_r\sqrt{\frac{\tau_\lambda}{\tau_r}}\right) + \tau_f\left(\tau_\lambda + \tau_\lambda\tau_r - 2{\tau_r}^2\sqrt{\frac{\tau_\lambda}{\tau_r}}\right)}{\left(\tau_f - \tau_\lambda\right){\tau_r}^2\sqrt{\frac{\tau_\lambda}{\tau_r}}}\right) = 0 \tag{3.40}$$

The value of τ_r for maximum thrust is determined from

$$\tau_\lambda\tau_r\left(1 - 3\tau_r + 2\tau_r\sqrt{\frac{\tau_\lambda}{\tau_r}}\right) + \tau_f\left(\tau_\lambda + \tau_\lambda\tau_r - 2{\tau_r}^2\sqrt{\frac{\tau_\lambda}{\tau_r}}\right) = 0. \tag{3.41}$$

The quantity τ_f is quite large and so the second term in parentheses in (3.41) clearly dominates the first term. For $f \ll 1$ the maximum thrust Mach number of a ramjet is found from

$${\tau_\lambda}^{1/2} = \frac{2(\tau_{r_{\max thrust}})^{3/2}}{\tau_{r_{\max thrust}} + 1}. \tag{3.42}$$

For the case shown above, with $\tau_\lambda = 8.4$, the optimum value of τ_r is 3.5 corresponding to a Mach number of 3.53. The ramjet is clearly best suited for high Mach number flight and

the optimum Mach number increases as the maximum engine temperature increases.

$$\frac{I_{sp}g}{a_0} = \frac{\left(\frac{2}{\gamma-1}\left(\tau_r - 1\right)\right)^{1/2}}{\frac{\tau_\lambda - \tau_r}{\tau_f - \tau_\lambda}} \left(\frac{\tau_f - \tau_r}{\tau_f - \tau_\lambda}\sqrt{\frac{\tau_\lambda}{\tau_r}} - 1\right) \tag{3.43}$$

The specific impulse also has an optimum but it is much more gentle than the thrust optimum, as shown in Figure 3.13.

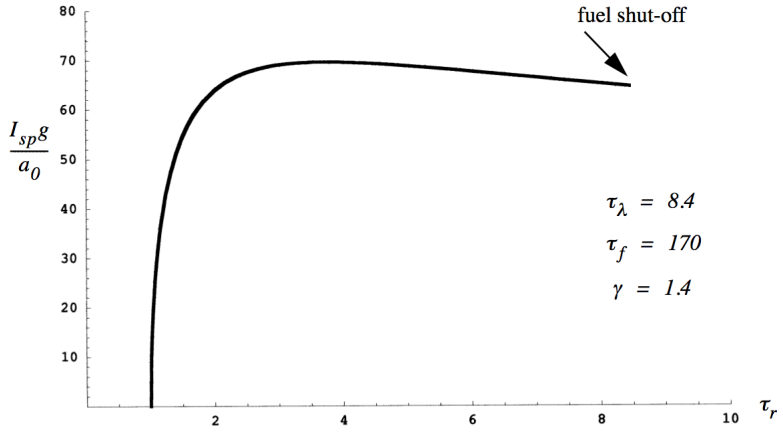

Figure 3.13: *Ramjet specific impulse.*

Optimizing the cycle with respect to thrust essentially gives close to optimal specific impulse. Notice that the specific impulse of the ideal cycle has a finite limit as the fuel flow reaches shut-off.

3.5 The non-ideal ramjet

The major non-ideal effects come from the stagnation pressure losses due to the inlet shock and the burner heat addition. We have already studied those effects fairly thoroughly. In addition there are stagnation pressure losses due to burner drag and skin friction losses in the inlet and nozzle where the Mach numbers tend to be quite high. A reasonable rule of thumb is that the stagnation pressure losses due to burner drag are comparable to the losses due to heat addition.

3.6 Ramjet control

Let's examine what happens when we apply some control to the ramjet. The two main control mechanisms at our disposal are the fuel flow and the nozzle exit area. The engine we will use for illustration is a stable ramjet with an inlet shock and simple convergent nozzle shown below. The inlet throat is designed to have a Mach number well above one so that it is not so sensitive to un-start if the free stream conditions, burner temperature or nozzle area change. Changes are assumed to take place slowly so that unsteady changes in the mass, momentum, and energy contained in the ramjet are negligible.

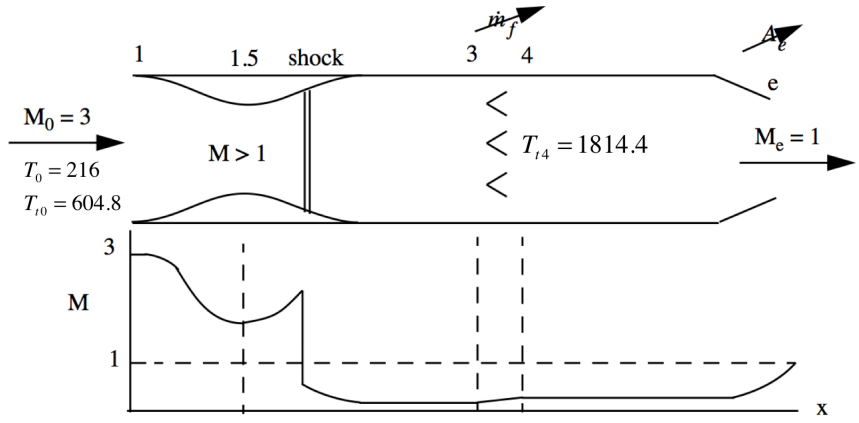

Figure 3.14: *Ramjet control model.*

The mass balance is

$$\dot{m}_e = \frac{\gamma}{\left(\frac{\gamma+1}{2}\right)^{\frac{\gamma+1}{2(\gamma-1)}}} \frac{P_{te} A_e}{\sqrt{\gamma R T_{te}}} f\left(M_e\right) = (1+f)\,\dot{m}_a. \tag{3.44}$$

The pressure in the engine is virtually certain to be very high at this free stream Mach number, and so the nozzle is surely choked, and we can write

$$\dot{m}_a = \frac{1}{(1+f)} \frac{\gamma}{\left(\frac{\gamma+1}{2}\right)^{\frac{\gamma+1}{2(\gamma-1)}}} \frac{P_{te} A_e}{\sqrt{\gamma R T_{te}}}. \tag{3.45}$$

The thrust equation is

$$\frac{T}{P_0 A_0} = \gamma {M_0}^2 \left((1+f)\frac{U_e}{U_0} - 1 \right) + \frac{A_e}{A_0}\left(\frac{P_e}{P_0} - 1 \right). \tag{3.46}$$

Our main concern is to figure out what happens to the velocity ratio and pressure ratio as we control the fuel flow and nozzle exit area.

Nozzle exit area control

First, suppose A_e is increased with T_{te} constant. In order for (3.45) to be satisfied P_{te} must drop keeping $P_{te}A_e$ constant. The shock moves downstream to a higher shock Mach number. The velocity ratio remains the same and, since the exit Mach number does not change, the product P_eA_e remains constant. Note that the thrust decreases. This can be seen by writing the second term in (3.46) as

$$\frac{A_e}{A_0}\frac{P_e}{P_0} - \frac{A_e}{A_0}. \tag{3.47}$$

The left term in (3.47) is constant but the right term increases leading to a decrease in thrust. If A_e is decreased, the reverse happens, the inlet operates more efficiently and the thrust goes up. But remember, the amount by which the area can be decreased is limited by the Mach number of the inlet throat.

Fuel flow control

Now, suppose T_{te} is decreased with A_e constant. In order for (3.45) to be satisfied, P_{te} must drop keeping $P_{te}/\sqrt{T_{te}}$ constant. Once again the shock moves downstream to a higher shock Mach number. The velocity ratio goes down since the exit stagnation temperature is down and the Mach numbers do not change.The pressure ratio also decreases since the exit stagnation pressure is down. The thrust clearly decreases in this case. If T_{te} is increased, the reverse happens, the inlet operates more efficiently and the thrust goes up. The amount by which the burner exit temperature can be increased is again limited by the Mach number of the inlet throat.

3.7 Example - Ramjet with un-started inlet

For simplicity, assume constant heat capacity with $\gamma = 1.4$, $C_p = 1005\, M^2/\left(\sec^2 - K\right)$. The gas constant is $R = 287\, M^2/\left(\sec^2 - K\right)$. The ambient temperature and pressure are $T_0 = 216K$ and $P_0 = 2 \times 10^4 N/M^2$. The fuel heating value is $h_f = 4.28 \times 10^7\, J/kg$. The sketch below shows a ramjet operating at a free stream Mach number of 3.0. A normal shock stands in front of the inlet. Heat is added between stations 3 and 4.

The stagnation temperature at station 4 is $T_{t4} = 2000\, K$. Relevant areas are $A_3/A_{1.5} = 8$, $A_1 = A_3 = A_4$ and $A_4/A_e = 3$. Determine the dimensionless thrust $T/(P_0A_1)$. Do not assume $f \ll 1$. Neglect stagnation pressure losses due to wall friction and burner drag. Assume that the static pressure outside the nozzle has recovered to the ambient value.

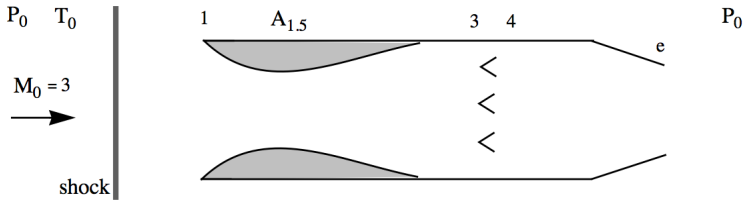

Figure 3.15: *Ramjet with normal shock ahead of the inlet.*

Suppose $A_{1.5}$ can be increased until $A_1 = A_{1.5} = A_3$. By what proportion would the air mass flow change?

Solution

The first point to recognize is that the stagnation pressure at station 4 exceeds the ambient by more than a factor of two - note the pressure outside the nozzle is assumed to have recovered to the ambient value. Thus the exit Mach number is one and the Mach number at station 4 is $M_4 = 0.1975$. The stagnation temperature at station 3 is $T_{t3} = 604.8\,K$. The fuel-air ratio is determined from the enthalpy balance

$$\dot{m}_f h_f = (\dot{m}_a + \dot{m}_f)\, h_{te} - \dot{m}_a h_{t0}. \tag{3.48}$$

For constant heat capacity

$$f = \frac{\frac{T_{t4}}{T_{t0}} - 1}{\frac{h_f}{C_p T_{t0}} - \frac{T_{t4}}{T_{t0}}} = \frac{\frac{2000}{604.8} - 1}{\frac{4.28\times10^7}{1005\times604.8} - \frac{2000}{604.8}} = 0.0344. \tag{3.49}$$

Now we need to determine the flow between stations 1 and 3. To get started we will neglect the fuel addition for the moment. Knowing the Mach number at 4 and the stagnation temperatures at 3 and 4 we can use Rayleigh line results to estimate the Mach number at station 3. The stagnation temperature ratio across the burner is

$$\begin{aligned} \frac{T_{t4}}{T_{t3}} &= \left.\frac{T_{t4}}{T_t^*}\right|_{M=0.1975} \left.\frac{T_t^*}{T_{t3}}\right|_{M=?} = \frac{2000}{604.8} = 3.3069 \\ \frac{T_{t4}}{T_{t3}} &= 0.2066 \left.\frac{T_t^*}{T_{t3}}\right|_{M=?} = \frac{2000}{604.8} = 3.3069. \end{aligned} \tag{3.50}$$

The Rayleigh line tables give

$$\left.\frac{T_t^*}{T_{t3}}\right|_{M=?} = \frac{3.3069}{0.2066} = 16.006 \Rightarrow M_3 = 0.103. \tag{3.51}$$

This is a reasonable approximation to the Mach number at station 3. The stagnation pressure ratio across the burner is

$$\frac{P_{t4}}{P_{t3}} = \left.\frac{P_{t4}}{P_t^*}\right|_{M=0.1975} \left.\frac{P_t^*}{P_{t3}}\right|_{M=0.103} = \frac{1.235}{1.258} = 0.981. \tag{3.52}$$

The subsonic critical Mach number for an area ratio of 8 is 0.0725. The fact that the Mach number at station 3 is higher than this value implies that there is a shock in the diverging part of the inlet and the inlet throat Mach number is equal to one. The stagnation pressure ratio between the inlet throat and the exit can be determined from a mass balance between stations 1.5 and e.

$$\begin{aligned} &\frac{P_{t_{1.5}} A_{1.5}\,(1+f)}{\sqrt{T_{t_{1.5}}}} = \frac{P_{te} A_e}{\sqrt{T_{te}}} = \\ &\frac{P_{te}}{P_{t_{1.5}}} = \frac{1.0344 \times 3}{8}\sqrt{\frac{2000}{604.8}} = 0.7054 \end{aligned} \tag{3.53}$$

The results (3.52) and (3.53) determine the stagnation pressure ratio across the inlet shock and this determines the Mach number of the inlet shock.

$$\pi_{shock} = \frac{0.7054}{0.981} = 0.719 \Rightarrow M_{shock} = 2.004 \tag{3.54}$$

Thus far the ramjet flow looks as shown in Figure 3.16.

The stagnation pressure ratio across the external shock is

$$\left.\frac{P_{t1}}{P_{t0}}\right|_{M=3} = 0.3283 \tag{3.55}$$

and so the overall stagnation pressure ratio is

$$\frac{P_{te}}{P_{t0}} = \frac{P_{t1}}{P_{t0}}\frac{P_{te}}{P_{t1.5}} = 0.3283 \times 0.7054 = 0.2316. \tag{3.56}$$

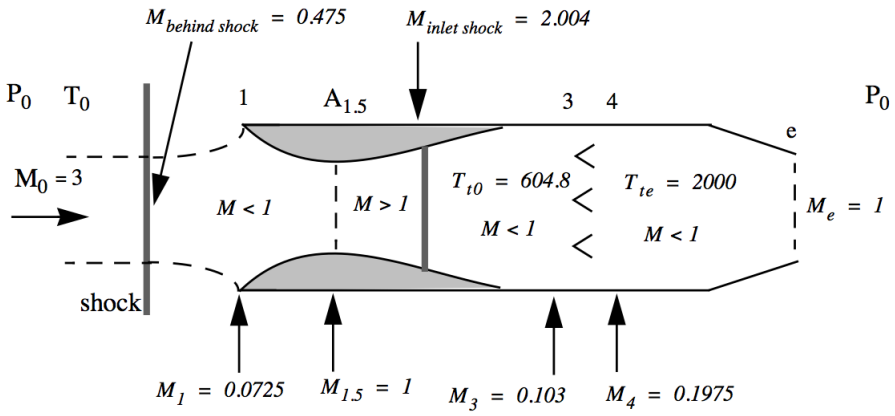

Figure 3.16: *State I.*

The static pressure ratio is

$$\frac{P_e}{P_0} = \frac{P_{te}}{P_{t0}} \left(\frac{1 + \frac{\gamma-1}{2} M_0{}^2}{1 + \frac{\gamma-1}{2} M_e{}^2} \right)^{\frac{\gamma}{\gamma-1}} = 0.2316 \times \left(\frac{2.8}{1.2} \right)^{3.5} = 4.494. \tag{3.57}$$

The temperature ratio is

$$\frac{T_e}{T_0} = \frac{T_{te}}{T_{t0}} \left(\frac{1 + \frac{\gamma-1}{2} M_0{}^2}{1 + \frac{\gamma-1}{2} M_e{}^2} \right) = \frac{2000}{604.8} \times \left(\frac{2.8}{1.2} \right) = 7.72. \tag{3.58}$$

The velocity ratio is

$$\frac{U_e}{U_0} = \frac{M_e}{M_0} \sqrt{\frac{T_e}{T_0}} = \frac{\sqrt{7.72}}{3} = 0.926. \tag{3.59}$$

Across the inlet, the mass balance is

$$P_{t1.5} A_{1.5} = P_{t0} A_0 f\left(M_0\right) \tag{3.60}$$

and so

$$\frac{A_0}{A_{1.5}} = \frac{P_{t1.5}}{P_{t0} f\left(M_0\right)} = 0.3283 \times 4.235 = 1.39. \tag{3.61}$$

Finally the thrust is

$$\frac{T}{P_0 A_1} = \gamma {M_0}^2 \frac{A_0}{A_{1.5}} \frac{A_{1.5}}{A_1} \left((1+f) \frac{U_e}{U_0} - 1 \right) + \frac{A_e}{A_1} \left(\frac{P_e}{P_0} - 1 \right) \tag{3.62}$$

and

$$\left. \frac{T}{P_0 A_1} \right|_{StateI} = 1.4 \times 9 \times 1.39 \times (1/8) \times (1.0344 \times 0.926 - 1) + (1/3) \times (4.494 - 1) =$$

$$-0.0923 + 1.165 = 1.0724. \tag{3.63}$$

State II

Now increase the inlet throat area to the point where the inlet un-chokes. As the inlet throat area is increased the Mach number at station 3 will remain the same since it is determined by the choking at the nozzle exit and the fixed enthalpy rise across the burner. The mass balance between the inlet throat and the nozzle exit is again

$$\frac{P_{t_{1.5}} A_{1.5} (1+f)}{\sqrt{T_{t_{1.5}}}} = \frac{P_{te} A_e}{\sqrt{T_{te}}}. \tag{3.64}$$

The stagnation pressure at station 1.5 is fixed by the loss across the external shock. The fuel-air ratio is fixed as are the temperatures in (3.64). As $A_{1.5}$ is increased, the equality (3.64) is maintained and the inlet shock moves to the left increasing P_{te} . At the point where the the inlet throat un-chokes the shock is infinitely weak and the only stagnation pressure loss between station 1.5 and the nozzle exit is across the burner.

$$\frac{A_{1.5\,State\,II}}{A_e} = \frac{1}{1+f} \frac{P_{te\,State\,II}}{P_{t1.5}} \sqrt{\frac{T_{t_{1.5}}}{T_{te}}} = \frac{0.982}{1.0344} \sqrt{\frac{604.8}{2000}} = 0.522 \tag{3.65}$$

This corresponds to

$$\frac{A_1}{A_{1.5\,State\,II}} = \left(\frac{A_1}{A_e} \right) \left(\frac{A_e}{A_{1.5\,State\,II}} \right) = \frac{3}{0.522} = 5.747. \tag{3.66}$$

The mass flow through the engine has increased by the ratio

$$\frac{\dot{m}_{a\,State\,II}}{\dot{m}_{a\,State\,I}} = \frac{A_{1.5\,State\,II}}{A_{1.5\,State\,I}} = \left(\frac{A_{1.5\,State\,II}}{A_1}\right)\left(\frac{A_1}{A_{1.5\,State\,I}}\right) = \frac{8}{5.747} = 1.392 = \frac{A_{0\,State\,II}}{A_{0\,State\,I}}. \tag{3.67}$$

At this condition the stagnation pressure ratio across the system is

$$\frac{P_{te\,State\,II}}{P_{t0}} = \left(\frac{P_{t1.5}}{P_{t0}}\right)\left(\frac{P_{te\,State\,II}}{P_{t1.5}}\right) = 0.3283 \times 0.982 = 0.3224. \tag{3.68}$$

The static pressure ratio is

$$\frac{P_{e\,State\,II}}{P_0} = \frac{P_{te\,State\,II}}{P_{t0}}\left(\frac{1+\frac{\gamma-1}{2}M_0{}^2}{1+\frac{\gamma-1}{2}M_e{}^2}\right)^{\frac{\gamma}{\gamma-1}} = 0.3224\left(\frac{2.8}{1.2}\right)^{3.5} = 6.256. \tag{3.69}$$

The Mach number at station 1 increases as $A_{1.5}$ increases and at the condition where the inlet is just about to un-choke reaches the same Mach number as station 3. At this condition the ramjet flow field looks like that shown in Figure 3.17.

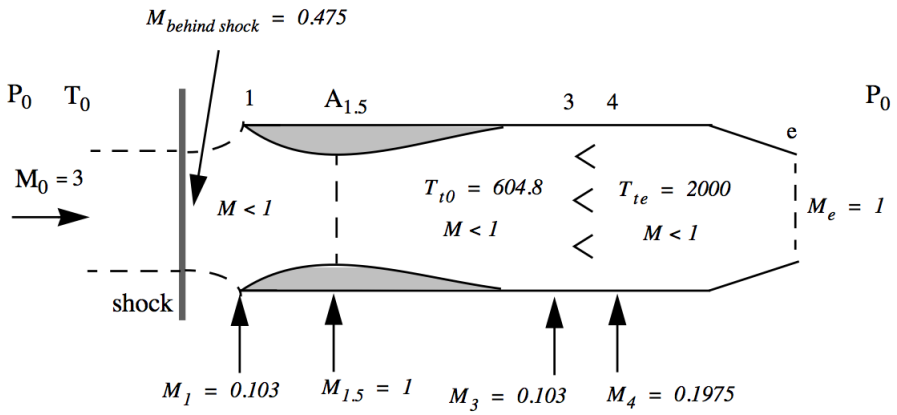

Figure 3.17: *State II.*

The inlet shock is gone, the inlet Mach number has increased to $M_1 = M_3$ and the external shock has moved somewhat closer to the inlet. Note that the capture area to throat area ratio is still

$$\frac{A_{0\,State\,II}}{A_{1.5\,State\,II}} = \frac{P_{t1.5}}{P_{t0}f\,(M_0)} = 0.3283 \times 4.235 = 1.39 \tag{3.70}$$

although both $A_{1.5}$ and A_0 have increased. Also

$$\frac{A_{0\,State\,II}}{A_1} = \frac{A_{0\,State\,II}}{A_{1.5\,State\,II}} \frac{A_{1.5\,State\,II}}{A_1} = \frac{1.39}{5.747} = 0.242. \tag{3.71}$$

The thrust formula is

$$\left.\frac{T}{P_0 A_1}\right|_{State\,II} = \gamma {M_0}^2 \left(\frac{A_{0\,State\,II}}{A_{1.5\,State\,II}}\right)\left(\frac{A_{1.5\,State\,II}}{A_1}\right)\left((1+f)\,\frac{U_e}{U_0} - 1\right) + \frac{A_e}{A_1}\left(\frac{P_{e\,State\,II}}{P_0} - 1\right). \tag{3.72}$$

The velocity ratio across the engine is unchanged by the increase in inlet throat area. The thrust of state II is

$$\left.\frac{T}{P_0 A_1}\right|_{State\,II} = 1.4 \times 9 \times 1.39 \times \left(\frac{1}{5.747}\right) \times (1.0344 \times 0.926 - 1) + \left(\frac{1}{3}\right) \times (6.256 - 1) =$$

$$-0.1284 + 1.752 = 1.624. \tag{3.73}$$

The reduced loss of stagnation pressure leads to almost a 60% increase in thrust at this condition.

State III

Now remove the inlet throat altogether.

Now, suppose $A_{1.5}$ is increased until $A_1 = A_{1.5} = A_3$. The ramjet flow field looks like Figure 3.18.

With the inlet throat absent, the Mach number is constant between 1 and 3. There is no change in mass flow, fuel-air ratio, stagnation pressure, or the position of the upstream shock. The capture area remains

$$\frac{A_{0\,State\,III}}{A_1} = \frac{A_{0\,State\,II}}{A_1} = \frac{A_{0\,State\,II}}{A_{1.5\,State\,II}} \frac{A_{1.5\,State\,II}}{A_1} = \frac{1.39}{5.747} = 0.242. \tag{3.74}$$

Therefore the thrust is the same as the thrust for State II, equation (3.74). If we want to position the upstream shock very near the entrance to the engine we have to increase the nozzle exit area and reduce the heat addition.

State IV

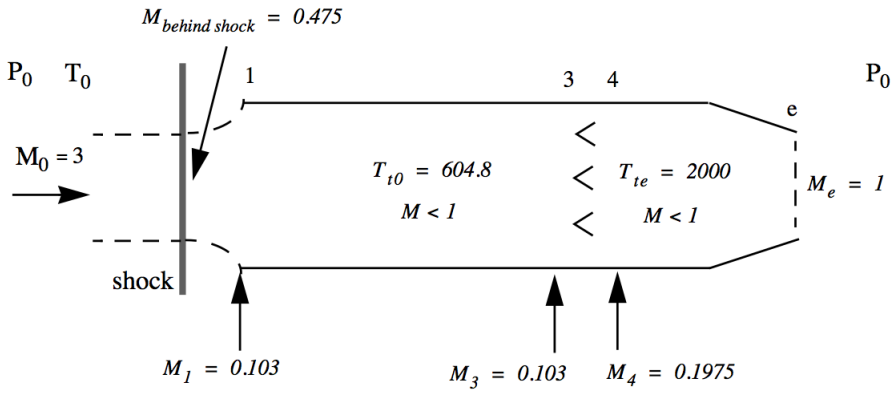

Figure 3.18: *State III.*

Open the nozzle exit fully.

First increase the exit area to the point where $A_1 = A_3 = A_4 = A_e$. If we maintain $T_{t4} = 2000\,K$ the Mach number at station 4 becomes one and the Mach number between 1 and 3 is, from the Rayleigh solution, $M_1 = M_3 = 0.276$. The ramjet flow at this condition is sketched in Figure 3.19.

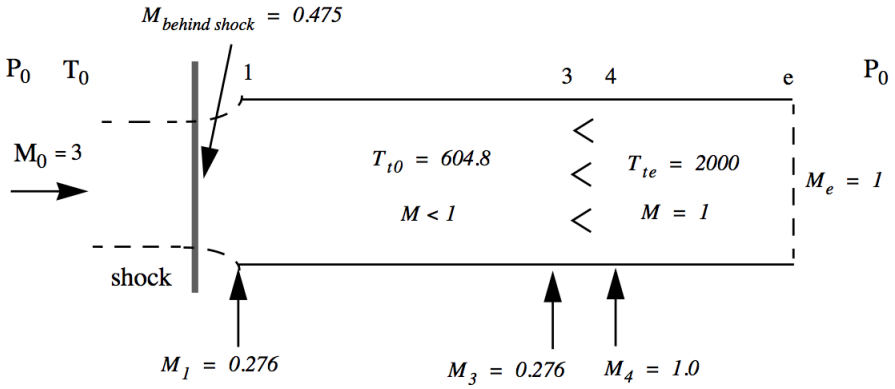

Figure 3.19: *State IV.*

The velocity ratio is still

$$\frac{U_e}{U_0} = \frac{M_e}{M_0}\sqrt{\frac{T_e}{T_0}} = \frac{\sqrt{7.72}}{3} = 0.926. \tag{3.75}$$

The stagnation pressure ratio across the burner is, from the Rayleigh solution,

$$\left.\frac{P_{te}}{P_{t1}}\right|_{State\,IV} = 0.8278. \tag{3.76}$$

Across the whole system

$$\left.\frac{P_{te}}{P_{t0}}\right|_{State\,IV} = \left.\frac{P_{t1.5}}{P_{t0}}\right|_{State\,IV} \left.\frac{P_{te}}{P_{t1.5}}\right|_{State\,IV} = 0.3283 \times 0.8278 = 0.2718 \tag{3.77}$$

and the static pressure ratio is

$$\frac{P_{e\,State\,IV}}{P_0} = \frac{P_{te\,State\,IV}}{P_{t0}} \left(\frac{1+\frac{\gamma-1}{2}{M_0}^2}{1+\frac{\gamma-1}{2}{M_e}^2}\right)^{\frac{\gamma}{\gamma-1}} = 0.2718\left(\frac{2.8}{1.2}\right)^{3.5} = 5.274. \tag{3.78}$$

The area ratio is

$$\frac{A_{0\,State\,IV}}{A_1} = \frac{P_{t1} f\left(M_1\right)}{P_{t0} f\left(M_0\right)} = 0.3283 \times \frac{0.4558}{0.2362} = 0.634. \tag{3.79}$$

The thrust formula for state IV is

$$\left.\frac{T}{P_0 A_1}\right|_{State\,IV} = \gamma {M_0}^2 \left(\frac{A_{0\,State\,IV}}{A_1}\right)\left(\left(1+f\right)\frac{U_e}{U_0} - 1\right) + \frac{A_e}{A_1}\left(\frac{P_{e\,State\,IV}}{P_0} - 1\right) \tag{3.80}$$

which evaluates to

$$\left.\frac{T}{P_0 A_1}\right|_{State\,IV} = 1.4 \times 9 \times 0.634 \times (1.0344 \times 0.926 - 1) + 1 \times (5.274 - 1) = \\ -0.3367 + 4.274 = 3.937. \tag{3.81}$$

Note the considerable increase in mass flow for state IV compared to state III. From (3.74)

$$\frac{\dot{m}_{a\,State\,IV}}{\dot{m}_{a\,State\,III}} = \left(\frac{A_{0\,State\,IV}}{A_1}\right)\left(\frac{A_1}{A_{0\,State\,III}}\right) = \frac{0.634}{0.242} = 2.62 \tag{3.82}$$

which accounts for much of the increased thrust in spite of the increase in stagnation pressure loss across the burner.

State V

Reduce the burner outlet temperature until the shock is very close to station 1.

Now reduce T_{te} until the Mach number at station 3 matches the Mach number behind the shock. From the Rayleigh solution, this occurs when $T_{te} = 924.8$. At this condition the ramjet flow field looks like Figure 3.20.

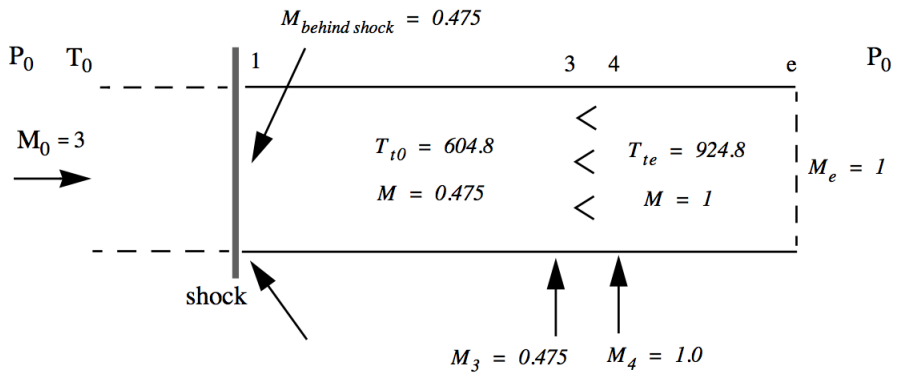

Figure 3.20: *State V.*

The static temperature ratio is

$$\frac{T_e}{T_0} = \frac{T_{te}}{T_{t0}} \left(\frac{1 + \frac{\gamma-1}{2} M_0{}^2}{1 + \frac{\gamma-1}{2} M_e{}^2} \right) = \frac{924.8}{604.8} \times \left(\frac{2.8}{1.2} \right) = 3.57. \tag{3.83}$$

The velocity ratio at this temperature is

$$\frac{U_e}{U_0} = \frac{M_e}{M_0} \sqrt{\frac{T_e}{T_0}} = \frac{\sqrt{3.57}}{3} = 0.630. \tag{3.84}$$

The stagnation pressure ratio across the burner at this condition is

$$\frac{P_{te}}{P_{t3}} = 0.889 \tag{3.85}$$

and across the system

$$\frac{P_{te}}{P_{t0}} = 0.889 \times 0.3283 = 0.292. \tag{3.86}$$

The static pressure ratio is

$$\frac{P_e}{P_0} = \frac{P_{te}}{P_{t0}} \left(\frac{1 + \frac{\gamma-1}{2} M_0{}^2}{1 + \frac{\gamma-1}{2} M_e{}^2} \right)^{\frac{\gamma}{\gamma-1}} = 0.292 \times \left(\frac{2.8}{1.2} \right)^{3.5} = 5.67. \tag{3.87}$$

Neglecting the fuel flow, the thrust is (Note that at this condition $A_0 = A_1 = A_e$).

$$\frac{T}{P_0 A_1} = \gamma M_0{}^2 \left(\frac{U_e}{U_0} - 1 \right) + \left(\frac{P_e}{P_0} - 1 \right) = 1.4 \times 9 \times (0.629 - 1) + (5.67 - 1) = -4.67 + 4.67 = 0 \tag{3.88}$$

State VI

Reduce the burner temperature slightly to establish supersonic flow up to the burner.

If the temperature at station 4 is decreased by an infinitesimal amount then supersonic flow will be established through the engine. Finally the flow is as shown in Figure 3.21.

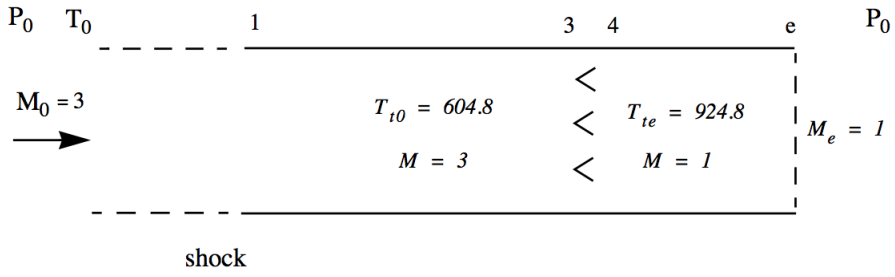

Figure 3.21: *State VI.*

The mass flow, velocity ratio, pressure ratio and thrust all remain the same as in state V. If we were to reduce the fuel flow to the burner to zero we would be back to the state of undisturbed Mach three flow through a straight tube.

3.8 Very high speed flight - scramjets

As the Mach number reaches values above 5 or so the ramjet cycle begins to become unusable and a new design has to be considered where the heat addition across the burner is carried out at supersonic Mach numbers. There are several reasons why this is so, all related to the very high stagnation temperature and stagnation pressure of high Mach number flight. To get started let's recall the thrust equation for the ramjet with a fully expanded nozzle.

$$\frac{T}{P_0 A_1} = \gamma {M_0}^2 \left((1+f) \frac{M_e}{M_0} \sqrt{\frac{T_e}{T_0}} - 1 \right) \tag{3.89}$$

Define the thrust coefficient as

$$C_{thrust} = \frac{Thrust}{\frac{1}{2}\rho_0 {U_0}^2 A_0} = \frac{T}{\frac{\gamma}{2} {M_0}^2 P_0 A_0}. \tag{3.90}$$

If we assume ideal behavior ($M_e = M_0$) the thrust coefficient becomes

$$C_{thrust} = 2 \left((1+f) \sqrt{\frac{T_{te}}{T_{t0}}} - 1 \right). \tag{3.91}$$

When we carried out the energy balance across the burner

$$\dot{m}_f h_f = (\dot{m}_a + \dot{m}_f)\, h_{t4} - \dot{m}_a h_{t3} \tag{3.92}$$

we assumed that the fuel enthalpy was simply added to the flow without regard to the chemistry of the process. In fact the chemistry highly limits the range of fuel-air ratios that are possible. The stoichiometric reaction of JP-4 with air where the fuel and oxygen are completely consumed is

$$CH_{1.94} + 1.485 O_2 + 5.536 N_2 \rightarrow CO_2 + 0.97 H_2O + 5.536 N_2. \tag{3.93}$$

corresponding to a fuel-air ratio

$$f = \frac{12.01 + 1.94 \times 1.008}{1.485 \times 32.00 + 5.536 \times 28.02} = 0.0689. \tag{3.94}$$

This is roughly the value of the fuel-air ratio that produces the maximum outlet temperature from the burner. If we choose the much more energetic hydrogen fuel, the reaction is

$$H_2 + 0.5O_2 + 1.864N_2 \rightarrow H_2O + 1.864N_2 \tag{3.95}$$

corresponding to a fuel-air ratio

$$f = \frac{2 \times 1.008}{16.00 + 1.864 \times 28.02} = 0.0295. \tag{3.96}$$

The fuel enthalpies are generally taken to be

$$\begin{aligned} h_{f_{JP-4}} &= 4.28 \times 10^7 \, J/kg \\ h_{f_{H_2}} &= 12.1 \times 10^7 \, J/kg. \end{aligned} \tag{3.97}$$

In the earlier discussion, we took the perspective that the ramjet cycle was limited by a red line temperature in the hot part of the engine. Let's relax this assumption and allow the maximum temperature to be free while keeping the fuel-air ratio constant. Furthermore let's continue to retain the assumption of constant heat capacities even at high Mach numbers. We will correct this eventually in Chapter 9, but for now we just want to see what happens to the ideal thrust coefficient (3.91) as we increase the free stream Mach number at constant fuel-air ratio. Using (3.92)), constant heat capacities, and assuming adiabatic flow in the inlet and nozzle we can express the stagnation temperature ratio across the engine as

$$\frac{T_{te}}{T_{t0}} = \left(\frac{f\tau_f}{1+f} \right) \left(\frac{1}{1 + \frac{\gamma-1}{2} {M_0}^2} \right) + \frac{1}{1+f} \tag{3.98}$$

where we recall that $\tau_f = h_f / (C_p T_0)$. Now the thrust coefficient becomes

$$C_{thrust} = 2 \left(\left(\frac{f\,(1+f)\,\tau_f}{1 + \frac{\gamma-1}{2} {M_0}^2} + (1+f) \right)^{1/2} - 1 \right). \tag{3.99}$$

The temperature ratio and thrust coefficient are plotted in Figures 3.22 and 3.23. The drag coefficient is defined as

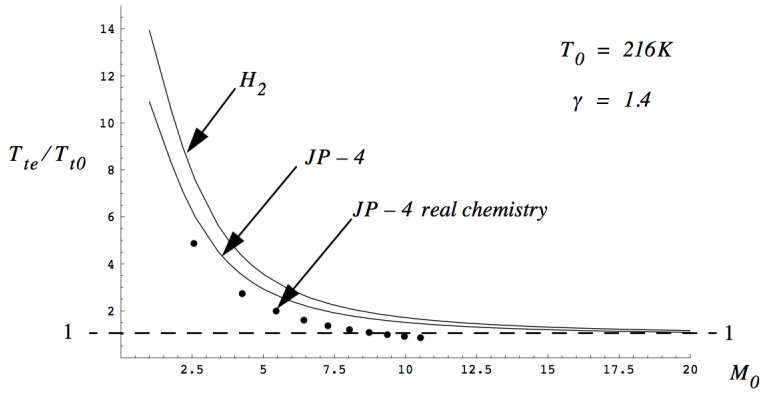

Figure 3.22: *Temperature ratio of an ideal ramjet at constant fuel-air ratio.*

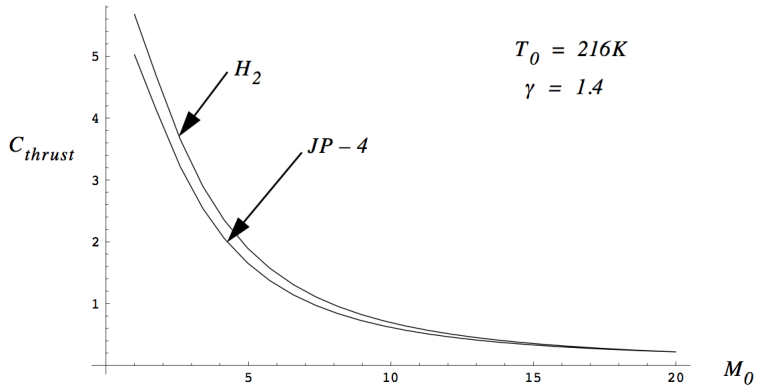

Figure 3.23: *Thrust coefficient of an ideal ramjet at constant fuel-air ratio.*

$$C_{drag} = \frac{Drag}{\frac{1}{2}\rho_0 {U_0}^2 A_0} = \frac{D}{\frac{\gamma}{2}{M_0}^2 P_0 A_0}. \tag{3.100}$$

At high Mach numbers the drag coefficient of a body tends toward a constant value. For a sphere the drag coefficient tends toward a constant slightly less than one, about 0.95. More streamlined bodies have lower drag and coefficients as low as 0.2 can be achieved. This observation together with Figure 3.23 indicates that as the Mach number increases it becomes harder and harder to produce thrust that exceeds drag. The thrust coefficient drops below one at a Mach number of about 7 to 8 for both fuels. As the Mach number increases a conventional ramjet (even an ideal one) simply cannot produce enough thrust to overcome drag. The limiting thrust coefficient at infinite Mach number is

$$\lim_{M_0 \to \infty} C_{thrust} = f. \tag{3.101}$$

This last result suggests that a scramjet can benefit from the choice of a fuel-rich mixture ratio as long as it does not exceed the flammability limit of the fuel. This would also provide additional fuel for cooling the vehicle. An advantage of a hydrogen system is that it can operate quite fuel rich. In addition, hydrogen has a higher heat capacity than any other fuel enabling it to be used to provide cooling for the vehicle that, in contrast to a re-entry body, has to operate in a very high temperature environment for long periods of time. The down side of hydrogen is that liquid hydrogen has to be stored at very low temperatures and the liquid density is only about 1/10 of that of JP-4. It is clear that small effects can be important. For example when we developed the thrust formula we neglected the momentum of the injected fuel. In a realistic scramjet analysis that would have to be taken into account.

3.8.1 Real chemistry effects

The real chemistry of combustion shows that the problem is even worse than just discussed. The plot points in Figure 3.21 are derived from an equilibrium chemistry computation of the combustion of JP-4 with air. Notice that the temperature reached by the combustion gases is substantially less than the ideal, and for high Mach numbers the temperature rise from the reaction is actually less than one due to the cooling effect of the added fuel.

The solution to this problem, which has been pursued since the 1960s, is to try to add heat with the burner operating with a supersonic Mach number on the order of two or so thereby cutting the static temperature of the air flowing into the combustor by almost a factor of two. This is the concept of a supersonically burning ramjet or scramjet. A

generic sketch of such a system is shown in Figure 3.24. Two Homework problems are used to illustrate basic concepts.

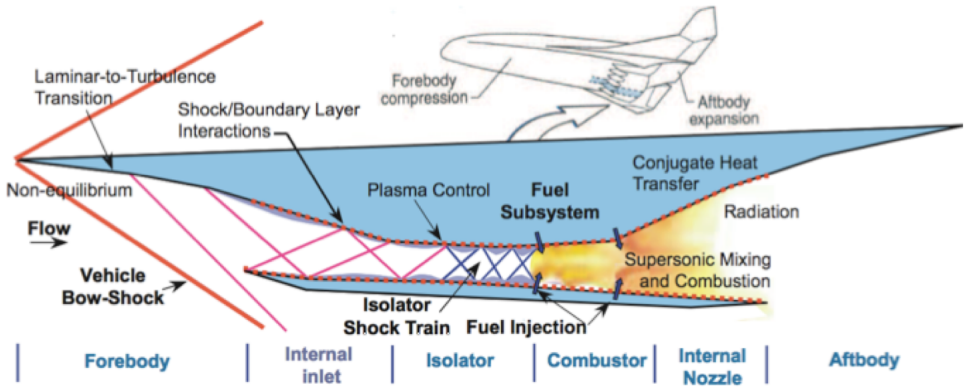

Figure 3.24: *Conceptual figure of a ramjet.*

3.8.2 Scramjet operating envelope

Figure 3.25 shows a widely circulated plot showing the altitude and Mach number regime where a scramjet might be expected to operate. Contours of constant free stream stagnation temperature and flow dynamic pressure are indicated on the plot.

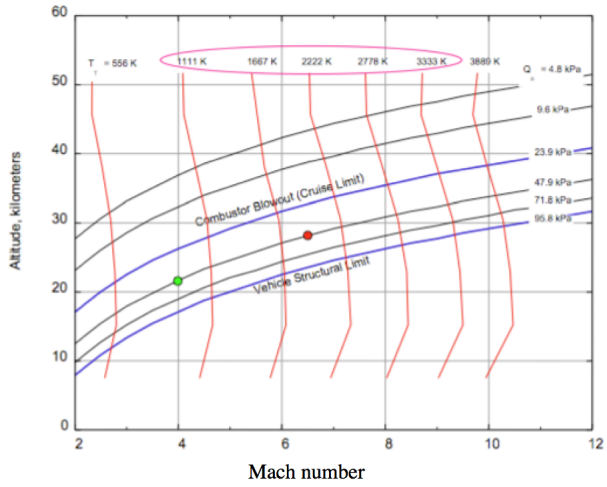

Figure 3.25: *Conceptual operating envelope of a scramjet.*

This figure somewhat accurately illustrates the challenges of scramjet flight. These can be listed as follows.

1) At high Mach numbers the vehicle is enveloped in an extremely high temperature gas for a long period of time perhaps more than an hour.

2)At high altittude, combustion is hard to sustain even at high Mach numbers because of the low atmospheric density and long chemical times. This defines the combustor blowout limit.

3) At lower altitude and high Mach number the free stream dynamic pressure increases to the point where the structural loads on the vehicle become untenable.

Let's take a look at the vehicle structural limit (item 3) in a little more detail. This limit is presented as a line of constant dynamic pressure coinciding with increasing Mach number and altitude. But in supersonic flow, the free stream dynamic pressure is really not a sufficient measure of the actual loads that are likely to act on the vehicle. Again let's make a constant heat capacity assumption and compare the free stream stagnation pressure to the free stream dynamic pressure as follows. Form the pressure coefficient

$$\frac{P_{t\infty}-P_\infty}{q_\infty}=\frac{P_\infty}{\frac{\gamma}{2}P_\infty {M_\infty}^2}\left(\left(1+\frac{\gamma-1}{2}{M_\infty}^2\right)^{\frac{\gamma}{\gamma-1}}-1\right)=\frac{\left(1+\frac{\gamma-1}{2}{M_\infty}^2\right)^{\frac{\gamma}{\gamma-1}}-1}{\frac{\gamma}{2}{M_\infty}^2}. \tag{3.102}$$

This function is plotted in Figure 3.26.

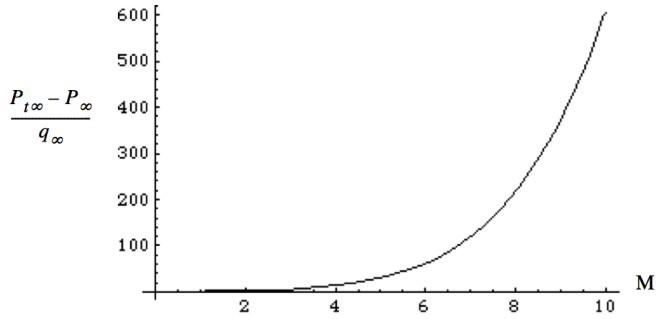

Figure 3.26: *Comparison of stagnation pressure and dynamic pressure in supersonic flow.*

If one repeats this calculation with real gas effects the stagnation pressures one calculates are even larger because of reduced values of γ.

Consider the downstream end of the inlet where the flow enters the combuster. According to Figure 3.26 if, at a free stream Mach number of 8, the internal flow is brought isentropically

to low Mach number at the entrance to the combustor, the combuster will experience a pressure 218 times the free stream dynamic pressure. For example, at an altitude of about 26 kilometers and $M_0 = 8.0$ a low Mach number combuster would operate at about 3200 psia (10,000 times the ambient atmospheric pressure at that altitude). This would require a very heavy structure making the whole idea impractical.

If instead, the flow Mach number entering the combuster can be maintained at about Mach 2 then the combuster will operate at a much more feasible value of 28 bar or about 410 psia (somewhat higher with real gas effects accounted for). This structural issue is at least as important as the thermochemistry issue in forcing the designer to consider operating the combuster at supersonic Mach numbers in order to attain hypersonic flight.

3.9 Problems

Problem 1 - Review 1-D gas dynamics with heat addition and area change. Consider the flow of a combustible gas mixture through a sudden expansion in a pipe shown in Figure 3.27.

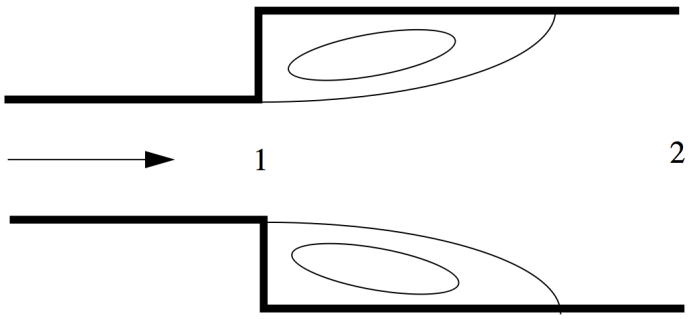

Figure 3.27: *Dump combustor.*

Combustion occurs between section 1 at the exit of the small pipe and section 2 in the large pipe where the flow is uniform. Wall friction may be assumed to be negligible throughout. The flow at station 1 has stagnation properties P_{t1} and T_{t1} . The Mach number at station 1, M_1 is subsonic and the pressure on the annular step is approximately equal to P_1 . The heat of reaction is denoted by Q.

(i) Show that the exit Mach number is given by

$$\frac{{M_2}^2\left(1+\frac{\gamma-1}{2}{M_2}^2\right)}{\left(1+\gamma{M_2}^2\right)^2}=\left(1+\frac{Q}{C_pT_{t1}}\right)\frac{{M_1}^2\left(1+\frac{\gamma-1}{2}{M_1}^2\right)}{\left(\frac{A_2}{A_1}+\gamma{M_1}^2\right)^2}. \tag{3.103}$$

(ii) Show that when $Q=0$ and A_2/A_1 goes to infinity

$$\frac{P_{t1}}{P_{t2}}=\left(1+\frac{\gamma-1}{2}{M_1}^2\right)^{\frac{\gamma}{\gamma-1}}. \tag{3.104}$$

This limit is the case of a simple jet coming from an orifice in an infinite plane.

Problem 2 - Show that for an ideal ramjet

$$\eta_{th}=\frac{\frac{\gamma-1}{2}{M_0}^2}{1+\frac{\gamma-1}{2}{M_0}^2}. \tag{3.105}$$

Do not assume $f \ll 1$.

Problem 3 - Figure 3.28 shows a ramjet operating at a free stream Mach number of 0.7. Heat is added between stations 3 and 4 and the stagnation temperature at station 4 is $T_{t4}=1000K$. The Mach number at station 3 is very low. The ambient temperature and pressure are $T_0=216\,K$ and $P_0=2\times10^4\,N/M^2$. Assume that $f \ll 1$.

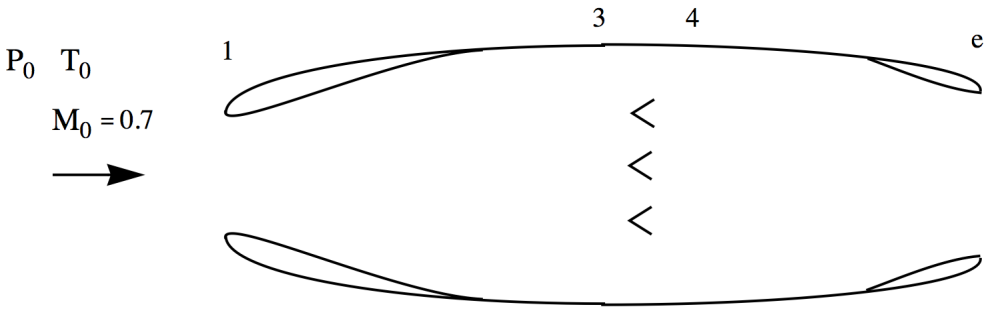

Figure 3.28: *Ramjet in subsonic flow.*

Using appropriate assumptions, estimate the dimensionless thrust $T/\left(P_0A_0\right)$ and the area ratio A_0/A_e.

Problem 4 - Figure 3.29 shows a ramjet operating at a free stream Mach number $M_0=1.5$, with a normal shock in front of the engine. Heat is added between stations 3 and 4 and

the stagnation temperature at station 4 is $T_{t4} = 1400\,K$. The Mach number at station 3 is very low. There is no shock in the inlet. The ambient temperature and pressure are $T_0 = 216\,K$ and $P_0 = 2 \times 10^4\,N/M^2$. Assume that $f \ll 1$.

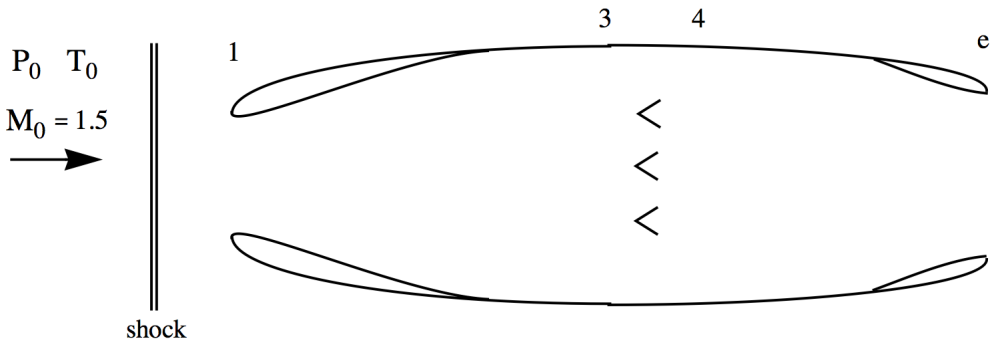

Figure 3.29: *Ramjet in supersonic flow with a shock ahead of the inlet.*

Using appropriate assumptions, estimate the dimensionless thrust $T/\left(P_0 A_0\right)$ and the area ratio A_0/A_e.

Problem 5 - In Figure 3.30 a ramjet operates at a freestream Mach number of 3. The inlet is a straight duct and the Mach number of the flow entering the burner at station 3 is three. Heat is added across the burner such that the Mach number of the flow exiting the burner at station 4 is two. The ambient temperature and pressure are $T_0 = 216\,K$ and $P_0 = 2 \times 10^4\,N/M^2$. Assume that $f \ll 1$.

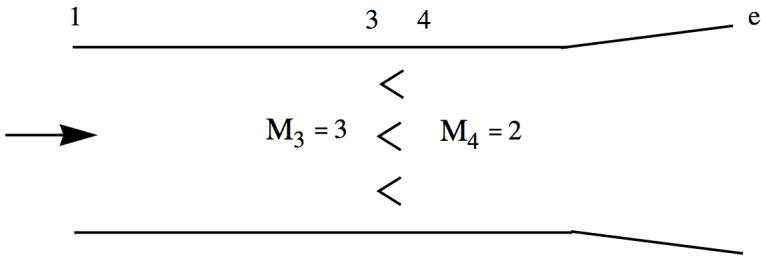

Figure 3.30: *Supersonically burning ramjet.*

The exit flow is expanded to $P_e = P_0$. Determine the dimensionless thrust, $T/\left(P_0 A_0\right)$.

Problem 6 - In Figure 3.31 a ramjet operates at a freestream Mach number of 2.5. The ambient temperature and pressure are $T_0 = 216\,K$ and $P_0 = 2 \times 10^4\,N/M^2$. The engine operates with a straight duct after the burner, $A_1/A_e = 1$. Supersonic flow is established at the entrance of the inlet and a normal shock is stabilized somewhere in the diverging

part of the inlet. The stagnation temperature exiting the burner is $T_{t4} = 1800\,K$. Neglect wall friction. Determine the dimensionless thrust, $T/(P_0 A_0)$.

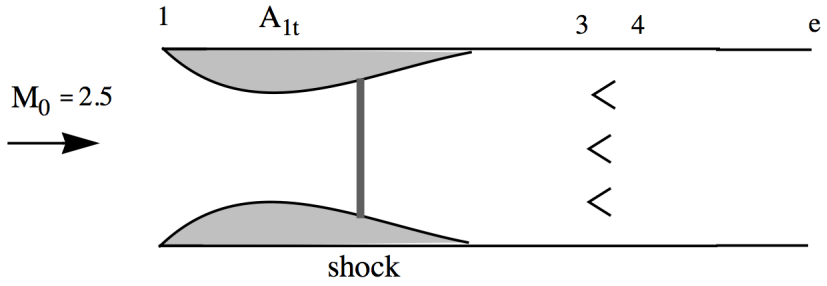

Figure 3.31: *Ramjet with a constant area nozzle.*

Problem 7 - Figure 3.32 shows a ramjet test facility. A very large plenum contains Air at constant stagnation pressure and temperature, P_{t0} , T_{t0}. Jet fuel ($h_f = 4.28 \times 10^7\,J/kg$) is added between stations 3 and 4 ($A_3 = A_4$) where combustion takes place. The flow exhausts to a large tank which is maintained at pressure P_0. Let $P_{t0}/P_0 = 100$. The upstream nozzle area ratio is $A_3/A_{1.5} = 8$. The exit area, A_e can be varied in order to change the flow conditions in the engine. The gas temperature in the plenum is $T_{t0} = 805.2\,K$. To simplify the analysis, assume adiabatic flow, neglect wall friction and assume constant specific heat throughout with $\gamma = 1.4$.

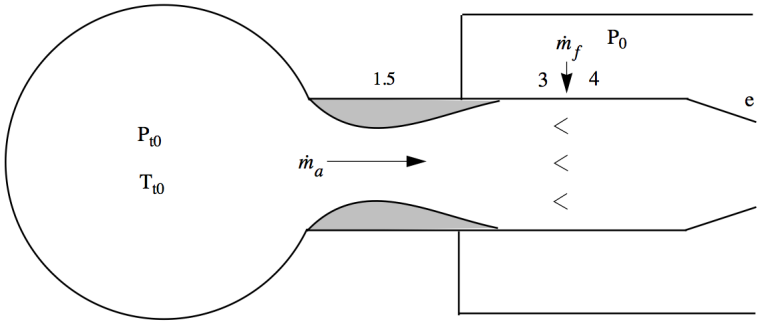

Figure 3.32: *Ramjet test facility.*

Initially, the valve controlling A_e is closed, $A_e = 0$ and the fuel mass flow is shut off. Consider a test procedure where the nozzle area is opened, then closed. In the process $A_e/A_{1.5}$ is slowly increased from zero causing Air to start flowing. The nozzle is opened until $A_e = A_3$. Then the nozzle area is slowly reduced until $A_e/A_{1.5} = 0$ once again. Plot the thrust normalized by the plenum pressure and upstream throat area, $T/(P_{t0} A_{1.5})$ and the fuel-Air ratio f as a function of $A_e/A_{1.5}$. Distinguish points corresponding to increasing

and decreasing A_e. The fuel flow is adjusted to maintain the stagnation temperature at 4 at a constant value. Plot the results for three cases.

$$T_{t4} = 805.2\,K \text{(zero fuel flow)}$$

$$\mathrm{T}_{t4} = 1200\,K \tag{3.106}$$

$$T_{t4} = 2700\,K$$

Neglect stagnation pressure loss across the burner due to aerodynamic drag of the burner, retain the loss due to heat addition. Do not assume $f \ll 1$. What flight Mach number and altitude are being simulated at this condition?

Problem 8 - In Figure 3.33 a ramjet operates at a free-stream Mach number of 3. The area ratio across the engine is $A_1/A_e = 2$. Supersonic flow is established at the entrance of the inlet and a normal shock is stabilized in the diverging part of the inlet. The inlet throat Mach number is 1.01. The stagnation temperature exiting the burner is $T_{t4} = 1944\,K$. Assume $\gamma = 1.4$, $R = 287\,M^2/\left(\sec^2 - K\right)$, $C_p = 1005\,M^2/\left(\sec^2 - K\right)$. The ambient temperature and pressure are $T_0 = 216\,K$ and $P_0 = 2 \times 10^4\,N/M^2$. Assume throughout that $f \ll 1$.

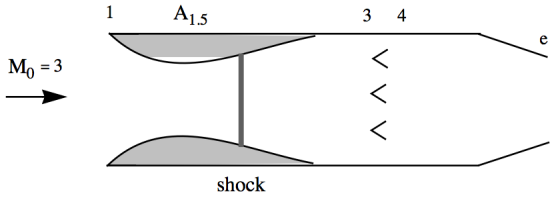

Figure 3.33: *Ramjet with a simple convergent nozzle.*

i) Suppose the fuel flow is increased with the geometry of the engine held fixed. Estimate the value of f that would cause the inlet to unstart. Plot the dimensionless thrust, $T/(P_0 A_{1.5})$, specific impulse, and overall efficiency of the engine as a function of f. Plot your result beyond the point where the inlet un-starts and assume the engine does not flame out. Assume the fuel flow is throttled so as to keep the fuel/air ratio constant. Note that the thrust is normalized by a fixed geometric area rather than the capture area A_0 that changes when the engine un-starts.

ii) With $T_{t4} = 1944\,K$, suppose A_e is reduced keeping the fuel flow the same. Estimate the value of A_1/A_e that would cause the inlet to un-start? Plot the dimensionless thrust, $T/(P_0 A_{1.5})$ specific impulse and overall efficiency of the engine as a function of A_1/A_e. As in part (i), plot your result beyond the point where the inlet un-starts and assume the engine does not flame out.

Problem 9 - In Figure 3.34 a ramjet operates at a free-stream Mach number of 3. The area ratio across the engine is $A_1/A_e = 2$. Supersonic flow is established at the entrance of the inlet and a normal shock is stabilized in the diverging part of the inlet. The stagnation temperature exiting the burner is $T_{t4} = 1944\,K$. The ambient temperature and pressure are $T_0 = 216\,K$ and $P_0 = 2 \times 10^4\,N/M^2$. Do not assume that $f \ll 1$. Do not neglect the effects of wall friction.

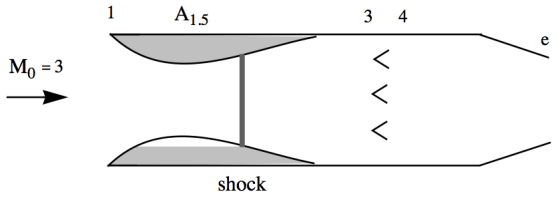

Figure 3.34: *Ramjet with a convergent nozzle and inlet shock.*

i) Determine the fuel-air ratio, f.

ii) Determine the dimensionless thrust, $T/(P_0 A_0)$.

Problem 10 - Assume $\gamma = 1.4$, $R = 287\,M^2/\left(\sec^2 - K\right)$, $C_p = 1005\,M^2/\left(\sec^2 - K\right)$. The ambient temperature and pressure are $T_0 = 216\,K$ and $P_0 = 2 \times 10^4\,N/M^2$. Figure 3.35 shows a ramjet operating at a free stream Mach number of 3.0. The incoming air is decelerated to a Mach number of 2.0 at station 3.

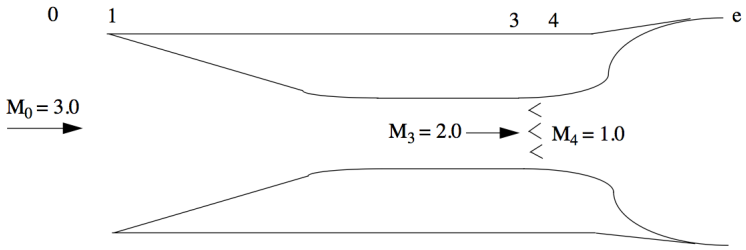

Figure 3.35: *A scramjet concept.*

Heat is added between 3 and 4 bringing the Mach number at station 4 to one. The flow is then ideally expanded to $P_e = P_0$. This type of engine with the combustion of fuel occurring in a supersonic stream is called a SCRAMJET (supersonic combustion ramjet). Determine the dimensionless thrust $T/(P_0 A_0)$. Assume $f \ll 1$ if you wish and neglect stagnation pressure losses due to friction.

Problem 11 - A ramjet operates in the upper atmosphere at a high supersonic Mach number as shown in Figure 3.36. Supersonic flow is established at the entrance of the

inlet and a normal shock is stabilized in the diverging part of the inlet. The stagnation temperature exiting the burner is sufficient to produce substantial positive thrust. A small flat plate is placed downstream of the burner as shown, causing a small drop in stagnation pressure between station "a" and station "b". The plate can be positioned so as to produce high drag as shown, or it can be rotated 90° so that the long dimension is aligned with the flow, producing lower drag. The engine operates with a convergent-divergent nozzle. The nozzle throat is choked and the nozzle exit is fully expanded.

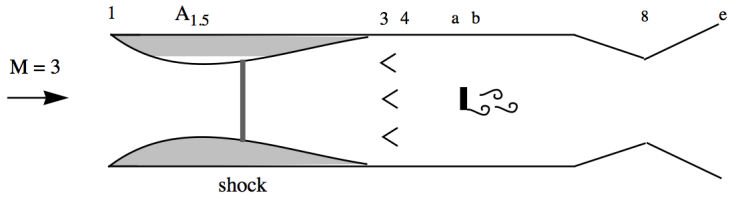

Figure 3.36: *Ramjet with variable drag loss.*

Suppose the plate is rotated from the high drag position to the low drag position. State whether each of the following area-averaged quantities increases, decreases or remains the same.

1) M_3 5) T_e

2) M_a 6) P_e

3) M_b 7) U_e

4) M_e 8) $Engine\,thrust$

Explain the answer to part 8) in terms of the drag force on the plate and the pressure forces that act on the engine inlet and nozzle.

Problem 12 - In Figure 3.37 a ramjet operates at a freestream Mach number of 3. The area ratio across the engine is $A_1/A_e = 2$. Supersonic flow is established at the entrance of the inlet and a normal shock is stabilized in the diverging part of the inlet. The stagnation temperature exiting the burner is $T_{t4} = 1512\,K$. The ambient temperature and pressure are $T_0 = 216\,K$ and $P_0 = 2 \times 10^4\,N/M^2$.

Do not neglect wall friction.

i) Determine the dimensionless thrust, $T/(P_0 A_0)$.

ii) Suppose the wall friction is increased slightly. Determine if each of the following increases, decreases or remains the same.

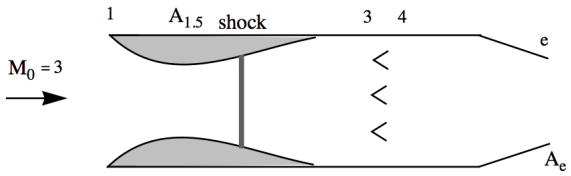

Figure 3.37: *Ramjet in supersonic flow.*

a) The Mach number at station 4

b) The Mach number at station 1.5

c) The shock Mach number

d) The dimensionless thrust $T/(P_0 A_0)$

Assume the inlet does not un-start.

Problem 13 - In Figure 3.38 a ramjet operates at a freestream Mach number of 3. The area ratio across the engine is $A_1/A_8 = 1.75$. Supersonic flow is established at the entrance of the inlet and a normal shock is stabilized in the diverging part of the inlet. The stagnation temperature exiting the burner is $T_{t4} = 1512\,K$. The nozzle is fully expanded $P_e = P_0$. The fuel enthalpy is $h_f = 4.28 \times 10^7\,J/kg$. The ambient temperature and pressure are $T_0 = 216\,K$ and $P_0 = 2 \times 10^4\,N/M^2$.

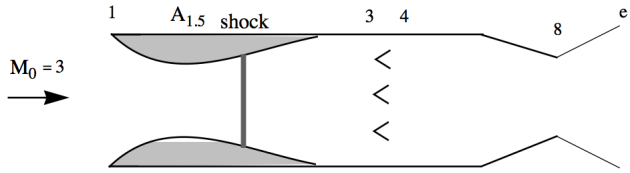

Figure 3.38: *Ramjet with a converging-diverging nozzle.*

i) Determine the dimensionless thrust, $T/(P_0 A_0)$.

ii) Suppose T_{t4} is decreased slightly. Determine if each of the following increases, decreases or remains the same.

a) The Mach number at station 4

b) The Mach number at station 3

c) The shock Mach number

d) The nozzle exit pressure P_e

Chapter 4

The Turbojet cycle

4.1 Thermal efficiency of the ideal turbojet

Recalling our discussion in Chapter 2, the thermal efficiency of a jet engine propulsion system is defined as

$$\eta_{th} = \frac{power\,to\,the\,vehicle + \frac{\Delta kinetic\,energy\,of\,air}{second} + \frac{\Delta kinetic\,energy\,of\,fuel}{second}}{\dot{m}_f h_f} \tag{4.1}$$

or

$$\eta_{th} = \frac{\mathrm{TU}_0 + \left[\frac{\dot{m}_a(U_e - U_0)^2}{2} - \frac{\dot{m}_a(0)^2}{2}\right] + \left[\frac{\dot{m}_f(U_e - U_0)^2}{2} - \frac{\dot{m}_f(U_0)^2}{2}\right]}{\dot{m}_f h_f}. \tag{4.2}$$

If the exhaust is fully expanded so that $P_e = P_0$ the thermal efficiency reduces to

$$\eta_{th} = \frac{\frac{(\dot{m}_a + \dot{m}_f){U_e}^2}{2} - \frac{\dot{m}_a {U_0}^2}{2}}{\dot{m}_f h_f}. \tag{4.3}$$

For the ideal ramjet we were able to rearrange the thermal efficiency as follows.

$$\eta_{th} = \frac{\frac{(\dot{m}_a+\dot{m}_f){U_e}^2}{2} - \frac{\dot{m}_a {U_0}^2}{2}}{\dot{m}_f h_f} = \frac{(\dot{m}_a + \dot{m}_f)(h_{te} - h_e) - \dot{m}_a (h_{t0} - h_0)}{(\dot{m}_a + \dot{m}_f) h_{te} - \dot{m}_a h_{t0}}$$

$$\eta_{th} = 1 - \frac{Q_{rejected\,during\,the\,cycle}}{Q_{input\,during\,the\,cycle}} = 1 - \frac{(\dot{m}_a + \dot{m}_f) h_e - \dot{m}_a h_0}{(\dot{m}_a + \dot{m}_f) h_{te} - \dot{m}_a h_{t0}} \tag{4.4}$$

$$\eta_{th} = 1 - \frac{T_0}{T_{t0}} \left(\frac{(1+f)\frac{T_e}{T_0} - 1}{(1+f)\frac{T_{te}}{T_{t0}} - 1} \right)$$

Noting that for the ideal ramjet $T_e/T_0 = T_{te}/T_{t0}$, the term in brackets is one, and the thermal efficiency of the ideal ramjet becomes

$$\eta_{th} = 1 - \frac{T_0}{T_{t0}} = 1 - \frac{1}{\tau_r} = \frac{\left(\frac{\gamma-1}{2}\right) {M_0}^2}{1 + \left(\frac{\gamma-1}{2}\right) {M_0}^2}. \tag{4.5}$$

The thermal efficiency of the ideal ramjet is entirely determined by the flight Mach number. As the Mach number goes to zero the thermal efficiency goes to zero and the engine produces no thrust.

To overcome this, we need an engine cycle that produces its own compression at zero Mach number. This is achieved through the use of a compressor driven by a turbine. A sketch of a turbojet engine is shown in Figure 4.1.

In an adiabatic system with no shaft bearing losses the work done by the gas on the turbine matches the work done by the compressor on the gas. This is expressed as a simple enthalpy balance.

$$(\dot{m}_a + \dot{m}_f)(h_{t4} - h_{t5}) = \dot{m}_a (h_{t3} - h_{t2}) \tag{4.6}$$

The enthalpy balance across the burner is

$$(\dot{m}_a + \dot{m}_f) h_{t4} = \dot{m}_a h_{t3} + \dot{m}_f h_f. \tag{4.7}$$

Subtract (4.6) from (4.7). The enthalpy balance across the engine is

$$(\dot{m}_a + \dot{m}_f) h_{t5} = \dot{m}_a h_{t2} + \dot{m}_f h_f. \tag{4.8}$$

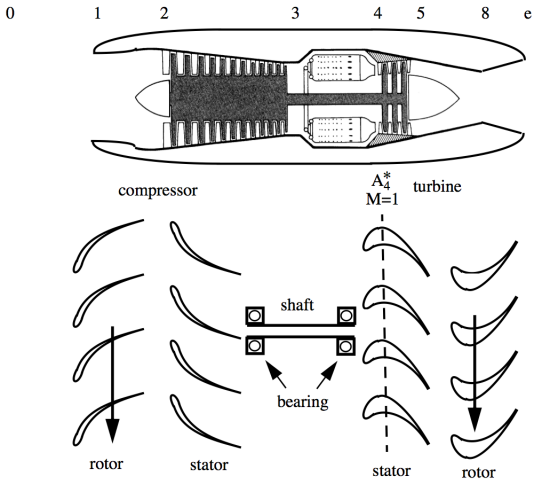

Figure 4.1: *Turbojet engine and compressor-turbine blade diagram.*

Assume that the inlet and nozzle flow are adiabatic. Then (4.8) is equivalent to

$$(\dot{m}_a + \dot{m}_f)\, h_{te} = \dot{m}_a h_{t0} + \dot{m}_f h_f. \tag{4.9}$$

Now the thermal efficiency (4.3) can be written as

$$\eta_{th} = \frac{(\dot{m}_a + \dot{m}_f)\,(h_{te} - h_e) - \dot{m}_a\,(h_{t0} - h_0)}{(\dot{m}_a + \dot{m}_f)\, h_{t4} - \dot{m}_a h_{t3}}. \tag{4.10}$$

Using (4.9) and (4.7), equation (4.10) becomes

$$\eta_{th} = \frac{(\dot{m}_a + \dot{m}_f)\, h_{t4} - \dot{m}_a h_{t3} - (\dot{m}_a + \dot{m}_f)\, h_e + \dot{m}_a h_0}{(\dot{m}_a + \dot{m}_f)\, h_{t4} - \dot{m}_a h_{t3}} \tag{4.11}$$

or

$$\begin{aligned} \eta_{th} &= 1 - \frac{Q_{rejected\,during\,the\,cycle}}{Q_{input\,during\,the\,cycle}} = 1 - \left(\frac{(\dot{m}_a + \dot{m}_f)\, h_e - \dot{m}_a h_0}{(\dot{m}_a + \dot{m}_f)\, h_{t4} - \dot{m}_a h_{t3}} \right) \\ \eta_{th} &= 1 - \frac{h_0}{h_{t3}} \left(\frac{(1+f)\,\frac{h_e}{h_0} - 1}{(1+f)\,\frac{h_{t4}}{h_{t3}} - 1} \right). \end{aligned} \tag{4.12}$$

If the gas is calorically perfect then (4.12) can be expressed in terms of the temperature.

$$\eta_{th} = 1 - \frac{T_0}{T_{t3}} \left(\frac{(1+f)\frac{T_e}{T_0} - 1}{(1+f)\frac{T_{t4}}{T_{t3}} - 1} \right) \tag{4.13}$$

In the ideal Brayton cycle the compression process from the free stream to station 3 is assumed to be adiabatic and isentropic. Similarly the expansion from station 4 to the exit is assumed to be isentropic. Thus

$$\begin{aligned} \frac{T_{t3}}{T_0} &= \left(\frac{P_{t3}}{P_0} \right)^{\frac{\gamma-1}{\gamma}} \\ \frac{T_{t4}}{T_e} &= \left(\frac{P_{t4}}{P_e} \right)^{\frac{\gamma-1}{\gamma}}. \end{aligned} \tag{4.14}$$

Also in the ideal Brayton cycle the heat adition and removal is assumed to occur at constant pressure. Therefore $P_{t4} = P_{t3}$, $P_e = P_0$ and we can write

$$\frac{T_{t4}}{T_e} = \frac{T_{t3}}{T_0}. \tag{4.15}$$

Therefore the expression in brackets in (4.13) is equal to one for the ideal turbojet cycle and the thermal efficiency is

$$\eta_{th_{idealturbojet}} = 1 - \frac{T_0}{T_{t3}} = 1 - \frac{1}{\tau_r \tau_c}. \tag{4.16}$$

When the Mach number is zero ($\tau_r = 1$), the thermal efficiency is positive and determined by the stagnation temperature ratio $\tau_c = T_{t3}/T_{t2}$ of the compressor.Thermodynamic diagrams of the turbojet cycle are shown in Figures 4.2 and 4.3.

The important impact of the compression process on thermal efficiency is a major factor behind the historical trend toward higher compression engines for both commercial and military applications.

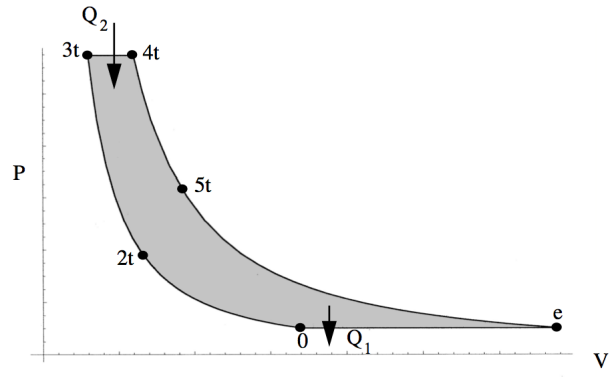

Figure 4.2: *P-V diagram of the ideal turbojet cycle. Station number with a "t" refers to the stagnation state of the gas at that point.*

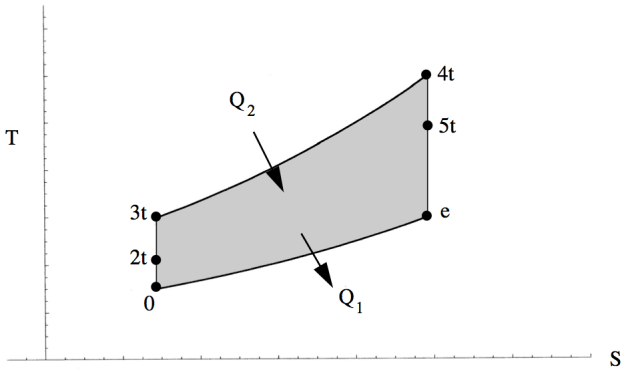

Figure 4.3: *T-S diagram of the ideal turbojet cycle.*

4.2 Thrust of an ideal turbojet engine

The thrust equation for a fully expanded nozzle is

$$\frac{T}{P_0 A_0} = \gamma {M_0}^2 \left((1+f)\frac{U_e}{U_0} - 1 \right). \tag{4.17}$$

To determine the thrust we need to work out the velocity ratio.

$$\frac{U_e}{U_0} = \frac{M_e}{M_0}\sqrt{\frac{T_e}{T_0}} \tag{4.18}$$

To determine the Mach numbers we focus on the variation of stagnation pressure through the engine. Begin with the following identity.

$$P_{te} = P_0 \left(\frac{P_{t0}}{P_0}\right)\left(\frac{P_{t2}}{P_{t0}}\right)\left(\frac{P_{t3}}{P_{t2}}\right)\left(\frac{P_{t4}}{P_{t3}}\right)\left(\frac{P_{t5}}{P_{t4}}\right)\left(\frac{P_{te}}{P_{t5}}\right) \tag{4.19}$$

Using our engine parameters this would be written as

$$P_{te} = P_0 \pi_r \pi_d \pi_c \pi_b \pi_t \pi_n. \tag{4.20}$$

Under the assumptions of the ideal cycle the stagnation pressure losses in the diffuser and nozzle are negligible. In other words, skin friction and shock losses are negligible.

$$\begin{aligned} \pi_d &= 1 \\ \pi_n &= 1 \end{aligned} \tag{4.21}$$

Similarly, the Mach number through the burner is assumed to be so low that the stagnation pressure losses due to heat addition and aerodynamic drag are assumed to be negligible.

$$\pi_b = 1 \tag{4.22}$$

Therefore

$$P_{te} = P_0 \pi_r \pi_c \pi_t = P_e \left(1 + \frac{\gamma - 1}{2} {M_e}^2\right)^{\frac{\gamma}{\gamma - 1}}. \tag{4.23}$$

Another assumption of the ideal cycle is that the nozzle is fully expanded.

$$\pi_r \pi_c \pi_t = \left(1 + \frac{\gamma - 1}{2} {M_e}^2\right)^{\frac{\gamma}{\gamma - 1}} \tag{4.24}$$

The final assumption of the ideal turbojet is that the compressor and turbine behave isentropically.

$$\begin{aligned} \pi_c &= {\tau_c}^{\frac{\gamma}{\gamma - 1}} \\ \pi_t &= {\tau_t}^{\frac{\gamma}{\gamma - 1}} \end{aligned} \tag{4.25}$$

Using (4.25) in (4.24) and the relation $\pi_r = {\tau_r}^{\gamma/(\gamma-1)}$, the exit Mach number can be determined from

$${M_e}^2 = \frac{2}{\gamma - 1} \left(\tau_r \tau_c \tau_t - 1\right) \tag{4.26}$$

and the Mach number ratio is

$$\frac{{M_e}^2}{{M_0}^2} = \left(\frac{\tau_r \tau_c \tau_t - 1}{\tau_r - 1}\right). \tag{4.27}$$

We take a similar approach to determining the temperature ratio across the engine. Begin with the identity

$$T_{te} = T_0 \left(\frac{T_{t0}}{T_0}\right) \left(\frac{T_{t2}}{T_{t0}}\right) \left(\frac{T_{t3}}{T_{t2}}\right) \left(\frac{T_{t4}}{T_{t3}}\right) \left(\frac{T_{t5}}{T_{t4}}\right) \left(\frac{T_{te}}{T_{t5}}\right) \tag{4.28}$$

or, in terms of component temperature parameters

$$T_{te} = T_0 \tau_r \tau_d \tau_c \tau_b \tau_t \tau_n. \tag{4.29}$$

In the ideal turbojet we assume that the diffuser and nozzle flows are adiabatic and so

$$T_{te} = T_0 \tau_r \tau_c \tau_b \tau_t = T_e \left(1 + \frac{\gamma - 1}{2} {M_e}^2\right) = T_e \tau_r \tau_c \tau_t. \tag{4.30}$$

From (4.30) we have the result

$$\frac{T_e}{T_0} = \tau_b = \frac{T_{t4}}{T_{t3}}. \tag{4.31}$$

This is the same result we deduced earlier in (4.15) when we analyzed the thermal efficiency. Actually it is more convenient to express the temperature ratio in terms of the all-important parameter $\tau_\lambda = T_{t4}/T_0$.

$$\frac{T_e}{T_0} = \frac{\tau_\lambda}{\tau_r \tau_c} \tag{4.32}$$

The reason is that τ_λ is a parameter that we would like to make as large as possible, but is limited by the highest temperature that can be tolerated by the turbine materials before they begin to lose strength and undergo creep. The maximum allowable turbine inlet temperature (and therefore the maximum design operating temperature) is one of the cycle variables that is essentially fixed when an engine manufacturer begins the development of a new engine. Enormous sums of money have been invested in turbine materials technology and turbine cooling schemes in an effort to enable jet engines to operate with as high a turbine inlet temperature as possible.

Our thrust formula is now

$$\frac{T}{P_0 A_0} = \frac{2\gamma}{\gamma - 1}(\tau_r - 1)\left((1+f)\left(\left(\frac{\tau_r \tau_c \tau_t - 1}{\tau_r - 1}\right)\frac{\tau_\lambda}{\tau_r \tau_c}\right)^{1/2} - 1\right). \tag{4.33}$$

The fuel/air ratio is found from

$$f = \frac{\tau_\lambda - \tau_r \tau_c}{\tau_f - \tau_\lambda}. \tag{4.34}$$

At this point it would appear that for fixed γ, and τ_f the thrust is a function of four variables.

$$\frac{T}{P_0 A_0} = F(\tau_r, \tau_c, \tau_\lambda, \tau_t) \tag{4.35}$$

But the turbine and compressor are not independent components. They are connected by a shaft and the work done across the compressor is the same as the work done across the

turbine. They are related by the work matching condition (4.6) repeated here in terms of the temperatures.

$$(\dot{m}_a + \dot{m}_f)\, C_P\, (T_{t4} - T_{t5}) = \dot{m}_a C_P\, (T_{t3} - T_{t2}) \tag{4.36}$$

For simplicity we have assumed the same value of C_p for the compressor and turbine. If we divide (4.36) by $C_p T_0$ then it becomes

$$(1 + f)\, \tau_\lambda\, (1 - \tau_t) = \tau_r\, (\tau_c - 1) \tag{4.37}$$

or

$$\tau_t = 1 - \frac{\tau_r\, (\tau_c - 1)}{(1 + f)\, \tau_\lambda} \tag{4.38}$$

where we have assumed $T_{t2} = T_{t0}$. The result (4.38) only assumes adiabatic flow in the inlet and no shaft losses. It is not tied to the other assumptions of the ideal cycle. The velocity ratio across the engine is now

$$\left(\frac{U_e}{U_0}\right)^2 = \frac{1}{(\tau_r - 1)} \left(\tau_\lambda - \tau_r\, (\tau_c - 1) - \frac{\tau_\lambda}{\tau_r \tau_c}\right) \tag{4.39}$$

where the fuel/air ratio has been neglected.

4.3 Maximum thrust ideal turbojet

How much compression should we use? If there is too little the engine is like a ramjet and may not produce enough thrust at low Mach number. If we use too much then the fuel flow has to be reduced to avoid raising the temperature above the "do not exceed" (redline) value of T_{t4}. The thrust and specific impulse of a typical ideal turbojet is shown in Figure 4.4. Recall that

$$\frac{I_{sp} g}{a_0} = \left(\frac{1}{f}\right) \left(\frac{1}{\gamma M_0}\right) \left(\frac{T}{P_0 A_0}\right). \tag{4.40}$$

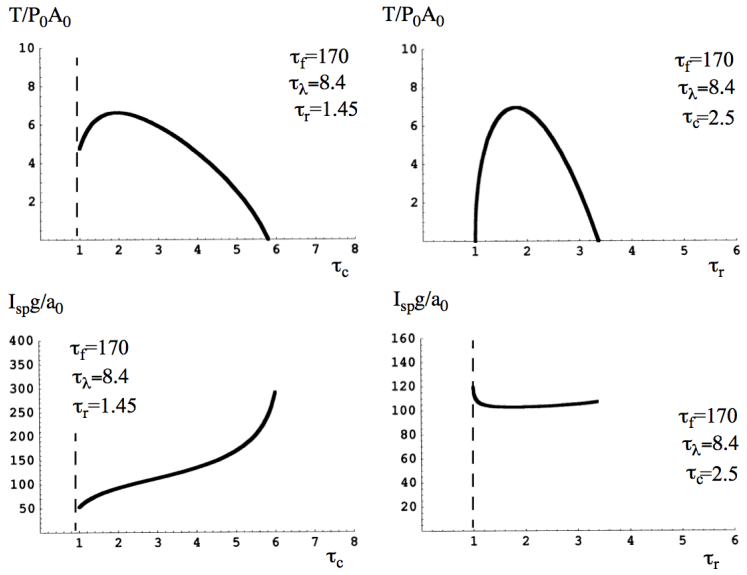

Figure 4.4: *Thrust and specific impulse curves for an ideal turbojet.*

It is clear from the upper left graph in Figure 4.4 that there is a choice of τ_c that maximizes the thrust for fixed values of the other three engine parameters. We can determine this compression ratio by maximizing $(U_e/U_0)^2$.

$$\frac{\partial}{\partial \tau_c}\left(\frac{U_e}{U_0}\right)^2 = \frac{1}{(\tau_r - 1)}\left(-\tau_r + \frac{\tau_\lambda}{\tau_r {\tau_c}^2}\right) = 0 \tag{4.41}$$

The maximum velocity ratio for the ideal turbojet occurs when

$$\tau_{c_{\text{maxthrust}}} = \frac{\sqrt{\tau_\lambda}}{\tau_r}. \tag{4.42}$$

Note that fuel shut-off and zero thrust occurs when $\tau_c = \tau_\lambda/\tau_r$. The relation (4.42) tells us a great deal about why engines look the way they do. An engine designed to cruise at low Mach number (a low value of τ_r) will be designed with a relatively large compressor generating a relatively high value of τ_c as indicated by (4.42). But as the flight Mach number increases the optimum compression decreases until at $\tau_r = \sqrt{\tau_\lambda}$ one would like to get rid of the compressor altogether and convert the engine to a ramjet. This also tells us something about the general trend of engine design with history. As higher temperature turbine materials and better cooling schemes have been developed over the years, newer engines tend to be designed with correspondingly higher compression ratios leading to higher specific

impulse and better fuel efficiency. Over the 40 year period since the introduction of the JT9D, allowable turbine inlet temperatures have increased over $1000F$.

One should note that (4.42) is not a particularly useful relationship for the design of an actual engine. This is partly because, strictly speaking, it only applies to the ideal cycle but mostly due to the fact that any real engine must operate effectively from take-off to cruise. If the compressor is rigorously designed to satisfy (4.42) at cruise then the engine will be seriously underpowered and inefficient at take-off when the desired compression is much larger. On the other hand if the compressor is too large, then the engine will tend to be over-designed and over-weight for cruise.

As (4.42) would indicate, this problem becomes more and more difficult to solve as the cruise Mach number of the engine increases. The J58 powered SR71 Blackbird cruises at Mach numbers greater than 3.

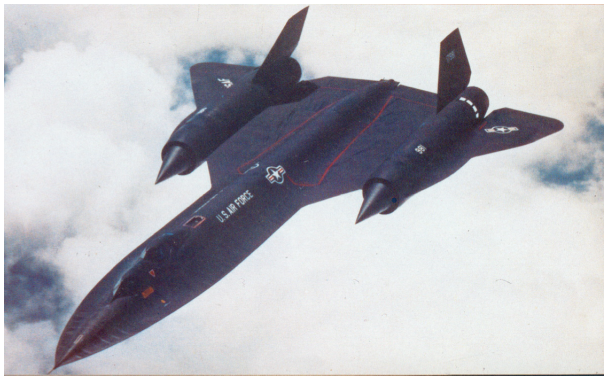

Figure 4.5: *The Mach 3+ SR71 Blackbird.*

The engine is designed to be a variable cycle system so that at cruise a large fraction of the inlet air bypasses the rotating machinery and enters the afterburner directly as it would in a ramjet. Despite this design the aircraft cannot take-off with a full load of fuel and has to be refueled in flight before beginning a mission. Another, unrelated reason for the partial fuel load at takeoff is that the braking power of the landing gear is too small for an emergency take-off abort with a full fuel load.

Designing a high Mach number engine for a supersonic transport faces the same problem. In an engine out situation the aircraft must be able to cruise subsonically to the nearest landing field and so the engine must be able to supply adequate thrust for long distances at subsonic Mach numbers.

4.4 Turbine-nozzle mass flow matching

The mass balance between the entrance of the turbine and the nozzle throat is

$$\begin{aligned} \dot{m}_4 &= \dot{m}_e \\ \frac{P_{t4}A_4}{\sqrt{\gamma RT_{t4}}} f\left(M_4\right) &= \frac{P_{t8}A_8}{\sqrt{\gamma RT_{t8}}} f\left(M_8\right). \end{aligned} \tag{4.43}$$

In general, the turbine is designed to provide a large pressure drop per stage. This is possible because of the favorable pressure gradient that stabilizes the boundary layers on the turbine airfoils. The result is a large amount of work per stage and this can be seen in the highly cambered, high lift shape of typical turbine airfoils shown in Figure 4.1. The large pressure drop across each stage implies that at some point near the entrance to the first stage turbine stator (also called the turbine nozzle) the flow is choked as indicated in Figure 4.1. At this point $A_4 f\left(M_4\right) = A_4^*$. The choked area occurs somewhere in the stator passage. Similarly for the vast range of practical engine operations the nozzle throat is also choked. Therefore the mass balance (4.43) can be written

$$\frac{P_{t4}A_4^*}{\sqrt{T_{t4}}} = \frac{P_{t8}A_8}{\sqrt{T_{t8}}}. \tag{4.44}$$

Under the assumption of an ideal cycle the turbine operates isentropically.

$$\frac{P_{t5}}{P_{t4}} = \left(\frac{T_{t5}}{T_{t4}}\right)^{\frac{\gamma}{\gamma-1}} \tag{4.45}$$

The skin friction losses in the nozzle duct are assumed to be negligible and the duct is adiabatic ($P_{t5} = P_{t8}$) and ($T_{t5} = T_{t8}$). Therefore

$$\tau_t = \frac{T_{t5}}{T_{t4}} = \left(\frac{A_4^*}{A_8}\right)^{\frac{2(\gamma-1)}{\gamma+1}}. \tag{4.46}$$

The temperature and pressure ratio across the turbine is determined entirely by the area ratio from the turbine inlet to the nozzle throat. As the fuel flow to the engine is increased or decreased with the areas fixed, the temperature drop across the turbine may increase or decrease changing the amount of work done while the temperature ratio remains constant. The turbine inlet and nozzle throat are choked over almost the entire practical range of engine operating conditions except during brief transients at start-up and shut-down.

4.5 Free-stream-compressor inlet flow matching

The mass balance between the free stream and the compressor face is

$$\begin{aligned} \dot{m}_a &= \dot{m}_2 \\ \frac{P_{t0}A_0}{\sqrt{T_{t0}}} f(M_0) &= \frac{P_{t2}A_2}{\sqrt{T_{t2}}} f(M_2). \end{aligned} \tag{4.47}$$

The flow from the free-stream to the compressor face is assumed to be adiabatic so that $T_{t2} = T_{t0}$. Thus the mass balance is

$$P_{t0}A_0 f(M_0) = P_{t2}A_2 f(M_2) \tag{4.48}$$

which we write as follows

$$f(M_2) = \frac{P_{t0}A_0 f(M_0)}{P_{t2}A_2}. \tag{4.49}$$

In terms of our engine parameters (4.49) is

$$f(M_2) = \left(\frac{1}{\pi_d}\right)\left(\frac{A_0}{A_2}\right) f(M_0). \tag{4.50}$$

We shall see that the fuel setting and nozzle throat area determine the value of $f(M_2)$ independently of what is happening in the free stream and inlet. In other words the engine demands a certain value of $f(M_2)$ and the gas dynamics of the inlet adjust A_0 and/or π_d in (4.50) to supply this value.

4.6 Compressor-turbine mass flow matching

The mass balance between the compressor face and the turbine inlet is

$$\begin{aligned} \dot{m}_2(1+f) &= \dot{m}_4 \\ (1+f)\frac{P_{t2}A_2}{\sqrt{T_{t2}}} f(M_2) &= \frac{P_{t4}A_4^*}{\sqrt{T_{t4}}}. \end{aligned} \tag{4.51}$$

We can write (4.51) in terms of our flow parameters as follows.

$$f(M_2) = \left(\frac{1}{1+f}\right)\frac{\pi_c\pi_b}{\sqrt{\tau_\lambda/\tau_r}}\left(\frac{A_4^*}{A_2}\right) \tag{4.52}$$

Under the ideal cycle assumption $\pi_b = 1$. Neglecting the fuel-air ratio, (4.52) becomes

$$f(M_2) = \frac{\pi_c}{\sqrt{\tau_\lambda/\tau_r}}\left(\frac{A_4^*}{A_2}\right). \tag{4.53}$$

Notice that we have written $f(M_2)$ on the left hand side of (4.53). In this point of view $f(M_2)$ is an outcome of the interaction of the nozzle with the turbine and compressor. The inlet behavior is then determined from (4.50).

4.7 Summary - engine matching conditions

In summary, the various component matching conditions needed to understand the operation of the turbojet in order, from the nozzle to the inlet are as follows.

$$\tau_t = \left(\frac{A_4^*}{A_8}\right)^{\frac{2(\gamma-1)}{\gamma+1}} \tag{4.54}$$

$$\tau_c - 1 = \frac{\tau_\lambda}{\tau_r}(1-\tau_t) \tag{4.55}$$

$$f(M_2) = \frac{\pi_c}{\sqrt{\tau_\lambda/\tau_r}}\left(\frac{A_4^*}{A_2}\right) \tag{4.56}$$

$$f(M_2) = \left(\frac{1}{\pi_d}\right)\left(\frac{A_0}{A_2}\right) f(M_0) \tag{4.57}$$

The quantity A_0 in (4.57) is the area of the external stream tube of air captured by the engine. At first this seems like a vaguely defined quantity. In fact it is precisely determined by the engine pumping characteristics as we shall see shortly.

4.7.1 Example - turbojet in supersonic flow with an inlet shock

A turbojet operates supersonically at $M_0 = 3$ and $T_{t4} = 1944\,K$. The compressor and turbine polytropic efficiencies are $\eta_{pc} = \eta_{pt} = 1$. At the condition shown, the engine operates semi-ideally with $\pi_b = \pi_n = 1$ but $\pi_d \neq 1$ and with a simple convergent nozzle. The relevant areas are $A_1/A_2 = 2$, $A_2/A_4^* = 14$ and $A_e/A_4^* = 4$. Supersonic flow is established at the entrance to the inlet with a normal shock downstream of the inlet throat. This type of inlet operation is called supercritical and will be discussed further in a later section.

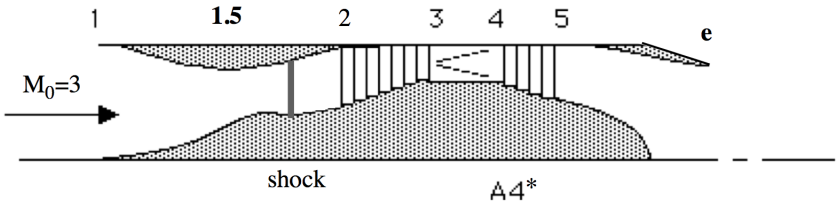

Figure 4.6: *Supersonic turbojet with inlet shock.*

1) Sketch the distribution of stagnation pressure, P_t/P_{t0} and stagnation temperature, T_t/T_{t0} through the engine. Assign numerical values at each station.

Solution - Note that $f(3) = 0.236$, $T_{t0} = 605\,K$ and

$$\frac{A_e}{A_1} = \left(\frac{A_e}{A_4^*}\right)\left(\frac{A_4^*}{A_2}\right)\left(\frac{A_2}{A_1}\right) = \frac{4}{14}\left(\frac{1}{2}\right) = 0.143. \tag{4.58}$$

We need to determine π_c, $f(M_2)$ and π_d. The analysis begins at the nozzle where the flow is choked. Choking at the turbine inlet and nozzle determines the turbine temperature and pressure ratio.

$$\tau_t = \left(\frac{A_4^*}{A_e}\right)^{\frac{2(\gamma-1)}{\gamma+1}} = \left(\frac{1}{4}\right)^{\frac{1}{3}} = 0.63 \tag{4.59}$$

$$\pi_t = \tau_t{}^{\frac{\gamma}{\gamma-1}} = 0.63^{3.5} = 0.198 \tag{4.60}$$

Matching turbine and compressor work gives the compressor temperature and pressure ratio.

$$\tau_c = 1 + \frac{\tau_\lambda}{\tau_r}(1 - \tau_t) = 1 + \frac{1944}{605}(1 - 0.63) = 2.19 \tag{4.61}$$

$$\pi_c = \tau_c{}^{\frac{\gamma}{\gamma-1}} = 2.19^{3.5} = 15.54 \tag{4.62}$$

Now the Mach number at the compressor face is determined.

$$f\left(M_2\right) = \frac{A_4^*}{A_2}\left(\frac{\tau_r}{\tau_\lambda}\right)^{1/2}\pi_c\pi_b = \frac{A_4^*}{A_2}\left(\frac{605}{1944}\right)^{1/2}15.54 = \frac{A_4^*}{A_2}8.67 = \frac{8.67}{14} = 0.62 \tag{4.63}$$

Use free-stream-compressor-mass-flow matching to determine the stagnation pressure loss across the inlet.

$$\pi_d = \frac{A_0 f\left(M_0\right)}{A_2 f\left(M_2\right)} = 2 \times \frac{0.236}{0.62} = 0.76 \tag{4.64}$$

Now determine the stagnation pressure ratio across the engine.

$$\frac{P_{te}}{P_{t0}} = \pi_d\pi_c\pi_t = 0.76\left(15.54\right)\left(0.198\right) = 2.34 \tag{4.65}$$

Now the exit static pressure ratio is determined

$$\frac{P_e}{P_0} = \frac{P_{te}}{P_{t0}}\left(\frac{1+\frac{\gamma-1}{2}{M_0}^2}{1+\frac{\gamma-1}{2}{M_e}^2}\right)^{\frac{\gamma}{\gamma-1}} = 2.34\left(\frac{2.8}{1.2}\right)^{3.5} = 45.4 \tag{4.66}$$

as is the stagnation temperature ratio,

$$\frac{T_{te}}{T_{t0}} = \frac{\tau_\lambda}{\tau_r}\tau_t = \frac{1944}{605}0.63 = 2.02 \tag{4.67}$$

static temperature ratio,

$$\frac{T_e}{T_0} = \frac{T_{te}}{T_{t0}}\left(\frac{1+\frac{\gamma-1}{2}{M_0}^2}{1+\frac{\gamma-1}{2}{M_e}^2}\right) = 2.02\left(\frac{2.8}{1.2}\right) = 4.71 \tag{4.68}$$

velocity ratio,

$$\frac{U_e}{U_0} = \frac{M_e}{M_0}\left(\frac{T_e}{T_0}\right)^{1/2} = \frac{1}{3}(4.71)^{1/2} = 0.723 \tag{4.69}$$

and thrust

$$\begin{aligned}\frac{T}{P_0 A_0} &= \gamma {M_0}^2 \left(\frac{U_e}{U_0} - 1\right) + \frac{A_e}{A_0}\left(\frac{P_e}{P_0} - 1\right) \\ \frac{T}{P_0 A_0} &= 1.4 \times 9 \times (0.723 - 1) + 0.143\,(45.4 - 1) = -3.49 + 6.35 = 2.86.\end{aligned} \tag{4.70}$$

At this point we have all the information we need (and then some) to answer the problem. The pressure ratios are

$$\begin{aligned}\frac{P_{t2}}{P_{t0}} &= \pi_d = 0.76 \\ \frac{P_{t3}}{P_{t0}} &= \pi_d \pi_c = 11.8 \\ \frac{P_{t4}}{P_{t0}} &= \pi_d \pi_c \pi_b = 11.8 \\ \frac{P_{te}}{P_{t0}} &= \pi_d \pi_c \pi_b \pi_t = 2.34\end{aligned} \tag{4.71}$$

and the relevant temperature ratios are

$$\begin{aligned}\frac{T_{t2}}{T_{t0}} &= \tau_d = 1 \\ \frac{T_{t3}}{T_{t0}} &= \tau_d \tau_c = 2.19 \\ \frac{T_{t4}}{T_{t0}} &= \tau_d \tau_c \tau_b = \frac{1944}{605} = 3.21 \\ \frac{T_{te}}{T_{t0}} &= \tau_d \tau_c \tau_b \tau_t = 2.02.\end{aligned} \tag{4.72}$$

The stagnation pressure and temperature ratios through the engine are sketched in Figure 4.7.

At this relatively high Mach number, the nozzle exit pressure is far higher than the ambient pressure. That suggests that it should be possible to increase the thrust by adding an

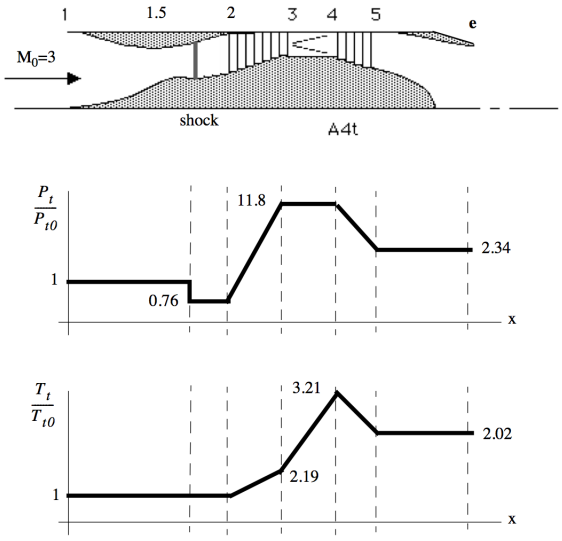

Figure 4.7: *Stagnation temperature and pressure through a supersonic turbojet.*

expansion section to the nozzle. Let's see how much improvement might be possible. The thrust is

$$\frac{T}{P_0 A_0} = \gamma {M_0}^2 \left(\frac{M_e}{M_0} \sqrt{\frac{T_e}{T_0}} - 1 \right) + \frac{A_e}{A_0} \left(\frac{P_e}{P_0} - 1 \right). \tag{4.73}$$

Let's express (4.73) in terms of the nozzle exit Mach number assuming isentropic flow in the nozzle.

$$\begin{aligned} &\frac{T}{P_0 A_0} = \gamma {M_0}^2 \left(\frac{M_e}{M_0} \sqrt{\frac{T_{te}}{T_0} \left(\frac{T_e}{T_{te}} \right)} - 1 \right) + \frac{A_8}{A_0} \frac{A_e}{A_8} \left(\frac{P_{te}}{P_0} \frac{P_e}{P_{te}} - 1 \right) \\ &\textit{or} \\ &\frac{T}{P_0 A_0} (M_e) = \gamma {M_0}^2 \left(\frac{M_e}{M_0} \sqrt{\frac{T_{te}}{T_0} \left(\frac{1}{1 + \frac{\gamma - 1}{2} {M_e}^2} \right)} - 1 \right) + \\ &\frac{A_8}{A_0} \frac{1}{f(M_e)} \left(\frac{P_{te}}{P_0} \left(\frac{1}{1 + \frac{\gamma - 1}{2} {M_e}^2} \right)^{\frac{\gamma}{\gamma - 1}} - 1 \right) \end{aligned} \tag{4.74}$$

The latter version of the thrust equation in (4.74) can be considered to be just a function of the Mach number for fixed stagnation pressure and temperature leaving the turbine.

Equation (4.74) is plotted in Figure 4.8 for selected values of pressure, temperature, and area ratio.

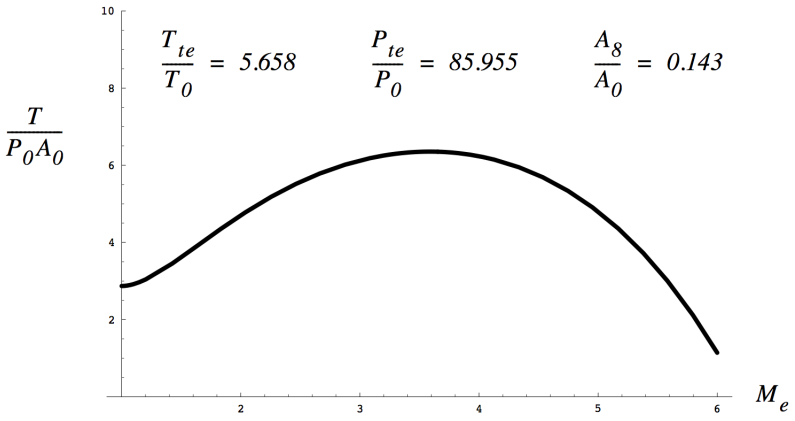

Figure 4.8: *Thrust variation with nozzle exit Mach number for example 4.7.1*

At this flight Mach number the thrust can be nearly doubled using the nozzle. The maximum thrust occurs when the nozzle is fully expanded to $P_e = P_0$. The corresponding exit Mach number is $M_e = 3.585$ at a nozzle area ratio of $A_e/A_8 = 7.34$. The overall engine area ratio is $A_e/A_1 = (A_e/A_8)\,(A_8/A_0) = 1.05$ which suggests that the expansion could be added without much increase in the frontal area that the engine presents to the flow and therefore without much drag penalty.

For an engine designed for a lower flight Mach number the performance gain by fully expanding the nozzle is relatively less. For a commercial engine designed to fly at subsonic Mach numbers the improvement is quite small and usually not worth the additional weight required to fully expand the nozzle.

4.8 How does a turbojet work?

The answer to this question lies in the various matching conditions that must be satisfied between engine components. These are mainly the requirements that the mass flow in and out of a component must be accommodated by the neighboring components and the work taken out of the flow by the turbine must equal the work done on the flow by the compressor. The analysis is simplified by the fact that under most practical operating conditions the nozzle and turbine inlet are choked. The rule of thumb, when trying to understand engine behavior, is to begin at the nozzle and work forward finishing with the inlet.

The total temperature ratio across the turbine is fixed by the turbine and nozzle choked areas. As a result, the turbine tends to operate at a single point. For example, if the pilot pushes the throttle forward, the turbine inlet temperature will go up and the temperature exiting the turbine will go up, but not as much. This leads to an increase in the temperature drop across the turbine. More work is taken out of the flow and the engine revs up while τ_t remains fixed. There are some variable cycle engine concepts that use a variable area turbine (VAT) to improve performance but the temperature and materials problems associated with movement of the turbine inlet vane make this very difficult to implement.

Many engines, especially military engines, designed to operate over a wide altitude and Mach number flight envelope, do incorporate variable area nozzles.

4.8.1 The compressor operating line

Now eliminate τ_λ/τ_r between (4.55) and (4.56) , using

$$\pi_c = {\tau_c}^{\frac{\gamma}{\gamma-1}}. \tag{4.75}$$

The result is

$$\frac{\pi_c}{\left({\pi_c}^{\frac{\gamma-1}{\gamma}} - 1\right)^{1/2}} = \left(\frac{1}{1 - \left(\frac{A_4^*}{A_8}\right)^{\frac{2(\gamma-1)}{\gamma+1}}}\right)^{1/2} \left(\frac{A_2}{A_4^*}\right) f\left(M_2\right). \tag{4.76}$$

Equation (4.76) defines the compressor operating line on a plot of π_c versus $f\left(M_2\right)$. Note that the denominator on the left hand side represents a relatively weak dependence on π_c except at unrealistically low values of π_c where the denominator can become singular. So, to a rough approximation (4.76) defines a nearly straight line relationship between π_c and $f\left(M_2\right)$. Equation (4.76) is sketched below.

Still missing from our understanding of turbojet operation is the relationship between the compressor temperature and pressure rise and the actual compressor speed. To determine this we will need to develop a model of the compressor aerodynamics.

4.8.2 The gas generator

The combination of compressor, burner and turbine shown below is called the gas generator.

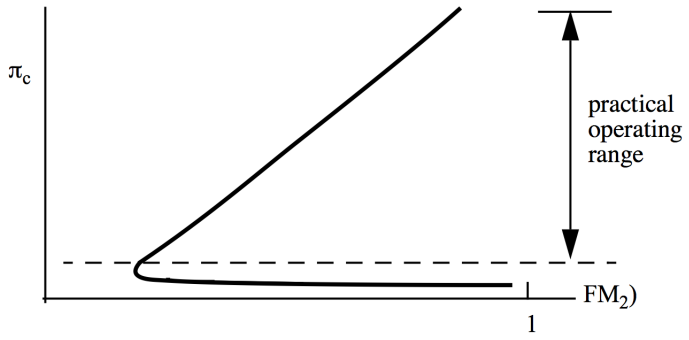

Figure 4.9: *Schematic of the compressor operating line Equation* (4.76).

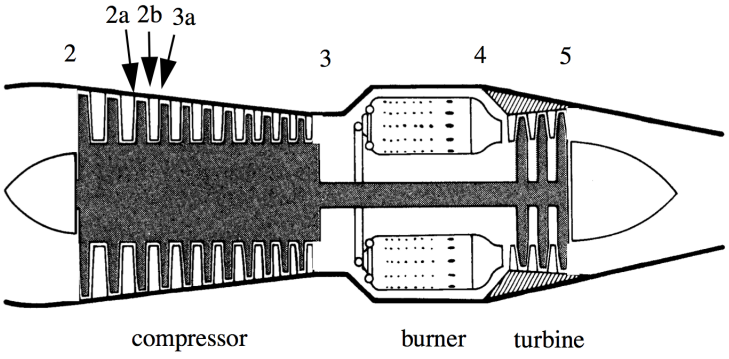

Figure 4.10: *Gas generator with imbedded station numbers.*

Compressor performance is characterized in terms of the compressor map which describes the functional relationship between compressor pressure ratio, mass flow and compressor speed. The compressor map from a J85 turbojet is shown below.

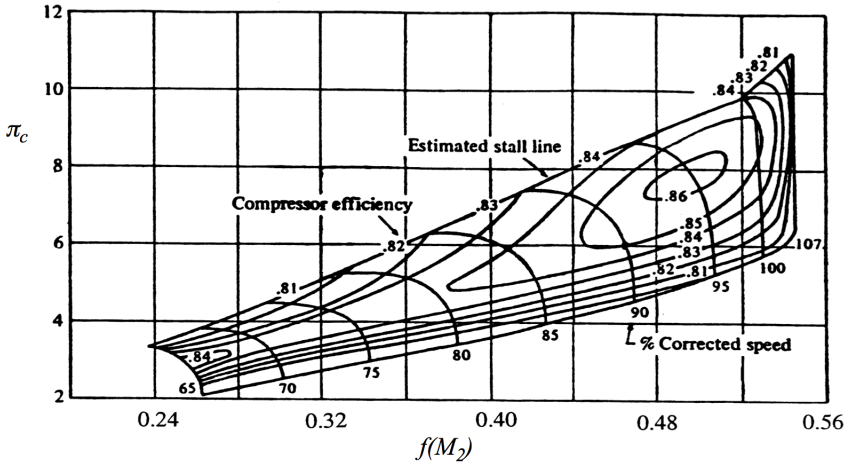

Figure 4.11: *Compressor map from a J-85 turbojet.*

In general the pressure ratio increases with increasing compressor rotation speed. At a given rotation speed the pressure ratio goes up as $f(M_2)$ is decreased. This latter behavior can be understood in terms of increasing relative angle of attack of the air flowing over the compressor blades leading to increased blade lift as the axial speed of the flow decreases. More will be said on this point later.

4.8.3 Corrected weight flow is related to $f(M_2)$.

Industry practice is to correct the mass flow for the effects of altitude and flight speed. One defines the corrected weight flow as

$$\dot{w}_c = \dot{m}_a g \frac{\sqrt{\theta}}{\delta} \tag{4.77}$$

where

$$\begin{aligned} \theta &= \frac{T_{t2}}{T_{SL}} \\ \delta &= \frac{P_{t2}}{P_{SL}}. \end{aligned} \tag{4.78}$$

The quantities T_{SL} and P_{SL} refer to sea level standard pressure and temperature. In English units

$$\begin{aligned} T_{SL} &= 518.67R \\ P_{SL} &= 2116.22\text{pounds/ft}^2. \end{aligned} \tag{4.79}$$

The gas constant for air is

$$R_{air} = 1710.2\text{ft}^2/\left(\text{sec}^2 - R\right). \tag{4.80}$$

We can write (4.77) as

$$\dot{w}_c = \dot{m}g\frac{\sqrt{\theta}}{\delta} = \left(\frac{1}{\left(\frac{\gamma+1}{2}\right)^{\frac{\gamma+1}{2(\gamma-1)}}}\frac{\gamma g P_{SL}}{\sqrt{\gamma R T_{SL}}}\right) A f\left(M\right). \tag{4.81}$$

Note that the quantity in parentheses is a constant. Thus the corrected mass flow is proportional to $f\left(M_2\right)$. At the compressor face

$$\dot{w}_c = 49.459 A_2 f\left(M_2\right)\text{pounds/sec} \tag{4.82}$$

where A_2 is expressed in terms of square feet. Throughout this course $f\left(M_2\right)$ will be the preferred measure of reduced mass flow through the compressor instead of the usual corrected weight flow. This quantity has several significant advantages. It is dimensionless, independent of compressor size and for practical purposes lies in a fairly narrow range of values that is more or less the same for all engines. The compressor entrance Mach number, M_2, is generally restricted to lie in the range between 0.2 and 0.6. Unusually low values of $f\left(M_2\right)$ imply that the engine diameter is too large. If $f\left(M_2\right)$ gets too large ($f\left(M_2\right)$ approaches one), the compressor blade passages begin to choke and stagnation pressure losses increase dramatically.

The compressor map can be regarded as a cross plot of three independent functions. The first is determined by the compressor-turbine inlet matching function (4.52). Rearranging variables (4.52) becomes

$$\pi_c = F_1\left(\frac{\tau_\lambda}{\tau_r}, f\left(M_2\right)\right) = \left(\frac{\left(1+f\right)}{\pi_b}\frac{A_2}{A_4^*}\right)\sqrt{\frac{\tau_\lambda}{\tau_r}} f\left(M_2\right) \tag{4.83}$$

where the contribution of the fuel/air ratio and burner pressure loss has been included. The factor in parentheses in (4.83) is approximately constant.

The second function relates the compressor efficiency to the pressure ratio and mass flow.

$$\eta_c = F_2\left(\pi_c, f\left(M_2\right)\right) \tag{4.84}$$

This is a function that can only be determined empirically through extensive compressor testing. The contours of constant efficiency in Figure 4.11 illustrate a typical case.

The third function relates the pressure ratio and mass flow to the rotational speed of the compressor. This function is of the form

$$\pi_c = F_3\left(\frac{M_{b0}}{\sqrt{\tau_r}}, f\left(M_2\right)\right) \tag{4.85}$$

where

$$M_{b0} = \frac{U_{blade}}{\sqrt{\gamma R T_0}} \tag{4.86}$$

is the compressor blade Mach number based on the free stream speed of sound and U_{blade} is the blade speed. Equation (4.85) is shown as lines of constant percent corrected speed in Figure 4.11.

4.8.4 A simple model of compressor blade aerodynamics

An accurate model of (4.85) can be derived from a detailed computation of the aerodynamics of the flow over the individual compressor blade elements. This is beyond the scope of this course but we can develop a simplified model of blade aerodynamics that reproduces the most important features of the relation between pressure ratio, mass flow and blade speed illustrated by the family of speed curves in Figure 4.11. Figure 4.12 shows the flow through a typical compressor stage called an imbedded stage. The stations labeled in Figure 4.12 are 2a (the space just ahead of the compressor rotor), 2b (the space between the rotor and stator) and 3a (the space after the stator and just ahead of the next rotor). The

velocity vectors at various points in the stage are indicated in Figure 4.12. The vector relationships are

$$W_{2a} = C_{2a} - U_{blade}$$
$$W_{2b} = C_{2b} - U_{blade}. \tag{4.87}$$

The axial velocity component is c_z. Tangential components are $c_{2a\theta}$ and $c_{2b\theta}$. Flow angles in non-moving coordinates are α_{2a}, α_{2b} and α_{3a}. Flow angles in moving coordinates are β_{2a}, β_{2b} and β_{3a}. The assumptions of the model are

$$\begin{aligned} &c_z \, is \, constant \, through \, the \, engine \\ &All \, stages \, are \, identical \\ &\alpha_{2a} = \alpha_{3a} \, and \, C_{2a} = C_{3a}. \end{aligned} \tag{4.88}$$

In addition, radial variations in the flow along the compressor blade elements are ignored (c_r is negligible). This is called a strip model of the compressor where the blades are approximated by an infinite 2-D cascade.

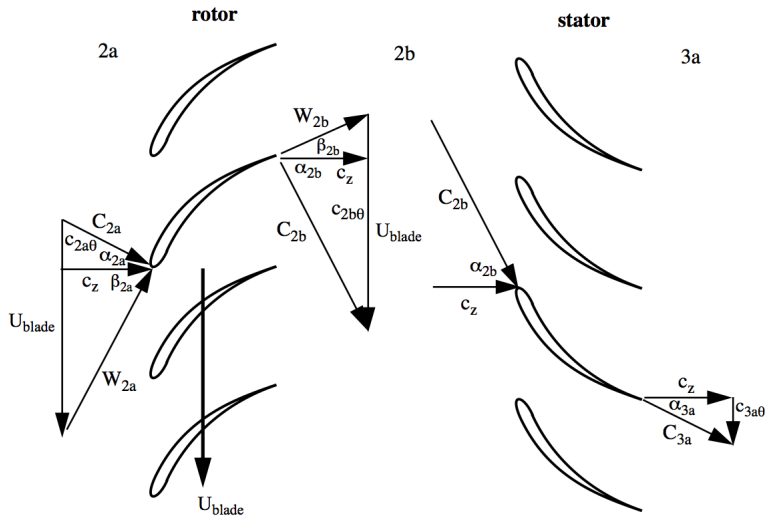

Figure 4.12: *Flow geometry in an imbedded stage.*

The basic aerodynamic principle utilized in this model is that the flow coming off the trailing edge of the compressor airfoils is guided by the wing surface and leaves the wing at the angle of the trailing edge. In contrast, the flow angle at the leading edge varies with

the axial flow speed and blade speed while the airfoil lift varies accordingly as suggested in Figure 4.13.

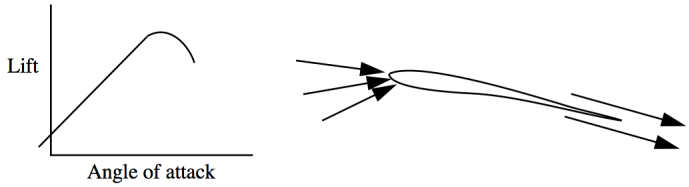

Figure 4.13: *Effect of angle of attack on airfoil lift.*

When the airfoil is one element of a cascade the guiding effect of the trailing edge is enhanced. One of the design parameters of a compressor cascade is the solidity which is defined as the blade chord divided by the vertical distance between compressor blade trailing edges. If the solidity is low (blades far apart) then the guiding effect of the cascade on the flow is reduced, the trailing edge flow is susceptible to stall (flow separation) and the work capability of the compressor is reduced. If the solidity gets too high then the drag losses of the compressor become excessive as does the compressor weight. A solidity of approximately one is fairly typical.

The tangential velocity components are

$$\begin{aligned} c_{2a\theta} &= c_z Tan\left(\alpha_{2a}\right) \\ c_{2b\theta} &= U_{blade} - c_z Tan\left(\beta_{2b}\right). \end{aligned} \tag{4.89}$$

The tangential velocity change of the flow induced by the tangential component of the lift force acting on the compressor blades is

$$\Delta c_\theta = c_{2b\theta} - c_{2a\theta} = U_{blade} - c_z Tan\left(\beta_{2b}\right) - c_z Tan\left(\alpha_{2a}\right). \tag{4.90}$$

Note that there is a considerable axial force component on the stage due to the pressure rise that the flow experiences as the stator removes the tangential velocity change. An energy balance on a control volume that encloses the rotor can be used to show that the work done across the rotor is

$$\dot{m}_a \left(h_{t2b} - h_{t2a}\right) = \bar{F} \cdot \bar{U}_{blade}. \tag{4.91}$$

In terms of the tangential velocity change

$$\dot{m}_a \left(h_{t2b} - h_{t2a}\right) = \dot{m}_a \Delta c_\theta U_{blade}. \tag{4.92}$$

This is a key equation that connects the work done across a cascade with the speed of the blade and the tangential velocity change. Note that all of the stage work is done by the rotor and so we can write

$$\left(h_{t3a} - h_{t2a}\right) = \Delta c_\theta U_{blade}. \tag{4.93}$$

Assume there are n identical stages. Then the enthalpy rise across the compressor is

$$\left(h_{t3} - h_{t2}\right) = n \left(\Delta c_\theta\right) U_{blade}. \tag{4.94}$$

Assume constant heat capacity and divide (4.94) by $C_p T_0$.

$$\tau_r \left(\tau_c - 1\right) = n \left(\gamma - 1\right) \frac{U_{blade}^2}{\gamma R T_0} \left(\frac{\Delta c_\theta}{U_{blade}}\right) \tag{4.95}$$

Solve for τ_c

$$\tau_c = 1 + n \left(\gamma - 1\right) \left(\frac{M_{b0}}{\sqrt{\tau_r}}\right)^2 \psi \tag{4.96}$$

where the stage load factor

$$\psi = \frac{\Delta c_\theta}{U_{blade}} \tag{4.97}$$

is introduced. The stage load factor compares the tangential velocity change of the flow across the rotor to the rotor speed. The upper limit of this parameter is about 1/4 and is a measure of the maximum pressure rise achievable in a stage. Equation (4.96) is expressed in terms of the basic compressor speed parameter introduced in (4.85). Now we need to express the stage load factor in terms of this speed parameter and $f\left(M\right)$. From (4.90).

$$\psi = 1 - \frac{c_z}{U_{blade}} \left(Tan\left(\beta_{2b}\right) + Tan\left(\alpha_{2a}\right)\right) \tag{4.98}$$

Equation (4.98) brings into play a second dimensionless velocity ratio, the flow coefficient which compares the flow axial speed to the blade speed.

$$\phi = \frac{c_z}{U_{blade}} \tag{4.99}$$

The basic aerodynamic design of the compressor boils down to two dimensionless velocity ratios, the flow coefficient and the stage load factor. Note that (4.98) is written in terms of the trailing edge flow angles. In our simple model these angles are assumed to be constant and so the stage load factor is a simple linear function of the flow coefficient. Now

$$\tau_c = 1 + n\left(\gamma - 1\right)\left(\frac{M_{b0}}{\sqrt{\tau_r}}\right)^2 \left(1 - \phi\left(Tan\left(\beta_{2b}\right) + Tan\left(\alpha_{2a}\right)\right)\right). \tag{4.100}$$

At station 2 where the Mach number is relatively low $f\left(M_2\right)$ can be approximated by

$$f\left(M_2\right) \cong \left(\frac{\gamma+1}{2}\right)^{\frac{\gamma+1}{2(\gamma-1)}} \frac{c_z}{\sqrt{\gamma R T_2}} \cong \left(\frac{\gamma+1}{2}\right)^{\frac{\gamma+1}{2(\gamma-1)}} \frac{U_{blade}}{\sqrt{\gamma R T_2}} \left(\frac{c_z}{U_{blade}}\right). \tag{4.101}$$

So to a reasonable approximation

$$\phi = \frac{1}{\left(\frac{\gamma+1}{2}\right)^{\frac{\gamma+1}{2(\gamma-1)}}} \frac{f\left(M_2\right)}{\left(\frac{M_{b0}}{\sqrt{\tau_r}}\right)}. \tag{4.102}$$

Finally our aerodynamic model of the compressor is

$$\tau_c = 1 + n\left(\gamma - 1\right)\left(\frac{M_{b0}}{\sqrt{\tau_r}}\right)^2 - \frac{n\left(\gamma - 1\right)}{\left(\frac{\gamma+1}{2}\right)^{\frac{\gamma+1}{2(\gamma-1)}}} \left(Tan\left(\beta_{2b}\right) + Tan\left(\alpha_{2a}\right)\right)\left(\frac{M_{b0}}{\sqrt{\tau_r}}\right) f\left(M_2\right). \tag{4.103}$$

The pressure ratio is generated from (4.103) using $\pi_c = {\tau_c}^{\gamma(\gamma-1)}$. A polytropic efficiency of compression (defined below) can also be included. Figure 4.14 shows a cross plot of (4.83) and (4.103) for a typical case.

The model does a reasonable job of reproducing the inverse relationship between pressure ratio and blade speed although the curvature of the speed characteristics (lines of constant $M_{b0}/\sqrt{\tau_r}$) is opposite to that observed in Figure 4.9. This is because the model does not include viscous effects at all. Such effects as the deviation in trailing edge flow angle due

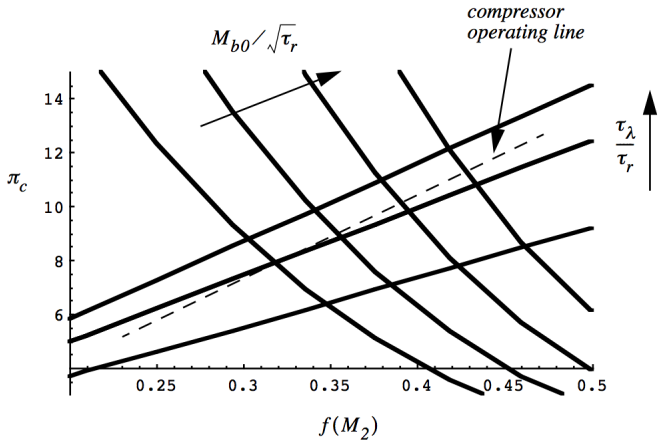

Figure 4.14: *Compressor map generated by the strip model.*

to boundary layer thickening at high pressure ratio are not accounted for. At high pressure ratio and low flow speed the trailing edge flow eventually separates and the compressor stalls. This is indicated in Figure 4.11 as the estimated stall line. Modern engine control systems are designed to prevent the engine from stalling although some trailing edge separation can be tolerated. Substantial stall can lead to a condition called surge where large flow oscillations can do substantial damage to the engine. In the most extreme case the high pressure in the engine cannot be maintained and the internal gas may be released in an nearly explosive manner similar to the release from a burst pressure vessel with gas (and possibly engine parts) coming out of the inlet.

4.8.5 Turbojet engine control

The two main inputs to the control of the engine are:

1) The throttle, which we can regard as controlling T_{t4}, or equivalently at a fixed altitude, τ_λ and,

2) the nozzle throat area A_8.

The logic of the engine operation is as follows.

Case 1- Increase A_8 keeping τ_λ constant. Equation (4.54) determines τ_t which is used in (4.55) to determine τ_c. This determines π_c through (4.75) and $f\left(M_2\right)$ through (4.56). Given $f\left(M_2\right)$, the combination $\left(1/\pi_d\right)\left(A_0/A_2\right)$ is now known. This quantity completely specifies the inlet operation. The increase of A_8 leads to an increase in both $f\left(M_2\right)$ and π_c due

to an increase in compressor speed as indicated on the compressor map. The compressor operating point moves along a constant τ_λ/τ_r characteristic.

Case 2 - Increase τ_λ keeping A_8 constant. The logic in this case is very similar to case 1 except that the compressor-turbine work matching condition, has $\tau_t = constant$. This determines π_c through (4.75) and $f(M_2)$ through the (in this case fixed) compressor operating line (4.76). Given $f(M_2)$ then $(1/\pi_d)(A_0/A_2)$ is known and the inlet operation is defined. As in case 1 the change of $f(M_2)$ and π_c is achieved by an increase in compressor speed according to the compressor map. The compressor operating point moves along the operating line (4.76) which crosses the constant τ_λ/τ_r characteristics as shown in Figure 4.12.

4.8.6 Inlet operation

There are two main points to take away from the previous discussion of engine control. The first is that to understand engine operation one begins at the nozzle and works forward. The other is that the inlet flow is essentially defined by the engine operating point through the value of $f(M_2)$. In effect, the engine sets the back pressure for the inlet. This is the fundamental purpose of the inlet; to provide the air mass flow to the engine at the Mach number dictated by the engine operating point with as small a stagnation pressure loss as possible. This whole mechanism is referred to as the pumping characteristic of the engine.

Lets look at the various possible modes of inlet operation recalling the discussion of capture area in Chapter 2. Figure 4.15 depicts an engine in subsonic flow. Shown is the variation in inlet flow as the nozzle throat A_8 area is increased with τ_λ held constant.

The Mach number at station 2 entering the compressor increases from top to bottom in Figure 4.15. In the top four figures (a, b, c, d) there is no inlet shock and so, neglecting skin friction, the only way the increase in the Mach number at station 2 can be accommodated according to the matching condition (4.57) is for the capture area A_0 to increase leading to an increase in the air mass flow through the engine with $\pi_d = 1$.

As A_8 is increased further the inlet eventually chokes (this is the situation shown as case d). The condition for inlet choking is determined from the mass balance between the inlet throat $A_{1.5}$ and compressor face A_2.

$$\frac{P_{t2}A_2}{\sqrt{T_{t2}}}f(M_2) = \frac{P_{t1.5}A_{1.5}}{\sqrt{T_{t1.5}}}f(M_{1.5}) \tag{4.104}$$

Neglecting skin friction and heat transfer, the flow from $A_{1.5}$ to A_2 is adiabatic and isen-

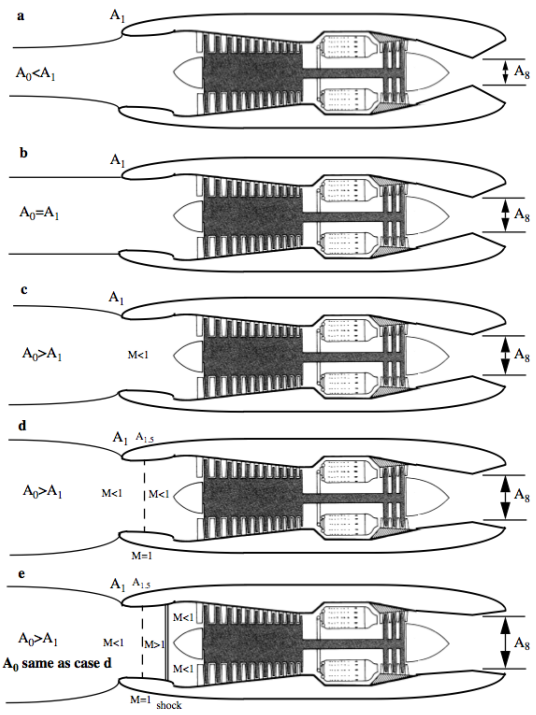

Figure 4.15: *Inlet behavior with increasing nozzle throat area in subsonic flow.*

tropic. The mass balance (4.104) becomes

$$A_2 f\left(M_2\right) = A_{1.5} f\left(M_{1.5}\right). \tag{4.105}$$

The inlet chokes when $f\left(M_{1.5}\right) = 1$. This occurs when

$$f\left(M_2\right)|_{inlet\,choking} = \frac{A_{1.5}}{A_2}. \tag{4.106}$$

If the nozzle area is increased beyond this point there is no change in A_0, the air mass flow remains fixed and a shock wave forms downstream of the inlet throat (this is depicted as case e in Figure 4.15). The matching condition (4.57) is satisfied by increasing stagnation pressure loss across the shock ($\pi_d < 1$). The shock becomes stronger as the Mach number at the compressor face is further increased. This whole mechanism is referred to as the pumping characteristic of the engine. Once a shock begins to form in the inlet, the engine performance (thrust and efficiency) begins to drop off rather rapidly. A well designed system is designed to avoid shock formation.

In supersonic flow the inlet is routinely designed to accommodate an inlet shock and/or a system of external shocks that may be needed to decelerate a high Mach number flow to the subsonic value at the compressor face dictated by the engine pumping characteristics. The basic operation of the inlet throat in supersonic flow is similar to that shown in Figure 4.15. Stagnation pressure losses may include fixed losses due to the external shock system as well as variable losses, due to the movement of the inlet shock. The figure below depicts the effect of increasing A_8 on the inlet flow for an engine operating in a supersonic stream.

In case a the Mach number at station 2 is low enough so that the Mach number at station 1 is less than the Mach number behind the normal shock ahead of the inlet as determined by A_2/A_1. The inlet operation is said to be sub-critical and after the system of oblique and normal shocks over the center body, the flow into the inlet is all subsonic . The inlet pressure ratio π_d is less than one due to the oblique and normal shocks. As the nozzle is opened up, the air mass flow into the engine increases with π_d approximately constant (exactly constant if the inlet is planar as opposed to axisymmetric). When the Mach number at station 2 has increased to the point where the Mach number at station 1 is just slightly less than the Mach number behind the normal shock, the normal shock will be positioned just ahead of the inlet lip and the inlet operation is said to be critical. The Mach number between stations 1 and 2 is all subsonic.

Further increasing A_8 leads to *starting* of the inlet flow and shock formation downstream of $A_{1.5}$. If the nozzle is opened up still more the engine will demand increasing values of $f\left(M_2\right)$. In this case the mass flow through the inlet can no longer increase and the mass flow

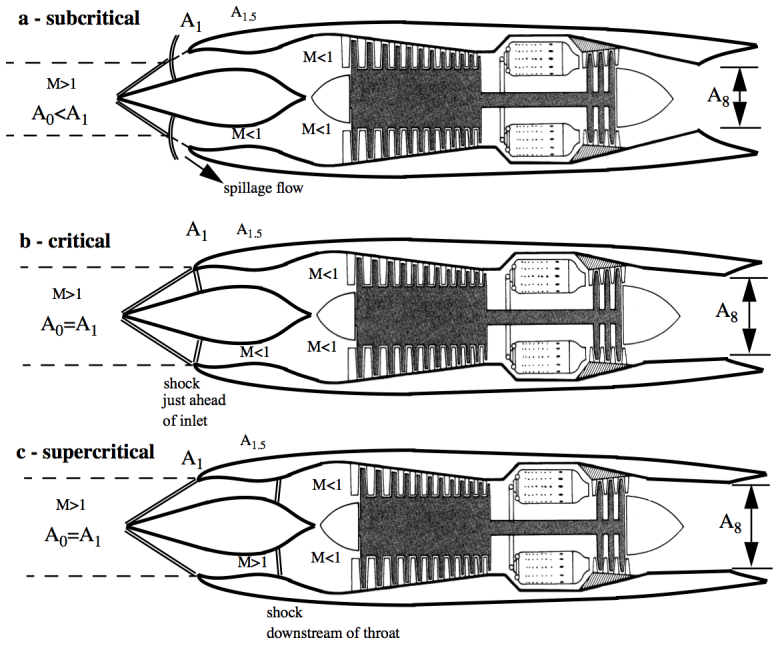

Figure 4.16: *Inlet behavior with increasing nozzle throat area in supersonic flow.*

balance between the free stream and compressor face (4.57) is satisfied through decreasing values of π_d (supercritical operation) due to downstream movement of the shock to higher shock Mach numbers. Similar inlet behavior occurs with fuel throttling. The shadowgraph photos in Figure 4.17 illustrate sub and supercritical flow on an axisymmetric spike inlet. A final point to be made here is to remind ourselves of the artificial nature of the ideal turbojet cycle which assumes $\pi_d = 1$. The first step toward a more realistic supersonic engine is to allow the inlet the freedom to accommodate some stagnation pressure loss. Just as in the ramjet cycle the inlet plays a crucial role in the stable operation of the engine.

4.9 The non-ideal turbojet cycle

We have already studied one of the most important mechanisms for non-ideal behavior; namely the formation of an inlet shock.

Less than full expansion of the nozzle $P_e < P_0$ generally leads to less than maximum thrust. The loss in performance of a nozzle is a strong function of flight Mach number and becomes less important as the flight Mach number falls below one. Most military engines employ

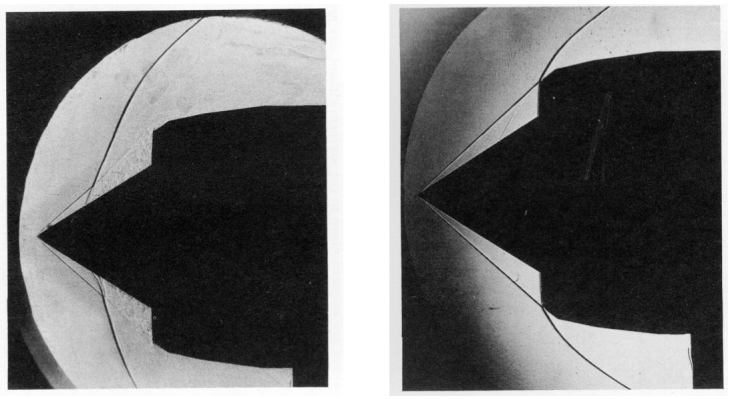

Figure 4.17: *Flow over a Mach 3 spike inlet, left photo subcritical behavior, right photo supercritical behavior.*

a converging-diverging nozzle for good supersonic performance whereas most commercial engines use a purely convergent nozzle for subsonic flight where the emphasis is on reducing weight and complexity. Most nozzle stagnation pressure losses are associated with viscous skin friction although some shock loss can occur at off design conditions. The nozzle operates in a strongly favorable pressure gradient environment and so stagnation pressure losses tend to be small and flow separation usually does not occur unless the nozzle becomes highly over-expanded. Flow separation can be an important issue in rocket nozzles when operating in the lower atmosphere but the problem is less severe in jet engines.

Stagnation pressure losses across the burner due to heat addition cause π_b to be always less than one. Additional reduction of π_b occurs due to wall friction and injector drag. Recall that the stagnation pressure loss due to heat addition and friction is proportional to , $\gamma M^2/2$. A rule of thumb is

$$\pi_b = 1 - \text{constant} \times \gamma \mathrm{M_3}^2 \tag{4.107}$$

where the constant is between one and two. In addition to the loss of stagnation pressure it is necessary to account for incomplete combustion as well as radiation and conduction of heat to the combustor walls. The combustor efficiency is defined directly from the energy balance across the burner.

$$\eta_b = \frac{(1+f)\,h_{t4} - h_{t3}}{f h_f} \tag{4.108}$$

The burner efficiency in a modern gas turbine engine is generally very close to one; Typically the efficiency is 0.99 or better.

The shaft that connects the turbine and compressor is subject to frictional losses in the bearings that support the shaft and a shaft mechanical efficiency is defined using the work balance across the compressor and turbine.

$$\eta_m = \frac{h_{t3} - h_{t2}}{(1+f)\,(h_{t4} - h_{t5})} \tag{4.109}$$

Typical shaft efficiencies are also very close to one.

4.9.1 The polytropic efficiency of compression

In the ideal turbojet cycle the compressor is assumed to operate isentropically. But this ignores the viscous frictional losses that are always present. An $h - s$ diagram illustrating the non-ideal operation of the compressor and turbine in an otherwise ideal turbojet cycle is shown in Figure 4.18.

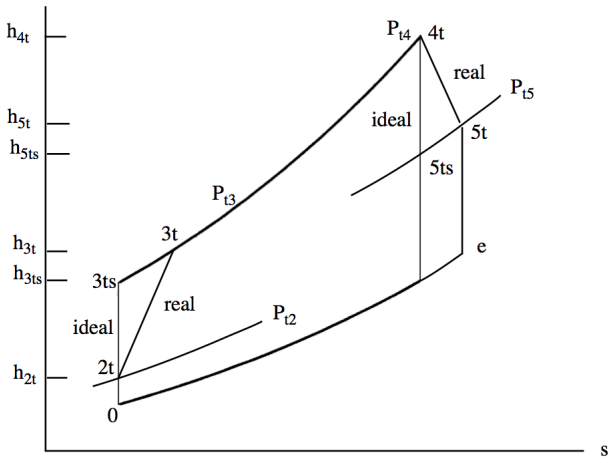

Figure 4.18: *Path of a turbojet in h-s coordinates with non-ideal compressor and turbine.*

The diagram shows the thermodynamic path of the gas flowing through a turbojet with ideal inlet, burner and nozzle but non-ideal compressor and turbine. As we consider the non-ideal cycle it is well to keep in mind that the engine is designed to produce thrust first and be efficient second. As an engine ages and various components begin to degrade, the engine control system is designed to increase fuel flow and the turbine inlet temperature so as to maintain the design thrust at the expense of efficiency.

A compressor is expected to reach the design pressure ratio regardless of its efficiency. and the same goes for the turbine. With this in mind Figure 4.18 suggests a reasonable

definition of compressor and turbine efficiency

$$\eta_c = \frac{\textit{The work input needed to reach } P_{t3}/P_{t2} \textit{ in an isentropic compression process}}{\textit{The work input needed to reach } P_{t3}/P_{t2} \textit{ in the real compression process}}$$

$$\eta_c = \frac{h_{t3s} - h_{t2}}{h_{t3} - h_{t2}} \tag{4.110}$$

and

$$\eta_e = \frac{\textit{The work output needed to reach } P_{t5}/P_{t4} \textit{ in the real expansion process}}{\textit{The work output needed to reach } P_{t5}/P_{t4} \textit{ in an isentropic expansion process}}$$

$$\eta_e = \frac{h_{t5} - h_{t4}}{h_{t5s} - h_{t4}} \tag{4.111}$$

In terms of the temperature for a calorically perfect gas these definitions become

$$\begin{aligned} \eta_c &= \frac{T_{t3s} - T_{t2}}{T_{t3} - T_{t2}} \\ \eta_e &= \frac{T_{t5} - T_{t4}}{T_{t5s} - T_{t4}}. \end{aligned} \tag{4.112}$$

These definitions are useful but a little hard to interpret when comparing one compressor with another if the compression ratios are not the same. We can use the approach suggested by Figure 4.18 to define an efficiency that characterizes the compression process itself. Consider an infinitesimal compression process defined by the $T - s$ diagram shown in Figure 4.19.

Define the polytropic efficiency of compression as the efficiency of an infinitesimal compression process.

$$\eta_{pc} = \left(\frac{T_{t3s} - T_{t2}}{T_{t3} - T_{t2}} \right)_{infinitesimal\, compression} = \frac{dT_{ts}}{dT_t} \tag{4.113}$$

For an isentropic process of a calorically perfect gas the Gibbs equation is

$$\frac{dT_{ts}}{T_t} = \left(\frac{\gamma - 1}{\gamma} \right) \frac{dP_t}{P_t}. \tag{4.114}$$

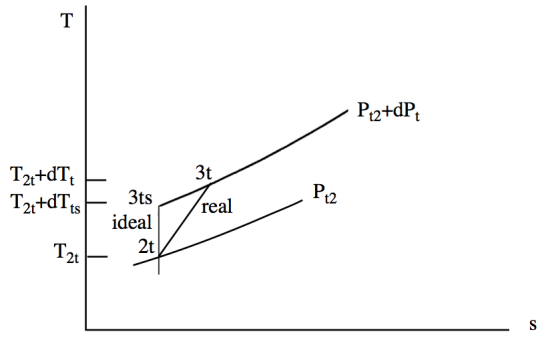

Figure 4.19: *Infinitesimal compression process.*

Using (4.113) the differential change in stagnation temperature for the real process is

$$\frac{dT_t}{T_t} = \left(\frac{\gamma - 1}{\gamma \eta_{pc}}\right) \frac{dP_t}{P_t}. \tag{4.115}$$

Now assume the polytropic efficiency is constant over the real finite compression from station 2 to station 3. Integrating (4.115) from 2 to 3 we get

$$\frac{P_{t3}}{P_{t2}} = \left(\frac{T_{t3}}{T_{t2}}\right)^{\frac{\gamma \eta_{pc}}{\gamma - 1}}. \tag{4.116}$$

The polytropic efficiency of compression allows us to analyze the flow through the compressor in terms of a relation that retains the simplicity of the isentropic relation. A lot of poorly understood physics is buried in the specification of η_{pc}. Modern compressors are designed to have values of η_{pc} in the range 0.88 to 0.92. Now the overall compressor efficiency becomes

$$\eta_c = \frac{\frac{T_{t3s}}{T_{t2}} - 1}{\frac{T_{t3}}{T_{t2}} - 1} = \frac{\left(\frac{P_{t3}}{P_{t2}}\right)^{\frac{\gamma-1}{\gamma}} - 1}{\left(\frac{P_{t3}}{P_{t2}}\right)^{\frac{\gamma-1}{\gamma \eta_{pc}}} - 1}. \tag{4.117}$$

Note that for pressure ratios close to one $\eta_c \cong \eta_{pc}$. The polytropic efficiency is a fundamental measure of the degree to which the compression process is isentropic. Given η_{pc} the overall compression efficiency is determined for any given pressure ratio.

4.10 The polytropic efficiency of expansion

Consider an infinitesimal expansion process defined by the $T-s$ diagram shown in Figure 4.20.

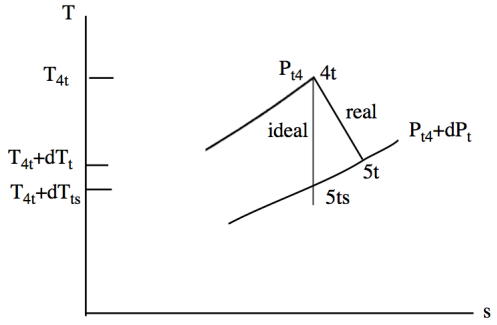

Figure 4.20: *Infinitesimal compression process.*

Define the polytropic efficiency of expansion as

$$\eta_{pe} = \left(\frac{T_{t5} - T_{t4}}{T_{t5s} - T_{t4}}\right)_{\text{infinitesimal expansion}} = \frac{dT_t}{dT_{ts}}. \tag{4.118}$$

For an isentropic process the Gibbs equation for an ideal, calorically perfect gas is

$$\frac{dT_{ts}}{T_t} = \left(\frac{\gamma - 1}{\gamma}\right)\frac{dP_t}{P_t}. \tag{4.119}$$

Using (4.118) the differential change in stagnation temperature for the real process is

$$\frac{dT_t}{T_t} = \left(\frac{(\gamma - 1)\,\eta_{pe}}{\gamma}\right)\frac{dP_t}{P_t}. \tag{4.120}$$

Now if we assume the polytropic efficiency is constant over the real finite expansion from station 4 to station 5, then integrating (4.115) from 4 to 5

$$\frac{P_{t5}}{P_{t4}} = \left(\frac{T_{t5}}{T_{t4}}\right)^{\frac{\gamma}{(\gamma-1)\eta_{pe}}}. \tag{4.121}$$

The polytropic efficiency of expansion allows us to analyze the flow through the turbine in terms of a relation that retains the simplicity of the isentropic relation. Similar to

the compression case, a lot of ignorance regarding the viscous turbulent flow through the turbine is buried in the specification of η_{pe}. Modern turbines are designed to values of η_{pe} in the range 0.91 to 0.94. The overall turbine efficiency is

$$\eta_e = \frac{\frac{T_{t5}}{T_{t4}} - 1}{\frac{T_{t5s}}{T_{t4}} - 1} = \frac{\left(\frac{P_{t5}}{P_{t4}}\right)^{\frac{(\gamma-1)\eta_{pe}}{\gamma}} - 1}{\left(\frac{P_{t5}}{P_{t4}}\right)^{\frac{\gamma-1}{\gamma}} - 1}. \tag{4.122}$$

Note that for pressure ratios close to one $\eta_e \cong \eta_{pe}$. Generally speaking turbine efficiencies are somewhat greater than compressor efficiencies because of the strongly favorable pressure gradient in the turbine.

4.11 The effect of afterburning

Figure 4.21 depicts a turbojet with an afterburner (also called an augmentor). The afterburner is a relatively simple device that includes a spray bar where fuel is injected and a flame holder designed to provide a low speed wake where combustion takes place. Note my drawing is not to scale. Usually the afterburner is considerably longer than the engine itself to permit complete mixing and combustion between the injected fuel and the vitiated air coming out of the turbine, before the flow reaches the exhaust nozzle.

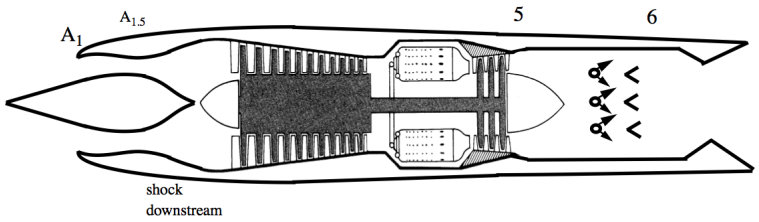

Figure 4.21: *Turbojet with afterburner.*

The main effect of the afterburner is to add a lot of heat to the turbine exhaust gases while producing relatively little stagnation loss since the heat addition is at relatively low Mach number. The exhaust Mach number is determined by the nozzle area ratio and for the same exit Mach number the exit velocity is increased in proportion to the increase in the square root of exhaust temperature. In terms of engine parameters

$$\pi_a = \frac{P_{t6}}{P_{t5}} \cong 1. \tag{4.123}$$

The fact that the nozzle area ratio is fixed (M_e is constant) and the stagnation pressure is the same, implies that the pressure contribution to the thrust is the same. The velocity ratio is

$$\frac{U_e}{U_0} = \frac{M_e}{M_0}\sqrt{\frac{T_e}{T_0}} = \frac{M_e}{M_0}\sqrt{\frac{1}{T_0}}\left(\frac{T_{te}}{1+\left(\frac{\gamma-1}{2}\right)M_e{}^2}\right)^{1/2}. \tag{4.124}$$

The exit stagnation temperature is

$$T_{te} = T_{t5}\left(\frac{T_{te}}{T_{t5}}\right) = T_{t5}\tau_a. \tag{4.125}$$

The bottom line is that $U_e \approx \sqrt{\tau_a}$. The afterburner provides a rapid increase in thrust on demand allowing the aircraft to respond quickly to changing mission circumstances; perhaps to escape a suddenly emerging threat. The price is a substantial increase in fuel burn rate. Most military engines only spend a few hundred hours in the after-burning mode over a typical engine lifetime of $3-4000$ hours before a major overhaul.

4.12 Nozzle operation

Commercial engines generally operate with fixed, purely convergent nozzles. There is a penalty for not fully expanding the flow but at low Mach numbers the performance loss is relatively small and the saving in weight and complexity is well worth it. For a commercial engine operating at $M_0 = 0.8$, π_n is on the order of 0.97 or better.

On the other hand military engines almost always employ some sort of variable area nozzle and in several modern systems the nozzle is also designed to be vectored. The most well known example is the planar nozzle of the F22. After-burning engines especially require a variable area nozzle. When the afterburner is turned on, and the exit gas temperature is increased according to (4.125), the nozzle throat area must be increased in a coordinated way to preserve the mass flow through the engine without putting an undue load on the turbine. Remember the exhaust nozzle is choked. With the augmentor on, the turbine temperature ratio is

$$\tau_t = \left(\frac{A_4^*}{A_8}\sqrt{\tau_a}\right)^{\frac{2(\gamma-1)}{\gamma+1}}. \tag{4.126}$$

In order to keep the turbine temperature ratio unchanged and the rest of the engine at the same operating point when the augmentor is turned on, it is necessary to program the nozzle area so that $\sqrt{\tau_a}/A_8$ remains constant. If this is not done the dimensionless mass flow through the engine will decrease, the actual mass flow may decrease and the desired thrust increment will not occur, or worse, the compressor might stall.

4.13 Problems

Problem 1 - Consider the turbojet engine shown in Figure 4.22.

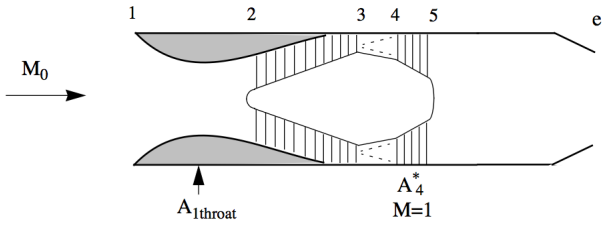

Figure 4.22: *Turbojet in subsonic flow.*

The engine operates at a free stream Mach number $M_0 = 0.8$. The ambient temperature is $T_0 = 216\,K$. The turbine inlet temperature is $T_{t4} = 1944\,K$ and $\pi_c = 20$. Relevant area ratios are $A_2/A_4^* = 10$ and $A_2/A_{1throat} = 1.2$. Assume the compressor, burner and turbine all operate ideally. The nozzle is of a simple converging type and stagnation pressure losses due to wall friction in the inlet and nozzle are negligible. Determine $f\,(M_2)$. Sketch the compressor operating line. Suppose T_{t4} is increased. What value of T_{t4} would cause the inlet to choke? Assume $f << 1$.

Problem 2 - A turbojet engine operates at a Mach number of 2.0 with a normal shock ahead of the inlet as shown in the sketch in Figure 4.23. The flow between the shock and station 2 is all subsonic. Assume $f << 1$ where appropriate and assume the static pressure outside the nozzle exit has recovered to the free stream value as indicated in the sketch. The ambient temperature and pressure are $T_0 = 216\,K$ and $P_0 = 2 \times 10^4\,N/m^2$.

The turbine inlet temperature is $T_{t4} = 1512\,K$, the compressor pressure ratio is $\pi_c = 20$ and $A_2/A_4^* = 18$. Assume the compressor, burner and turbine all operate ideally and stagnation pressure losses due to wall friction in the inlet and nozzle are negligible. Assume $f << 1$. Determine A_2/A_0, the pressure ratio P_e/P_0, temperature ratio T_e/T_0 and dimensionless thrust T/P_0A_0.

Problem 3 - Consider the turbojet engine shown in Figure 4.24.

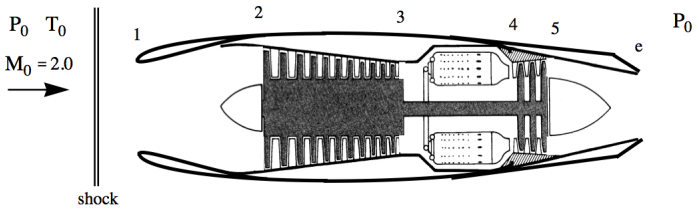

Figure 4.23: *Turbojet with upstream normal shock.*

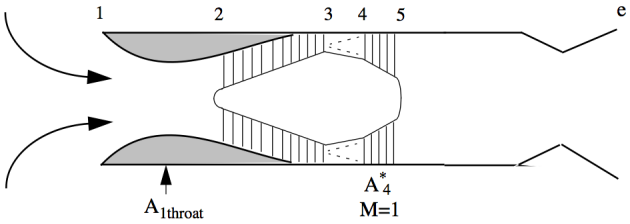

Figure 4.24: *Operating turbojet at rest.*

The engine operates at zero free stream Mach number $M_0 = 0$. The ambient temperature and pressure are $T_0 = 273K$ and $P_0 = 1.01 \times 10^5 N/m^2$. The turbine inlet temperature is $T_{t4} = 1638K$ and $\pi_c = 20$. Relevant area ratios are $A_2/A_4^* = 10$ and $A_2/A_{1throat} = 1.2$. Assume the compressor, burner and turbine all operate ideally. The nozzle is fully expanded $P_e = P_0$ and stagnation pressure losses due to wall friction in the inlet and nozzle are negligible. Assume $f << 1$. Determine the overall pressure ratio P_{te}/P_0 and dimensionless thrust T/P_0A_2.

Problem 4 - Figure 4.25 shows a typical turbojet engine flying supersonically. In Figure 4.26 are typical stagnation pressure and stagnation temperature ratios at various points inside the engine (the figures are not drawn to scale).

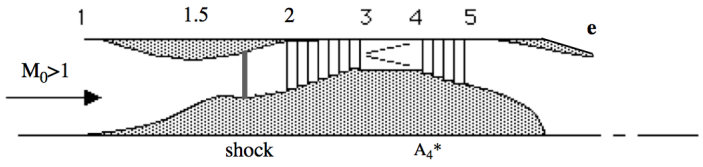

Figure 4.25: *Turbojet in supersonic flow.*

The turbine inlet and nozzle exit are choked, and the compressor, burner and turbine operate ideally. Supersonic flow is established in the inlet and a normal shock is positioned downstream of the inlet throat. The inlet and nozzle are adiabatic. Neglect wall friction and assume $f << 1$.

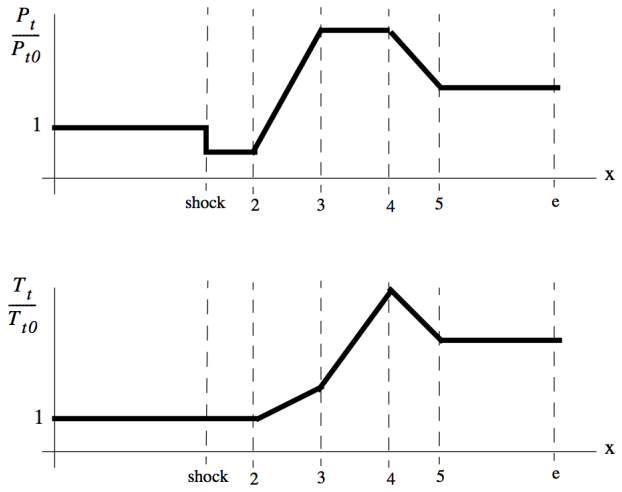

Figure 4.26: *Stagnation pressure and stagnation temperature through a turbojet engine with inlet shock.*

Suppose τ_λ is increased while the flight Mach number and engine areas including the nozzle throat area are constant.

1) Show whether P_{t3}/P_{t0} increases, decreases or remains the same.

2) At each of the stations indicated above explain how the stagnation pressure and stagnation temperature change in response to the increase in τ_λ.

Problem 5 - A turbojet operates supersonically at $M_0 = 2$ with $f\,(M_2) = 0.5$, $\pi_c = 20$ and $T_{t4} = 2160\,K$. The compressor and turbine polytropic efficiencies are $\eta_{pc} = \eta_{pt} = 1$. At the condition shown in Figure 4.27, the engine operates semi-ideally with $\pi_d = \pi_b = \pi_n = 1$ but with a simple convergent nozzle. The relevant inlet areas are $A_1/A_{1.5} = 1.688$ and $A_2/A_{1.5} = 2$. Assume $\gamma = 1.4$, $R = 287\,m^2/\left(\sec^2 - K\right)$, $C_p = 1005\,m^2/\left(\sec^2 - K\right)$. The fuel heating value is $h_f = 4.28 \times 10^7\,J/kg$. The ambient temperature and pressure are $T_0 = 216\,K$ and $P_0 = 2 \times 10^4\,N/m^2$. These are typical values in the atmosphere at an altitude of about $12,000$ meters.

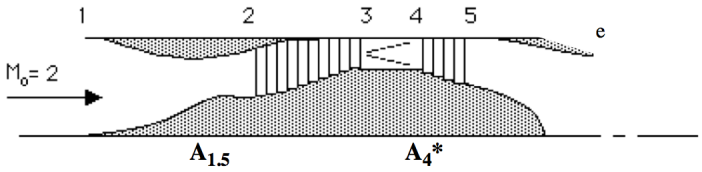

Figure 4.27: *Turbojet at Mach 2.0.*

Assume throughout that the fuel/air ratio is much less than one and that all areas of the engine structure remain fixed.

1) Determine A_2/A_4^* and A_4^*/A_e.

2) For each of the following three cases determine $f(M_2)$, $f(M_{1.5})$, $f(M_1)$, A_0/A_1 and T/P_0A_1.

Case I - First T_{t4} is slowly raised to $2376\,K$.

Case II - Then T_{t4} is reduced to $1944\,K$.

Case III - Finally T_{t4} is increased back to $2160\,K$.

Problem 6 - Consider the turbojet engine shown in Figure 4.28.

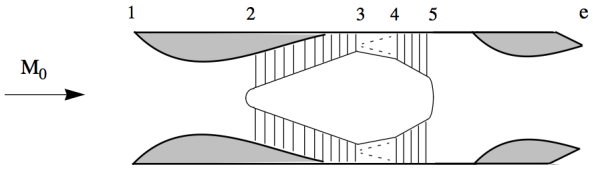

Figure 4.28: *Generic turbojet engine.*

The engine has a converging-diverging nozzle and operates at a free stream Mach number $M_0 = 0.8$. The turbine inlet temperature is $T_{t4} = 1800\,K$. Instead of me giving you a lot of information from which you can determine engine thrust, I would like to turn the question around and have you supply me with the information necessary to design the engine. Since this is a very preliminary design you may assume ideal behavior where appropriate. Note however that the polytropic efficiency of the compressor is $\eta_{pc} = 0.85$ and that of the turbine is $\eta_{pe} = 0.90$. Note also that my crude engine drawing is not to scale! After you finish the design, make a sketch for yourself that is more to scale.

The goal of the design is to produce as much thrust per unit area as possible for the given operating conditions. You are asked to supply the following.

1) The compressor pressure ratio, π_c.

2) The fuel/air ratio.

3)The compressor face mass flow parameter, $f(M_2)$.

4) All relevant area ratios, $A_{4_{throat}}/A_{5_{throat}}$, $A_{5_{throat}}/A_e$, $A_2/A_{4_{throat}}$, $A_0/A_{4_{throat}}$, $A_{1_{throat}}/A_2$, $A_{1_{throat}}/A_1$

5) The engine thrust, T/P_0A_0.

You may find that not every quantity that you are asked to supply is fixed by specifying the engine operating point. Where this is the case, you will need to use your experience to choose reasonable values. Be sure to explain your choices.

Assume $\gamma = 1.4$, $R = 287\,m^2/\left(\sec^2 - K\right)$, $C_p = 1005\,m^2/\left(\sec^2 - K\right)$. The fuel heating value is $h_f = 4.28 \times 10^7 J/kg$. The ambient temperature and pressure are $T_0 = 216\,K$ and $P_0 = 2 \times 10^4\,N/m^2$. These are typical values in the atmosphere at an altitude of about $12,000$ meters.

Problem 7 - A test facility designed to measure the mass flow and pressure characteristics of a jet engine compressor is shown in Figure 4.29. An electric motor is used to power the compressor. The facility draws air in from the surroundings which is at a pressure of one atmosphere and a temperature of $300\,K$. The air passes through the inlet throat at station 1, is compressed from 2 to 3 and then exhausted through a simple convergent nozzle at station e. Assume the compressor (2-3) has a polytropic efficiency of $\eta_{pc} = 0.95$.

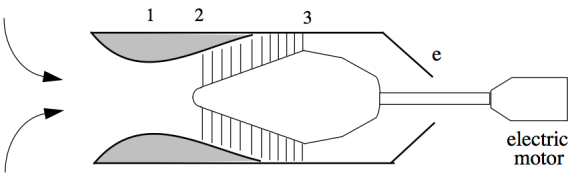

Figure 4.29: *A compressor test facility.*

Relevant area ratios of the rig are $A_1/A_e = 8$ and $A_1/A_2 = 0.5$. Suppose the power to the compressor is slowly increased from zero.

1) Determine the compressor pressure ratio P_{t3}/P_{t2} at which the nozzle chokes.

2) Determine the compressor pressure ratio P_{t3}/P_{t2} at which the inlet throat chokes.

3) Plot the overall pressure ratio P_{te}/P_0 versus the temperature ratio T_{te}/T_0 over the full range from less than sonic flow at e to beyond the point where a normal shock forms in the inlet.

Problem 8 - Because of their incredible reliability, surplus jet engines are sometimes used for power generation in remote locations. By de-rating the engine a bit and operating at lower than normal temperatures, the system can run twenty four hours a day for many years with little or no servicing. Figure 4.30 shows such an engine supplying shaft power P to an electric generator. Assume that there are no mechanical losses in the shaft.

The ambient temperature and pressure are $T_0 = 273\,K$ and $P_0 = 1.01 \times 10^5\,N/m^2$. The turbine inlet temperature is $T_{t4} = 1638\,K$ and $\pi_c = 20$. Relevant area ratios are $A_2/A_4^* = 15$ and $A_2/A_{1_{throat}} = 1.5$. Assume the compressor, burner and turbine all operate ideally. The

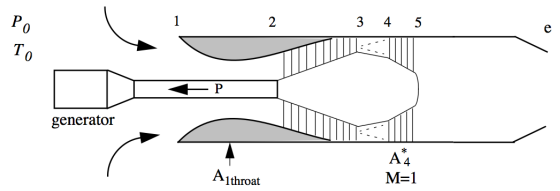

Figure 4.30: *A gas-turbine based power plant.*

nozzle is a simple convergent design and stagnation pressure losses due to wall friction in the inlet and nozzle are negligible. Assume $f << 1$. Let the nozzle area be set so that $P_{t5}/P_0 = 2$.

1) Is there a shock in the inlet?

2) How much dimensionless shaft power $P/\left(\dot{m}_a C_p T_0\right)$ is generated at this operating condition?

Problem 9 - Consider the afterburning turbojet shown in Figure 4.31. The inlet operates with a normal shock in the diverging section. The nozzle is of simple convergent type.

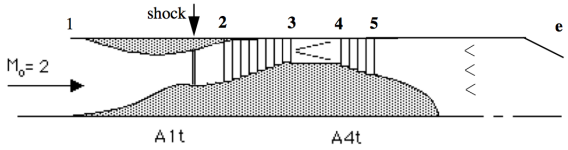

Figure 4.31: *Turbojet with afterburner.*

Initially the afterburner is off so that $P_{te} = P_{t5}$ and $T_{te} = T_{t5}$. At the condition shown the overall engine pressure ratio is $P_{te}/P_{t1} = 5.6$ and the temperature ratio is $T_{te}/T_{t1} = 3.1$.

1) Determine A_e/A_1.

2) Determine the thrust $T/P_0 A_0$.

3) Suppose the afterburner is turned on increasing the exit temperature to $T_{te}/T_{t5} = 1.5$. Assume that, as the afterburner is turned on, the nozzle area is increased so that P_{t5} remains constant thus avoiding any disturbance to the rest of the engine. Determine the new value of $T/P_0 A_0$. State any assumptions used to solve the problem.

Problem 10 - For this problem assume the properties of air are $\gamma = 1.4$, $R = 287\, m^2/\left(\sec^2 - K\right)$, $C_p = 1005\, m^2/\left(\sec^2 - K\right)$. Where appropriate assume $f << 1$. Figure 4.32 shows a flow facility used to test a small turbojet engine. The facility is designed to simulate various flight Mach numbers by setting the value of $P_{t0}/P_0 > 1$.

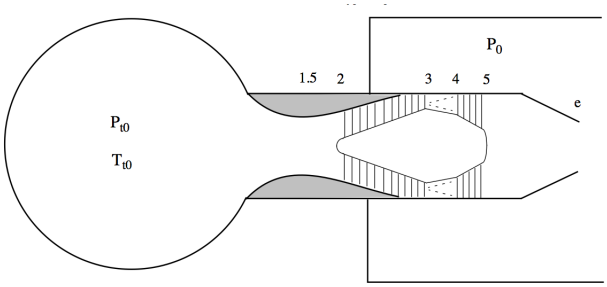

Figure 4.32: *A turbojet test facility.*

The relevant areas are $A_{4t}/A_e = 1/2$, $A_{1.5}/A_{4t} = 5$, $A_2/A_{1.5} = 2$. Assume that the compressor, burner and turbine operate ideally and that there is no stagnation pressure or stagnation temperature loss in the nozzle.

1)Let $T_{t4}/T_{t0} = 6$. Determine, π_c, π_d, $f(M_2)$ and the engine stagnation pressure ratio, $\pi_d\pi_c\pi_t$. Assuming $P_{t0}/P_0 > 1$ can you be certain that A_e is choked?

2) Let $P_{t0}/P_0 = 7.82$ and $T_{t4}/T_{t0} = 6$. What flight Mach number is being simulated at this facility pressure ratio? Determine P_e/P_0.

3) On the compressor map, (π_c versus $f(M_2)$ indicate the operating point for part 1. Sketch the change in engine operating point when A_e is increased with T_{t4}/T_{t0} held fixed.

Problem 11 - Consider an ideal turbojet with after-burning. Show that for a given total fuel flow, part to the main burner and part to the afterburner, the compressor temperature ratio for maximum thrust is

$$\tau_c|_{max\ thrust\ turbojet\ with\ afterburning} = \frac{1}{2}\left(1 + \frac{\tau_\lambda}{\tau_r}\right). \tag{4.127}$$

Recall that for a non-afterburning turbojet $\tau_c|_{max\ thrust\ turbojet} = \sqrt{\tau_\lambda}/\tau_r$. For typical values of τ_λ and τ_r the compressor pressure ratio with after-burning will be somewhat larger than that without after-burning.

Problem 12 - In the movie Top Gun there is depicted a fairly realistic sequence where two F-14s are engaged in a dogfight at subsonic Mach numbers with another aircraft. During a maneuver, one F-14 inadvertently flies through the hot wake of the other. This causes both engines of the trailing F-14 to experience compressor stall and subsequently flame-out leading to loss of the aircraft and crew. Can you explain what happened? Why might the sudden ingestion of hot air cause the compressor to stall?

Problem 13 - Figure 4.33 below depicts the flow across a compressor rotor. The axial

speed is $c_z = 200\,m/\,\text{sec}$ and the blade speed is $U_{blade} = 300\,m/\,\text{sec}$. Relevant angles are $\alpha_{2a} = 30^\circ$ and $\beta_{2b} = 30^\circ$. Determine T_{t2_b}/T_{t2_a} where $T_{t2_a} = 260\,K$.

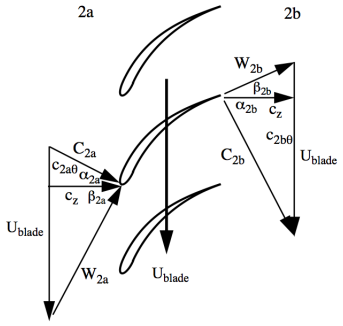

Figure 4.33: *Compressor rotor flow diagram.*

Problem 14 - Figure 4.34 depicts the flow across a compressor stage composed of two counter-rotating rotors.

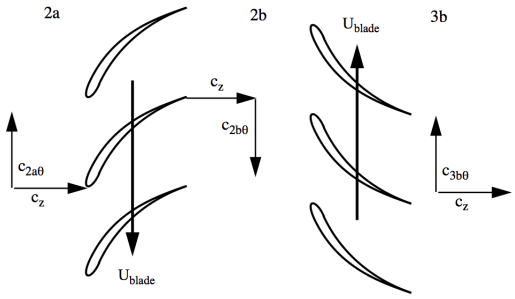

Figure 4.34: *Compressor stage flow diagram.*

The axial speed is $c_z = 200\,m/\,\text{sec}$ and the blade speed is $U_{blade} = 300\,m/\,\text{sec}$. Tangential velocities are $c_{2a\theta} = 50\,m/\,\text{sec}$, $c_{2b\theta} = -50\,m/\,\text{sec}$ and $c_{3b\theta} = 50\,m/\,\text{sec}$.

1)!Determine T_{t3_b}/T_{t2_a} where $T_{t2_a} = 300\,K$.

2)Let the polytropic efficiency of compression be $\eta_{pc} = 0.85$. Determine P_{t3_b}/P_{t2_a}.

3) What benefits can you see in this design, what disadvantages?

Problem 15 - Figure 4.35 depicts the flow across a compressor rotor. The axial speed is $c_z = 150\,m/\,\text{sec}$ and the blade speed is $U_{blade} = 250\,m/\,\text{sec}$.

Relevant angles are $\alpha_{2a} = 30^\circ$ and $\beta_{2b} = 30^\circ$.

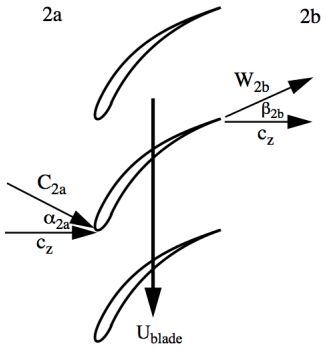

Figure 4.35: *Compressor rotor.*

1) Determine T_{t2_b}/T_{t2_a} where $T_{t2_a} = 350\,K$.

2) Let the polytopic efficiency of compression be $\eta_{pc} = 0.9$. Determine P_{t2_b}/P_{t2a}.

Problem 16 - Consider the turbojet engine shown in Figure 4.36.

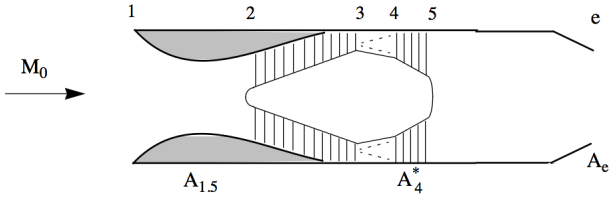

Figure 4.36: *Turbojet schematic.*

The engine operates at a free stream Mach number $M_0 = 0.8$. The turbine inlet temperature is $T_{t4} = 1296\,K$ and $\pi_c = 15$. The compressor face to turbine inlet area ratio is $A_2/A_4^* = 10$. Assume the compressor, and turbine operate ideally and there is no stagnation pressure loss across the burner. The nozzle is of a simple converging type and stagnation pressure losses due to wall friction in the inlet and nozzle are negligible. The nozzle throat area A_e can be varied. The ambient temperature and pressure are $T_0 = 216\,K$ and $P_0 = 2 \times 10^4\,N/m^2$.

1) Determine τ_t, A_4^*/A_e, and $f\,(M_2)$.

2) Now suppose that the compressor operates non-ideally with $\eta_{pc} = 0.8$. The turbine inlet temperature is kept at $T_{t4} = 1296\,K$. What value of A_4^*/A_e is required to maintain the same value of $\pi_c = 15$?

Problem 17 - An aircraft powered by a turbojet engine shown in Figure 4.37 is ready for

take-off. The ambient temperature and pressure are $T_0 = 300\,K$ and $P_0 = 10^5\,N/m^2$. The turbine inlet temperature is $T_{t4} = 1500\,K$. The compressor pressure ratio is $\pi_c = 25$ and $A_2/A_4^* = 15$. The compressor polytropic efficiency is $\eta_{pc} = 0.85$ and the turbine polytropic efficiency is $\eta_{pe} = 0.9$. Assume that stagnation pressure losses in the inlet, burner and nozzle are negligible. Determine the pressure ratio P_e/P_0, temperature ratio T_e/T_0 and dimensionless thrust T/P_0A_2. The fuel heating value is $h_f = 4.28 \times 10^7\,J/kg$. The nozzle is of simple converging type as shown.

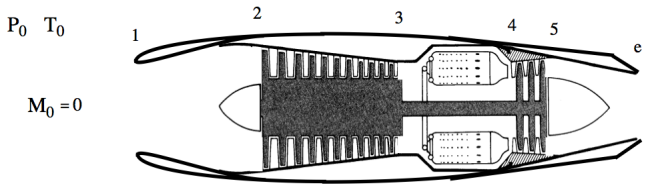

Figure 4.37: *Turbojet schematic.*

Problem 18 - Consider the turbojet engine shown in Figure 4.38.

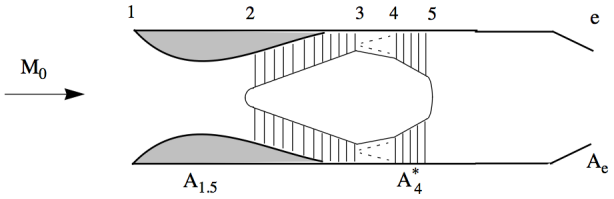

Figure 4.38: *Turbojet schematic.*

The engine operates at a free stream Mach number $M_0 = 0.6$. The turbine inlet temperature is $T_{t4} = 1296\,K$ and $\pi_c = 15$. The compressor face to turbine inlet area ratio is $A_2/A_4^* = 10$ and $A_{1.5}/A_2 = 0.8$. Assume the compressor, burner and turbine operate ideally. The nozzle is of a simple converging type and stagnation pressure losses due to wall friction in the inlet and nozzle are negligible.

1) Determine τ_t, A_4^*/A_e, and $f\,(M_2)$.

2) Suppose T_{t4} is increased. What value of T_{t4} would cause the inlet to choke?

Problem 19 - In the 1950s engine designers sought to decrease engine weight by increasing the compression achieved per stage of a jet engine compressor. In their endeavors they toyed with the idea of greatly increasing the relative Mach number of the flow entering the compressor to values exceeding Mach one. Thus was born the concept of a supersonically operating compressor and today the fans of most turbofan engines do in fact operate with blade tip Mach numbers that are greater than one. Axial Mach numbers still remain well

below one. One of the most innovative design ideas during this period came from Arthur Kantrowitz of Cornell University. He conceived the idea of a *shock in rotor* compressor that could operate at Mach numbers considerably greater than one. The idea is illustrated in Figure 4.39.

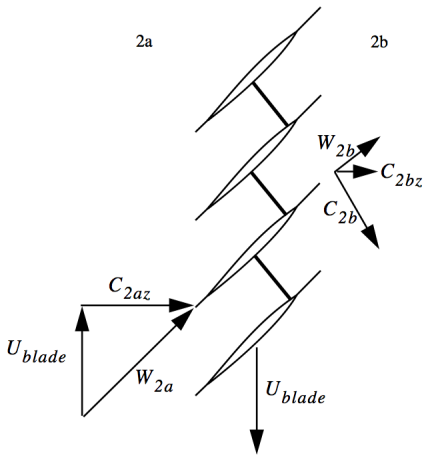

Figure 4.39: *Shock-in-rotor supersonic compressor.*

Let $T_{2a} = 354\,K$, $U_{blade} = 800\,m/\text{sec}$ and $C_{2a_z} = 800\,m/\text{sec}$. The velocity vector entering the compressor is exactly aligned with the leading edge of the rotor blade as seen by an observer attached to the rotor. This is shown in the figure above. The tangential (swirl) velocity entering the stage is zero. The flow through the rotor passes through a $M = 2.0$ shock wave and then exits the rotor at the same angle it entered. In other words there is no turning of the flow by the blade in the frame of reference of the blade.

a) In a frame of reference attached to the rotor determine

1) M_{2a}, P_{t2b}/P_{t2a} and M_{2b}

2) T_{t2b}/T_{t2a} and P_{t2b}/P_{t2a}.

b) In the frame of a non-moving observer determine

1) $T_{t2b_{rest\,frame}}/T_{t2a_{rest\,frame}}$

2) $P_{t2b_{rest\,frame}}/P_{t2a_{rest\,frame}}$.

c) Determine the polytropic efficiency of the compression process in the non-moving frame.

Chapter 5

The Turbofan cycle

5.1 Turbofan thrust

Figure 5.1 illustrates two generic turbofan engine designs. The upper figure shows a modern high bypass ratio engine designed for long distance cruise at subsonic Mach numbers around 0.83 typical of a commercial aircraft. The fan utilizes a single stage composed of a large diameter fan (rotor) with wide chord blades followed by a single nozzle stage (stator). The bypass ratio is 5.8 and the fan pressure ratio is 1.9. The lower figure shows a military turbofan designed for high performance at supersonic Mach numbers in the range of 1.1 to 1.5. The fan on this engine has three stages with an overall pressure ratio of about 6 and a bypass ratio of only about 0.6. One of the goals of this chapter is to understand why these engines look so different in terms the differences in flight condition for which they are designed. In this context we will begin to appreciate that the thermodynamic and gas dynamic analysis of these engines defines a continuum of cycles as a function of Mach number. We had a glimpse of this when we determined that the maximum thrust turbojet is characterized by

$$\tau_{c_{\max thrust}} = \frac{\sqrt{\tau_\lambda}}{\tau_r}. \tag{5.1}$$

For fixed turbine inlet temperature and altitude, as the Mach number increases the optimum compression decreases and at some point it becomes desirable to convert the turbojet to a ramjet. We will see a similar kind of trend emerge for the turbofan where it replaces the turbojet as the optimum cycle for lower Mach numbers. Superimposed on all this is a historical technology trend where, with better materials and cooling schemes, the allowable turbine inlet temperature has increased with time. This tends to lead to an optimum cycle with higher compression and higher bypass ratio at a given Mach number.

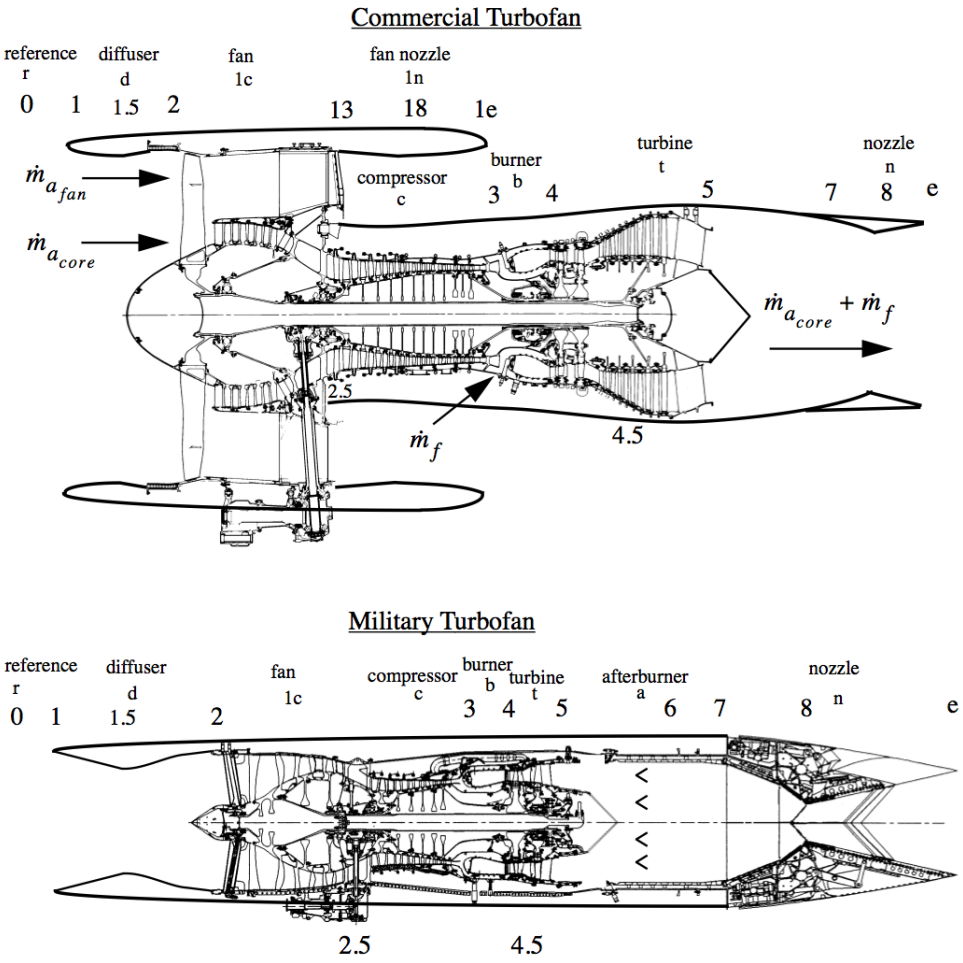

Figure 5.1: *Turbofan engine numbering and component notation.*

The thrust equation for the turbofan is similar to the usual relation except that it includes the thrust produced by the fan.

$$T = \dot{m}_{a_{core}} (U_e - U_0) + \dot{m}_{a_{fan}} (U_{e1} - U_0) + \dot{m}_f U_e + (P_e - P_0) A_e + (P_{e1} - P_0) A_{1e} \quad (5.2)$$

The total air mass flow is

$$\dot{m}_a = \dot{m}_{a_{core}} + \dot{m}_{a_{fan}}. \quad (5.3)$$

The fuel/air ratio is defined in terms of the total air mass flow.

$$f = \frac{\dot{m}_f}{\dot{m}_a} \quad (5.4)$$

The bypass fraction is defined as

$$B = \frac{\dot{m}_{a_{fan}}}{\dot{m}_{a_{fan}} + \dot{m}_{a_{core}}} \quad (5.5)$$

and the bypass ratio is

$$\beta = \frac{\dot{m}_{a_{fan}}}{\dot{m}_{a_{core}}}. \quad (5.6)$$

Note that

$$\begin{aligned} \beta &= \frac{B}{1-B} \\ B &= \frac{\beta}{1+\beta}. \end{aligned} \quad (5.7)$$

5.2 The ideal turbofan cycle

The ideal turbofan cycle is characterized by the following assumptions

$$\begin{aligned} P_e &= P_0 \\ P_{e1} &= P_0 \end{aligned} \quad (5.8)$$

and

$$\begin{aligned} \pi_d &= 1 \\ \pi_b &= 1 \\ \pi_n &= 1 \\ \pi_{n1} &= 1 \end{aligned} \tag{5.9}$$

and

$$\begin{aligned} \pi_c &= \tau_c{}^{\frac{\gamma}{\gamma-1}} \\ \pi_{c1} &= \tau_{c1}{}^{\frac{\gamma}{\gamma-1}} \\ \pi_t &= \tau_t{}^{\frac{\gamma}{\gamma-1}}. \end{aligned} \tag{5.10}$$

For a fully expanded exhaust the normalized thrust is

$$\frac{T}{\dot{m}_a a_0} = M_0 \left((1 - B + f) \left(\frac{U_e}{U_0} - 1 \right) + B \left(\frac{U_{e1}}{U_0} - 1 \right) + f \right) \tag{5.11}$$

or, in terms of the bypass ratio with $f << 1$,

$$\frac{T}{\dot{m}_a a_0} = M_0 \left(\left(\frac{1}{1+\beta} \right) \left(\frac{U_e}{U_0} - 1 \right) + \left(\frac{\beta}{1+\beta} \right) \left(\frac{U_{e1}}{U_0} - 1 \right) \right). \tag{5.12}$$

5.2.1 The fan bypass stream

First work out the velocity ratio for the fan stream.

$$\frac{U_{e1}}{U_0} = \frac{M_{e1}}{M_0} \sqrt{\frac{T_{e1}}{T_0}} \tag{5.13}$$

The exit Mach number is determined from the stagnation pressure.

$$P_{te1} = P_0 \pi_r \pi_{c1} = P_{e1} \left(1 + \frac{\gamma - 1}{2} {M_{e1}}^2 \right)^{\frac{\gamma}{\gamma-1}} \tag{5.14}$$

Since the nozzle is fully expanded and the fan is assumed to behave isentropically, we can write

$$\tau_r \tau_{c1} = \left(1 + \frac{\gamma - 1}{2} {M_{e1}}^2\right) \tag{5.15}$$

therefore

$$\frac{{M_{e1}}^2}{{M_0}^2} = \frac{\tau_r \tau_{c1} - 1}{\tau_r - 1}. \tag{5.16}$$

The exit temperature is determined from the stagnation temperature.

$$T_{te1} = T_0 \tau_r \tau_{c1} = T_{e1} \left(1 + \frac{\gamma - 1}{2} {M_{e1}}^2\right) \tag{5.17}$$

Noting (5.15) we can conclude that for the ideal fan

$$T_{e1} = T_0. \tag{5.18}$$

The exit static temperature is equal to the ambient static temperature. The velocity ratio of the fan stream is

$$\left(\frac{U_{e1}}{U_0}\right)^2 = \frac{\tau_r \tau_{c1} - 1}{\tau_r - 1}. \tag{5.19}$$

5.2.2 The core stream

The velocity ratio across the core is

$$\frac{U_e}{U_0} = \frac{M_e}{M_0} \sqrt{\frac{T_e}{T_0}}. \tag{5.20}$$

The analysis of the stagnation pressure and temperature is exactly the same as for the ideal turbojet.

$$P_{te} = P_0 \pi_r \pi_c \pi_t = P_e \left(1 + \frac{\gamma - 1}{2} {M_e}^2\right)^{\frac{\gamma}{\gamma - 1}} \tag{5.21}$$

Since the nozzle is fully expanded and the compressor and turbine operate ideally the Mach number ratio is

$$\frac{{M_e}^2}{{M_0}^2} = \frac{\tau_r \tau_c \tau_t - 1}{\tau_r - 1}. \tag{5.22}$$

The temperature ratio is also determined in the same way in terms of component temperature parameters.

$$T_{te} = T_0 \tau_r \tau_d \tau_c \tau_b \tau_t \tau_n \tag{5.23}$$

In the ideal turbofan we assume that the diffuser and nozzle flows are adiabatic and so

$$T_{te} = T_0 \tau_r \tau_c \tau_b \tau_t = T_e \left(1 + \frac{\gamma - 1}{2} {M_e}^2\right) = T_e \tau_r \tau_c \tau_t \tag{5.24}$$

from which is determined

$$\frac{T_e}{T_0} = \tau_b = \frac{\tau_\lambda}{\tau_r \tau_c}. \tag{5.25}$$

The velocity ratio across the core is

$$\left(\frac{U_e}{U_0}\right)^2 = \left(\frac{\tau_r \tau_c \tau_t - 1}{\tau_r - 1}\right) \frac{\tau_\lambda}{\tau_r \tau_c}. \tag{5.26}$$

5.2.3 Turbine-compressor-fan matching

The work taken out of the flow by the high and low pressure turbine is used to drive both the compressor and the fan.

$$\left(\dot{m}_{a_{core}} + \dot{m}_f\right)\left(h_{t4} - h_{t5}\right) = \dot{m}_{a_{core}}\left(h_{t3} - h_{t2}\right) + \dot{m}_{a_{fan}}\left(h_{t31} - h_{t2}\right) \tag{5.27}$$

Divide (5.27) by $\dot{m}_a C_p T_0$ and rearrange. The work matching condition for a turbofan is

$$\tau_t = 1 - \frac{\tau_r}{\tau_\lambda}\left(\frac{1 - B}{1 - B + f}\left(\tau_c - 1\right) + \frac{B}{1 - B + f}\left(\tau_{c1} - 1\right)\right). \tag{5.28}$$

The approximation $f \ll 1$ is generally pretty good for a turbofan. Using this approximation the work matching condition becomes

$$\tau_t = 1 - \frac{\tau_r}{\tau_\lambda}\left((\tau_c - 1) + \beta\left(\tau_{c1} - 1\right)\right) \tag{5.29}$$

where the bypass ratio β appears for the first time. If the bypass ratio goes to zero the matching condition reduces to the usual turbojet formula.

5.2.4 The fuel/air ratio

The fuel/air ratio is determined from the energy balance across the burner.

$$\dot{m}_f\left(h_f - h_{t4}\right) = \dot{m}_{a_{core}}\left(h_{t4} - h_{t3}\right) \tag{5.30}$$

Divide (5.30) by $\dot{m}_a C_p T_0$ and rearrange. The result is

$$f = \left(\frac{1}{1+\beta}\right)\frac{\tau_\lambda - \tau_r\tau_c}{\tau_f - \tau_\lambda}. \tag{5.31}$$

5.3 Maximum specific impulse ideal turbofan

The non-dimensionalized specific impulse can be expressed in terms of thrust and fuel/air ratio as

$$\frac{I_{sp}g}{a_0} = \left(\frac{T}{\dot{m}_f g}\right)\left(\frac{g}{a_0}\right) = \left(\frac{T}{\dot{m}_a a_0}\right)\left(\frac{1}{f}\right). \tag{5.32}$$

Substitute (5.12) and (5.31) into (5.32). The result is

$$\frac{I_{sp}g}{a_0} = M_0\left(\frac{\tau_f - \tau_\lambda}{\tau_\lambda - \tau_r\tau_c}\right)\left(\left(\frac{U_e}{U_0} - 1\right) + \beta\left(\frac{U_{e1}}{U_0} - 1\right)\right). \tag{5.33}$$

The question is: what value of β maximizes the specific impulse? Differentiate (5.33) with respect to β and note that β appears in (5.29).

$$\frac{\partial}{\partial\beta}\left(\frac{I_{sp}g}{a_0}\right) = M_0\left(\frac{\tau_f - \tau_\lambda}{\tau_\lambda - \tau_r\tau_c}\right)\left(\frac{\partial}{\partial\beta}\left(\frac{U_e}{U_0}\right) + \left(\frac{U_{e1}}{U_0} - 1\right)\right) = 0 \tag{5.34}$$

We can write (5.34) as

$$\frac{1}{2\left(U_e/U_0\right)}\frac{\partial}{\partial\beta}\left(\frac{U_e}{U_0}\right)^2+\left(\frac{U_{e1}}{U_0}-1\right)=0 \tag{5.35}$$

or

$$\frac{1}{2\left(U_e/U_0\right)}\left(\frac{\tau_\lambda}{\tau_r-1}\right)\frac{\partial\tau_t}{\partial\beta}=-\left(\frac{U_{e1}}{U_0}-1\right). \tag{5.36}$$

Equation (5.36) becomes

$$\frac{1}{2\left(U_e/U_0\right)}\left(\frac{\tau_r\left(\tau_{c1}-1\right)}{\tau_r-1}\right)=\left(\frac{U_{e1}}{U_0}-1\right). \tag{5.37}$$

From (5.19),the expression in parentheses on the left side of (5.37) can be written

$$\frac{1}{2\left(U_e/U_0\right)}\left(\left(\frac{U_{e1}}{U_0}\right)^2-1\right)=\left(\frac{U_{e1}}{U_0}-1\right). \tag{5.38}$$

Factor the left side of (5.38) and cancel common factors on both sides. The velocity condition for a maximum impulse ideal turbofan is

$$\left(\frac{U_{e1}}{U_0}-1\right)=2\left(\frac{U_e}{U_0}-1\right). \tag{5.39}$$

According to this result, for an ideal turbofan one would want to design the turbine such that the velocity increment across the fan was twice that across the core in order to achieve maximum specific impulse. Recall that U_e/U_0 depends on β through (5.29) (and weakly though (5.31) which we neglect). The value of β that produces the condition (5.39) corresponding to the maximum impulse ideal turbofan is

$$\beta_{\,max\ impulse\ ideal\ turbofan}= \frac{1}{\tau_{c1}-1}\left(\left(\frac{\tau_\lambda}{\tau_r\tau_c}-1\right)\left(\tau_c-1\right)+\frac{\tau_\lambda\left(\tau_r-1\right)}{{\tau_r}^2\tau_c}-\frac{1}{4}\left(\frac{\tau_r-1}{\tau_r}\right)\left(\left(\frac{\tau_r\tau_{c1}-1}{\tau_r-1}\right)^{1/2}+1\right)\right). \tag{5.40}$$

Figure 5.2 shows how the optimum bypass ratio (5.40) varies with flight Mach number for a given set of engine parameters.

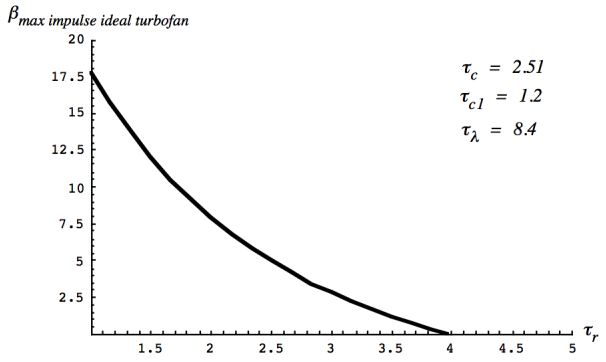

Figure 5.2: *Ideal turbofan bypass ratio for maximum specific impulse as a function of Mach number.*

It is clear from this figure that, as the Mach number increases, the optimum bypass ratio decreases until a point is reached where one would like to get rid of the fan altogether and convert the engine to a turbojet. For the ideal cycle the turbojet limit occurs at an unrealistically high Mach number of approximately 3.9. Non-ideal component behavior greatly reduces this optimum Mach number. Figure 5.3 provides another cut on this issue. Here the optimum bypass ratio is plotted versus the fan temperature (or pressure) ratio. Several curves are shown for increasing Mach number.

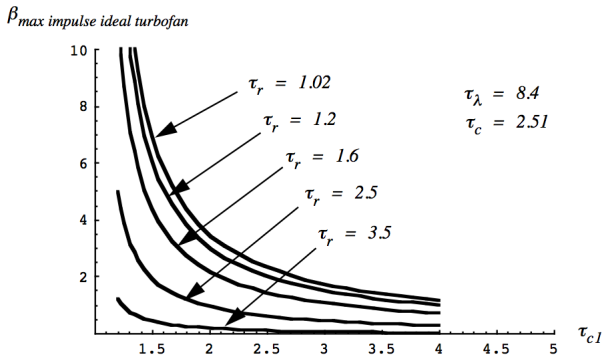

Figure 5.3: *Ideal turbofan bypass ratio for maximum specific impulse as a function of fan temperature ratio for several Mach numbers.*

It is clear that increasing the fan pressure ratio leads to an optimum at a lower bypass ratio. The curves all seem to allow for optimum systems at very low fan pressure ratios and high bypass ratios. This is an artifact of the assumptions underlying the ideal turbofan. As soon as non-ideal effects are included the low fan pressure ratio solutions reduce to much lower bypass ratios. To see this, we will shortly study the non-ideal case.

5.4 Turbofan thermal efficiency

Recall the definition of thermal efficiency from Chapter 2.

$$\eta_{th} = \frac{Power\ to\ the\ vehicle + \frac{\Delta\ kinetic\ energy\ of\ air}{second} + \frac{\Delta\ kinetic\ energy\ of\ fuel}{second}}{\dot{m}_f h_f} \tag{5.41}$$

For a turbofan with a core and bypass stream the thermal efficiency is

$$\eta_{th} = \frac{TU_0 + \left(\frac{\dot{m}_{a_{core}}(U_e - U_0)^2}{2} + \frac{\dot{m}_{a_{fan}}(U_{e1} - U_0)^2}{2}\right) + \left(\frac{\dot{m}_f(U_e - U_0)^2}{2} - \frac{\dot{m}_f(U_0)^2}{2}\right)}{\dot{m}_f h_f}. \tag{5.42}$$

Remember, the frame of reference for Equation (5.42) is one where the air ahead of the engine is at rest. If both exhausts are fully expanded, so that $P_e = P_0$; $P_{e1} = P_0$ the thermal efficiency becomes

$$\eta_{th} = \frac{\left(\dot{m}_{a_{core}}(U_e - U_0) + \dot{m}_{a_{fan}}(U_{e1} - U_0) + \dot{m}_f U_e\right) U_0}{\dot{m}_f h_f} + \frac{\left(\frac{\dot{m}_{a_{core}}(U_e - U_0)^2}{2} + \frac{\dot{m}_{a_{fan}}(U_{e1} - U_0)^2}{2}\right) + \left(\frac{\dot{m}_f(U_e - U_0)^2}{2} - \frac{\dot{m}_f(U_0)^2}{2}\right)}{\dot{m}_f h_f} \tag{5.43}$$

which reduces to

$$\eta_{th} = \frac{\left(\dot{m}_{a_{core}}\left(\frac{{U_e}^2}{2} - \frac{{U_0}^2}{2}\right) + \dot{m}_{a_{fan}}\left(\frac{{U_{e1}}^2}{2} - \frac{{U_0}^2}{2}\right) + \dot{m}_f \frac{{U_e}^2}{2}\right) U_0}{\dot{m}_f h_f}. \tag{5.44}$$

We can recast (5.44) in terms of enthalpies using the following relations

$$\begin{aligned} \dot{m}_f\left(h_f - h_{t4}\right) &= \dot{m}_{a_{core}}\left(h_{t4} - h_{t3}\right) \\ h_{t5} &= h_e + \frac{{U_e}^2}{2} \\ h_{t31} &= h_{e1} + \frac{{U_{e1}}^2}{2} \end{aligned} \tag{5.45}$$

where the fan and core nozzle streams are assumed to be adiabatic. Now

$$\eta_{th} = \frac{\dot{m}_{a_{core}} \left((h_{t5} - h_e) - (h_{t0} - h_0) \right) + \dot{m}_{a_{fan}} \left((h_{t31} - h_{1e}) - (h_{t0} - h_0) \right) + \dot{m}_f \left(h_{t5} - h_e \right)}{\left(\dot{m}_f + \dot{m}_{a_{core}} \right) h_{t4} - \dot{m}_{a_{core}} h_{t3}}. \tag{5.46}$$

Rearrange (5.46) to read

$$\eta_{th} = \frac{\left(\dot{m}_{a_{core}} + \dot{m}_f \right) h_{t5} + \dot{m}_{a_{fan}} h_{t31} - \left(\dot{m}_{a_{core}} + \dot{m}_{a_{fan}} \right) h_{t0}}{\left(\dot{m}_f + \dot{m}_{a_{core}} \right) h_{t4} - \dot{m}_{a_{core}} h_{t3}} - \frac{\dot{m}_{a_{core}} \left(h_e - h_0 \right) + \dot{m}_{a_{fan}} \left(h_{e1} - h_0 \right) + \dot{m}_f h_e}{\left(\dot{m}_f + \dot{m}_{a_{core}} \right) h_{t4} - \dot{m}_{a_{core}} h_{t3}}. \tag{5.47}$$

Recall the turbofan work balance (5.27). This relation can be rearranged to read

$$\left(\dot{m}_f + \dot{m}_{a_{core}} \right) h_{t4} - \dot{m}_{a_{core}} h_{t3} = \left(\dot{m}_{a_{core}} + \dot{m}_f \right) h_{t5} + \dot{m}_{a_{fan}} h_{t31} - \left(\dot{m}_{a_{core}} + \dot{m}_{a_{fan}} \right) h_{t0} \tag{5.48}$$

where it has been assumed that the inlet is adiabatic $h_{t2} = h_{t0}$. Now use (5.48) to replace the numerator or denominator in the first term of (5.47). The thermal efficiency finally reads

$$\eta_{th} = 1 - \frac{Q_{rejected\ during\ the\ cycle}}{Q_{input\ during\ the\ cycle}} = 1 - \frac{\left(\dot{m}_{a_{core}} + \dot{m}_f \right) \left(h_e - h_0 \right) + \dot{m}_{a_{fan}} \left(h_{e1} - h_0 \right) + \dot{m}_f h_0}{\left(\dot{m}_f + \dot{m}_{a_{core}} \right) h_{t4} - \dot{m}_{a_{core}} h_{t3}}. \tag{5.49}$$

The expression in (5.49) for the heat rejected during the cycle

$$Q_{rejected\ during\ the\ cycle} = \left(\dot{m}_{a_{core}} + \dot{m}_f \right) \left(h_e - h_0 \right) + \dot{m}_{a_{fan}} \left(h_{e1} - h_0 \right) + \dot{m}_f h_0 \tag{5.50}$$

brings to mind the discussion of thermal efficiency in Chapter 2. The heat rejected comprises heat conduction to the surrounding atmosphere from the fan and core mass flows plus physical removal from the thermally equilibrated nozzle flow of a portion equal to the added fuel mass flow. From this perspective the added fuel mass carries its fuel enthalpy into the system and the exhausted fuel mass carries its ambient enthalpy out of the system and there is no net mass increase or decrease to the system.

The main assumptions underlying (5.49) are that the engine operates adiabatically, the shaft mechanical efficiency is one, and the burner combustion efficiency is one. Engine components are not assumed to operate ideally; They are not assumed to be isentropic.

5.4.1 Thermal efficiency of the ideal turbofan

For the ideal cycle, assuming constant C_p, equation (5.49) in terms of temperatures becomes

$$\eta_{th_{ideal\ \ turbofan}} = 1 - \left(\frac{(1+(1+\beta)\,f)\,T_e - T_0}{(1+(1+\beta)\,f)\,T_{t4} - T_{t3}} \right) = 1 - \left(\frac{1}{\tau_r \tau_c} \right) \left(\frac{(1+(1+\beta)\,f)\,\frac{T_e}{T_0} - 1}{(1+(1+\beta)\,f)\,\frac{\tau_\lambda}{\tau_r \tau_c} - 1} \right). \tag{5.51}$$

Using (5.25) Equation (5.51) becomes

$$\eta_{th\,ideal\,turbofan} = 1 - \left(\frac{1}{\tau_r \tau_c} \right) \tag{5.52}$$

which is identical to the thermal efficiency of the ideal turbojet. Notice that for the ideal turbofan with

$$h_{e1} = h_0$$

the heat rejected by the fan stream is zero. Therefore the thermal efficiency of the ideal turbofan is independent of the parameters of the fan stream.

5.5 The non-ideal turbofan

The fan, compressor and turbine polytropic relations are

$$\begin{aligned} \pi_{c1} &= \tau_{c1}^{\frac{\gamma \eta_{pc1}}{\gamma - 1}} \\ \pi_c &= \tau_c^{\frac{\gamma \eta_{pc}}{\gamma - 1}} \\ \pi_t &= \tau_t^{\frac{\gamma}{(\gamma - 1)\eta_{pe}}} \end{aligned} \tag{5.53}$$

where η_{pc1} is the polytropic efficiency of the fan. The polytropic efficiencies η_{pc}, η_{pc1} and η_{pe} are all less than one. The inlet, burner and nozzles all operate with some stagnation pressure loss.

$$\begin{aligned} \pi_d &< 1 \\ \pi_{n1} &< 1 \\ \pi_n &< 1 \\ \pi_b &< 1 \end{aligned} \tag{5.54}$$

5.5.1 Non-ideal fan stream

The stagnation pressure ratio across the fan is

$$P_{te1} = P_0 \pi_r \pi_d \pi_{c1} \pi_{n1} = P_{e1} \left(1 + \frac{\gamma - 1}{2} {M_{e1}}^2 \right)^{\frac{\gamma}{\gamma - 1}}. \tag{5.55}$$

The fan nozzle is still assumed to be fully expanded and so the Mach number ratio for the non-ideal turbofan is

$$\left(\frac{M_{e1}}{M_0} \right)^2 = \frac{\tau_r {\tau_{c1}}^{\eta_{pc1}} (\pi_d \pi_{n1})^{\frac{\gamma - 1}{\gamma}} - 1}{\tau_r - 1}. \tag{5.56}$$

The stagnation temperature is (assuming the inlet and fan nozzle are adiabatic)

$$T_{te1} = T_0 \tau_r \tau_{c1} = T_{e1} \left(1 + \frac{\gamma - 1}{2} {M_{e1}}^2 \right) = T_{e1} \tau_r {\tau_{c1}}^{\eta_{pc1}} (\pi_d \pi_{n1})^{\frac{\gamma - 1}{\gamma}} \tag{5.57}$$

and

$$\frac{T_{e1}}{T_0} = \frac{{\tau_{c1}}^{1 - \eta_{pc1}}}{(\pi_d \pi_{n1})^{\frac{\gamma - 1}{\gamma}}}. \tag{5.58}$$

Now the velocity ratio across the non-ideal fan is

$$\left(\frac{U_{e1}}{U_0} \right)^2 = \frac{1}{\tau_r - 1} \left(\tau_r \tau_{c1} - \frac{{\tau_{c1}}^{1 - \eta_{pc1}}}{(\pi_d \pi_{n1})^{\frac{\gamma - 1}{\gamma}}} \right). \tag{5.59}$$

5.5.2 Non-ideal core stream

The stagnation pressure across the core is

$$P_{te1} = P_0 \pi_r \pi_d \pi_c \pi_b \pi_t \pi_n = P_e \left(1 + \frac{\gamma - 1}{2} {M_e}^2 \right)^{\frac{\gamma}{\gamma - 1}}. \tag{5.60}$$

The core nozzle is fully expanded and so the Mach number ratio across the non-ideal core is

$$\left(\frac{M_e}{M_0} \right)^2 = \frac{\tau_r {\tau_c}^{\eta_{pc}} {\tau_t}^{\frac{1}{\eta_{pe}}} \left(\pi_d \pi_b \pi_n \right)^{\frac{\gamma - 1}{\gamma}} - 1}{\tau_r - 1}. \tag{5.61}$$

In the non-ideal turbofan we continue to assume that the diffuser and nozzle flows are adiabatic and so

$$T_{te} = T_e \tau_r {\tau_c}^{\eta_{pc}} {\tau_t}^{\frac{1}{\eta_{pe}}} \left(\pi_d \pi_b \pi_n \right)^{\frac{\gamma - 1}{\gamma}} \tag{5.62}$$

from which is determined

$$\frac{T_e}{T_0} = \frac{{\tau_c}^{1 - \eta_{pc}} {\tau_t}^{\left(1 - \frac{1}{\eta_{pe}} \right)} \tau_\lambda}{\tau_r \tau_c \left(\pi_d \pi_b \pi_n \right)^{\frac{\gamma - 1}{\gamma}}}. \tag{5.63}$$

The velocity ratio across the non-ideal core is

$$\left(\frac{U_e}{U_0} \right)^2 = \frac{1}{\tau_r - 1} \left(\tau_\lambda \tau_t - \frac{{\tau_c}^{1 - \eta_{pc}} {\tau_t}^{\left(1 - \frac{1}{\eta_{pe}} \right)} \tau_\lambda}{\tau_r \tau_c \left(\pi_d \pi_b \pi_n \right)^{\frac{\gamma - 1}{\gamma}}} \right). \tag{5.64}$$

The work balance across the engine remains essentially the same as in the ideal cycle

$$\tau_t = 1 - \frac{\tau_r}{\eta_m \tau_\lambda} \left(\left(\tau_c - 1 \right) + \beta \left(\tau_{c1} - 1 \right) \right) \tag{5.65}$$

where the shaft mechanical efficiency is defined as

$$\eta_m = \frac{\dot{m}_{a_{core}} \left(h_{t3} - h_{t2} \right) + \dot{m}_{a_{fan}} \left(h_{t31} - h_{t2} \right)}{\left(\dot{m}_f + \dot{m}_{a_{core}} \right) \left(h_{t4} - h_{t5} \right)}. \tag{5.66}$$

5.5.3 Maximum specific impulse non-ideal cycle

Equation (5.35) remains the same as for the ideal cycle.

$$\frac{1}{2\left(U_e/U_0\right)}\frac{\partial}{\partial\beta}\left(\frac{U_e}{U_0}\right)^2+\left(\frac{U_{e1}}{U_0}-1\right)=0 \tag{5.67}$$

The derivative is

$$\frac{\partial}{\partial\beta}\left(\frac{{U_e}^2}{{U_0}^2}\right)=\frac{-\tau_r\left(\tau_{c1}-1\right)}{\eta_m\left(\tau_r-1\right)}\left(1-\frac{\left(1-\frac{1}{\eta_{pe}}\right){\tau_c}^{1-\eta_{pc}}{\tau_t}^{\left(-\frac{1}{\eta_{pe}}\right)}}{\tau_r\tau_c\left(\pi_d\pi_b\pi_n\right)^{\frac{\gamma-1}{\gamma}}}\right) \tag{5.68}$$

Equations (5.59), (5.64), (5.65) and (5.68) are inserted into (5.67) and the optimal bypass ratio for a set of selected engine parameters is determined implicitly. A typical numerically determined result is shown in Figure 5.4 and Figure 5.5.

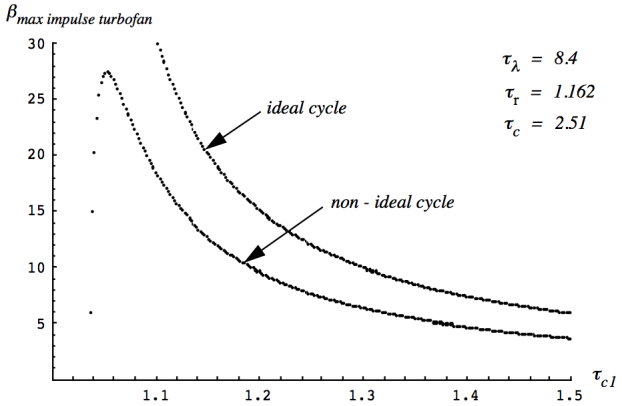

Figure 5.4: *Turbofan bypass ratio for maximum specific impulse as a function of fan temperature ratio comparing the ideal with a non-ideal cycle. Parameters of the non-ideal cycle are* $\pi_d = 0.95$, $\eta_{pc1} = 0.86$, $\pi_{n1} = 0.96$, $\eta_{pc} = 0.86$, $\pi_b = 0.95$, $\eta_m = 0.98$, $\eta_{pe} = 0.86$, $\pi_n = 0.96$.

These figures illustrate the strong dependence of the optimum bypass ratio on the non-ideal behavior of the engine. As the losses increase, the bypass ratio optimizes at a lower value. But note that the optimum bypass ratio of the non-ideal engine is still somewhat higher than the values generally used in real engines. The reason for this is that our analysis does not include the optimization issues connected to integrating the engine onto an aircraft where there is a premium on designing to a low frontal area so as to reduce drag

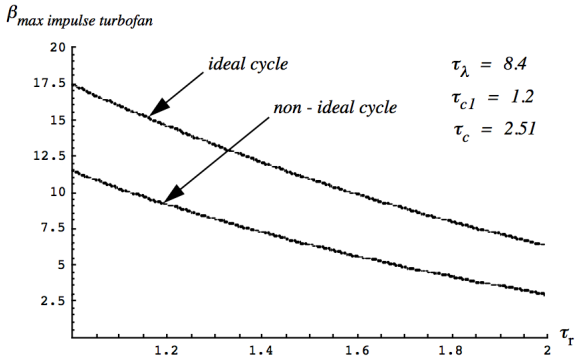

Figure 5.5: *Turbofan bypass ratio for maximum specific impulse as a function of Mach numbers comparing the ideal with a non-ideal cycle. Parameters of the non-ideal cycle are* $\pi_d = 0.95$, $\eta_{pc1} = 0.86$, $\pi_{n1} = 0.96$, $\eta_{pc} = 0.86$, $\pi_b = 0.95$, $\eta_m = 0.98$, $\eta_{pe} = 0.86$, $\pi_n = 0.96$.

while maintaining a certain clearance between the engine and the runway. Nevertheless, our analysis helps us to understand the historical trend toward higher bypass engines as turbine and fan efficiencies have improved along with increases in the turbine inlet temperature.

5.6 Problems

Problem 1 - Assume $\gamma = 1.4$, $R = 287\,m^2/\left(\sec^2 - K\right)$, $C_p = 1005\,m^2/\left(\sec^2 - K\right)$. The fuel heating value is $4.28 \times 10^7\,J/kg$. Where appropriate assume $f \ll 1$. The ambient temperature and pressure are $T_0 = 216\,K$ and $P_0 = 2 \times 10^4\,N/m^2$. Consider a turbofan with the following characteristics.

$$\begin{aligned} M_0 &= 0.85 \\ \tau_\lambda &= 8.0 \\ \pi_c &= 30 \\ \pi_{c1} &= 1.6 \\ \beta &= 5 \end{aligned} \tag{5.69}$$

The compressor, fan and turbine polytropic efficiencies are

$$\eta_{pc} = 0.9$$
$$\eta_{pc1} = 0.9 \tag{5.70}$$
$$\eta_{pt} = 0.95.$$

Let the burner efficiency and pressure ratio be $\eta_b = 0.99$ and $\pi_b = 0.97$. Assume the shaft efficiency is one. Both the fan and core streams use ideal simple convergent nozzles. Determine the dimensionless thrust T/P_0A_0, specific fuel consumption, and overall efficiency of the engine. Suppose the engine is expected to deliver 8,000 pounds of thrust at cruise conditions. What must be the area of the fan face A_2?

Problem 2 - Use Matlab or Mathematica to develop a program that reproduces Figure 5.4 and Figure 5.5.

Problem 3 - Figure 5.6 shows an ideal turbofan operating with a heat exchanger at its aft end.

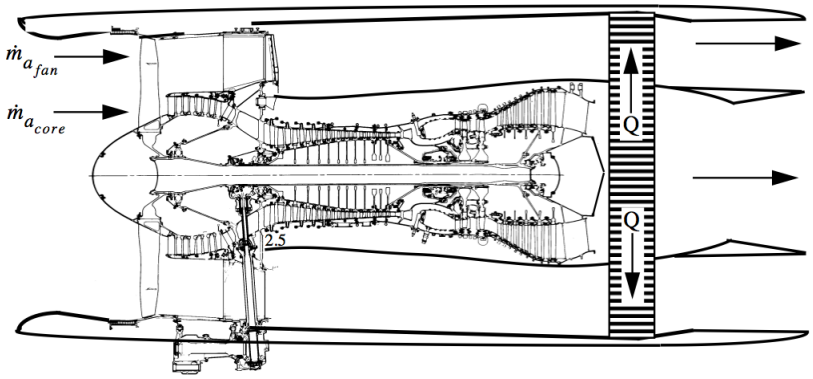

Figure 5.6: *Turbofan with an aft heat exchanger.*

The heat exchanger causes a certain amount of thermal energy Q (Joules/sec) to be transferred from the hot core stream to the cooler fan stream. Let the subscript x refer to the heat exchanger. Assume that the heat exchanger operates without any loss of stagnation pressure $\pi_x = \pi_{x1} = 1$ and that both nozzles are fully expanded. Let $\tau_x = T_{te}/T_{t5}$ and $\tau_x 1 = T_{te1}/T_{t51}$. The thrust is given by

$$\frac{T}{\dot{m}_{a_{core}} a_0} = M_0 \left(\left(\frac{U_e}{U_0} - 1 \right) + \beta \left(\frac{U_{e1}}{U_0} - 1 \right) \right) \tag{5.71}$$

where we have assumed $f \ll 1$.

1) Derive an expression for $T/\left(\dot{m}_{a_{core}} a_0\right)$ in terms of τ_λ, τ_r, τ_c, τ_{c1}, β and τ_x, τ_{x1}.

2) Write down an energy balance between the core and fan streams. Suppose an amount of heat Q is exchanged. Let $\tau_x = 1 - \alpha$ where $\alpha = Q/\dot{m}_{a_{core}} C_p T_{t5}$, $Q > 0$. Show that

$$\tau_{x1} = 1 + \left(\frac{\tau_\lambda \tau_t}{\beta \tau_r \tau_{c1}}\right) \alpha. \tag{5.72}$$

3) Consider an ideal turbofan with the following characteristics.

$$\begin{aligned} T_0 &= 216K \\ M_0 &= 0.85 \\ \tau_\lambda &= 7.5 \\ \pi_c &= 30 \\ \pi_{c1} &= 1.6 \\ \beta &= 5 \end{aligned} \tag{5.73}$$

Plot $T/\dot{m}_{a_{core}} a_0$ versus α for $0 < \alpha < \alpha_{\max}$ where $\alpha_{\max}$ corresponds to the value of α such that the two streams are brought to the same stagnation temperature coming out of the heat exchanger.

Problem 4 - Figure 5.7 shows a turbojet engine supplying shaft power to a lift fan. Assume that there are no mechanical losses in the shaft but the clutch and gear box that transfers power to the fan has an efficiency of 80%. That is, only 80% of the shaft power is used to increase the enthalpy of the air flow through the lift fan. The air mass flow rate through the lift fan is equal to twice the air mass flow rate through the engine $\dot{m}_{Lift\ Fan} = 2\dot{m}_a$. The polytropic efficiency of the lift fan is $\eta_{p_{Lift\ Fan}} = 0.9$ and the air flow through the lift fan is all subsonic. The flight speed is zero.

The ambient temperature and pressure are $T_0 = 300\,K$ and $P_0 = 1.01 \times 10^5\,N/m^2$. The turbine inlet temperature is $T_{t4} = 1800\,K$ and $\pi_c = 25$. Relevant area ratios are $A_2/A_4^* = 15$ and $A_{1_{throat}}/A_2 = 0.5$. Assume the compressor, burner and turbine all operate ideally. The nozzle is a simple convergent design and stagnation pressure losses due to wall friction in the inlet and nozzle are negligible. Assume $f \ll 1$. Let the nozzle area be set so that $P_{t5}/P_0 = 3$.

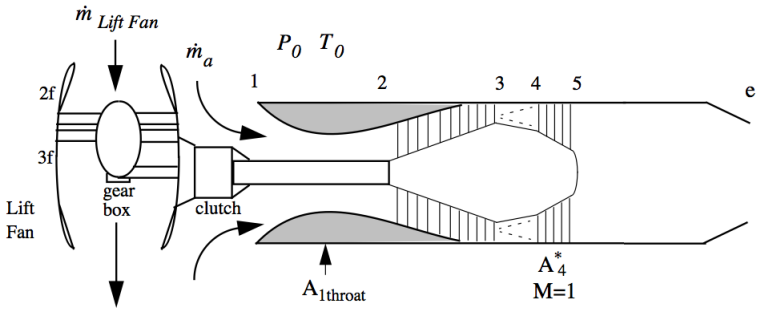

Figure 5.7: *Turbojet engine driving a lift fan.*

1) Is there a shock in the inlet of the turbojet?

2) Determine the stagnation temperature and pressure ratio across the lift fan

$$\tau_{Lift\,Fan} = \frac{T_{t3\,Lift\,Fan}}{T_{t2\,Lift\,Fan}}$$
$$\pi_{Lift\,Fan} = \frac{P_{t3\,Lift\,Fan}}{P_{t2\,Lift\,Fan}}. \tag{5.74}$$

Chapter 6

The Turboprop cycle

6.1 Propellor efficiency

The turboprop cycle can be regarded as a very high bypass limit of a turbofan. Recall that the propulsive efficiency of a thruster with $P_e = P_0$ and $f \ll 1$ is

$$\eta_{pr} = \frac{2}{1 + U_e/U_0}. \tag{6.1}$$

This expression is relevant to a propeller also where U_e is replaced by U_∞ the velocity, shown schematically in Figure 6.1, that would occur far downstream of the propeller if there were no mixing of the propeller wake.

The achievement of high propulsive efficiency at a given thrust requires a large mass flow with a small velocity increment. The turboprop accomplishes this by using a low pressure turbine to produce shaft power to drive a propeller. Since the propeller disc is quite large the mass flow rate is large and a high propulsive efficiency can be achieved.

The power output of a turbine is proportional to the square of the blade speed and so turbines generally operate at high rotational speeds limited by compressibility effects at the blade tips. The propeller diameter is much larger than the turbine diameter and so to avoid compressibility losses over the outer portion of the propeller a gearbox is required to step the turbine rotational speed down to values that keep the propeller tip Mach numbers below one.

It should be pointed out that Figure 6.1 is purely a schematic and the relative size of the gearbox shown in this figure is quite unrealistic. The figure below shows a cross section of

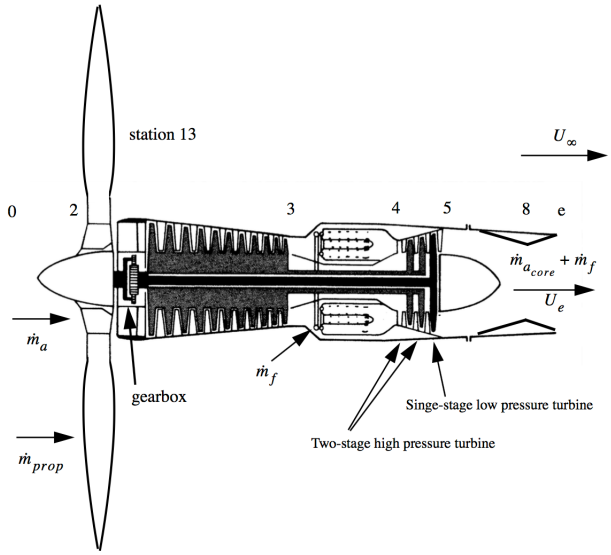

Figure 6.1: *Schematic of a turboprop engine.*

a current model of the Allison T56 turboprop engine. This is a widely used engine that has been in operation since 1954.

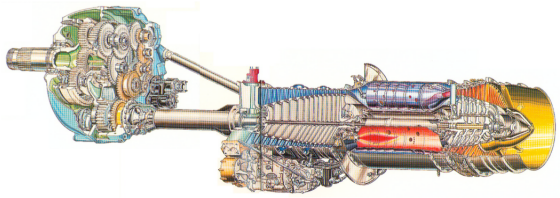

Figure 6.2: *Turboprop engine with its gearbox.*

As the figure shows, the gearbox is massive and contains a dizzyingly complex system of gears and bearings. In fact the main disadvantage of the turboprop is the weight and maintenance cost of the gearbox as well as the maintenance cost of the propeller. In terms of cycle performance, the power losses through the gearbox are also a significant factor.

In any case if an efficient gearbox and propeller system can be developed, a turboprop should be a more efficient cycle than a turbojet or a turbofan at low Mach number. Actual cycle analysis shows that at low to moderate subsonic flight Mach numbers fuel consumption is lower for the turboprop cycle. However in the transonic and supersonic flight regime propeller driven aircraft are prohibitively noisy and propeller efficiency falls off rapidly with

Mach number due to stagnation pressure losses at the blade tips.

Part of the thrust of a turboprop comes from the flow through the core engine. We can analyze the core flow using the same approach used in the turbojet. But a major portion of the thrust comes from the propeller and because the flow through the propeller is unducted there is no simple way to relate the thrust produced by the propeller to the usual flow variables that we can analyze using basic gas-dynamic tools. Such an analysis would require a means of determining the flow speed induced by the propeller infinitely far down stream of the engine. For this reason, the analysis of the turboprop begins with a definition of the propeller efficiency.

$$\eta_{prop} = \frac{T_{prop} U_0}{W_p} \tag{6.2}$$

where W_p is the power supplied to the propeller by the low pressure turbine. As long as the propeller efficiency is known then the propeller thrust is known in terms of the flow through the turbine. To understand the nature of the propeller efficiency it is useful to factor (6.2) as follows. The thrust produced by the propeller is

$$T_{prop} = \dot{m}_{prop} \left(U_\infty - U_0 \right). \tag{6.3}$$

Using (6.3) the propeller efficiency can be factored as

$$\eta_{prop} = \left(\frac{\dot{m}_{prop} \left(U_\infty - U_0 \right) U_0}{\frac{1}{2} \dot{m}_{prop} \left({U_\infty}^2 - {U_0}^2 \right)} \right) \left(\frac{\frac{1}{2} \dot{m}_{prop} \left({U_\infty}^2 - {U_0}^2 \right)}{W_p} \right). \tag{6.4}$$

The propeller efficiency factors into a product of a propulsive efficiency multiplying a term that compares the change in kinetic energy across the propeller to the shaft work.

$$\eta_{prop} = \left(\frac{2 U_0}{U_\infty + U_0} \right) \left(\frac{\frac{1}{2} \dot{m}_{prop} \left({U_\infty}^2 - {U_0}^2 \right)}{W_p} \right) \tag{6.5}$$

Let's look at this from a thermodynamic point of view. The stagnation enthalpy rise across the propeller produced by the shaft work is

$$W_p = \dot{m}_{prop} \left(h_{t13} - h_{t2} \right). \tag{6.6}$$

In the simplest model of propeller flow, the propeller is treated as an actuator disc, a uniform disc over which there is a pressure and temperature rise that is constant over the

disc area. The flow velocity increases up to and through the disc while the flow velocity is the same just ahead and just behind the disc as shown in Figure 6.3. According to Froude's theorem the velocity change ahead of the propeller is the same as behind and so

$$U_2 = U_{13} = \frac{U_0 + U_\infty}{2}. \tag{6.7}$$

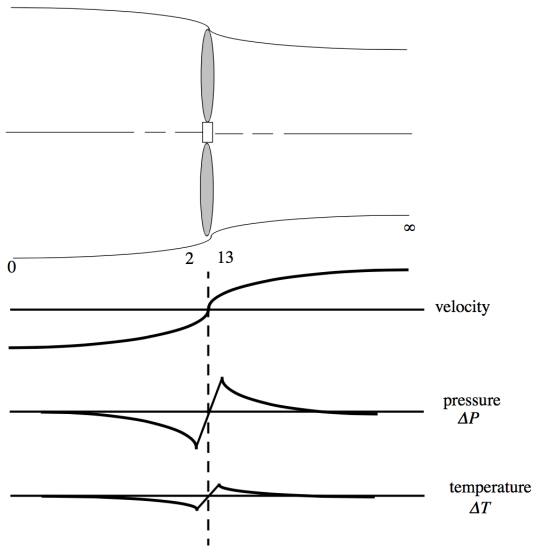

Figure 6.3: *Effect of propeller actuator disc on flow velocity, pressure and temperature.*

Since the velocity is the same before and after the propeller we can write

$$W_p = \dot{m}_{prop} C_p \left(T_{13} - T_2\right). \tag{6.8}$$

The stagnation pressure and stagnation temperature across the propeller are related by a polytropic efficiency of compression which accounts for the entropy rise across the propeller.

$$\frac{P_{t13}}{P_{t2}} = \left(\frac{T_{t13}}{T_{t2}}\right)^{\frac{\gamma \eta_{pc}}{\gamma - 1}} \tag{6.9}$$

Equation (6.9) can be written as

$$\frac{P_{13}}{P_2}\left(\frac{1+\frac{\gamma-1}{2}{M_{13}}^2}{1+\frac{\gamma-1}{2}{M_2}^2}\right)^{\frac{\gamma}{\gamma-1}} = \left(\frac{T_{13}}{T_2}\right)^{\frac{\gamma\eta_{pc}}{\gamma-1}}\left(\frac{1+\frac{\gamma-1}{2}{M_{13}}^2}{1+\frac{\gamma-1}{2}{M_2}^2}\right)^{\frac{\gamma\eta_{pc}}{\gamma-1}}. \tag{6.10}$$

The Mach number change across the propeller is small due to the small temperature change and to a good approximation (6.10) relates the static temperatures and pressures

$$\frac{P_{13}}{P_2} = \left(\frac{T_{13}}{T_2}\right)^{\frac{\gamma\eta_{pc}}{\gamma-1}} \tag{6.11}$$

which we can write as

$$1+\left(\frac{P_{13}-P_2}{P_2}\right) = \left(1+\frac{T_{13}-T_2}{T_2}\right)^{\frac{\gamma\eta_{pc}}{\gamma-1}}. \tag{6.12}$$

For a propeller that is lightly loaded, (6.12) can be approximated as

$$\frac{P_{13}-P_2}{P_2} \cong \frac{\gamma\eta_{pc}}{\gamma-1}\left(\frac{T_{13}-T_2}{T_2}\right) \tag{6.13}$$

or

$$P_{13}-P_2 \cong \eta_{pc}\rho_2 C_p\left(T_{13}-T_2\right). \tag{6.14}$$

The propeller thrust is

$$T = \left(P_{13}-P_2\right)A \tag{6.15}$$

where A is the effective area of the actuator disc. Now combine (6.8), (6.14) and (6.15) to form the propeller efficiency.

$$\eta_{prop} = \frac{\eta_{pc}\rho_2 U_0 A C_p\left(T_{13}-T_2\right)}{\dot{m}_{prop}C_p\left(T_{13}-T_2\right)} = \frac{\eta_{pc}\rho_2 U_0 A}{\rho_2 U_2 A} \tag{6.16}$$

Using (6.7), the propeller efficiency becomes finally

$$\eta_{prop} = \left(\frac{2U_0}{U_0+U_\infty}\right)\eta_{pc} \tag{6.17}$$

which should be compared with (6.5). We can now interpret the energy factor in (6.5) as

$$\eta_{pc} \cong \frac{\frac{1}{2}\dot{m}_{prop}\left({U_\infty}^2 - {U_0}^2\right)}{W_p}. \tag{6.18}$$

The polytropic efficiency is also related to the entropy change across the propeller. From (6.13)

$$\frac{dP}{P} = \eta_{pc}\left(\frac{\gamma}{\gamma - 1}\right)\frac{dT}{T}. \tag{6.19}$$

According to the Gibbs equation, the entropy change across a differential part of the compression process is

$$\frac{ds}{C_p} = \frac{dT}{T} - \left(\frac{\gamma - 1}{\gamma}\right)\frac{dP}{P} = (1 - \eta_{pc})\frac{dT}{T} \tag{6.20}$$

and so the propeller efficiency can also be written as

$$\eta_{prop} = \left(\frac{2U_0}{U_0 + U_\infty}\right)\left(1 - \frac{T}{C_p}\frac{ds}{dT}\right). \tag{6.21}$$

These results tell us that the propeller efficiency is determined by two distinct mechanisms. The first is the propulsive efficiency that is directly related to the propeller loading (Thrust/Area). The higher the loading, the more power is lost to increasing the kinetic energy of the flow. A very highly loaded propeller is sensitive to blade stall and one of the advantages of putting a duct around the propeller, turning it into a fan, is that a higher thrust per unit area can be achieved.

The second mechanism is the entropy rise across the propeller due to viscous friction and stagnation pressure losses due to compressibility effects. A well designed propeller should achieve as low an entropy rise per unit temperature rise, ds/dT, as possible. Note that even if we could design a propeller that operated isentropically it would still have an efficiency that is less than one.

6.2 Work output coefficient

The thrust equation for the turboprop is

$$T_{total} = T_{core} + T_{prop}$$

$$or \tag{6.22}$$

$$T = \dot{m}_a \left(U_e - U_0\right) + \dot{m}_f U_e + \left(P_e - P_0\right) A_e + \dot{m}_{prop} \left(U_\infty - U_0\right).$$

Substitute the propeller efficiency

$$T_{total} = \dot{m}_a \left(U_e - U_0\right) + \dot{m}_f U_e + \left(P_e - P_0\right) A_e + \eta_{prop} \frac{W_p}{U_0}. \tag{6.23}$$

The core thrust has the usual form

$$\frac{T_{core}}{\dot{m}_a a_0} = M_0 \left(\left(1 + f\right) \frac{M_e}{M_0} \sqrt{\frac{T_e}{T_0}} - 1 \right) \tag{6.24}$$

where the nozzle is taken to be fully expanded $P_e = P_0$.

The presence of U_0 in the denominator of (6.23) indicates the inadequacy of the propeller efficiency for describing propeller thrust at low speeds. As a consequence the performance of a turboprop is usually characterized in terms of power output instead of thrust. Define the work output coefficient as

$$C_{total} = \frac{T_{total} U_0}{\dot{m}_a C_p T_0} = C_{core} + C_{prop} \tag{6.25}$$

where from (6.23)

$$C_{core} = \left(\gamma - 1\right) {M_0}^2 \left(\left(1 + f\right) \frac{M_e}{M_0} \sqrt{\frac{T_e}{T_0}} - 1 \right) \tag{6.26}$$

and

$$C_{prop} = \eta_{prop} \frac{W_p}{\dot{m}_a C_p T_0}. \tag{6.27}$$

The work output coefficient and the dimensionless thrust are directly proportional to one another

$$\frac{T}{P_0 A_0} = \frac{\gamma}{\gamma - 1} C_{total}. \tag{6.28}$$

The fuel efficiency of the turboprop is expressed in terms of the specific horsepower

$$SHP = \frac{pounds\ of\ fuel\ burned\ per\ hour}{output\ horsepower} = 3600 \frac{\dot{m}_f g}{T_{total} U_0}$$

$$or \tag{6.29}$$

$$SHP = \frac{2545}{C_p T_0} \left(\frac{f}{C_{total}} \right)$$

where the temperature is in degrees Rankine and the heat capacity is in BTU/lbm-hr.

6.3 Power balance

The turbine drives both the compressor and propeller. The power to the propeller is

$$W_p = \eta_g \left((\dot{m}_a + \dot{m}_f) \eta_m \left(h_{t4} - h_{t5} \right) - \dot{m}_a \left(h_{t3} - h_{t2} \right) \right) \tag{6.30}$$

where η_g is the gearbox efficiency and η_m is the shaft mechanical efficiency. Substitute (6.30) into (6.27) and assume the gas is calorically perfect. The work output coefficient of the propeller is expressed in terms of cycle parameters as

$$C_{prop} = \eta_{prop} \eta_g \left((1 + f) \eta_m \tau_\lambda \left(1 - \tau_t \right) - \tau_r \left(\tau_c - 1 \right) \right). \tag{6.31}$$

6.4 The ideal turboprop

The assumptions of the ideal turboprop are essentially the same as for the ideal turbojet,

namely

$$\begin{aligned} \pi_d &= 1 \\ \eta_{pc} &= 1 \\ \pi_b &= 1 \\ \eta_{pe} &= 1 \\ \pi_n &= 1 \end{aligned} \tag{6.32}$$

along with $P_e = P_0$. Notice that the propeller efficiency is not assumed to be one. The ideal turboprop cycle begins with a propeller efficiency below one as reflected in the proportionality of the propeller efficiency to a propulsive efficiency that is inherently less than one. There is a little bit of an inconsistency here in that the compressor is assumed to be isentropic, whereas a small part of the compression of the core air is accomplished by the propeller. This portion of the compression is assumed to be isentropic even though the rest of the propeller may behave non-isentropically. In any case there is no way to distinguish between the propulsive and frictional parts of the propeller efficiency in practice and so all of the entropy change across the propeller can be assigned to the portion of the mass flow that passes outside of the core engine.

The exit Mach number is generated in the same manner as for the ideal turbojet. The Mach number ratio is

$$\left(\frac{M_e}{M_0}\right)^2 = \left(\frac{\tau_r\tau_c\tau_t - 1}{\tau_r - 1}\right). \tag{6.33}$$

The temperature ratio is also generated in the same way.

$$\frac{T_e}{T_0} = \frac{\tau_\lambda}{\tau_r\tau_c} \tag{6.34}$$

The work output coefficient of the core is

$$C_{core} = 2\left(\tau_r - 1\right)\left(\left(1+f\right)\left(\frac{\tau_\lambda}{\tau_r\tau_c}\right)^{1/2}\left(\frac{\tau_r\tau_c\tau_t - 1}{\tau_r - 1}\right)^{1/2} - 1\right). \tag{6.35}$$

6.4.1 Optimization of the ideal turboprop cycle

The question now is: what fraction of the total thrust should be generated by the core in order to produce the maximum work output coefficient. The answer to this question is required in order to properly select the size of the turbine. Now determine an extremum in C_{total} with respect to τ_t.

$$\frac{\partial C_{total}}{\partial \tau_t} = \frac{\partial C_{core}}{\partial \tau_t} + \frac{\partial C_{prop}}{\partial \tau_t} = 0 \tag{6.36}$$

Substitute C_{core}, (6.35) and C_{prop}, (6.31) into (6.36) and carry out the differentiation

$$2\left(\tau_r - 1\right)\left(1 + f\right)\left(\frac{\tau_\lambda}{\tau_r \tau_c}\right)^{1/2} \frac{1}{2}\left(\frac{\tau_r \tau_c \tau_t - 1}{\tau_r - 1}\right)^{-1/2}\left(\frac{\tau_r \tau_c}{\tau_r - 1}\right) - \eta_{prop}\eta_g\left(1 + f\right)\eta_m \tau_\lambda = 0 \tag{6.37}$$

which simplifies to

$$\left(\tau_\lambda \tau_r \tau_c\right)^{1/2}\left(\frac{\tau_r \tau_c \tau_t - 1}{\tau_r - 1}\right)^{-1/2} = \eta_{prop}\eta_g\eta_m\tau_\lambda. \tag{6.38}$$

Notice that the propeller, gearbox and shaft efficiencies enter the analysis as one product. Let

$$\eta = \eta_{prop}\eta_g\eta_m. \tag{6.39}$$

Square (6.38) and solve for τ_t.

$$\tau_t\big|_{\ max\ \ thrust\ \ ideal\ \ turboprop} = \frac{1}{\tau_r \tau_c} + \frac{\left(\tau_r - 1\right)}{\eta^2 \tau_\lambda} \tag{6.40}$$

This result essentially defines the size of the turbine needed to achieve maximum work output coefficient which is equivalent to maximum thrust. Lets see what core engine velocity ratio this corresponds to.

$$\left(\frac{U_e}{U_0}\right)^2\Bigg|_{max\,thrust\,ideal\,turboprop} = \frac{\tau_\lambda}{\tau_r \tau_c}\left(\frac{1}{\tau_r - 1}\right)\left(\tau_r \tau_c\, \tau_t\big|_{max\,thrust\,ideal\,turboprop} - 1\right) \tag{6.41}$$

Substitute (6.40) into (6.41). The result is the very simple relationship

$$\left.\frac{U_e}{U_0}\right|_{max\,thrust\,ideal\,turboprop} = \frac{1}{\eta}. \tag{6.42}$$

As the propeller-gearbox-shaft efficiency improves, the optimum turboprop cycle takes a larger and larger fraction of the thrust out of the propeller. This is accomplished with a larger turbine and a smaller core thrust.

The result (6.42) gives us some additional insight into the nature of the propeller efficiency. An ideal turboprop with a propeller that produced isentropic compression would have a core velocity that satisfies

$$U_e|_{\,max\,thrust\,ideal\,turboprop} = \frac{U_0 + U_\infty}{2}. \tag{6.43}$$

The core exit speed would be the average of the upstream and far downstream velocities. Referring back to (6.7) we can see that in this limit the core thruster becomes an indistinguishable part of the propeller actuator disc.

6.4.2 Compression for maximum thrust of an ideal turboprop

Once the turbine has been sized according to the above, then the thrust due to the core engine is fixed by (6.42). It is then a matter of choosing the compressor that maximizes C_{prop}. Differentiate (6.31) with respect to τ_c. Neglect f.

$$\frac{\partial C_{prop}}{\partial \tau_c} = \eta_{prop}\eta_g\left(-\eta_m\tau_\lambda\left(\frac{\partial \tau_t}{\partial \tau_c}\right) - \tau_r\right) = \eta_{prop}\eta_g\left(-\eta_m\tau_\lambda\left(\frac{-1}{\tau_r{\tau_c}^2}\right) - \tau_r\right) \tag{6.44}$$

Maximum C_{prop} is achieved for

$$\tau_c = \frac{\sqrt{\eta_m\tau_\lambda}}{\tau_r} \tag{6.45}$$

which is essentially the same result we obtained for the turbojet (exactly the same if we had included the shaft efficiency in the turbojet analysis). At this point the required turbine temperature ratio can determined from (6.40).

6.5 Turbine sizing for the non-ideal turboprop

The optimization problem is still essentially the same; we need to select the turbine temperature ratio so as to maximize the total work output coefficient.

$$\frac{\partial C_{total}}{\partial \tau_t} = \frac{\partial C_{core}}{\partial \tau_t} + \frac{\partial C_{prop}}{\partial \tau_t} = 0 \tag{6.46}$$

Assume the core flow is fully expanded. The squared velocity ratio across the non-ideal core is

$$\left(\frac{U_e}{U_0}\right)^2 = \frac{1}{\tau_r - 1}\left(\frac{\tau_\lambda}{\tau_r \tau_c}\right)\left(\tau_r\tau_c\tau_t - \frac{{\tau_c}^{1-\eta_{pc}}{\tau_t}^{\left(1-\frac{1}{\eta_{pe}}\right)}}{\left(\pi_d\pi_b\pi_n\right)^{\frac{\gamma-1}{\gamma}}}\right) \tag{6.47}$$

and the core work output coefficient of the non-ideal turboprop is

$$C_{core} = 2\left(\tau_r - 1\right)\left(\frac{(1+f)}{\left(\tau_r-1\right)^{1/2}}\left(\frac{\tau_\lambda}{\tau_r\tau_c}\right)^{1/2}\left(\tau_r\tau_c\tau_t - \frac{{\tau_c}^{1-\eta_{pc}}{\tau_t}^{\left(1-\frac{1}{\eta_{pe}}\right)}}{\left(\pi_d\pi_b\pi_n\right)^{\frac{\gamma-1}{\gamma}}}\right)^{1/2} - 1\right). \tag{6.48}$$

For the non-ideal cycle the condition (6.46) becomes

$$\begin{aligned}\left(\tau_r-1\right)^{1/2}\left(\frac{\tau_\lambda}{\tau_r\tau_c}\right)^{1/2}\left(\tau_r\tau_c\tau_t - \frac{{\tau_c}^{1-\eta_{pc}}{\tau_t}^{\left(1-\frac{1}{\eta_{pe}}\right)}}{\left(\pi_d\pi_b\pi_n\right)^{\frac{\gamma-1}{\gamma}}}\right)^{-1/2} \times \\ \left(\tau_r\tau_c - \left(1-\frac{1}{\eta_{pe}}\right)\frac{{\tau_c}^{1-\eta_{pc}}{\tau_t}^{\left(-\frac{1}{\eta_{pe}}\right)}}{\left(\pi_d\pi_b\pi_n\right)^{\frac{\gamma-1}{\gamma}}}\right) - \eta_{prop}\eta_g\eta_m\tau_\lambda = 0.\end{aligned} \tag{6.49}$$

Various flow parameters are specified in (6.49) and the turbine temperature ratio for maximum work output coefficient is determined implicitly. Figure 6.4 shows a typical calculation.

The optimum turbine temperature ratio increases with non-ideal effects indicating that a larger fraction of the total thrust is developed across the core engine of a non-ideal turboprop.

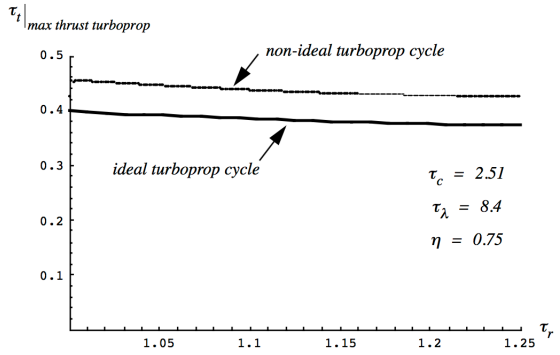

Figure 6.4: *Comparison of turbine selection for the ideal and non-ideal turboprop cycle. Parameters of the non-ideal cycle are* $\pi_d = 0.97$, $\eta_{pc} = 0.93$, $\pi_b = 0.96$, $\eta_{pe} = 0.95$, $\pi_n = 0.98$.

6.6 Problems

Problem 1 - Consider the propeller shown in Figure 6.5.

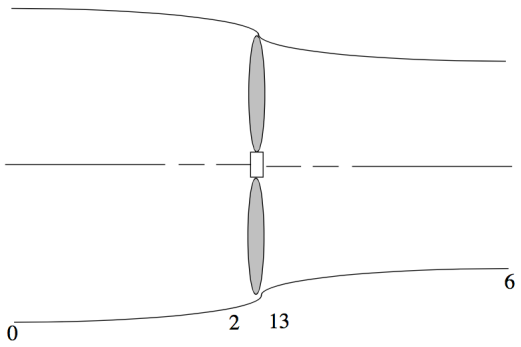

Figure 6.5: *Flow through an actuator disc.*

Show that for small Mach number, the velocity at the propeller is approximately

$$U_2 = U_{13} = \frac{U_0 + U_\infty}{2}. \tag{6.50}$$

In other words one-half the velocity change induced by the propeller occurs upstream of the propeller. This is known as Froude's theorem and is one of the cornerstones of propeller theory.

Problem 2 - Compare ducted versus unducted fans. Let the fan area be the same in both cases.

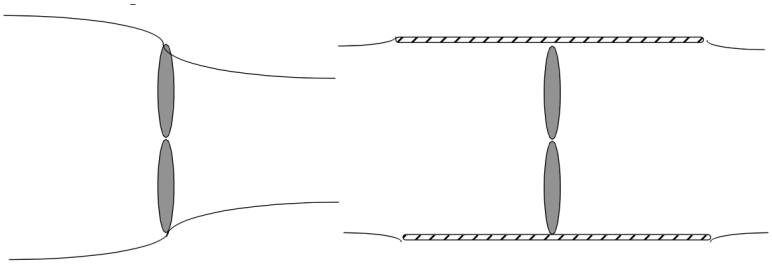

Figure 6.6: *Ducted and unducted fans.*

Show that, for the same power input, the ducted case produces more thrust. Note that the operating point of the ducted fan is chosen to produce a capture area equal to the area of the duct. Suppose the operating point were changed. How would your answer change?

Problem 3 - Derive equation (6.28).

Problem 4 - Use Matlab or Mathematica to develop a program that reproduces Figure 6.4.

Problem 5 - An ideal turboprop engine operates at a free stream Mach number, $M_0 = 0.7$. The propeller efficiency is, $\eta_{prop} = 0.8$ and the gearbox and shaft efficiencies are both 1.0. The turbine is chosen to maximize the total work output coefficient. The compressor is chosen according to, $\tau_c = \sqrt{\tau_\lambda}/\tau_r$ and $\tau_\lambda = 6$. Determine the dimensionless thrust, T/P_0A_0 where A_0 is the capture area corresponding to the air flow through the core engine. Assume $f \ll 1$. Is the exit nozzle choked?.

Problem 6 - A non-ideal turboprop engine operates at a free stream Mach number, $M_0 = 0.6$. The propeller efficiency is, $\eta_{prop} = 0.8$ and the gearbox and shaft efficiencies are both 1.0. The operating parameters of the engine are $\tau_\lambda = 7$, $\tau_c = 2.51$, $\pi_d = 0.97$, $\eta_{pc} = 0.93$, $\pi_b = 0.96$, $\eta_{pe} = 0.95$, $\pi_n = 0.98$. Determine the dimensionless thrust, T/P_0A_0 where A_0 is the capture area corresponding to the air flow through the core engine. Do not assume $f \ll 1$.

Problem 7 - A turboprop engine operates at a free stream Mach number, $M_0 = 0.6$. The propeller efficiency is $\eta_{prop} = 0.85$, the gearbox efficiency is $\eta_g = 0.95$, and the shaft efficiency is $\eta_m = 1$. All other components operate ideally and the exhaust is fully expanded $P_e = P_0$. The operating parameters of the engine are $\tau_\lambda = 7$ and $\tau_c = 2.51$. Assume the turbine is sized to maximize C_{total} and assume $f \ll 1$. Determine the total work output coefficient C_{total} and dimensionless thrust T/P_0A_0. The ambient temperature and pressure

are $T_0 = 216\,K$ and $P_0 = 2 \times 10^4 N/m^2$.

Problem 8 - A propulsion engineer is asked by her supervisor to determine the thrust of a turboprop engine at cruise conditions. The engine is designed to cruise at $M_0 = 0.5$. At that Mach number the engine is known to be operating close to its maximum total work output coefficient C_{total}. She responds by asking the supervisor to provide some data on the operation of the engine at this condition. List the minimum information she would need in order to provide a rough estimate of the thrust of the engine. What assumptions would she need to make in order to produce this estimate?

Chapter 7

Rocket performance

7.1 Thrust

Figure 7.1 shows a sketch of a rocket in a test stand. The rocket produces thrust, T , by expelling propellant mass from a thrust chamber with a nozzle. The test stand applies an opposite force on the rocket holding it at rest. The propellant (fuel+oxidizer) mass flow rate is $\dot{m}$ and the ambient pressure of the surrounding air is P_0.

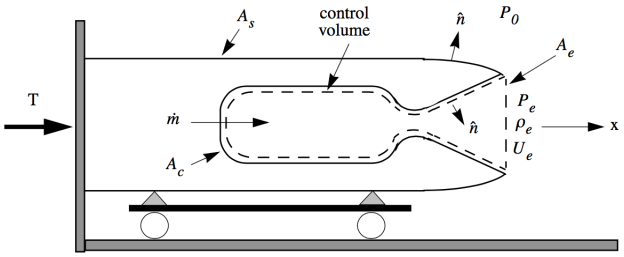

Figure 7.1: *Rocket thrust schematic.*

Other quantities defined in Figure 7.1 are as follows.

$$
\begin{aligned}
&A_s = outside\ surface\ of\ the\ vehicle\ exposed\ to\ P_0 \\
&A_c = inside\ surface\ of\ the\ combustion\ chamber \\
&A_e = nozzle\ exit\ area \\
&\hat{n} = outward\ unit\ normal \\
&P_e = area\ averaged\ exit\ gas\ pressure \\
&\rho_e = area\ averaged\ exit\ gas\ density \\
&U_e = area\ averaged\ x-component\ of\ velocity\ at\ the\ nozzle\ exit
\end{aligned}
\tag{7.1}
$$

The vehicle is at rest and so the total force acting on it is zero.

$$0 = T + \int_{A_s} \left(P\overline{\overline{I}} - \overline{\overline{\tau}} \right) \cdot \hat{n} dA \Big|_x + \int_{A_c} \left(P\overline{\overline{I}} - \overline{\overline{\tau}} \right) \cdot \hat{n} dA \Big|_x + \dot{m} U_{xm} \tag{7.2}$$

The variable P is the gas pressure acting at any point on the surface of the rocket, $\overline{\overline{\tau}}$ is the viscous stress tensor, and $\dot{m}U_{xm}$ is the x-momentum of the propellant injected into the thrust chamber. If the rocket were inactive so that there was no force on the restraint and the outside surface and thrust chamber were all at a pressure P_0 then

$$0 = \int_{A_s} P_0 \overline{\overline{I}} \cdot \hat{n} dA \Big|_x + \int_{A_c} P_0 \overline{\overline{I}} \cdot \hat{n} dA \Big|_x . \tag{7.3}$$

In this situation the control volume contains fluid all at rest and

$$0 = \int_{A_c} P_0 \overline{\overline{I}} \cdot \hat{n} dA \Big|_x + \int_{A_e} P_0 \overline{\overline{I}} \cdot \hat{n} dA \Big|_x . \tag{7.4}$$

The last relation can be written as

$$0 = \int_{A_c} P_0 \overline{\overline{I}} \cdot \hat{n} dA \Big|_x + P_0 A_e . \tag{7.5}$$

Note that a unit normal vector that is consistent between the control volume and the outside surface of the vehicle points inward on A_e. Thus equation (7.3) becomes

$$0 = \int_{A_s} P_0 \overline{\overline{I}} \cdot \hat{n} dA \Big|_x - P_0 A_e \tag{7.6}$$

and the original force balance (7.2) can be written as

$$0 = T + P_0 A_e + \int_{A_c} \left(P\overline{\overline{I}} - \overline{\overline{\tau}} \right) \cdot \hat{n} dA \Big|_x + \dot{m} U_{xm} . \tag{7.7}$$

Built into (7.7) is the assumption that when the engine is operating the external surface pressure and stress distribution is unchanged.

$$\left(\int_{A_s} \left(P\overline{\overline{I}} - \overline{\overline{\tau}} \right) \cdot \hat{n} dA \Big|_x \right)_{after\ engine\ turn\ on} = \left(\int_{A_s} P_0 \overline{\overline{I}} \cdot \hat{n} dA \Big|_x \right)_{before\ engine\ turn\ on} \tag{7.8}$$

In fact, the jet from the rocket mixes with the surrounding air setting the air near the vehicle into motion leading to slight deviations in the pressure acting on the outside of the vehicle. For a rocket of reasonable size and thrust, this is a very small effect.

With the engine on, a balance of momentum over the control volume gives

$$\frac{D}{Dt}\int_V (\rho\bar{U})dV = \int_V \left(\frac{\partial \rho\bar{U}}{\partial t}\right)dV = -\int_V \nabla\cdot\left(\rho\bar{U}\bar{U} + P\bar{\bar{I}} - \bar{\bar{\tau}}\right)dV. \tag{7.9}$$

We are treating the case where the flow in the combustion chamber is stationary and the integral on the left hand side of (7.9) is zero. Our goal is to relate the thrust of the engine to flow conditions on A_e and with this in mind we convert the right hand side to an integral over the surface of the control volume.

$$\begin{aligned} 0 = &\int_V \nabla\cdot\left(\rho\bar{U}\bar{U} + P\bar{\bar{I}} - \bar{\bar{\tau}}\right)dV = \\ &\int_{A_c}\left(\rho\bar{U}\bar{U} + P\bar{\bar{I}} - \bar{\bar{\tau}}\right)\cdot\hat{n}dA + \int_{A_e}\left(\rho\bar{U}\bar{U} + P\bar{\bar{I}} - \bar{\bar{\tau}}\right)\cdot\hat{n}dA \end{aligned} \tag{7.10}$$

Note that the unit normal that appears in the surface integrals in (7.10) is an inward pointing unit normal. On the surface A_c, the velocity is zero by the no-slip condition (except over the injector holes) and on the surface A_e we use area-averaged values of velocity, pressure, and density

$$\int_{A_c}\left(P\bar{\bar{I}} - \bar{\bar{\tau}}\right)\cdot\hat{n}dA\Big|_x + \dot{m}U_{xm} + \rho_e {U_e}^2 A_e + P_e A_e = 0 \tag{7.11}$$

where the momentum of the propellant injected into the combustion chamber has been included. Small viscous normal forces on A_e are neglected. Our force balance (7.7) now becomes

$$0 = T + P_0 A_e - \left(\rho_e {U_e}^2 A_e + P_e A_e\right). \tag{7.12}$$

Finally our rocket thrust formula is

$$T = \rho_e {U_e}^2 A_e + \left(P_e - P_0\right)A_e. \tag{7.13}$$

The propellant mass flow is

$$\dot{m} = \rho_e U_e A_e \tag{7.14}$$

and the rocket thrust formula is often written

$$T = \dot{m} U_e + (P_e - P_0) A_e. \tag{7.15}$$

7.2 Momentum balance in center-of-mass coordinates

Let's look at the question of defining the thrust from a rather different point of view. Figure 7.2 depicts a rocket referenced to a system of center-of-mass coordinates. In the analysis to follow, gravity is taken to be zero. The effects of gravitational acceleration will be taken into account later.

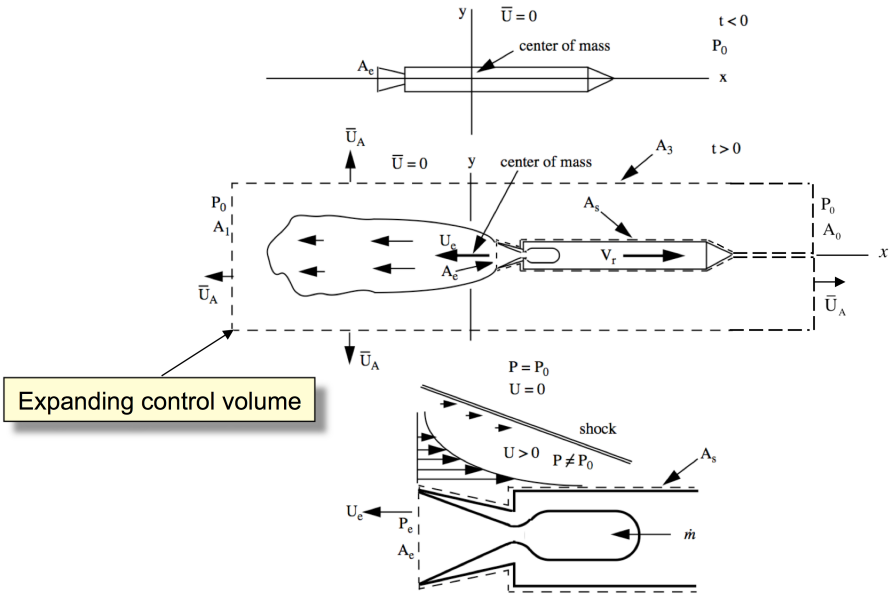

Figure 7.2: *Center-of-mass description of the rocket and expelled propellant mass.*

For $t < 0$ the rocket, its propellant and the surrounding atmosphere are all at rest. Sometime after ignition the rocket has translated to the right and the exhaust gases form a cloud off to the left of the center-of-mass. Because there is no external force on the system the center of mass remains at rest at the origin for all time. Conservation of momentum for the whole system of rocket vehicle, expelled combustion gases as well as the air set into

motion by the drag forces on the rocket can be stated as

$$\frac{D}{Dt}\left(\int_{V(t)}\left(\rho\bar{U}\right)dV\Bigg|_x + M_r\left(t\right)V_r\left(t\right)\right) = 0 \tag{7.16}$$

where $M_r\left(t\right)$ is the time-dependent rocket mass. At any given instant the rocket mass comprises all of the hardware and all of the propellant contained in the tanks, piping, pumps and combustion chamber up to the exit plane of the nozzle. The time-dependent rocket velocity is $V_r\left(t\right)$. We shall assume that all of the propellant mass contained in the rocket is moving at this velocity although there is always a small amount moving through the piping and combustion chamber at a slightly different velocity.

The gas momentum is integrated over a control volume V(t) that completely encloses all of the moving gas outside the vehicle as shown in Figure 7.2. Since there is a continuous flow of propellant mass into the combustion chamber and out of the rocket nozzle the volume required to contain the expelled gas must grow with time. This is depicted in Figure 7.2. The control volume is cylindrical in shape. The left face A_1 moves to the left at a speed sufficient to fully contain all the moving gas as well as any unsteady pressure disturbances generated by the rocket plume. The surface A_3 moves outward for the same reason. The upstream face A_2 moves to the right at velocity $V_r\left(t\right)$ with the rocket. Finally the surface A_s is attached to the rocket fuselage and outer nozzle surface. On the solid surface, the fluid velocity is equal to the rocket velocity $V_r\left(t\right)$ by the no slip condition. The last surface of the control volume is A_e which coincides with the nozzle exit plane and translates to the right at the rocket velocity. The momentum equation integrated over $V\left(t\right)$ is

$$\frac{D}{Dt}\int_{V(t)}\left(\rho\bar{U}\right)dV\Bigg|_x = -\int_{A(t)}\left(\rho\bar{U}\left(\bar{U}-\bar{U}_A\right)+P\bar{\bar{I}}-\bar{\bar{\tau}}\right)\cdot\hat{n}dA\Bigg|_x . \tag{7.17}$$

The control volume is sufficiently large so that the fluid velocity on A_1 , A_2 and A_3 is zero and the pressure is P_0. Therefore over most of the surface of the selected control volume no additional momentum is being enclosed as the surface moves outward. The pressure forces on A_1 and A_2 nearly cancel except for a small deviation in pressure near the rocket nose in subsonic flight. For now we will cancel these forces but they will be included later when we develop an expression for the vehicle drag. The pressure forces on A_3 have no

component in the x direction. Thus the momentum balance (7.17) becomes

$$\frac{D}{Dt}\int_{V(t)}\left(\rho\bar{U}\right)dV\Big|_x =$$

$$-\int_{A_s(t)}\left(\rho\bar{U}\left(\bar{U}-\bar{U}_A\right)+P\bar{\bar{I}}-\bar{\bar{\tau}}\right)\cdot\hat{n}dA\Big|_x - \tag{7.18}$$

$$\int_{A_e(t)}\left(\rho\bar{U}\left(\bar{U}-\bar{U}_A\right)+P\bar{\bar{I}}-\bar{\bar{\tau}}\right)\cdot\hat{n}dA\Big|_x .$$

Now we can use an argument similar to that used in the previous section to relate the surface integral of the ambient pressure to an integral over the nozzle area. Recall

$$0=\int_{A_s}P_0\bar{\bar{I}}\cdot\hat{n}dA\Big|_x+P_0A_e. \tag{7.19}$$

The sign change in (7.19) compared to (7.6) comes from the change in the direction of the outward normal on A_e compared to the control volume used in Section 7.1. Subtract (7.19) from (7.18) to get

$$\frac{D}{Dt}\int_{V(t)}\left(\rho\bar{U}\right)dV\Big|_x =$$

$$-\int_{A_s(t)}\left(\rho\bar{U}\left(\bar{U}-\bar{U}_A\right)+(P-P_0)\bar{\bar{I}}-\bar{\bar{\tau}}\right)\cdot\hat{n}dA\Big|_x - \tag{7.20}$$

$$\int_{A_e(t)}\left(\rho\bar{U}\left(\bar{U}-\bar{U}_A\right)+(P-P_0)\bar{\bar{I}}-\bar{\bar{\tau}}\right)\cdot\hat{n}dA\Big|_x .$$

On the no-slip surface of the rocket, the fluid velocity satisfies $\bar{U}=(V_r,0,0)$ and the control volume surface velocity is $\bar{U}_A=(V_r,0,0)$. Therefore

$$\int_{A_s(t)}\rho\bar{U}\left(\bar{U}-\bar{U}_A\right)\cdot\hat{n}dA\Big|_x=0. \tag{7.21}$$

Now

$$\frac{D}{Dt}\int_{V(t)}\left(\rho\bar{U}\right)dV\Bigg|_x =$$

$$-\int_{A_s(t)}\left((P-P_0)\bar{\bar{I}}-\bar{\bar{\tau}}\right)\cdot\hat{n}dA\Bigg|_x - \tag{7.22}$$

$$\int_{A_e(t)}\left(\rho\bar{U}\left(\bar{U}-\bar{U}_A\right)+(P-P_0)\bar{\bar{I}}-\bar{\bar{\tau}}\right)\cdot\hat{n}dA\Bigg|_x .$$

Near the rocket, the surrounding air is dragged along due to the no-slip condition and due to compressibility effects that may generate shock waves as sketched in Figure 7.2. Note that it is the deviation of the surface pressure from ambient, $P-P_0$, that contributes to the change in air momentum due to the drag of the rocket. The combination of viscous skin friction drag, base pressure drag and wave drag are all accounted for by the integral over A_s on the right-hand-side of (7.22). Thus let

$$D=-\int_{A_s(t)}\left(\left(P-P_0\right)\bar{\bar{I}}-\bar{\bar{\tau}}\right)\cdot\hat{n}dA\Bigg|_x . \tag{7.23}$$

Equation (7.22) becomes

$$\frac{D}{Dt}\int_{V(t)}\left(\rho\bar{U}\right)dV\Bigg|_x = D-\int_{A_e(t)}\left(\rho\bar{U}\left(\bar{U}-\bar{U}_A\right)+\left(P-P_0\right)\bar{\bar{I}}-\bar{\bar{\tau}}\right)\cdot\hat{n}dA\Bigg|_x . \tag{7.24}$$

Now consider the integral over A_e on the right side of (7.24). All variables are area-averaged over A_e. The x-component of velocity of the gas passing through A_e in the center-of-mass frame of reference is

$$U=V_r+U_e. \tag{7.25}$$

The nozzle exhaust velocity is the same velocity defined in section 7.1 (the velocity relative to the rocket) except that in this system of coordinates U_e is negative. In this frame the

speed of the surface A_e is $V_r(t)$.

$$\int_{A_e(t)} \left(\rho\bar{U}\left(\bar{U}-\bar{U}_A\right)+\left(P-P_0\right)\bar{\bar{I}}-\bar{\bar{\tau}}\right)\cdot\hat{n}dA\Big|_x = \rho_e A_e\left(U_e+V_r\right)\left(U_e+V_r-V_r\right)+\left(P_e-P_0\right)A_e. \tag{7.26}$$

Now the momentum change of the expelled gas is

$$\frac{D}{Dt}\int_{V(t)}\left(\rho\bar{U}\right)dV\Big|_x = D-\left(\rho_e A_e\left(U_e+V_r\right)\left(U_e+V_r-V_r\right)+\left(P_e-P_0\right)A_e\right). \tag{7.27}$$

Substitute (7.27) into (7.16)

$$\frac{D}{Dt}\left(M_r(t)V_r(t)\right)+D-\left(\rho_e A_e U_e\left(U_e+V_r\right)+\left(P_e-P_0\right)A_e\right)=0 \tag{7.28}$$

or

$$M_r(t)\frac{dV_r(t)}{dt}+V_r(t)\frac{dM_r(t)}{dt}+D-\left(\rho_e A_e U_e\left(U_e+V_r\right)+\left(P_e-P_0\right)A_e\right)=0. \tag{7.29}$$

Note that

$$\frac{dM_r(t)}{dt}=\rho_e U_e A_e \tag{7.30}$$

and the second and fifth terms in (7.29) cancel. Remember that in the chosen set of coordinates, U_e is negative and (7.30) is consistent with the fact that $dM_r/dt<0$. Finally our momentum balance in the center-of-mass system boils down to

$$M_r(t)\frac{dV_r(t)}{dt}=\left(\rho_e {U_e}^2 A_e+\left(P_e-P_0\right)A_e\right)-D. \tag{7.31}$$

In words, Equation (7.31) simply states

$$Rocket\ mass\times Acceleration = Thrust - Drag. \tag{7.32}$$

The first term on the right-hand-side of (7.31) is the same thrust expression derived in the previous section.

7.3 Effective exhaust velocity

The total mechanical impulse (total change of momentum) generated by an applied force, T, is

$$I = \int_0^t T dt. \tag{7.33}$$

The total propellant mass expended is

$$M_p = \int_0^t \dot{m} dt. \tag{7.34}$$

The instantaneous change of momentum per unit expenditure of propellant mass defines the effective exhaust velocity.

$$C = \frac{dI}{dM_p} = \frac{T}{\dot{m}} = U_e + \frac{A_e}{\dot{m}} (P_e - P_0) \tag{7.35}$$

This can be expressed in terms of the exit Mach number as follows

$$C = U_e \left(1 + \frac{P_e A_e}{\rho_e {U_e}^2 A_e} \left(1 - \frac{P_0}{P_e} \right) \right) \tag{7.36}$$

or

$$C = U_e \left(1 + \frac{1}{\gamma {M_e}^2} \left(1 - \frac{P_0}{P_e} \right) \right). \tag{7.37}$$

For a large area ratio exhaust with a large exit Mach number the pressure part of the thrust becomes a small fraction of the overall thrust.

Let's estimate the theoretical maximum exhaust velocity that can be generated by a given set of propellants characterized by the heating value per unit propellant mass, q. Consider the simple model of a rocket thrust chamber shown in Figure 7.3.

Between stations 1 and 2 combustion takes place leading to a change in stagnation enthalpy of the propellant mass.

$$h_{t2} = h_{t1} + q = h_e + \frac{1}{2} {U_e}^2 \tag{7.38}$$

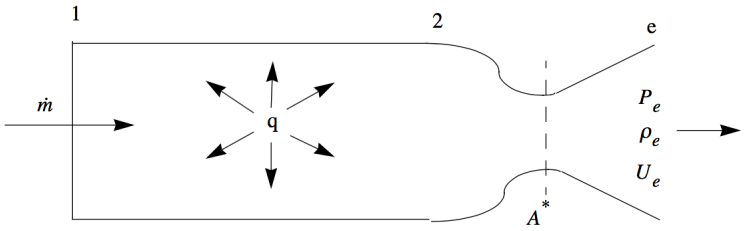

Figure 7.3: *Thrust chamber propellant injection, heat release and nozzle expulsion.*

The last equality assumes adiabatic conditions between station 2 and the nozzle exit. The quantity, h_{t1} is the stagnation enthalpy of the gases entering the combustion chamber and, in general, is much smaller than the heat added $h_{t1} \ll q$. If the nozzle pressure ratio is very large $P_{t2}/P_0 \gg 1$, and the area ratio is large $A_e/A^* \gg 1$, then ${U_e}^2/2 \gg h_e$ and so we can define the theoretical maximum exhaust velocity as

$$C_{\max} \cong \sqrt{2q}. \tag{7.39}$$

The exit velocity is directly proportional to the amount of heat added through the combustion process. Making the approximation of constant specific heat and introducing the stagnation temperature, $h_{t2} = C_p T_{t2}$, the maximum velocity becomes,

$$C_{\max} \cong \sqrt{2C_p T_{t2}} = \sqrt{\frac{2\gamma}{\gamma - 1} R T_{t2}}. \tag{7.40}$$

The gas constant in (7.40) is related to the universal gas constant by

$$R = \frac{R_u}{M_w} \tag{7.41}$$

where M_w is the mean molecular weight of the combustion gas. For this highly expanded rocket engine, the exhaust velocity is approximated by

$$C_{\max} \cong \sqrt{\frac{2\gamma}{\gamma - 1} \left(\frac{R_u}{M_w}\right) T_{t2}}. \tag{7.42}$$

This last relation shows the key role of the molecular weight of the combustion gases on the exhaust velocity of the nozzle. The highest performing engines generally have the lightest

weight exhaust gases. The most outstanding example of this is the Space Shuttle Main Engine (SSME) which uses hydrogen and oxygen, with water vapor as the main exhaust constituent.

7.4 C^* efficiency

A very important characteristic velocity that is widely used in rocket motor testing is C^* defined by the mass balance

$$\dot{m} = \frac{P_{t2} A^*}{C^*}. \tag{7.43}$$

The reason (7.43) is so useful is that it can be used to express the combustion efficiency in the rocket chamber in terms of quantities that are relatively easy to measure: chamber pressure, propellant mass flow rate and nozzle throat area. These variables are much easier and less expensive to measure than the combustion chamber temperature and chemical composition. The C^* efficiency of a motor is defined as

$$\eta_{C^*} = \frac{\left(\frac{P_{t2} A^*}{\dot{m}}\right)_{measured}}{\left(\frac{P_{t2} A^*}{\dot{m}}\right)_{ideal}}. \tag{7.44}$$

The ideal value of C^* is determined using a thermochemical calculator such as CEA discussed in Chapter 9. Since the ideal calculation is assumed to take place at the same propellant mass flow rate and nozzle throat area, A^* , the C^* efficiency reduces to a simple comparison between the achieved chamber pressure and the chamber pressure that would be reached if there was complete mixing and complete combustion under adiabatic conditions.

$$\eta_{C^*} = \frac{P_{t2_{measured}}}{P_{t2_{ideal}}} \tag{7.45}$$

7.5 Specific impulse

For historical reasons, the specific impulse has always been defined as the thrust per unit weight flow of propellant and so the gravitational acceleration at the surface of the Earth

is always inserted. The specific impulse is defined as

$$I_{sp} = \frac{T}{\dot{m} g_0} = \frac{C}{g_0} \tag{7.46}$$

even though the parameter $g_0 = 9.8 m/\sec^2$ has no particular relevance to the problem. Generally one distinguishes between the sea level specific impulse of a vehicle where the ambient pressure detracts from the thrust and the ideal vacuum specific impulse where the exhaust is assumed to be expanded to the exhaust pressure P_e with $P_0 = 0$. From the previous discussion of the theoretical maximum exhaust velocity, it is clear that the vacuum specific impulse at a very large area ratio effectively characterizes a given propellant combination. Typical solid propellant systems have specific $I_{sp_{vac}}$ in the range $230 - 290\,\sec$. Liquid propellant systems using a hydrocarbon fuel with liquid oxygen have $I_{sp_{vac}}$ around 360 seconds with hydrogen-oxygen systems reaching 455 seconds. One needs to not take these I_{sp} numbers too literally. Such values are often quoted for some typical real system such as the Space Shuttle Main Engine without stating the actual chamber pressure and area ratio and in some cases without identifying the system. The question of the area ratio corresponding to the ideal specific impulse is particularly important. For example, for a hydrogen-oxygen system at an area ratio of, say, $4,000$ the ideal I_{sp} is over 500 seconds.

An accurate specification of the specific impulse of a working system requires a knowledge of the chamber pressure, nozzle area ratio, combustion efficiency and nozzle efficiency. The chamber pressure is needed to determine the composition of the combustion chamber gas at the chamber temperature. This will become clear when we study the thermochemistry of gases in Chapter 9.

7.6 Chamber pressure

The mass flow of propellant injected into the rocket engine and the amount of heat added between stations 1 and 2 through combustion determine the engine chamber pressure. We can see this by considering the relationship between the mass exiting the nozzle and the stagnation conditions of the gas at station 2. In general, at any point in a channel flow of a compressible gas, the mass flow can be expressed as

$$\dot{m} = \rho U A = \frac{1}{\left(\frac{\gamma+1}{2}\right)^{\frac{\gamma+1}{2(\gamma-1)}}} \frac{\gamma P_t A}{\sqrt{\gamma R T_t}} f(M) \tag{7.47}$$

where $f(M)$ is the well known area-Mach number relation

$$f(M) = \frac{A^*}{A} = \left(\frac{\gamma+1}{2}\right)^{\frac{\gamma+1}{2(\gamma-1)}} \frac{M}{\left(1+\frac{\gamma-1}{2}M^2\right)^{\frac{\gamma+1}{2(\gamma-1)}}}. \tag{7.48}$$

Equation (7.48) is plotted in Figure 7.4 for several values of $\gamma = C_p/C_v$.

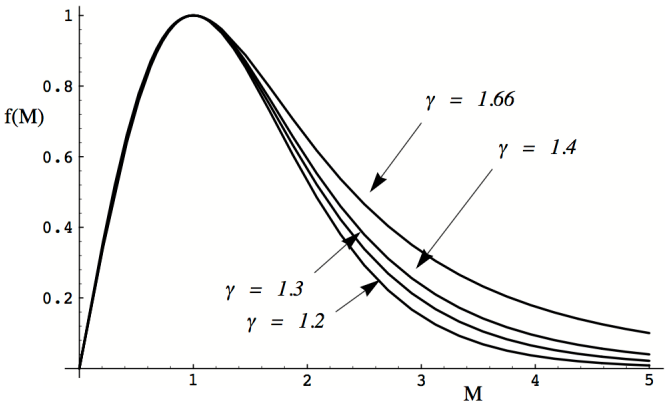

Figure 7.4: *Area-Mach number relation.*

The stagnation temperature at station 2 is determined by the heat released through combustion.

$$T_{t2} = T_{t1} + \frac{q}{C_p} \tag{7.49}$$

To a first approximation, T_{t2} is nearly independent of chamber pressure, P_{t2} and is approximately known once the propellants are specified. Generally the chamber pressure is much larger than the ambient pressure $P_{t2}/P_0 \gg 1$ and so the nozzle throat is choked, $M^* = 1$ and $f(M^*) = 1$. The chamber pressure is then determined by evaluating the mass flow at the nozzle throat

$$P_{t2} = \left(\frac{\gamma+1}{2}\right)^{\frac{\gamma+1}{2(\gamma-1)}} \frac{\sqrt{\gamma R T_t}}{\gamma A^*} \dot{m} \tag{7.50}$$

where adiabatic, isentropic conditions are assumed between station 2 and the nozzle throat.

7.7 Combustion chamber stagnation pressure drop

The stagnation pressure drop between stations 1 (near the injector) and station 2 due to the heat addition is given by the conventional Rayleigh line relations.

$$\frac{P_{t2}}{P_{t1}} = \left\{\frac{1+\gamma {M_1}^2}{1+\gamma {M_2}^2}\right\}\left(\frac{1+\frac{\gamma-1}{2}{M_2}^2}{1+\frac{\gamma-1}{2}{M_1}^2}\right)^{\frac{\gamma}{\gamma-1}}. \tag{7.51}$$

The static pressure is

$$\frac{P_2}{P_1} = \left\{\frac{1+\gamma {M_1}^2}{1+\gamma {M_2}^2}\right\}. \tag{7.52}$$

At station 1, ${M_1}^2 \ll 1$, and we can approximate conditions at station 2 in terms of just the Mach number at 2.

$$\begin{aligned}\frac{P_{t2}}{P_{t1}} &= \left\{\frac{1}{1+\gamma {M_2}^2}\right\}\left(1+\frac{\gamma-1}{2}{M_2}^2\right)^{\frac{\gamma}{\gamma-1}} \\ \frac{P_2}{P_1} &= \left\{\frac{1}{1+\gamma {M_2}^2}\right\}\end{aligned} \tag{7.53}$$

The Mach number at station 2 is determined by the internal nozzle area ratio from 2 to the throat. Assume isentropic, adiabatic, flow between A_2 and A^*.

$$\frac{A^*}{A_2} = \left(\frac{\gamma+1}{2}\right)^{\frac{\gamma+1}{2(\gamma-1)}} \frac{M_2}{\left(1+\frac{\gamma-1}{2}M^2\right)^{\frac{\gamma+1}{2(\gamma-1)}}} \tag{7.54}$$

The relations (7.53) and (7.54) effectively define a relationship between A_2/A^*, P_{t2}/P_{t1} and P_2/P_1, plotted in Figure 7.5 for several values of γ.

The desire to keep stagnation pressure losses relatively small, while avoiding an excessively large diameter combustion chamber, dictates the internal area ratio selected for the combustion chamber. It is clear from Figure 7.5 that an area ratio of about 3 is sufficient to keep the stagnation pressure losses across the combustion chamber negligibly small. Practically all rocket thrust chambers have an area ratio of about 3 for this reason.

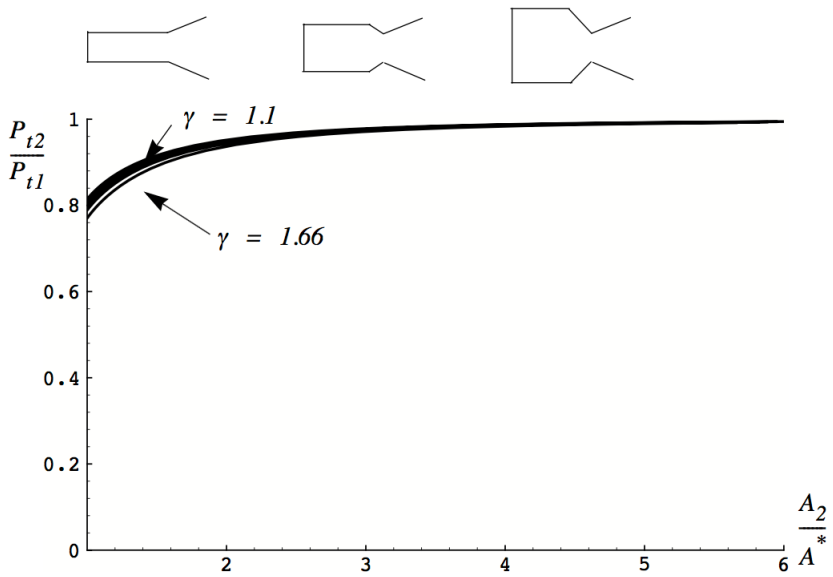

Figure 7.5: *Combustion chamber stagnation pressure loss.*

7.8 The Tsiolkovsky rocket equation

Consider the force balance on a rocket in flight shown in Figure 7.6.

The variables identified in the figure are as follows.

$$\begin{aligned} &T = vehicle\ thrust \\ &D = vehicle\ aerodynamic\ drag \\ &V_r = vehicle\ velocity \\ &\theta = angle\ with\ respect\ to\ the\ horizontal \\ &\dot{m} = nozzle\ mass\ flow \\ &M_r = vehicle\ mass \\ &g = gravitational\ acceleration \end{aligned} \tag{7.55}$$

The balance of forces along the direction of flight was derived earlier. Here we add the gravitational component of the force balance

$$M_r \frac{dV_r}{dt} = T - M_r g Sin\,(\theta) - D \tag{7.56}$$

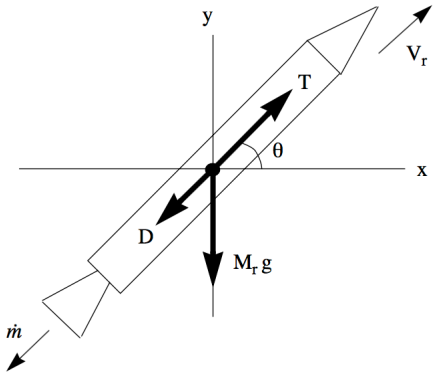

Figure 7.6: *Rocket free body diagram.*

or

$$M_r \frac{dV_r}{dt} = -C\frac{dM_r}{dt} - M_r g Sin\,(\theta) - D \tag{7.57}$$

where C is the effective exhaust velocity. Divide (7.57) through by M_r.

$$\frac{dV_r}{dt} = -C\frac{d\,(\ln M_r)}{dt} - gSin\,(\theta) - \frac{D}{M_r} \tag{7.58}$$

Let

$$\begin{aligned} &M_{ri} = initial\ mass\ at\ t = 0 \\ &M_{rf} = final\ mass\ at\ t = t_b \\ &t_b = time\ of\ burnout. \end{aligned} \tag{7.59}$$

Integrate (7.58) assuming constant C. The velocity change of the vehicle is

$$\Delta V_r = V_{rb} - V_{r0} = \Delta V_r|_{ideal} - \Delta V_r|_{gravitational} - \Delta V_r|_{drag} \tag{7.60}$$

where

$$\Delta V_r|_{gravitational} = \int_0^{t_b} gSin\,(\theta)dt$$
$$\Delta V_r|_{drag} = \int_0^{t_b} \left(\frac{D}{M_r}\right)dt. \tag{7.61}$$

For a typical launch vehicle headed to orbit, aerodynamic drag losses are generally quite small on the order of 100 to 500 $m/$ sec. Gravitational losses are larger, generally ranging from 700 to 1500 $m/$ sec depending on the shape of the trajectory to orbit. By far the largest term is the equation for the ideal velocity increment

$$\Delta V_r|_{ideal} = C \ln\left(\frac{M_{ri}}{M_{r_f}}\right) \tag{7.62}$$

first derived in 1903 by the soviet rocket pioneer Konstantin Tsiolkovsky who is credited with developing much of the early theory of rocket flight. Equation (7.62) shows the dependence of the velocity achieved by a rocket on the effective exhaust velocity (determined by the choice of propellants) and the initial to final mass ratio which is determined by what might be termed the structural efficiency of the vehicle and the density of the propellants. Notice the similarity of (7.62) to the Bruguet range equation discussed in chapter 2. In general, one seeks a very lightweight vehicle to carry high density propellants which after combustion produce very lightweight products. In practice these requirements conflict. Generally solid rockets use relatively dense, low energy propellants which do not produce very lightweight products of combustion. Whereas liquid rockets use more energetic propellants that produce light products but are not particularly dense.

7.9 Reaching orbit

Orbital velocity at an altitude of 115 miles, which is about the lowest altitude where a stable orbit can be maintained, is approximately 7777 $m/$ sec. To reach this velocity from the Kennedy Space Center where the velocity due to the rotation of the Earth is approximately 427 $m/$ sec, assuming gravitational plus drag losses of 1700 $m/$ sec, requires an ideal velocity increment of 9050 $m/$ sec. A hydrogen-oxygen system with an effective average exhaust velocity (from sea- level to vacuum) of 4000 $m/$ sec would require $M_i/M_f = 9.7$. This represents a very high level of structural efficiency and is the fundamental challenge being addressed by single-stage-to-orbit concepts. At the present time existing launch vehicles require multiple stages to achieve orbit with a reasonable payload size.

Strategies for reducing gravitational losses are mainly limited to optimizing the trajectory to orbit and expending the maximum amount of propellant as possible near the earth's surface (to avoid the work required to lift it to altitude). The latter strategy suggests that the most efficient way to orbit would be an artillery shell, however practical limitations prevent large acceleration loads on the payload. Most large launch vehicles are relatively delicate and require throttling back on thrust at low altitude to avoid large dynamic pressure loads on the vehicle.

The drag losses can be minimized by designing a slender vehicle. This can be seen as follows

$$\Delta V_r|_{drag} = \int_0^{t_b} \left(\frac{D}{M_r}\right) dt = \int_0^{t_b} \frac{1}{2} \frac{\rho {V_r}^2 A C_D}{M_{ri}} \left(\frac{M_{ri}}{M_r}\right) dt = \frac{A}{2M_{ri}} \int_0^{t_b} \left(\rho {V_r}^2 C_D\right) \left(\frac{M_{ri}}{M_r}\right) dt \tag{7.63}$$

where A is the cross-sectional area of the vehicle. The integral on the right-hand-side is approximately independent of vehicle size and the initial mass of the vehicle is approximately proportional to the vehicle volume, $M_{ri} \cong \rho_{vehicle} V_{vehicle}$.

$$\Delta V_{rocket}|_{drag} \cong \frac{FrontalArea_{rocket}}{2density_{rocket} Volume_{rocket}} \int_0^{t_b} \left(\rho {V_{rocket}}^2 C_D\right) \left(\frac{M_{rocket_i}}{M_{rocket}}\right) dt \sim \frac{1}{Length_{rocket}} \tag{7.64}$$

The last result suggests that the vehicle should be long and thin, roughly like a pencil. Note that the drag losses go down as the mass goes up, and so the velocity loss due to drag tends to become smaller as the vehicle absolute size goes up. The length to diameter ratio of the vehicle does not come into the analysis directly but, in general, the drag coefficient, C_d, decreases as the L/D goes up.

7.10 The thrust coefficient

The thrust coefficient provides a useful dimensionless measure of engine thrust.

$$C_F = \frac{T}{P_{t2} A^*} = \frac{\dot{m} U_e + (P_e - P_0) A_e}{P_{t2} A^*} = \left(\frac{P_e}{P_{t2}}\right) \left(\frac{A_e}{A^*}\right) \left(\gamma {M_e}^2 + 1 - \frac{P_0}{P_e}\right) \tag{7.65}$$

This rather complicated looking expression can be written in terms of the nozzle exit Mach

number and pressure

$$C_F = \frac{1}{\left(\frac{\gamma+1}{2}\right)^{\frac{\gamma+1}{2(\gamma-1)}}} \frac{\left(\gamma {M_e}^2 + 1 - \frac{P_0}{P_e}\right)}{M_e\left(1 + \frac{\gamma-1}{2}{M_e}^2\right)^{\frac{1}{2}}} \tag{7.66}$$

where the nozzle flow has been assumed to be isentropic. For a rocket operating in a vacuum, with a very large expansion ratio $M_e \to large$, the thrust coefficient has an upper limit of

$$C_{F_{\max}} = \frac{\gamma}{\left(\frac{\gamma-1}{2}\right)^{\frac{1}{2}}\left(\frac{\gamma+1}{2}\right)^{\frac{\gamma+1}{2(\gamma-1)}}}. \tag{7.67}$$

The thrust coefficient is plotted in Figure 7.7 for several values of γ as a function of exit Mach number.

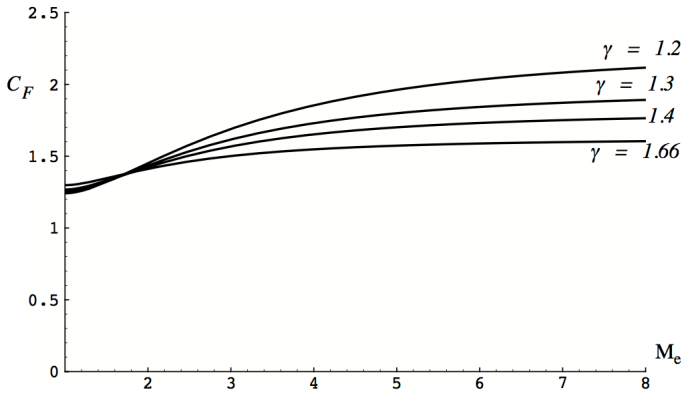

Figure 7.7: *Thrust coefficient versus Mach number.*

The thrust coefficient is also plotted in Figure 7.8 for several values of γ as a function of nozzle exit area ratio.

The thrust coefficient gives us a useful measure of the effect of nozzle expansion on thrust. It is clear from Figure 7.7 that, in principle, expanding a gas with low γ would have the greatest benefit. However Figure 7.4 indicates that a large area ratio nozzle is required to reach the high exit Mach number required to obtain this benefit. We can see from Figure 7.7 and Figure 7.8 that fully expanding the flow, versus no expansion at all (a simple convergent nozzle), represents as much as a 50 % increase in the thrust generated by the nozzle. Generally, high temperature combustion gases have values of γ between 1.2 and 1.3

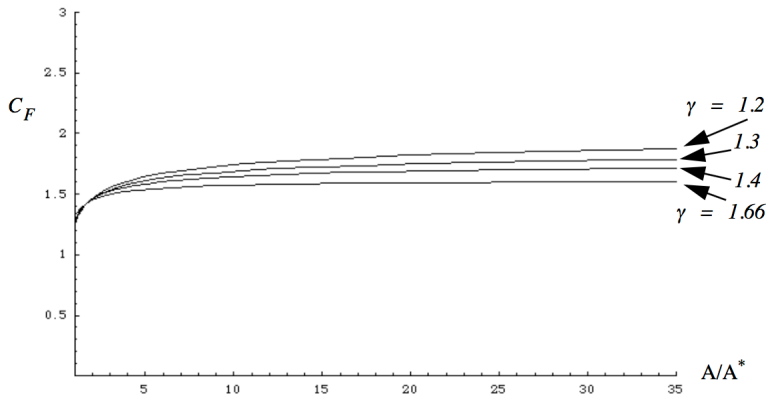

Figure 7.8: *Thrust coefficient versus area ratio.*

with the lower values characterizing high molecular weight products of combustion typical of solid rockets.

7.11 Problems

Problem 1 - A monopropellant thruster using Argon gas at $100\,psia$ and $1500\,K$ exhausts through a large area ratio convergent-divergent nozzle to the vacuum of space. Determine the energy per unit mass of a parcel of gas at three locations: in the plenum, at the nozzle throat, and at the end of the expansion where the gas pressure approaches vacuum. What mechanism is responsible for the change of energy from one position to the next? How does your answer change if the gas is changed to Helium?

Problem 2 - The designer of a spacecraft maneuvering system needs to choose between Argon (atomic weight 40) and Helium (atomic weight 4) as propellants for a monopropellant thruster. The gas pressure and temperature in the propellant tank are $5 \times 10^6\,N/m^2$ and $300\,K$ respectively. The propellant tank volume is $1.0\,m^3$ and the empty mass of the vehicle is $10\,kg$.

1) Which propellant gas will give the largest velocity change to the vehicle? Estimate the vehicle velocity change for each gas?

2) Suppose the vehicle mass is $1000\,kg$, which propellant would deliver the largest velocity change?

Problem 3 - Consider two different systems used for space propulsion. System A uses propellants with an average density of $2\,gm/cm^3$ and specific impulse of 200 seconds while

system B uses propellants with an average density of $1\,gm/cm^3$ and specific impulse 300 seconds. The ideal velocity increment generated by either system is given by

$$\Delta V = I_{sp} g_0 \ln\left(\frac{m_{initial}}{m_{final}}\right) \tag{7.68}$$

where $g_0 = 9.8\,m/\text{sec}^2$. Two missions are under consideration.

1) Mission I involves maneuvering of a large satellite where the satellite empty mass (mfinal) is 2000 kg and the required velocity increment is 100 m/sec.

2) Mission II involves a deep space mission where the vehicle empty mass (m_{final}) is $200\,kg$ and the required velocity increment is $6000\,m/$ sec.

The design requirement in both cases is to keep the tank volume required for the propellant as small as possible. Which propellant choice is best for each mission?

Problem 4 - Recently one of the popular toys being sold was called a stomp rocket. The launcher consists of a flexible plastic bladder connected to a $1.5\,cm$ diameter rigid plastic tube. The rocket is a slightly larger diameter rigid plastic tube, closed at the top end, about $20\,cm$ long. The rocket weighs about $10\,gm$. The rocket slips over the tube as shown in Figure 7.9.

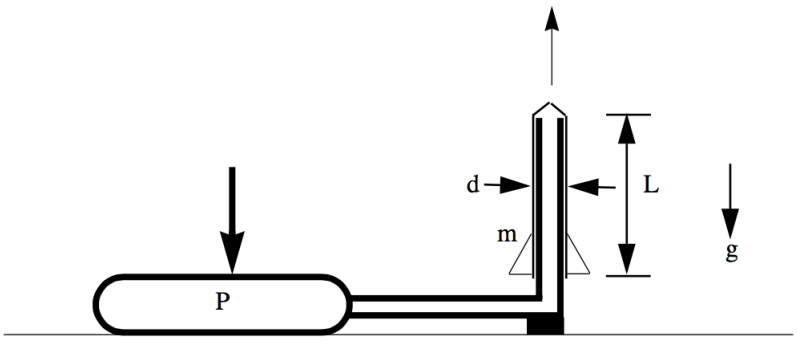

Figure 7.9: *Stomp rocket toy.*

Jumping on the bladder pressurizes the air inside and launches the rocket to a height which the manufacturer claims can exceed $50\,m$. The area of the bladder in contact with the ground is approximately $100\,cm^2$. Use basic principles of mechanics to roughly estimate how much a child would have to weigh to be able to achieve this height.

Problem 5 - Consider a class of monopropellant thrusters based on the use of the noble gases including Helium ($M_w = 4$), Neon ($M_w = 20$), Argon ($M_w = 40$), Krypton, ($M_w =$

84) and Xenon ($M_w = 131$). Radon ($M_w = 222$) is excluded because of its radioactivity. The thruster is comprised of a tank that exhausts through a simple convergent nozzle to the vacuum of space. Onboard heaters are used to maintain the gas in the tank at a constant stagnation temperature T_{t2} as it is exhausted.

1) The thrust is often expressed in terms of an effective exhaust velocity $T = \dot{m}C$. Show that the effective exhaust velocity of this system can be expressed as

$$C = \left(\frac{2\left(\gamma + 1\right)}{\gamma} \left(\frac{R_u}{M_w} \right) T_{t2} \right)^{1/2}. \tag{7.69}$$

2) The mass of propellant contained in the tank is

$$M_{propellant} = \frac{P_{t2_{initial}} V_{\tan k} M_w}{R_u T_{t2}}. \tag{7.70}$$

The initial tank pressure is some rated value (a do-not-exceed pressure) independent of the type of gas used. The designer would like to choose the propellant gas so that the velocity increment produced by the propulsion system ΔV is as large as possible for fixed tank volume, initial pressure and gas temperature. The problem is to decide whether to choose a gas with low M_w, thus achieving a high value of C but low propellant mass, or a gas with high M_w reducing C but increasing propellant mass. By mixing two or more gases, any mean atomic mass between 4 and 131 can be selected by the designer. Note that γ is the same regardless of what gas or mixture of gases is used.

Show that the maximum ΔV occurs when the ratio $M_{propellant}/M_{structure}$ is approximately 4 (actually 3.922). In other words, once the tank volume, pressure and temperature are determined and the vehicle empty mass is known, show that for maximum ΔV the gas should be selected to have a mean atomic weight M_w such that

$$\frac{P_{t2_{initial}} V_{\tan k} M_w}{R_u T_{t2} M_{structure}} = 3.922. \tag{7.71}$$

Problem 6 - The space shuttle main engine has a nozzle throat diameter of $10.22\,in$ a nozzle area ratio of 77.5 and produces $418,000$ pounds of thrust at lift-off from Cape Canaveral. Determine the engine thrust when it reaches the vacuum of space.

Chapter 8

Multistage Rockets

8.1 Notation

With current technology and fuels, and without greatly increasing the effective I_{sp} by air-breathing, a single stage rocket to Earth orbit is still not possible. So it is necessary to reach orbit using a multistage system where a certain fraction of the vehicle mass is dropped off after use, thus allowing the non-payload mass carried to orbit to be as small as possible. The final velocity of an n stage launch system is the sum of the velocity gains from each stage.

$$V_n = \Delta v_1 + \Delta v_2 + \Delta v_3 + \ldots\ldots + \Delta v_n \tag{8.1}$$

The performance of an n -stage system can be optimized by proper selection of the structural mass, propellant mass and specific impulse of each of the n stages.

Let the index i refer to the ith stage of an n stage launch system.The structural and propellant parameters of the system are as follows.

M_{0i} - The total initial mass of the ith vehicle prior to firing including the payload mass, ie, the mass of i, $i+1$, $i+2$, $i+3$,...., n stages.

M_{pi} - The mass of propellant in the ith stage.

M_{si} - Structural mass of the ith stage alone including the mass of its engine, controllers and instrumentation as well as any residual propellant which is not expended by the end of the stage burn.

M_L - The payload mass

Figure 8.1 schematically shows a three stage rocket at each regime of flight.

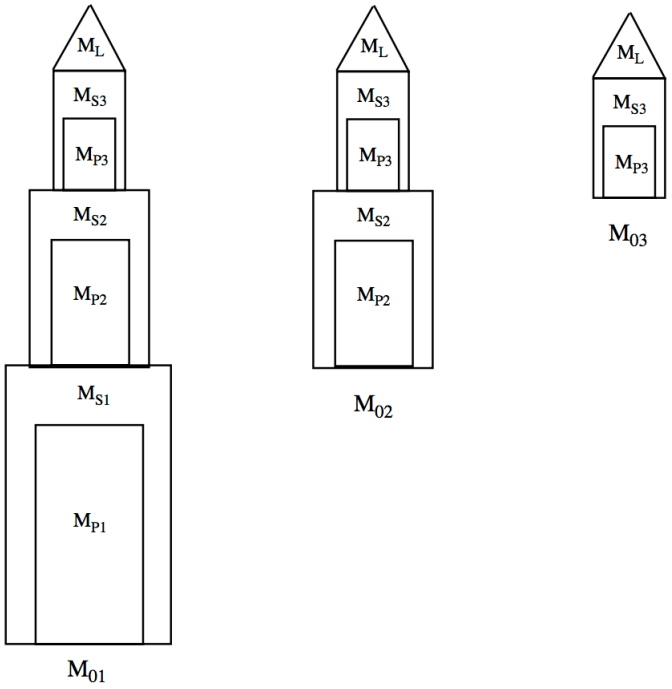

Figure 8.1: *Three stage rocket notation.*

Define the following variables.

Payload ratio

$$\lambda_i = \frac{M_{0(i+1)}}{M_{0i} - M_{0(i+1)}}$$
$$\lambda_n = \frac{M_{0(n+1)}}{M_{0n} - M_{0(n+1)}} = \frac{M_L}{M_{0n} - M_L} \tag{8.2}$$

Structural coefficient

$$\varepsilon_i = \frac{M_{S_i}}{M_{0i} - M_{0(i+1)}} = \frac{M_{S_i}}{M_{S_i} + M_{P_i}} \tag{8.3}$$

Mass ratio

$$R_i = \frac{M_{0i}}{M_{0i} - M_{Pi}} = \frac{1+\lambda_i}{\varepsilon_i + \lambda_i}. \tag{8.4}$$

Ideal velocity increment

$$V_n = \sum_{i=1}^{n} C_i ln\left(R_i\right) = \sum_{i=1}^{n} C_i ln\left(\frac{1+\lambda_i}{\varepsilon_i + \lambda_i}\right). \tag{8.5}$$

Payload fraction

$$\begin{aligned} \Gamma = \frac{M_L}{M_{01}} &= \left(\frac{M_{02}}{M_{01}}\right)\left(\frac{M_{03}}{M_{02}}\right)\left(\frac{M_{04}}{M_{03}}\right)\ldots\ldots\left(\frac{M_L}{M_{0n}}\right) \\ &= \left(\frac{\lambda_1}{1+\lambda_1}\right)\left(\frac{\lambda_2}{1+\lambda_2}\right)\left(\frac{\lambda_3}{1+\lambda_3}\right)\ldots\ldots\left(\frac{\lambda_n}{1+\lambda_n}\right). \end{aligned} \tag{8.6}$$

Take the logarithm of (8.6) to express the payload fraction as a sum in terms of the payload ratios

$$\ln\left(\Gamma\right) = \sum_{i=1}^{n} \ln\left(\frac{\lambda_i}{1+\lambda_i}\right). \tag{8.7}$$

8.2 The variational problem

The structural coefficients, ε_i and effective exhaust velocities, C_i, are known constants based on some prior choice of propellants and structural design for each stage. The question is: how should we distribute the total mass of the vehicle among the various stages? In other words, given V_n, choose the distribution of stage masses so as to maximize the payload fraction, Γ. It turns out that the alternative statement; given Γ maximize the final velocity V_n, leads to the same distribution of stage masses.

The mathematical problem is to maximize

$$\ln\left(\Gamma\right) = G\left(\lambda_1, \lambda_2, \lambda_3, \ldots\ldots, \lambda_n\right) \tag{8.8}$$

for fixed

$$V_n = F\left(\lambda_1, \lambda_2, \lambda_3, \ldots\ldots, \lambda_n\right) \tag{8.9}$$

or, equivalently, maximize (8.9) for fixed (8.8). The approach is to vary the payload ratios, $(\lambda_1, \lambda_2, \lambda_3, \ldots\ldots, \lambda_n)$, so as to maximize Γ. Near a maximum, a small change in the λ_i will not change G.

$$\delta G = \left(\frac{\partial G}{\partial \lambda_i}\right) \delta\lambda_i = 0 \tag{8.10}$$

The basic idea is shown in Figure 8.2.

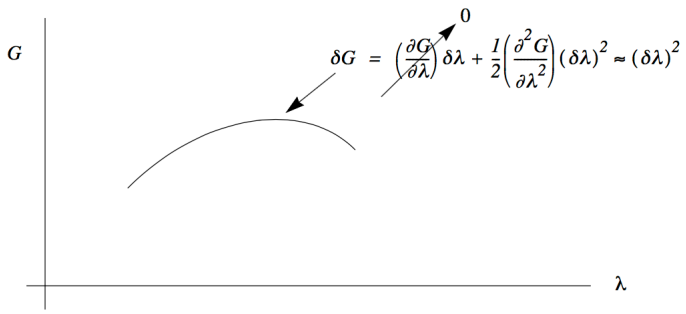

Figure 8.2: *Variation of G near a maximum.*

The $\delta\lambda_i$ are not independent, they must be chosen so that V_n is kept constant.

$$\delta F = \left(\frac{\partial F}{\partial \lambda_i}\right) \delta\lambda_i = 0 \tag{8.11}$$

Thus only $n-1$ of the λ_i can be treated as independent. Without loss of generality let's choose λ_n to be determined in terms of the other payload ratios. The sums (8.10) and (8.11) are

$$\left.\begin{aligned} \sum_{i=1}^{n-1} \left(\frac{\partial G}{\partial \lambda_i}\right) \delta\lambda_i + \left(\frac{\partial G}{\partial \lambda_n}\right) \delta\lambda_n = 0 \\ \sum_{i=1}^{n-1} \left(\frac{\partial F}{\partial \lambda_i}\right) \delta\lambda_i + \left(\frac{\partial F}{\partial \lambda_n}\right) \delta\lambda_n = 0 \end{aligned}\right\}. \tag{8.12}$$

Use the second sum in (8.12) to replace λ_n in the first

$$\sum_{i=1}^{n-1} \left\{ \left(\frac{\partial G}{\partial \lambda_i} \right) + \frac{1}{\alpha} \left(\frac{\partial F}{\partial \lambda_i} \right) \right\} \delta\lambda_i = 0 \tag{8.13}$$

where

$$\alpha = - \left(\frac{\partial F}{\partial \lambda_n} \right) / \left(\frac{\partial G}{\partial \lambda_n} \right) \tag{8.14}$$

plays the role of a Lagrange multiplier. Since the equality (8.13) must hold for arbitrary $\delta\lambda_i$, the coefficients in brackets must be individually zero.

$$\left(\frac{\partial G}{\partial \lambda_i} \right) + \frac{1}{\alpha} \left(\frac{\partial F}{\partial \lambda_i} \right) = 0; \qquad i = 1, 2, 3, \ldots, n-1 \tag{8.15}$$

From the definition of α given by (8.14)

$$\left(\frac{\partial G}{\partial \lambda_n} \right) + \frac{1}{\alpha} \left(\frac{\partial F}{\partial \lambda_n} \right) = 0. \tag{8.16}$$

We now have $n+1$ equations in the $n+1$ unknowns $(\lambda_1, \lambda_2, \lambda_3, \ldots\ldots, \lambda_n, \alpha)$.

$$\left.\begin{aligned} &\left(\frac{\partial G}{\partial \lambda_i} \right) + \frac{1}{\alpha} \left(\frac{\partial F}{\partial \lambda_i} \right) = 0; \qquad i = 1, 2, 3, \ldots, n \\ &V_n = \sum_{i=1}^{n} C_i \ln \left(\frac{1 + \lambda_i}{\varepsilon_i + \lambda_i} \right) \end{aligned}\right\} \tag{8.17}$$

If we supply the expressions for F and G in (8.17) the result for the optimal set of payload ratios is (no sum on the index i)

$$\lambda_i = \frac{\alpha \varepsilon_i}{(C_i - C_i \varepsilon_i - \alpha)}. \tag{8.18}$$

The Lagrange multiplier is determined from the expression for V_n.

$$V_n = \sum C_i \ln \left(\frac{C_i - \alpha}{\varepsilon_i C_i} \right) \tag{8.19}$$

Note that α has units of velocity. Finally, the optimum overall payload fraction is

$$\ln(\Gamma) = \sum_{i=1}^{n} \ln\left(\frac{\alpha\varepsilon_i}{(C_i - C_i\varepsilon_i - \alpha + \alpha\varepsilon_i)}\right). \tag{8.20}$$

8.3 Example - exhaust velocity and structural coefficient the same for all stages

Let $C_i = C$ and $\varepsilon_i = \varepsilon$ be the same for all stages. In this case

$$\alpha = C\left(1 - \varepsilon e^{\left(\frac{V_n}{nC}\right)}\right). \tag{8.21}$$

The payload ratio is

$$\lambda = \frac{1 - \varepsilon e^{\left(\frac{V_n}{nC}\right)}}{e^{\left(\frac{V_n}{nC}\right)} - 1}. \tag{8.22}$$

The payload fraction is

$$\Gamma = \left(\frac{1 - \varepsilon e^{\left(\frac{V_n}{nC}\right)}}{(1-\varepsilon)\, e^{\left(\frac{V_n}{nC}\right)}}\right)^n \tag{8.23}$$

and the mass ratio is

$$R = e^{\left(\frac{V_n}{nC}\right)}. \tag{8.24}$$

Consider a liquid oxygen, kerosene system. Take the specific impulse to be 360 *sec* implying $C = 3528\, m/\,\text{sec}$; a very high performance system. Let $V_n = 9077\, m/\,\text{sec}$ needed to reach orbital speed. The structural coefficient is $\varepsilon = 0.1$ and let the number of stages be $n = 3$. The stage design results are $\alpha = 2696\, m/\,\text{sec}$, $\lambda = 0.563$, $R = 2.3575$ and the payload fraction is

$$\Gamma = 0.047. \tag{8.25}$$

Less than 5% of the overall mass of the vehicle is payload. It is of interest to see how much better we can do by increasing the number of stages in this problem. Equation (8.23) is plotted in Figure 8.3 using the parameters of the problem.

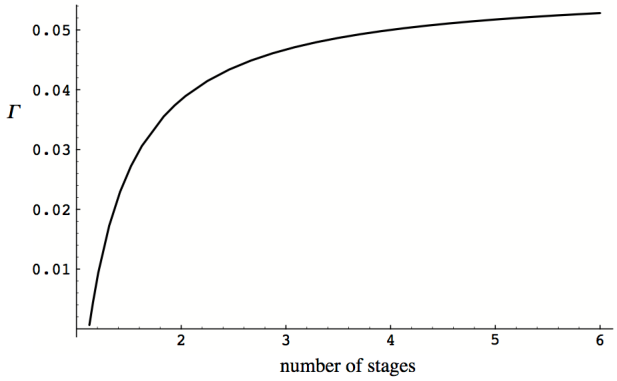

Figure 8.3: *Payload fraction as a function of number of stages for a constant parameter high performance launch vehicle.*

It is clear that beyond three stages, there is very little increase in payload. Note also that one stage cannot make orbit even with zero payload for the assumed value of ε.

8.4 Problems

Problem 1 - A two stage rocket is to be used to put a payload of $1000\,kg$ into low earth orbit. The vehicle will be launched from Kennedy Space Center where the speed of rotation of the Earth is $427\,m/\,\text{sec}$. Assume gravitational velocity losses of about $1200\,m/\,\text{sec}$ and aerodynamic velocity losses of $500\,m/\,\text{sec}$. The first stage burns kerosene and oxygen producing a mean specific impulse of $320\,sec$ averaged over the flight, while the upper stage burns hydrogen and oxygen with an average specific impulse of $450\,sec$. The structural coefficient of the first stage is 0.05 and that of the second is 0.07. Determine the payload ratios and the total mass of the vehicle. Suppose the same vehicle is to be used to launch a satellite into a north-south orbit from a launch complex on Kodiak island in Alaska. How does the mass of the payload change?

Problem 2 - A group of universities join together to launch a four stage rocket with a small payload to the Moon. The fourth stage needs to reach the earth escape velocity of $11,176\,m/\,\text{sec}$. The vehicle will be launched from Kennedy Space Center where the speed of rotation of the Earth is $427\,m/\,\text{sec}$. Assume gravitational velocity losses of about $1500\,m/\,\text{sec}$ and aerodynamic velocity losses of $600\,m/\,\text{sec}$. To keep cost down, four stages with the same effective exhaust velocity C and structural coefficient ε are used. Each stage burns kerosene and oxygen producing a mean specific impulse of $330\,sec$ averaged over each segment of the flight. The structural coefficient of each stage is $\varepsilon = 0.1$. Is the payload

fraction greater than zero?

Problem 3 - A low-cost four stage rocket is to be used to launch small payloads to orbit. The concept proposed for the system utilizes propellants that are safe and cheap but provide a specific impulse of only 200 *sec*. All four stages are identical. What structural efficiency is required to reach orbit with a finite payload?

Chapter 9

Thermodynamics of reacting mixtures

9.1 Introduction

For an open system containing several reacting chemical species that can exchange mass and work with its surroundings the fundamental Gibbs equation relating equilibrium states is

$$TdS = dE + PdV - \sum_{i=1}^{I} \mu_i dn_i + \sum_{k=1}^{K} F_k dl_k. \tag{9.1}$$

The F_k are forces that can act on the system through differential displacements. Ordinarily, lower case letters will be used to denote intensive (per unit mole) quantities (h, s, e, etc) and upper case will designate extensive quantities (H, S, E, etc). Heat capacities, pressure and temperature are symbolized in capital letters. One mole is an Avagadro's number of molecules, 6.0221415×10^{23}.

The chemical potential energy per unit mole μ_i is the amount by which the extensive energy of the system is changed when a differential number of moles dn_i of species i is added or removed from the system. If the system is closed so no mass can enter or leave and if it is isolated from external forces, the Gibbs equation becomes

$$TdS = dE + PdV - \sum_{i=1}^{I} \mu_i dn_i \tag{9.2}$$

where the differential changes in the number of moles of species i occur through chemical reactions that may take place within the closed volume. The main difference between (9.1) and (9.2) is that, in the closed system, changes in mole numbers are subject to the constraint that the number of atoms of each element in the system is strictly constant. The precise expression of the chemical potential in terms of conventional thermodynamic variables of state will be established shortly. For the present it can be regarded as a new, intensive state variable for the species i. Mathematically, equation (9.2) implies that

$$\mu_i\left(E, V, n_1, \ldots, n_I\right) = -T\left(\frac{\partial S}{\partial n_i}\right)_{E,V,n_{j\neq i}}. \tag{9.3}$$

If no reactions occur then (9.2) reduces to the familiar form

$$TdS = dE + PdV. \tag{9.4}$$

According to the second law of thermodynamics, for *any* process of a closed, isolated system

$$TdS \geq dE + PdV. \tag{9.5}$$

Spatial gradients in any variable of the system can lead to an increase in the entropy. Smoothing out of velocity gradients (kinetic energy dissipation) and temperature gradients (temperature dissipation) constitute the two most important physical mechanisms that contribute to the increase in entropy experienced by a non-reacting system during a non-equilibrium process. If the system contains a set of chemical species that can mix, then changes in entropy can also occur through the smoothing out of concentration gradients for the various species. If the species can react, then entropy changes will occur through changes in the chemical binding energy of the various species undergoing reactions.

The inequality (9.5) can be used to establish the direction of a thermodynamic system as it evolves toward a state of equilibrium.

9.2 Ideal mixtures

Consider a mixture of species with mole numbers $(n_1, n_2, \ldots, n_I)$. The extensive internal energy of the system is E and the volume is V. The extensive entropy of the system is the function, $S\left(E, V, n_1, n_2, \ldots, n_I\right)$. An ideal mixture is one where all molecules experience the same intermolecular forces. In an ideal mixture surface effects, (surface energy and surface tension) can be neglected and the enthalpy change when the constituents are mixed is

zero. Ideal mixtures obey Raoult's law that states that the vapor pressure of a component of an ideal mixture is equal to the vapor pressure of the pure component times the mole fraction of that component in the mixture. In the ideal approximation the volume of the system is the sum of the volumes occupied by the pure species alone. Similarly the internal energy is the sum of internal energies of the pure species. Most real mixtures approximate ideal behavior to one degree or another. A mixture of ideal gases is perhaps the best example of an ideal mixture. Liquid mixtures where the component molecules are chemically similar, such as a mixture of benzene and toluene, behave nearly ideally. Mixtures of strongly different molecules such as water and alcohol deviate considerably from ideal behavior.

Let the mole numbers of the mixture be scaled by a common factor α.

$$n_1 = \alpha\tilde{n}_1,\ n_2 = \alpha\tilde{n}_2,\ n_3 = \alpha\tilde{n}_3, \ldots,\ n_I = \alpha\tilde{n}_I \tag{9.6}$$

According to the ideal assumption, the extensive properties of the system will scale by the same factor.

$$E = \alpha\tilde{E},\ V = \alpha\tilde{V} \tag{9.7}$$

Similarly the extensive entropy of the system scales as

$$S\left(E, V, n_1, \ldots, n_I\right) = \alpha\tilde{S}\left(\tilde{E}, \tilde{V}, \tilde{n}_1, \ldots, \tilde{n}_I\right). \tag{9.8}$$

Functions that follow this scaling are said to be homogeneous functions of order one. Differentiate (9.8) with respect to α.

$$\tilde{E}\frac{\partial S}{\partial E} + \tilde{V}\frac{\partial S}{\partial V} + \sum_{i=1}^{I}\tilde{n}_i\frac{\partial S}{\partial n_i} = \tilde{S}\left(\tilde{E}, \tilde{V}, \tilde{n}_1, \ldots, \tilde{n}_I\right) \tag{9.9}$$

Multiply (9.9) by α and substitute (9.8).

$$E\frac{\partial S}{\partial E} + V\frac{\partial S}{\partial V} + \sum_{i=1}^{I}n_i\frac{\partial S}{\partial n_i} = S\left(E, V, n_1, \ldots, n_I\right) \tag{9.10}$$

The Gibbs equation is

$$dS = \frac{dE}{T} + \frac{P}{T}dV - \sum_{i=1}^{I} \frac{\mu_i}{T} dn_i. \tag{9.11}$$

According to (9.11) the partial derivatives of the entropy are

$$\begin{aligned} \frac{\partial S}{\partial E} &= \frac{1}{T} \\ \frac{\partial S}{\partial V} &= \frac{P}{T} \\ \frac{\partial S}{\partial n_i} &= -\frac{\mu_i}{T}. \end{aligned} \tag{9.12}$$

Inserting (9.12) into (9.10) leads to a remarkable result for an ideal mixture.

$$E + PV - TS = \sum_{i=1}^{I} n_i \mu_i \tag{9.13}$$

Equation (9.13) is called the Duhem-Gibbs relation. The combination of state variables that appears in (9.13) is called the Gibbs free energy.

$$G = E + PV - TS = H - TS \tag{9.14}$$

Equation (9.13) expresses the extensive Gibbs free energy of an ideal mixture in terms of the mole numbers and chemical potentials.

$$G = \sum_{i=1}^{I} n_i \mu_i \tag{9.15}$$

This important result shows that the chemical potential of species i is not really a new state variable but is defined in terms of the familiar state variables, enthalpy, temperature and entropy. The chemical potential of species i is its *molar* Gibbs free energy.

$$\mu_i = g_i = h_i - Ts_i \tag{9.16}$$

The enthalpy in (9.16) includes the chemical enthalpy associated with the formation of the species from its constituent elements.

9.3 Criterion for equilibrium

The Gibbs free energy is sometimes described as the "escaping tendency" of a substance. At low temperatures the enthalpy dominates. A chemical species with a positive enthalpy would like to break apart releasing some of its chemical enthalpy as heat and producing products with lower enthalpy. A few examples are ozone (O_3), hydrogen peroxide (H_2O_2), and nitrous oxide (N_2O). These are stable chemicals at room temperature but will decompose readily if their activation energy is exceeded in the presence of a heat source or a catalyst. The entropy of any substance is positive and at high temperatures the entropy term dominates the Gibbs free energy. In a chemical reaction the Gibbs free energy of any species or mixture will increasingly tend toward a state of higher entropy and lower Gibbs free energy as the temperature is increased. Take the differential of the Gibbs free energy.

$$dG = dE + PdV + VdP - TdS - SdT \tag{9.17}$$

For a process that takes place at constant temperature and pressure $dT = dP = 0$. The Second Law (9.5) leads to the result that for such a process

$$dG = dE + PdV - TdS \leq 0. \tag{9.18}$$

A spontaneous change of a system at constant temperature and pressure leads to a decrease of the Gibbs free energy. Equilibrium of the system is established when the Gibbs free energy reaches a minimum. This result leads to a complete theory for the equilibrium of a reacting system.

9.4 The entropy of mixing

Consider the adiabatic system shown in Figure 9.1 consisting of a set of $(n_1, n_2, \ldots, n_i, \ldots, n_I)$ moles of gas species segregated into volumes of various sizes such that the volumes are all at the same temperature and pressure.

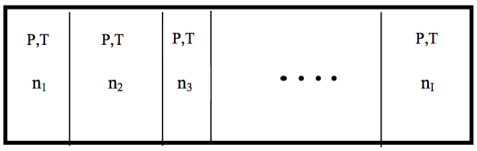

Figure 9.1: *A system of gases separated by partitions.*

The total number of moles in the system is

$$N = \sum_{i=1}^{I} n_i. \tag{9.19}$$

The entropy per unit mole of an ideal gas is determined using the Gibbs equation

$$ds = C_p \frac{dT}{T} - R_u \frac{dP}{P} \tag{9.20}$$

where the units of C_P are $Joules/(mole-Kelvin)$. Tabulations of gas properties are always defined with respect to a reference temperature and standard pressure. The reference temperature is universally agreed to be $T_{ref} = 298.15\,K$ and the standard pressure is

$$P^\circ = 10^5\, N/m^2 = 10^5\, Pascals = 10^2\, kPa = 1\, bar. \tag{9.21}$$

All pressures are referred to P° and the superscript '$^\circ$' denotes a species property evaluated at standard pressure. A cautionary note: In 1999 the International Union of Pure and Applied Chemistry (IUPAC) recommended that for evaluating the properties of all substances, the standard pressure should be taken to be precisely $100kPa$. Prior to this date, the standard pressure was taken to be one atmosphere at sea level, which is $101.325kPa$. Tabulations prior to 1999 are standardized to this value. The main effect is a small change in the standard entropy of a substance at a given temperature tabulated before and after 1999. There are also small differences in heat capacity and enthalpy as well. The IUPAC continues to provide standards for chemistry calculations and chemical nomenclature.

The pressure has no effect on the heat capacity of ideal gases, and for many condensed species the effect of pressure on heat capacity is relatively small. For this reason, tabulations of thermodynamic properties at standard pressure can be used to analyze a wide variety of chemical phenomena involving condensed and gas phase mixtures. Inaccuracies occur when evaluations of thermodynamic properties involve phase changes or critical phenomena where wide deviations from the ideal gas law occur, or condensed phases exhibit significant compressibility.

Integrating (9.20) from the reference temperature at standard pressure, the entropy per unit mole of the *ith* gas species is

$$s_i(T,P) - s_i^\circ(T_{ref}) = \int_{T_{ref}}^{T} C_{pi}^\circ(T)\frac{dT}{T} - R_u \ln\left(\frac{P}{P^\circ}\right). \tag{9.22}$$

where the molar heat capacity C_{pi}° is tabulated as a function of temperature at standard pressure. The standard entropy of a gas species at the reference temperature is

$$s_i^\circ(T_{ref}) = \int_0^{T_{ref}} C^\circ{}_{pi}(T)\frac{dT}{T} + s_i{}^\circ(0) \tag{9.23}$$

where the integration is carried out at $P = P^\circ$. To evaluate the standard entropy, heat capacity data is required down to absolute zero. For virtually all substances, with the exception of superfluid helium (II), the heat capacity falls off rapidly as $T \to 0$ so that the integral in (9.23) converges despite the apparent singularity at $T = 0$. From the third law, the entropy constant at absolute zero, $s_i^\circ(0)$, is generally taken to be zero for a pure substance in its simplest crystalline state. For alloys and pure substances such as CO where more than one crystalline structure is possible, the entropy at absolute zero may be nonzero and tabulated entropy data for a substance may be revised from time to time as new research results become available. Generally the entropy constant is very small.

The entropy per unit mole of the *ith* gas species is

$$s_i(T,P) = s_i^\circ(T) - R_u \ln\left(\frac{P}{P^\circ}\right). \tag{9.24}$$

The entire effect of pressure on the system is in the logarithmic term of the entropy. The extensive entropy of the whole system before mixing is

$$S_{before} = \sum_{i=1}^{I} n_i s_i(T,P) = \sum_{i=1}^{I} n_i s_i^\circ(T) - \sum_{i=1}^{I} n_i R_u \ln\left(\frac{P}{P^\circ}\right). \tag{9.25}$$

If the partitions are removed as shown in Figure 9.2 then, after complete mixing, each gas takes up the entire volume and the entropy of the *ith* species is

$$s_i(T,P_i) = s_i^\circ(T) - R_u \ln\left(\frac{P_i}{P^\circ}\right). \tag{9.26}$$

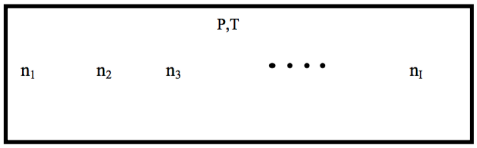

Figure 9.2: *System of gases with the partitions removed at the same pressure, temperature and total volume as in Figure 9.1.*

where P_i is the partial pressure of the *ith* species. The mixture is ideal so there is no enthalpy change during the mixing. If the pressure was so high that the potential energy associated with inter-molecular forces was significant then the enthalpy of mixing would be non-zero.

The entropy of the system after mixing is

$$S_{after} = \sum_{i=1}^{I} n_i s_i \left(T, P\right) = \sum_{i=1}^{I} n_i s_i^{\circ} \left(T\right) - \sum_{i=1}^{I} n_i R_u \ln\left(\frac{P_i}{P^{\circ}}\right). \tag{9.27}$$

The change of entropy due to mixing is

$$S_{after} - S_{before} = \left(\sum_{i=1}^{I} n_i s_i^{\circ} \left(T\right) - \sum_{i=1}^{I} n_i R_u \ln\left(\frac{P_i}{P^{\circ}}\right)\right) - \left(\sum_{i=1}^{I} n_i s_i^{\circ} \left(T\right) - \sum_{i=1}^{I} n_i R_u \ln\left(\frac{P}{P^{\circ}}\right)\right). \tag{9.28}$$

Cancel common terms in (9.28).

$$S_{after} - S_{before} = R_u \sum_{i=1}^{I} n_i \ln\left(\frac{P}{P_i}\right) > 0 \tag{9.29}$$

Mixing clearly leads to an increase in entropy. To determine the law that governs the partial pressure let's use the method of Lagrange multipliers to seek a maximum in the entropy after mixing subject to the constraint that

$$P = \sum_{i=1}^{I} P_i. \tag{9.30}$$

That is, we seek a maximum in the function

$$W\left(T,n_1,n_2,...,n_I,P_1,P_2,...,P_I,\lambda\right)=\sum_{i=1}^{I}n_i{s^\circ}_i\left(T\right)-\sum_{i=1}^{I}n_iR_u\ln\left(\frac{P_i}{P^\circ}\right)+\lambda\left(\sum_{i=1}^{I}P_i-P\right) \tag{9.31}$$

where λ is an, as yet unknown, Lagrange multiplier. The temperature of the system and number of moles of each species in the mixture are constant. Differentiate (9.31) and set the differential to zero for an extremum.

$$dW=\frac{\partial W}{\partial P_1}dP_1+\frac{\partial W}{\partial P_2}dP_2+.....+\frac{\partial W}{\partial P_I}dP_I+\frac{\partial W}{\partial \lambda}d\lambda=0 \tag{9.32}$$

Now

$$dW=-\sum_{i=1}^{I}n_iR_u\left(\frac{dP_i}{P_i}\right)+\lambda\left(\sum_{i=1}^{I}dP_i\right)+d\lambda\left(\sum_{i=1}^{I}P_i-P\right)=0. \tag{9.33}$$

The last term in (9.33) is zero by the constraint and the maximum entropy condition becomes.

$$\sum_{i=1}^{I}\left(-\frac{n_iR_u}{P_i}+\lambda\right)dP_i=0 \tag{9.34}$$

Since the dP_i are completely independent, the only way (9.34) can be satisfied is if the Lagrange multiplier satisfies

$$\lambda=\frac{n_iR_u}{P_i} \tag{9.35}$$

for all i. In the original, unmixed, system each species satisfies the ideal gas law.

$$PV_i=n_iR_uT \tag{9.36}$$

Using (9.35) and (9.36) we can form the sum

$$\lambda\sum_{i=1}^{I}P_i=\sum_{i=1}^{I}\frac{PV_i}{T}\quad . \tag{9.37}$$

Finally the Lagrange multiplier is

$$\lambda = \frac{V}{T} \tag{9.38}$$

where, $V = \sum_{i=1}^{I} V_i$. Using (9.35) and (9.38) the partial pressure satisfies

$$P_i V = n_i R_u T \tag{9.39}$$

which is Dalton's law of partial pressures. What we learn from this exercise is, not only that the entropy increases when the gases mix, but that the equilibrium state is one where the entropy is a maximum. Using Dalton's law, the mole fraction of the *ith* gas species is related to the partial pressure as follows

$$x_i = \frac{n_i}{N} = \frac{P_i}{P} \tag{9.40}$$

The entropy of a mixture of ideal gases expressed in terms of mole fractions is

$$S_{gas} = \sum_{i=1}^{I} n_i \left({s^\circ}_{i_{gas}} (T) - R_u \ln (x_i) \right) - N R_u \ln \left(\frac{P}{P^\circ} \right) \tag{9.41}$$

and the entropy change due to mixing, (9.29), is expressed as

$$S_{after} - S_{before} = -N R_u \sum_{i=1}^{I} x_i \ln (x_i) > 0. \tag{9.42}$$

9.5 Entropy of an ideal mixture of condensed species

The extensive entropy of an ideal mixture of condensed species (liquid or solid) with mole numbers $n_1, \ldots, n_I$ is $S(T, P, n_1, \ldots, n_I)$. If $s_{i_{pure}}(T, P)$ is the entropy of the pure form of the *ith* component, then in a system where the mole numbers are fixed, the differential of the entropy is

$$dS(T, P, n_1, \ldots, n_I) = \sum_{i=1}^{I} n_i ds_{i_{pure}}(T, P) \tag{9.43}$$

since $dn_1 = 0, \ldots, dn_I = 0$. If we integrate (9.43) the result is

$$S\left(T, P, n_1, \ldots, n_I\right) = \sum_{i=1}^{I} n_i s_{i_{pure}}\left(T, P\right) + C\left(n_1, \ldots, n_I\right) \tag{9.44}$$

with a constant of integration that is at most a function of the mole numbers.

In order to determine this constant we will use an argument first put forth by Max Planck in 1932 and also described by Enrico Fermi in his 1956 book *Thermodynamics* (page 114). Since the temperature and pressure in (9.44) are arbitrary let the pressure be reduced and the temperature be increased until all of the condensed species in the system are fully vaporized and behave as ideal gases as shown in Figure 9.3.

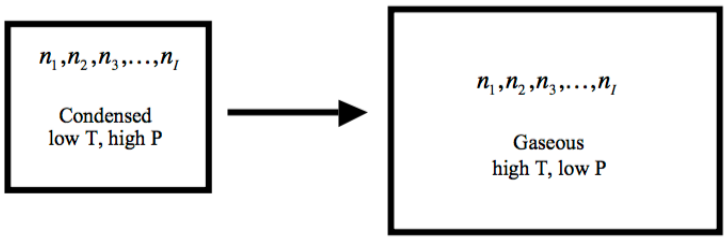

Figure 9.3: *System of condensed species with the temperature increased and pressure decreased to fully vaporize the mixture.*

Since the number of moles of each constituent has not changed, the constant of integration must be the same. The entropy of a system of ideal gases was discussed in the previous section and is given by equation (9.41).

$$S_{gas} = \sum_{i=1}^{I} n_i \left(s^{\circ}{}_{i_{gas}}\left(T\right) - R_u \ln\left(\frac{P}{P^{\circ}}\right)\right) - \sum_{i=1}^{I} n_i R_u \ln\left(\frac{n_i}{N}\right) \tag{9.45}$$

Comparing (9.44) with (9.45) we can conclude that the constant of integration must be

$$C\left(n_1, \ldots, n_I\right) = -R_u \sum_{i=1}^{I} n_i \ln\left(\frac{n_i}{N}\right). \tag{9.46}$$

Therefore, the entropy of a mixture of condensed species is

$$S\left(T,P,n_1,\ldots,n_I\right)=\sum_{i=1}^{I}n_i\left(s_{i_{pure}}\left(T,P\right)-R_u\ln\left(x_i\right)\right) \tag{9.47}$$

where the mole fraction, $x_i = n_i/N$ is used. Finally, the contribution of each component to the extensive entropy of the mixture of condensed species is

$$s_i\left(T,P\right)=s_{i_{pure}}\left(T,P\right)-R_u\ln\left(x_i\right). \tag{9.48}$$

The form of this equation is very similar to that for gases and comes as something of a surprise since it involves the ideal gas constant which would seem to have no particular relevance to a liquid or a solid. According to Kestin (*A Course in Thermodynamics*, Ginn Blaisdell 1966) when (9.48) was first introduced it was "met with general incredulity, but its validity has since been confirmed experimentally beyond any reasonable doubt whatever."

It can be noted that if the gases in the mixing problem described in the last section were replaced by ideal liquids, and those liquids were allowed to evolve from the unmixed to the mixed state, the entropy change would be given by an expression identical to (9.29).

$$\left(S_{after}-S_{before}\right)_{ideal\ liquids}=-NR_u\sum_{i=1}^{I}x_i\ln\left(x_i\right) \tag{9.49}$$

9.6 Thermodynamics of incompressible liquids and solids

For a single homogeneous substance the Gibbs equation is

$$dS=\frac{dE}{T}+\frac{P}{T}dV. \tag{9.50}$$

If the substance is an incompressible solid or liquid the Gibbs equation reduces to

$$dS=C_v(T)\frac{dT}{T} \tag{9.51}$$

and the entropy is

$$S - S_{ref} = \int_{T_{ref}}^{T} C_v(T) \frac{dT}{T}. \tag{9.52}$$

The entropy and internal energy of an incompressible substance depend only on its temperature. The constant volume and constant pressure heat capacities are essentially equivalent $C_p(T) = C_v(T) = C(T)$.

Since liquids and solids tend to be nearly incompressible, the entropy $s_{i_{pure}}(T, P)$ tends to be independent of pressure and in most circumstances one can use

$$s_{i_{pure}}(T, P) = s_i^{\circ}(T). \tag{9.53}$$

Now the entropy of a condensed species in a mixture really does resemble that of an ideal gas, but without the dependence on mixture pressure.

$$s_i(T, P) = s_i^{\circ}(T) - R_u \ln(x_i) \tag{9.54}$$

For a general substance, the differential of the Gibbs function is

$$dG = dE + PdV + VdP - TdS - SdT = -SdT + VdP \tag{9.55}$$

where the Gibbs equation (9.4) has been used. The cross derivative test applied to the right side of (9.55) produces the Maxwell relation

$$\left(\frac{\partial S}{\partial P}\right)_T = -\left(\frac{\partial V}{\partial T}\right)_P. \tag{9.56}$$

For an incompressible material, the entropy is independent of the pressure and (9.56) implies that the coefficient of thermal expansion of the material is also zero. Therefore, for

an incompressible substance

$$\begin{aligned}
&\left(\frac{\partial V}{\partial P}\right)_T = 0 \\
&\left(\frac{\partial V}{\partial T}\right)_P = 0 \\
&V = \text{constant} \\
&\mathrm{C}_P = C_V = C \\
&dE = CdT \\
&dS = \frac{C}{T}dT \\
&dH = CdT + VdP.
\end{aligned} \tag{9.57}$$

On a per unit mole basis, the enthalpy of an incompressible material referenced to the standard state is

$$h(T,P) = h^{\circ}(T) + (P - P^{\circ})\, v^{\circ} \tag{9.58}$$

where $v^{\circ} = constant$ is the molar volume of the material. The superscript on v° is not really necessary since it assumed to be a constant at all pressures and temperatures but as a practical matter, when using (9.58) as an approximation for a real condensed solid or liquid, the value of the molar density will be taken to be at the standard pressure $10^5 Pa$ and the reference temperature $298.15K$. Often the pressure term in (9.58) is neglected when dealing with reacting systems of gases and condensed materials. The reason is that, while the molar enthalpy of the condensed and gaseous form of a species are of the same order, the molar volume of a solid or liquid is generally two to three orders of magnitude smaller than the gaseous molar volume.

9.7 Enthalpy

The enthalpy per unit mole of a gas is determined from

$$dh = C_p(T)dT. \tag{9.59}$$

The enthalpy of a gas species is

$$h_i(T) - h_i(T_{ref}) = h_i^{\circ}(T) - h_i^{\circ}(T_{ref}) = \int_{Tref}^{T} C_{pi}^{\circ}(T)dT. \tag{9.60}$$

In principle the standard enthalpy of the ith gas species at the reference temperature could be taken as

$$h_i^\circ(T_{ref}) = \int_0^{T_{ref}} C_{pi}^\circ dT + h_i^\circ(0). \tag{9.61}$$

In this approach the enthalpy constant is the enthalpy change associated with chemical bond breaking and making that occurs when the atoms composing the species are brought together from infinity to form the molecule at absolute zero. Note that even for an atomic species, the enthalpy constant is not exactly zero. A quantum mechanical system contains energy or enthalpy arising from ground state motions that cannot be removed completely even at absolute zero temperature. In practice, enthalpies for most substances are tabulated as differences from the enthalpy at the reference temperature of $298.15K$ which is much more easily accessible than absolute zero so the question of the zero point enthalpy rarely comes up. Thus the standard enthalpy of a species is

$$h_i^\circ(T) = \int_{Tref}^{T} C_{pi}^\circ(T) dT + \Delta h_{fi}^\circ(T_{ref}) \tag{9.62}$$

where $\Delta h_{fi}^\circ(T)$ is the enthalpy change that occurs when the atoms of the species are brought together from at infinity at the finite temperature T. The enthalpy including the heat of formation (9.62) is sometimes called the complete enthalpy. In practice certain conventions are used to facilitate the tabulation of the heat of formation of a substance.

9.7.1 Enthalpy of formation and the reference reaction

The enthalpy of formation of a substance, denoted $\Delta h_f^\circ(T_{ref})$, is defined as the enthalpy change that occurs when one mole of the substance is formed from its elements in their reference state at the given temperature T and standard pressure P°. The reference state for an element is generally taken to be its most stable state at the given temperature and standard pressure. The reference reaction for a substance is one where the substance is the single product of a chemical reaction between its elements in their most stable state.

This convention for defining the heat of formation of a substance is useful even if the reference reaction is physically unlikely to ever actually occur. A consequence of this definition is that the heat of formation of a pure element in its reference state at any temperature is always zero. For example, the enthalpy of formation of any of the diatomic gases is zero at all temperatures. This is clear when we write the trivial reaction to form,

for example hydrogen, from its elements in their reference state.

$$H_2 \rightarrow H_2 \tag{9.63}$$

The enthalpy change is clearly zero. In fact the change in any thermodynamic variable for any element in its reference state is zero at all temperatures. A similar reference reaction applies to any of the other diatomic species $O_2, N_2, F_2, Cl_2, Br_2, I_2$, and the heat of formation of these substances is zero at all temperatures. The most stable form of carbon is solid carbon or graphite and the reference reaction is

$$C_{(s)} \rightarrow C_{(s)} \tag{9.64}$$

with zero heat of formation at all temperatures.

The reference reaction for carbon dioxide at $298.15K$ is

$$C_{(s)} + O_2 \rightarrow CO_2 \qquad \Delta h^\circ_{f_{CO_2}}(298.15) = -393.522\, kJ/mole. \tag{9.65}$$

Here the carbon is taken to be in the solid (graphite) form and the oxygen is taken to be the diatomic form. Both are the most stable forms over a wide range of temperatures. Even if the temperature is well above the point where carbon sublimates to a gas ($3915\,K$) and significant oxygen is dissociated, the heats of formation of $C_{(s)}$ and O_2 remain zero even though the most stable form of carbon at this temperature is carbon gas.

The heats of formation of metal elements are treated a little differently. The heat of formation of crystalline aluminum is zero at temperatures below the melting point and the heat of formation of liquid aluminum is zero at temperatures above the melting point. The same applies to boron, magnesium, sulfur, titanium and other metals.

The enthalpy (9.62) is usually expressed in terms of tabulated data as

$$h_i(T) = h_i^\circ(T) = \Delta h^\circ_{fi}(T_{ref}) + \left\{h_i^\circ(T) - h_i^\circ(T_{ref})\right\}. \tag{9.66}$$

For a general reaction the enthalpy balance is

$$\Delta h^\circ(T_{final}) = \sum_{i_{product}}^{I_{product}} n_{i_{product}} h^\circ_{i_{product}}(T_{final}) - \sum_{i_{reactant}}^{I_{reactant}} n_{i_{reactant}} h^\circ_{i_{reactant}}\left(T_{initial_{i_{reactant}}}\right). \tag{9.67}$$

So for example, to determine the heat of formation of CO_2 at $1000\,K$ where the initial reactants are also at $1000\,K$, the calculation would be

$$\begin{aligned}
&\Delta h^{\circ}_{f_{CO_2}}(1000) = \\
&\left(\Delta h^{\circ}_{f_{CO_2}}(298.15) + \left\{h^{\circ}_{CO_2}(1000) - h^{\circ}_{CO_2}(298.15)\right\}\right) - \\
&\left(\Delta h^{\circ}_{f_{C_{(s)}}}(298.15) + \left\{h^{\circ}_{C_{(s)}}(1000) - h^{\circ}_{C_{(s)}}(298.15)\right\}\right) - \\
&\left(\Delta h^{\circ}_{f_{O_2}}(298.15) + \left\{h^{\circ}_{O_2}(1000) - h^{\circ}_{O_2}(298.15)\right\}\right).
\end{aligned} \tag{9.68}$$

Putting in the numbers from tabulated data (See Appendix 2) gives

$$\begin{aligned}
&\Delta h^{\circ}_{f_{CO_2}}(1000) = \\
&[-393.522 + 33.397] - [0 + 11.795] - [0 + 22.703] = -394.623
\end{aligned} \tag{9.69}$$

which is the tabulated value of the heat of formation of carbon dioxide at $1000\,K$. Note that the enthalpy of the reference reactants at the reaction temperature must be included in the calculation of the heat of formation calculation. Further discussion of heats of formation can be found in Appendix 1 and tables of thermo-chemical data for selected species can be found in Appendix 2.

9.8 Condensed phase equilibrium

The pressure and temperature of the system may be such that one or more or all of the species may be evolving with their condensed phase. In this case it may be necessary to vary the volume to keep the temperature and pressure constant until the system reaches equilibrium.

Figure 9.4 depicts the various species of the system in several phases all of which are in contact with each other. Let the total number of moles in each phase be $N_1, N_2, \ldots, N_p, \ldots, N_P$. Generally only a subset of the species will be evolving with their condensed phase and so there is a different maximal index I_p for each phase. Effects of surface tensions between phases are ignored.

Note the total numbers of moles in each phase are related to the species mole numbers

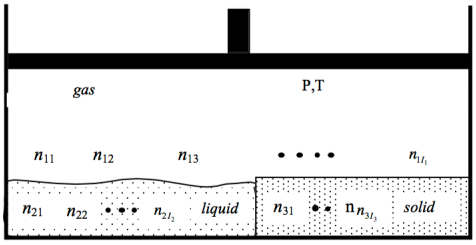

Figure 9.4: *System of molecular species with several phases.*

by

$$N_1 = \sum_{i=1}^{I_1} n_{1i} \quad N_2 = \sum_{i=1}^{I_2} n_{2i} \quad \cdots \quad N_P = \sum_{i=1}^{I_P} n_{Pi}. \tag{9.70}$$

The mole fractions in each phase are

$$x_{pi} = \frac{n_{pi}}{N_p}. \tag{9.71}$$

In the gas phase, the partial pressures of the gas species add up to the mixture pressure

$$P = \sum_{i=1}^{I_1} P_i. \tag{9.72}$$

The mole fractions of the species in the gas phase are related to the partial pressures by

$$x_{1i} = \frac{P_i}{P}. \tag{9.73}$$

Finally the mole fractions in each phase add to one.

$$\sum_{i=1}^{I_p} x_{pi} = 1 \tag{9.74}$$

The extensive Gibbs free energies in each phase are

$$
\begin{aligned}
G_1\left(T,P,n_{11},n_{12},n_{13},...,n_{1I_1}\right) &= N_1\left\{\sum_{i=1}^{I_1} x_{1i}\left(g_{1i}^{\circ}(T)+R_uT\ln\left(x_{1i}\right)\right)+R_uT\ln\left(\frac{P}{P^{\circ}}\right)\right\}\\
G_2\left(T,P,n_{21},n_{22},n_{23},...,n_{2I_2}\right) &= N_2\sum_{i_2=1}^{I_2} x_{2i}\left(g_{2i}(T,P)+R_uT\ln\left(x_{2i}\right)\right)\\
&\vdots\\
G_P\left(T,P,n_{P1},n_{P2},n_{P3},...,n_{PI_P}\right) &= N_P\sum_{i_P=1}^{I_P} x_{pi}\left(g_{pi}(T,P)+R_uT\ln\left(x_{pi}\right)\right)
\end{aligned}
\tag{9.75}
$$

where phase 1 is assumed to be the gas phase. In (9.75) we have assumed that all condensed phases are ideal mixtures and the entropy per mole of the condensed phase of species i does not depend on the pressure. This is a reasonable assumption for a condensed phase that is approximately incompressible as was argued earlier in conjunction with equation (9.58). There are a few examples of liquids such as liquid helium and liquid nitrous oxide that are quite compressible and the assumption would break down. This treatment of the condensed phases is similar to that used by Bill Reynolds in the development of STANJAN. The NASA Glenn code CEA is a little different. In CEA, each condensed phase is treated as a pure substance. For example, if there are two species that condense out as liquids, each is treated as a separate, distinct phase. In the approach used by CEA the mole fractions of each condensed species are one by definition. In CEA the pressure term in (9.58) is neglected. See equation 2.11 in NASA Reference Publication 1311 (1994) by Gordon and McBride.

In the case of a gas, the Gibbs free energy does depend on pressure through the dependence of entropy on pressure. This is connected to the fact that, as quantum mechanics tells us, the number of energy states that a gas can occupy (and therefore the entropy of the gas) increases with the volume containing the gas (see Appendix 1 of the AA210a notes).

The Gibbs free energy of the whole system is

$$
\begin{aligned}
&G\left(T,P,n_{11},n_{12},\ldots,n_{1I_1},n_{21},n_{22},\ldots,n_{2I_2},...,n_{P1},n_{P2},...,n_{PI_P}\right) =\\
&\sum_{p=1}^{P}\sum_{i=1}^{I_P} n_{pi}g_{pi}\left(T,P,n_{pi}\right).
\end{aligned}
\tag{9.76}
$$

With the gas phase written separately Equation (9.76) is

$$\begin{aligned} &G\left(T,P,n_{11},n_{12},\ldots,n_{1I_1},n_{21},n_{22},\ldots,n_{2I_2},...,n_{P1},n_{P2},...,n_{PI_P}\right)= \\ &\sum_{p=1}^{P}\sum_{i=1}^{I_P} n_{1i}\left(g_{1i}^{\circ}\left(T\right)+R_uT\ln\left(n_{1i}\right)-R_uT\ln\left(\sum_{\hat{i}=1}^{I_1}n_{1\hat{i}}\right)\right)+ \\ &\sum_{p=2}^{P}\sum_{i=1}^{I_P} n_{pi}\left(g_{pi}\left(T,P\right)+R_uT\ln\left(n_{pi}\right)-R_uT\ln\left(\sum_{\hat{i}=1}^{I_P}n_{p\hat{i}}\right)\right). \end{aligned} \tag{9.77}$$

Differentiate (9.77).

$$\begin{aligned} dG=&\frac{\partial G}{\partial T}dT+\frac{\partial G}{\partial P}dP+ \\ &\frac{\partial G}{\partial n_{11}}dn_{11}+\frac{\partial G}{\partial n_{12}}dn_{12}+\cdots+\frac{\partial G}{\partial n_{1I_1}}dn_{1I_1}+ \\ &\frac{\partial G}{\partial n_{21}}dn_{21}+\frac{\partial G}{\partial n_{22}}dn_{22}+\cdots+\frac{\partial G}{\partial n_{2I_2}}dn_{2I_2}+\ldots+ \\ &\frac{\partial G}{\partial n_{P1}}dn_{P1}+\frac{\partial G}{\partial n_{P2}}dn_{P2}+\cdots+\frac{\partial G}{\partial n_{PI_P}}dn_{PI_P}. \end{aligned} \tag{9.78}$$

Written out fully (9.78) is

$$
\begin{aligned}
dG = &\sum_{i=1}^{I_1} dn_{1i}\left(g^\circ_{1i}(T) + R_uT\ln\left(n_{1i}\right) - R_uT\ln\left(\sum_{\widehat{i}=1}^{I_1} n_{1\,\widehat{i}}\right)\right) + \\
&\sum_{i=1}^{I_1} n_{1i}\left(R_uT\left(\frac{dn_{1i}}{n_{1i}}\right) - R_uT\left(\frac{\sum_{\widehat{i}=1}^{I_1} dn_{1\,\widehat{i}}}{\sum_{\widehat{i}=1}^{I_1} n_{1\,\widehat{i}}}\right)\right) + R_uT\ln\left(\frac{P}{P^\circ}\right)\sum_{i=1}^{I_1} dn_{1i} + \\
&\sum_{i=1}^{I_1} n_{1i}\left(\frac{\partial g^\circ_{1i}(T)}{\partial T} + R_u\ln\left(n_{1i}\right) - R_u\ln\left(\sum_{\widehat{i}=1}^{I_1} n_{1\,\widehat{i}}\right)\right)dT + \\
&\left(\sum_{i=1}^{I_1} n_{1i}\right)R_uT\left(\frac{dP}{P}\right) + \left(\sum_{i=1}^{I_1} n_{1i}\right)R_u\ln\left(\frac{P}{P^\circ}\right)dT + \\
&\sum_{p=2}^{P}\sum_{i=1}^{I_p} dn_{pi}\left(g_{pi}(T,P) + R_uT\ln\left(n_{pi}\right) - R_uT\ln\left(\sum_{\widehat{i}=1}^{I_p} n_{p\,\widehat{i}}\right)\right) + \\
&\sum_{p=2}^{P}\sum_{i=1}^{I_p} n_{pi}\left(R_uT\left(\frac{dn_{pi}}{n_{pi}}\right) - R_uT\left(\frac{\sum_{\widehat{i}=1}^{I_p} dn_{p\,\widehat{i}}}{\sum_{i=1}^{I_p} n_{p\,\widehat{i}}}\right)\right) + \\
&\sum_{p=2}^{P}\sum_{i=1}^{I_p} n_{pi}\left(\frac{\partial g_{pi}(T,P)}{\partial T} + R_u\ln\left(n_{1i}\right) - R_u\ln\left(\sum_{\widehat{i}=1}^{I_p} n_{1\,\widehat{i}}\right)\right)dT + \sum_{p=2}^{P}\sum_{i=1}^{I_p} n_{pi}\left(\frac{\partial g_{pi}(T,P)}{\partial T}\right)dP.
\end{aligned}
\tag{9.79}
$$

Note that

$$
\sum_{i=1}^{I_p} n_{pi}\left(\frac{dn_{pi}}{n_{pi}} - \frac{\sum_{\widehat{i}=1}^{I_p} dn_{p\,\widehat{i}}}{\sum_{\widehat{i}=1}^{I_p} n_{p\,\widehat{i}}}\right) = dN_p - dN_p = 0. \tag{9.80}
$$

At constant temperature and pressure $dT = dP = 0$ and(9.79) becomes

$$dG = \sum_{i=1}^{I_1} dn_{1i} \left(g^\circ_{1i}(T) + R_u T \ln\left(n_{1i}\right) - R_u T \ln\left(\sum_{\widehat{i}=1}^{I_1} n_{1\,\widehat{i}} \right) + R_u T \ln\left(\frac{P}{P^\circ}\right) \right) + \sum_{p=2}^{P} \sum_{i=1}^{I_p} dn_{pi} \left(g_{pi}(T,P) + R_u T \ln\left(n_{pi}\right) - R_u T \ln\left(\sum_{\widehat{i}=1}^{I_p} n_{p\,\widehat{i}} \right) \right). \tag{9.81}$$

In terms of mole fractions (9.81) reads

$$dG = \sum_{i=1}^{I_1} dn_{1i} \left(g^\circ_{1i}(T) + R_u T \ln\left(x_{1i}\right) + R_u T \ln\left(\frac{P}{P^\circ}\right) \right) + \sum_{p=2}^{P} \sum_{i=1}^{I_p} dn_{pi} \left(g_{pi}(T,P) + R_u T \ln\left(x_{pi}\right) \right). \tag{9.82}$$

At equilibrium $dG = 0$. For species that are only present in one phase, $dn_{pi} = 0$ at equilibrium. For those species that are in equilibrium with another phase, $dn_{phase1i} = -dn_{phase\,pi}$ and equation $dG = 0$ can only be satisfied if

$$g_{phase1i} = g_{phase\,pi}. \tag{9.83}$$

If phase 1 is a gas species (9.83) is

$$g^\circ_{phase1i}(T) + R_u T \ln\left(x_{phase1i}\right) + R_u T \ln\left(\frac{P}{P^\circ}\right) = g_{phase\,pi}(T,P) + R_u T \ln\left(x_{phase\,pi}\right). \tag{9.84}$$

At equilibrium, the Gibbs free energy (or chemical potential) of species i is the same regardless of its phase. For example if gas species 1 is in equilibrium with its liquid phase, then $g_{gas1}\left(T,P\right) = g_{liquid1}\left(T,P\right)$. There can also be more than one solid phase and so the total number of phases can exceed three. For example, in helium at very low temperature there can be multiple liquid phases.

Suppose phase p in is a pure liquid so the mole fraction is one. Also assume the liquid is incompressible so that the Gibbs function of the liquid is given by

$$g^\circ_{gas_i}(T) + R_u T \ln\left(x_{gas_i}\right) + R_u T \ln\left(\frac{P}{P^\circ}\right) = g^\circ_{liquid_i}(T) + \left(P - P^\circ\right) v^\circ{}_{liquid}. \tag{9.85}$$

Solve for the partial pressure of the species in the gas phase.

$$\frac{P_i}{P^\circ} = e^{\frac{(P-P^\circ)v^\circ_{liquid_i}}{R_u T}} \left(e^{\frac{g^\circ_{liquid_i}(T) - g^\circ_{gas_i}(T)}{R_u T}} \right) \tag{9.86}$$

The term in brackets is the classical form of the Clausius-Clapeyron equation that relates the vapor pressure of a gas in equilibrium with its condensed phase to the temperature of the system.

9.9 Chemical equilibrium, the method of element potentials

If the species are allowed to react at constant temperature and pressure, the mole fractions will evolve toward values that minimize the extensive Gibbs free energy of the system subject to the constraint that the number of moles of each element in the mixture remains fixed. The number of moles of each atom in the system is given by

$$a_j = \sum_{p=1}^{P} \sum_{i=1}^{I_p} n_{pi} A_{pij} \tag{9.87}$$

where A_{pij} is the number of atoms of the jth element in the ith molecular species of the pth phase. The appropriate picture of our system is shown in Figure 9.5.

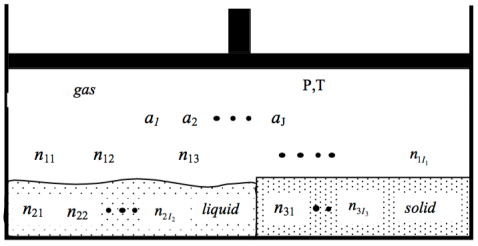

Figure 9.5: *System of reacting molecular species in several phases at constant temperature and pressure with fixed number of moles of each element.*

Generally the number of species in each phase will be different. This may be the case even in a situation where, at a given temperature and pressure, there is phase equilibrium for a given species. Consider graphite in equilibrium with its vapor at low temperature, the mole fraction in the vapor phase may be so small as to be essentially zero and the species

may be rightly excluded from the vapor mixture. The volume required to maintain the system at constant pressure and temperature must be allowed to vary.

The Gibbs free energy of the system is

$$G\left(T,P,n_{11},n_{12},...,n_{p1},...,n_{PI_P}\right)=\sum_{p=1}^{P}N_p\sum_{i=1}^{I_p}x_{pi}g_{pi}\left(T,P,x_{pi}\right). \tag{9.88}$$

With the gas phase written separately

$$G\left(T,P,n_{11},n_{12},...,n_{21},...,n_{PI_P}\right)=N_1\sum_{i=1}^{I_1}x_{1i}\left(g_{1i}^{\circ}(T)+R_uT\ln\left(x_{1i}\right)\right)+N_1R_uT\ln\left(\frac{P}{P^{\circ}}\right)+\sum_{p=2}^{P}N_p\sum_{i=1}^{I_p}x_{pi}\left(g_{pi}(T,P)+R_uT\ln\left(x_{pi}\right)\right) \tag{9.89}$$

We will use the method of Lagrange multipliers to minimize the Gibbs free energy subject to the atom constraints. Minimize the function

$$\begin{aligned}&W\left(T,P,n_{11},n_{12},...,n_{1I_1},n_{21},n_{22},...,n_{2I_2},....,n_{p1},n_{p2},...,n_{pI_p},\lambda_1,...,\lambda_J\right)=\\&G\left(T,P,n_{11},n_{12},...,n_{1I_1},n_{21},n_{22},...,n_{2I_2},....,n_{p1},n_{p2},...,n_{pI_p}\right)-\\&R_uT\sum_{j=1}^{J}\lambda_j\left(\sum_{p=1}^{P}\sum_{i=1}^{I_p}n_{pi}A_{pij}-a_j\right).\end{aligned} \tag{9.90}$$

where the J unknown Lagrange multipliers, λ_j, are dimensionless. Our modified equilibrium condition is

$$dW=\frac{\partial W}{\partial T}dT+\frac{\partial W}{\partial P}dP+\frac{\partial W}{\partial n_{11}}dn_{11}+....+\frac{\partial W}{\partial n_{pI}}dn_{pI_P}+\frac{\partial W}{\partial\lambda_1}d\lambda_1+....+\frac{\partial W}{\partial\lambda_J}d\lambda_J=0. \tag{9.91}$$

Substitute (9.76) into (9.91) and impose $dP = dT = 0$.

$$dW = \sum_{p=1}^{P}\sum_{i=1}^{I_p}\left(n_{pi}dg_{pi}\left(T,P,x_{pi}\right) + g_{pi}\left(T,P,x_{pi}\right)dn_{pi}\right) - R_uT\sum_{j=1}^{j}\lambda_j\sum_{p=1}^{P}\sum_{i=1}^{I_p}dn_{pi}A_{pij} \tag{9.92}$$

The order of the sums can be rearranged so (9.92) can be written as

$$dW = \sum_{p=1}^{P}\sum_{i=1}^{I_p}n_{pi}dg_{pi}\left(T,P,x_{pi}\right) + \sum_{p=1}^{P}\sum_{i=1}^{I_p}\left(g_{pi}\left(T,P,x_{pi}\right) - R_uT\sum_{j=1}^{J}\lambda_jA_{pij}\right)dn_{pi} = 0. \tag{9.93}$$

The differential of the molar Gibbs free energy is

$$dg_{pi} = \frac{\partial g_{pi}}{\partial T}dT + \frac{\partial g_{pi}}{\partial P}dP + R_uT\frac{dx_{pi}}{x_{pi}}. \tag{9.94}$$

For a process that takes place at constant temperature and pressure

$$dW = R_uT\sum_{p=1}^{P}\sum_{i=1}^{I_p}n_{pi}\frac{dx_{pi}}{x_{pi}} + \sum_{p=1}^{P}\sum_{i=1}^{I_p}\left(g_{pi}\left(T,P,x_{pi}\right) - R_uT\sum_{j=1}^{J}\lambda_jA_{pij}\right)dn_{pi} = 0. \tag{9.95}$$

The first sum in (9.95) can be re-written as follows

$$dW = R_uT\sum_{p=1}^{P}N_p\sum_{i=1}^{I_p}x_{pi}\frac{dx_{pi}}{x_{pi}} + \sum_{p=1}^{P}\sum_{i=1}^{I_p}\left(g_{pi}\left(T,P,x_{pi}\right) - R_uT\sum_{j=1}^{J}\lambda_jA_{pij}\right)dn_{pi} = 0 \tag{9.96}$$

or

$$dW = R_uT\sum_{p=1}^{P}N_p\sum_{i=1}^{I_p}dx_{pi} + \sum_{p=1}^{P}\sum_{i=1}^{I_p}\left(g_{pi}\left(T,P,x_{pi}\right) - R_uT\sum_{j=1}^{J}\lambda_jA_{pij}\right)dn_{pi} = 0. \tag{9.97}$$

But the normalization conditions for the mole fractions of each phase imply that

$$\sum_{i=1}^{I_p} dx_{pi} = d\left(\sum_{i=1}^{I_p} x_{pi}\right) = d\left(1\right) = 0. \tag{9.98}$$

Finally our modified equilibrium condition is

$$dW = \sum_{p=1}^{P}\sum_{i=1}^{I_p}\left(g_{pi}\left(T,P,x_{pi}\right) - R_uT\sum_{j=1}^{J}\lambda_j A_{pij}\right)dn_{pi} = 0. \tag{9.99}$$

Since the dn_{pi} are completely free, the condition (9.99) can only be satisfied if

$$g_{pi}\left(T,P,x_{pi}\right) = R_uT\sum_{j=1}^{J}\lambda_j A_{pij}. \tag{9.100}$$

The Gibbs free energy of the system is

$$G\left(T,P,n_{11},n_{12},...,n_{p1},...,n_{PI_P}\right) = R_uT\sum_{p=1}^{P}\sum_{i=1}^{I_p}\sum_{j=1}^{J} n_{pi}\lambda_j A_{pij}. \tag{9.101}$$

Each atom in the mixture contributes equally to the extensive Gibbs free energy regardless of which molecule it is in or which phase it is in. The molar Gibbs free energy of the *ith* gas phase species is

$$g_{1i}(T,P) = g^{\circ}_{1i}(T) + R_uT\ln\left(x_{1i}\right) + R_uT\ln\left(\frac{P}{P^{\circ}}\right). \tag{9.102}$$

Insert into (9.100). For the gas phase species

$$\frac{g^{\circ}_{1i}(T)}{R_uT} + \ln\left(x_{1i}\right) + \ln\left(\frac{P}{P^{\circ}}\right) = \sum_{j=1}^{J}\lambda_j A_{1ij}. \tag{9.103}$$

For the condensed phase species

$$\frac{g_{pi}(T,P)}{R_uT} + \ln\left(x_{pi}\right) = \sum_{j=1}^{J}\lambda_j A_{pij} \qquad p = 2,\ldots,P\ . \tag{9.104}$$

Solve for the mole fraction of the *ith* species in the *pth* phase.

$$\begin{aligned} x_{1i} &= Exp\left\{ -\frac{g^{\circ}_{1i}(T)}{R_u T} - \ln\left(\frac{P}{P^{\circ}}\right) + \sum_{j=1}^{J} \lambda_j A_{1ij} \right\} \\ x_{pi} &= Exp\left\{ -\frac{g_{pi}(T,P)}{R_u T} + \sum_{j=1}^{J} \lambda_j A_{pij} \right\} \qquad p = 2, \ldots, P \end{aligned} \quad . \tag{9.105}$$

The constraints on the atoms are

$$a_j = \sum_{p=1}^{P} N_p \sum_{i=1}^{I_p} x_{pi} A_{pij}. \tag{9.106}$$

Substitute (9.105) into (9.106).

$$\begin{aligned} a_j = N_1 \sum_{i=1}^{I_1} A_{1ij} Exp\left\{ -\frac{g^{\circ}_{1i}(T)}{R_u T} - \ln\left(\frac{P}{P^{\circ}}\right) + \sum_{j_1=1}^{J} \lambda_{j_1} A_{1ij_1} \right\} + \\ \sum_{p=2}^{P} N_p \sum_{i=1}^{I_p} A_{pij} Exp\left\{ -\frac{g_{pi}(T,P)}{R_u T} + \sum_{j_1=1}^{J} \lambda_{j_1} A_{pij_1} \right\} \qquad j = 1, ..., J. \end{aligned} \tag{9.107}$$

Note that we have to introduce the dummy index j_1 in the formula for x_{pi} when we make the substitution. The normalization conditions on the mole fractions give

$$\sum_{i=1}^{I_1} Exp\left\{ -\frac{g^{\circ}_{1i}(T)}{R_u T} - \ln\left(\frac{P}{P^{\circ}}\right) + \sum_{j=1}^{J} \lambda_j A_{1ij} \right\} = 1 \tag{9.108}$$

and

$$\sum_{i=1}^{I_p} Exp\left\{ -\frac{g_{pi}(T,P)}{R_u T} + \sum_{j=1}^{J} \lambda_j A_{pij} \right\} = 1 \qquad p = 2, ..., P \ . \tag{9.109}$$

The total number of moles in the mixture is

$$\sum_{p=1}^{P} N_p = N. \tag{9.110}$$

Equations, (9.107), (9.108), (9.109) and (9.110) are $J + P + 1$ equations in the unknowns $\lambda_1, ..., \lambda_J$, $N_1, ..., N_P$ and N.

As a practical matter, it is easier to compute the solution to equations (9.107), (9.108), (9.109) and (9.110) by reformulating the equations to get rid of the exponentials. Define

$$B_{1i}(T) \equiv Exp\left\{-\frac{g^{\circ}_{1i}(T)}{R_u T}\right\} \tag{9.111}$$

and for the condensed species, $p > 1$

$$B_{pi}(T, P) \equiv Exp\left\{-\frac{g_{pi}(T, P)}{R_u T}\right\}. \tag{9.112}$$

In addition, define

$$y_j = Exp\left(\lambda_j\right). \tag{9.113}$$

The mole fractions become

$$\begin{aligned} x_{1i} &= \left(\frac{P^{\circ}}{P}\right) B_{1i} \prod_{j=1}^{J} \left(y_j\right)^{A_{1ij}} \\ x_{pi} &= B_{pi} \prod_{j=1}^{J} \left(y_j\right)^{A_{pij}} \qquad p = 2, \ldots, P. \end{aligned} \tag{9.114}$$

The system of equations that needs to be solved now becomes

$$\begin{aligned}
&\left(\frac{P^\circ}{P}\right) N_1 \sum_{i=1}^{I_1} A_{1ij} B_{1i} \prod_{j_1=1}^{J} (y_{j_1})^{A_{1ij_1}} + \sum_{p=2}^{P} N_p \sum_{i=1}^{I_p} A_{pij} B_{pi} \prod_{j_1=1}^{J} (y_{j_1})^{A_{pij_1}} = a_j, \quad j = 1, \ldots, J \\
&\left(\frac{P^\circ}{P}\right) \sum_{i=1}^{I_1} B_{1i} \prod_{j=1}^{J} (y_j)^{A_{1ij}} = 1 \\
&\sum_{i=1}^{I_p} B_{pi} \prod_{j=1}^{J} (y_j)^{A_{pij}} = 1, \qquad p = 2, \ldots, P \\
&\sum_{p=1}^{P} N_p = N.
\end{aligned} \tag{9.115}$$

Note that in this formulation only the always positive y_j are needed to determine the mole fractions. The element potentials λ_j, which are the logarithm of the y_j, never actually need to be calculated.

A key advantage of this formulation of the problem is that the equations that need to be solved for the unknown y_i and N_p are multivariate polynomials, and algorithms are available that enable the roots to be determined without requiring an initial guess of the solution. Typically a number of real and complex roots are returned. The correct root is the one with all positive real values of the y_i and N_p. In general, there is only one such root.

9.9.1 Rescaled equations

The equations (9.115) admit an interesting scaling invariance where any constants, say α_j, $j = 1, \ldots, J$ can be added to the normalized Gibbs free energies as long as the coefficients and unknowns are transformed as

$$\begin{aligned}
B_{pi} &= \tilde{B}_{pi} \prod_{j=1}^{J} (\alpha_j)^{A_{pij}} \\
y_j &= \frac{\tilde{y}_j}{\alpha_j}.
\end{aligned} \tag{9.116}$$

If the transformations (9.116) are substituted into (9.115) the system of equations remains the same but expressed in tildaed variables. This leads to the following reformulation of

the problem.

Rewrite (9.111) and (9.112) by adding and subtracting the standard Gibbs free energies of the elements that make up the given species.

$$\begin{aligned} B_{1i} &= Exp\left\{ -\frac{g^{\circ}_{1i}(T)}{R_u T} + \sum_{j=1}^{J} A_{1ij} \frac{g^{\circ}{}_{j}(T)}{R_u T} - \sum_{j=1}^{J} A_{1ij} \frac{g^{\circ}_{j}(T)}{R_u T} \right\} \\ B_{pi} &= Exp\left\{ -\frac{g_{pi}(T,P)}{R_u T} + \sum_{j=1}^{J} A_{pij} \frac{g_j(T,P)}{R_u T} - \sum_{j=1}^{J} A_{pij} \frac{g_j(T,P)}{R_u T} \right\} \qquad p > 1 \end{aligned} \tag{9.117}$$

The first two terms in the bracket in equation (9.117) constitute the *Gibbs free energy of formation* of the given species from its individual elements

$$\begin{aligned} B_{1i} &= Exp\left\{ -\frac{\Delta g^{\circ}_{1i}(T)}{R_u T} - \sum_{j=1}^{J} A_{1ij} \frac{g^{\circ}_{j}(T)}{R_u T} \right\} \\ B_{pi} &= Exp\left\{ -\frac{\Delta g_{pi}(T,P)}{R_u T} - \sum_{j=1}^{J} A_{pij} \frac{g_j(T,P)}{R_u T} \right\} \qquad p > 1 \end{aligned} \tag{9.118}$$

where

$$\begin{aligned} \Delta g^{\circ}_{1i}(T) &= g^{\circ}_{1i}(T) - \sum_{j=1}^{J} A_{1ij} g^{\circ}_{j}(T) \\ \Delta g_{pi}(T,P) &= g_{pi}(T,P) - \sum_{j=1}^{J} A_{pij} g_j(T,P) \qquad p > 1. \end{aligned} \tag{9.119}$$

We can write (9.118) as

$$\begin{aligned} B_{1i} &= \tilde{B}_{1i} \prod_{j=1}^{J} Exp\left(-A_{1ij} \frac{g^{\circ}_{j}(T)}{R_u T} \right) \\ B_{pi} &= \tilde{B}_{pi} \prod_{j=1}^{J} Exp\left(-A_{pij} \frac{g_j(T,P)}{R_u T} \right) \qquad p > 1 \end{aligned} \tag{9.120}$$

where

$$\begin{aligned}\tilde{B}_{1i} &= Exp\left\{-\frac{\Delta g^{\circ}_{1i}(T)}{R_u T}\right\} \\ \tilde{B}_{pi} &= Exp\left\{-\frac{\Delta g_{pi}(T,P)}{R_u T}\right\} \qquad p>1.\end{aligned} \tag{9.121}$$

The system of equations (9.115) can now be written as

$$\begin{aligned}&\left(\frac{P^{\circ}}{P}\right) N_1 \sum_{i=1}^{I_1} A_{1ij}\tilde{B}_{1i} \prod_{j_1=1}^{J} (\tilde{y}_{j_1})^{A_{1ij_1}} + \sum_{p=2}^{P} N_p \sum_{i=1}^{I_p} A_{pij}\tilde{B}_{pi} \prod_{j_1=1}^{J} (\tilde{y}_{j_1})^{A_{pij_1}} = a_j, \quad j=1,\ldots,J \\ &\left(\frac{P^{\circ}}{P}\right) \sum_{i=1}^{I_1} \tilde{B}_{1i} \prod_{j=1}^{J} (\tilde{y}_j)^{A_{1ij}} = 1 \\ &\sum_{i=1}^{I_p} \tilde{B}_{pi} \prod_{j=1}^{J} (\tilde{y}_j)^{A_{pij}} = 1 \qquad\qquad p=2,\ldots,P \\ &\sum_{p=1}^{P} N_p = N\end{aligned} \tag{9.122}$$

where

$$\tilde{y}_j = y_j Exp\left(-\frac{g^{\circ}_j(T)}{R_u T}\right) \qquad j=1,\ldots,J. \tag{9.123}$$

The mole fractions in scaled variables are

$$\begin{aligned}x_{1i} &= \left(\frac{P^{\circ}}{P}\right) \tilde{B}_{1i} \prod_{j=1}^{J} (\tilde{y}_j)^{A_{1ij}} \\ x_{pi} &= \tilde{B}_{pi} \prod_{j=1}^{J} (\tilde{y}_j)^{A_{pij}} \qquad p=2,\ldots,P.\end{aligned} \tag{9.124}$$

Note that the governing equations (9.115) and (9.122) have exactly the same form and the $\tilde{y}_j$ determine the mole fractions. The implication of this result is that the calculation of mole fractions can be carried out either in terms of the standard Gibbs free energy of a species or the Gibbs free energy of formation of the species.

Generally the Gibbs free energy of formation of a substance is less than the Gibbs free energy itself and so usually $\tilde{B}_{pi} < B_{pi}$ making the numerical solution of (9.122) simpler than (9.115). This is especially important for gas calculations at low temperature where ${g^\circ}_j/R_uT$ can be quite large producing values of the B_{pi} that can range over many orders of magnitude. For many calculations, the Gibbs free energy of formation of a substance is the only data tabulated. This is especially true for reactions in aqueous solution.

9.10 Example - combustion of carbon monoxide

If we mix carbon monoxide (CO) and oxygen (O_2) at $10^5 Pa$ and $298.15\,K$ then ignite the mixture, the result is a strongly exothermic reaction. The simplest model of such a reaction takes one mole of CO plus half a mole of O_2 to produce one mole of carbon dioxide.

$$CO + \frac{1}{2}O_2 \rightarrow CO_2 \tag{9.125}$$

But this model is not very meaningful without some information about the temperature of the process. If the reaction occurs in an adiabatic system at constant pressure, the final temperature is very high and at that temperature the hot gas consists of a mixture of a number of species beside CO_2. A more realistic model assumes that the composition includes virtually all of the combinations of carbon and oxygen that one can think of including

$$C, CO, CO_2, O, O_2. \tag{9.126}$$

Other more complex molecules are possible such as C_2 and O_3 but are only present in extraordinarily low concentrations. For the composition (9.125) the temperature of the mixture at one atmosphere turns out to be $2975.34\,K$. This is called the adiabatic flame temperature.

Let's use the minimization of the Gibbs free energy to determine the relative concentrations of each molecular species for the mixture (9.126) at the equilibrium temperature $2975.34\,K$. We will order the species as in (9.126). In this case all the species are in the gas phase and the matrix of element coefficients A_{ij} is shown in Figure 9.6.

For this system of molecular species, (9.107) and (9.108) lead to the following equations governing the mole fractions and the total number of moles. Note that $P = P^\circ$ in this

	Atom	C	O
Molecule		$j=1$	$j=2$
C	$i=1$	1	0
CO	$i=2$	1	1
CO_2	$i=3$	1	2
O	$i=4$	0	1
O_2	$i=5$	0	2

Figure 9.6: *Matrix of element coefficients for the CO, O_2 system.*

case.

$$a_1 = N\left(A_{11}Exp\left(-\frac{g_1^\circ}{R_uT}+\lambda_1A_{11}+\lambda_2A_{12}\right)+A_{21}Exp\left(-\frac{g_2^\circ}{R_uT}+\lambda_1A_{21}+\lambda_2A_{22}\right)+ A_{31}Exp\left(-\frac{g_3^\circ}{R_uT}+\lambda_1A_{31}+\lambda_2A_{32}\right)+A_{41}Exp\left(-\frac{g_4^\circ}{R_uT}+\lambda_1A_{41}+\lambda_2A_{42}\right)+ A_{51}Exp\left(-\frac{g_5^\circ}{R_uT}+\lambda_1A_{51}+\lambda_2A_{52}\right)\right) \tag{9.127}$$

$$a_2 = N\left(A_{12}Exp\left(-\frac{g_1^\circ}{R_uT}+\lambda_1A_{11}+\lambda_2A_{12}\right)+A_{22}Exp\left(-\frac{g_2^\circ}{R_uT}+\lambda_1A_{21}+\lambda_2A_{22}\right)+ A_{32}Exp\left(-\frac{g_3^\circ}{R_uT}+\lambda_1A_{31}+\lambda_2A_{32}\right)+A_{42}Exp\left(-\frac{g_4^\circ}{R_uT}+\lambda_1A_{41}+\lambda_2A_{42}\right)+ A_{52}Exp\left(-\frac{g_5^\circ}{R_uT}+\lambda_1A_{51}+\lambda_2A_{52}\right)\right) \tag{9.128}$$

$$1 = Exp\left(-\frac{g_1^\circ}{R_uT}+\lambda_1A_{11}+\lambda_2A_{12}\right)+Exp\left(-\frac{g_2^\circ}{R_uT}+\lambda_1A_{21}+\lambda_2A_{22}\right)+ Exp\left(-\frac{g_3^\circ}{R_uT}+\lambda_1A_{31}+\lambda_2A_{32}\right)+Exp\left(-\frac{g_4^\circ}{R_uT}+\lambda_1A_{41}+\lambda_2A_{42}\right)+ Exp\left(-\frac{g_5^\circ}{R_uT}+\lambda_1A_{51}+\lambda_2A_{52}\right) \tag{9.129}$$

The unknowns in this system are the two Lagrange multipliers λ_1 and λ_2 corresponding to each element in the mixture and the total number of moles . The number of moles of carbon atoms is $a_1 = 1$ and the number of moles of oxygen atoms is $a_2 = 2$. The great advantage of this method is that the number of unknowns is limited to the number of

elements in the mixture not the number of molecular species. Use (9.111) and (9.113) to rewrite (9.127), (9.128) and (9.129) in the form of (9.115).

$$a_1/N = A_{11}B_1{y_1}^{A_{11}}{y_2}^{A_{12}} + A_{21}B_2{y_1}^{A_{21}}{y_2}^{A_{22}} + A_{31}B_3{y_1}^{A_{31}}{y_2}^{A_{32}} + A_{41}B_4{y_1}^{A_{41}}{y_2}^{A_{42}} + A_{51}B_5{y_1}^{A_{51}}{y_2}^{A_{52}} \tag{9.130}$$

$$a_2/N = A_{12}B_1{y_1}^{A_{11}}{y_2}^{A_{12}} + A_{22}B_2{y_1}^{A_{21}}{y_2}^{A_{22}} + A_{32}B_3{y_1}^{A_{31}}{y_2}^{A_{32}} + A_{42}B_4{y_1}^{A_{41}}{y_2}^{A_{42}} + A_{52}B_5{y_1}^{A_{51}}{y_2}^{A_{52}} \tag{9.131}$$

$$1 = B_1{y_1}^{A_{11}}{y_2}^{A_{12}} + B_2{y_1}^{A_{21}}{y_2}^{A_{22}} + B_3{y_1}^{A_{31}}{y_2}^{A_{32}} + B_4{y_1}^{A_{41}}{y_2}^{A_{42}} + B_5{y_1}^{A_{51}}{y_2}^{A_{52}} \tag{9.132}$$

According to (9.116) these equations can be rescaled as follows. Let

$$\begin{aligned} B_1 &= \tilde{B}_1{\alpha_1}^{A_{11}}{\alpha_2}^{A_{12}} \\ B_2 &= \tilde{B}_2{\alpha_1}^{A_{21}}{\alpha_2}^{A_{22}} \\ B_3 &= \tilde{B}_3{\alpha_1}^{A_{31}}{\alpha_2}^{A_{32}} \\ B_4 &= \tilde{B}_4{\alpha_1}^{A_{41}}{\alpha_2}^{A_{42}} \\ B_5 &= \tilde{B}_5{\alpha_1}^{A_{51}}{\alpha_2}^{A_{52}} \end{aligned} \tag{9.133}$$

and

$$\begin{aligned} y_1 &= \frac{\tilde{y}_1}{\alpha_1} \\ y_2 &= \frac{\tilde{y}_2}{\alpha_2}. \end{aligned} \tag{9.134}$$

If (9.133) and (9.134) are substituted into (9.130), (9.131) and (9.132) the resulting equations read exactly the same except in terms of tildaed variables. This invariance can be exploited to reduce the range of magnitudes of the coefficients in the equation if needed. Now

$$1 = N\left(B_1y_1 + B_2y_1y_2 + B_3y_1{y_2}^2\right) \tag{9.135}$$

$$2 = N\left(B_2y_1y_2 + 2B_3y_1{y_2}^2 + B_4y_2 + 2B_5{y_2}^2\right) \tag{9.136}$$

$$1 = B_1y_1 + B_2y_1y_2 + B_3y_1{y_2}^2 + B_4y_2 + B_5{y_2}^2 \tag{9.137}$$

where the coefficients are

$$\begin{aligned} B_1 &= e^{-\frac{g_C^\circ}{R_u T}} \\ B_2 &= e^{-\frac{g_{CO}^\circ}{R_u T}} \\ B_3 &= e^{-\frac{g_{CO_2}^\circ}{R_u T}} \\ B_4 &= e^{-\frac{g_O^\circ}{R_u T}} \\ B_5 &= e^{-\frac{g_{O_2}^\circ}{R_u T}}. \end{aligned} \tag{9.138}$$

At this point we need to use tabulated thermodynamic data to evaluate the coefficients. The Gibbs free energy of the ith molecular species is

$$g_i^\circ(T) = \Delta h_{fi}^\circ(T_{ref}) + \{h_i^\circ(T) - h_i^\circ(T_{ref})\} - T s_i^\circ(T). \tag{9.139}$$

Data for each species is as follows (See appendix 2). In the same order as (9.126)

$$\begin{aligned} &g_C^\circ(2975.34) = 715.004 + 56.208 - 2975.34\,(0.206054) = 158.131\,kJ/mole \\ &g_{CO}^\circ(2975.34) = -110.541 + 92.705 - 2975.34\,(0.273228) = -830.782\,kJ/mole \\ &g_{CO_2}^\circ(2975.34) = -393.522 + 151.465 - 2975.34\,(0.333615) = -1234.68\,kJ/mole \\ &g_O^\circ(2975.34) = 249.195 + 56.1033 - 2975.34\,(0.209443) = -317.866\,kJ/mole \\ &g_{O_2}^\circ(2975.34) = 0.00 + 97.1985 - 2975.34\,(0.284098) = -748.09\,kJ/mole. \end{aligned} \tag{9.140}$$

The universal gas constant in appropriate units is

$$R_u = 8.314472 \times 10^{-3}\,kJ/mole - K \tag{9.141}$$

and $R_uT = 24.7384\,kJ/mole$. Now the coefficients are

$$\begin{aligned}
B_1 &= Exp\left(-\frac{g^\circ_C}{R_uT}\right) = Exp\left(-\frac{158.131}{24.7382}\right) = 1.67346\times10^{-3}\\
B_2 &= Exp\left(-\frac{g^\circ_{CO}}{R_uT}\right) = Exp\left(\frac{830.782}{24.7382}\right) = 3.84498\times10^{14}\\
B_3 &= Exp\left(-\frac{g^\circ_{CO_2}}{R_uT}\right) = Exp\left(\frac{1234.68}{24.7382}\right) = 4.73778\times10^{21}\\
B_4 &= Exp\left(-\frac{g^\circ_{O}}{R_uT}\right) = Exp\left(\frac{317.866}{24.7382}\right) = 3.80483\times10^{5}\\
B_5 &= Exp\left(-\frac{g^\circ_{O_2}}{R_uT}\right) = Exp\left(\frac{748.090}{24.7382}\right) = 1.35889\times10^{13}.
\end{aligned} \tag{9.142}$$

Notice the ill conditioned nature of this problem. The constants in (9.142) vary over many orders of magnitude requiring high accuracy and very careful numerical analysis. The scaling (9.133) is

$$\begin{aligned}
B_1 &= \tilde{B}_1\alpha_1\\
B_2 &= \tilde{B}_2\alpha_1\alpha_2\\
B_3 &= \tilde{B}_3\alpha_1{\alpha_2}^2\\
B_4 &= \tilde{B}_4\alpha_2\\
B_5 &= \tilde{B}_5{\alpha_2}^2.
\end{aligned} \tag{9.143}$$

Choose $\alpha_2 = \sqrt{1.35889\times10^{13}}$ so that $\tilde{B}_5 = 1$ and $\alpha_1 = 1.67346\times10^{-3}$ so that $\tilde{B}_1 = 1$. The scaled coefficients are

$$\begin{aligned}
\tilde{B}_1 &= B_1/\alpha_1 = 1.67346\times10^{-3}/1.67346\times10^{-3} = 1\\
\tilde{B}_2 &= B_2/\alpha_1\alpha_2 = 3.84498\times10^{14}/\left(1.67346\times10^{-3}\sqrt{1.35889\times10^{13}}\right) = 6.23285\times10^{10}\\
\tilde{B}_3 &= B_3/\alpha_1{\alpha_2}^2 = 4.73778\times10^{21}/\left(1.67346\times10^{-3}\left(1.35889\times10^{13}\right)\right) = 2.08341\times10^{11}\\
\tilde{B}_4 &= B_4/\alpha_2 = 3.80483\times10^{5}/\sqrt{1.35889\times10^{13}} = 0.103215\\
\tilde{B}_5 &= B_5/{\alpha_2}^2 = 1.35889\times10^{13}/1.35889\times10^{13} = 1.
\end{aligned} \tag{9.144}$$

Using this procedure we have reduced the range of the coefficients from 24 down to 11 orders of magnitude, a very significant reduction. The equations we need to solve are as follows.

$$1 = N\left(\tilde{B}_1\tilde{y}_1 + \tilde{B}_2\tilde{y}_1\tilde{y}_2 + \tilde{B}_3\tilde{y}_1\tilde{y}_2^2\right) \tag{9.145}$$

$$2 = N\left(\tilde{B}_2\tilde{y}_1\tilde{y}_2 + 2\tilde{B}_3\tilde{y}_1\tilde{y}_2^2 + \tilde{B}_4\tilde{y}_2 + 2\tilde{B}_5\tilde{y}_2^2\right) \tag{9.146}$$

$$1 = \tilde{B}_1\tilde{y}_1 + \tilde{B}_2\tilde{y}_1\tilde{y}_2 + \tilde{B}_3\tilde{y}_1\tilde{y}_2^2 + \tilde{B}_4\tilde{y}_2 + \tilde{B}_5\tilde{y}_2^2 \tag{9.147}$$

I used Mathematica to solve the system, (9.145), (9.146), and (9.147). The result is

$$\begin{aligned} \tilde{y}_1 &= 1.42474 \times 10^{-11} \\ \tilde{y}_2 &= 0.392402 \\ n &= 1.24144 \end{aligned} \tag{9.148}$$

At the mixture temperature $T = 2975.34\,K$, the mole fractions of the various species are

$$\begin{aligned} x_C &= \tilde{B}_1\tilde{y}_1 = 1.42474 \times 10^{-11} \\ x_{CO} &= \tilde{B}_2\tilde{y}_1\tilde{y}_2 = 6.23285 \times 10^{10} \times 1.42474 \times 10^{-11} \times 0.392402 = 0.34846 \\ x_{CO_2} &= \tilde{B}_3\tilde{y}_1\tilde{y}_2^2 = 2.08341 \times 10^{11} \times 1.42474 \times 10^{-11} \times 0.392402^2 = 0.45706 \\ x_O &= \tilde{B}_4\tilde{y}_2 = 0.103215 \times 0.392402 = 0.0405018 \\ x_{O_2} &= \tilde{B}_5\tilde{y}_2^2 = 0.392402^2 = 0.153979. \end{aligned} \tag{9.149}$$

Note that there is almost no free carbon at this temperature. We could have dropped C from the mixture (9.126) and still gotten practically the same result.

9.10.1 CO Combustion at $2975.34K$ using Gibbs free energy of formation.

The Gibbs free energies of formation of the various species are

$$\begin{aligned} \Delta g_C^\circ\,(2975.34) &= 250.012\,kJ/mole \\ \Delta g_{CO}^\circ\,(2975.34) &= -365.761\,kJ/mole \\ \Delta g_{CO_2}^\circ\,(2975.34) &= -395.141\,kJ/mole \\ \Delta g_O^\circ\,(2975.34) &= 55.8281\,kJ/mole \\ \Delta g_{O_2}^\circ\,(2975.34) &= 0.0\,kJ/mole. \end{aligned} \tag{9.150}$$

These values can be found in the JANAF tables in Appendix 2. Using the Gibbs free energies of formation, the coefficients of the element potential equations are

$$\begin{aligned}
B_1 &= Exp\left[-\frac{\Delta g_C^\circ\,(2975.34)}{R_u T}\right] = Exp\left[-\frac{250.012}{24.7382}\right] = 4.0821\times 10^{-5}\\
B_2 &= Exp\left[-\frac{\Delta g_{CO}^\circ\,(2975.34)}{R_u T}\right] = Exp\left[\frac{365.761}{24.7382}\right] = 2.63731\times 10^{6}\\
B_3 &= Exp\left[-\frac{\Delta g_{CO_2}^\circ\,(2975.34)}{R_u T}\right] = Exp\left[\frac{395.141}{24.7382}\right] = 8.6486\times 10^{6}\\
B_4 &= Exp\left[-\frac{\Delta g_{O}^\circ\,(2975.34)}{R_u T}\right] = Exp\left[-\frac{55.8281}{24.7382}\right] = 0.104689\\
B_5 &= Exp\left[-\frac{\Delta g_{O_2}^\circ\,(2975.34)}{R_u T}\right] = Exp\left[-\frac{0.0}{24.7382}\right] = 1.00.
\end{aligned} \tag{9.151}$$

The results using Mathematica to solve this system are

$$\begin{aligned}
y_1 &= 3.382049\times 10^{-7}\\
y_2 &= 0.3935536\\
n &= 1.24391
\end{aligned} \tag{9.152}$$

and the mole fractions are

$$\begin{aligned}
x_C &= B_1 y_1 = 1.380743\times 10^{-11}\\
x_{CO} &= B_2 y_1 y_2 = 0.3509709\\
x_{CO_2} &= B_3 y_1 {y_2}^2 = 0.4529426\\
x_O &= B_4 y_2 = 0.04120202\\
x_{O_2} &= B_5 {y_2}^2 = 0.15488445.
\end{aligned} \tag{9.153}$$

These results agree closely with the results in (9.149) and with calculations using CEA. Now transfer heat out of the gas mixture to bring the temperature back to $298.15\,K$ at one atmosphere. The standard Gibbs free energies of the species at this temperature are

$$\begin{aligned}
g_C^\circ\,(298.15) &= 669.54219\,kJ/mole\\
g_{CO}^\circ\,(298.15) &= -169.46747\,kJ/mole\\
g_{CO_2}^\circ\,(298.15) &= -457.25071\,kJ/mole\\
g_O^\circ\,(298.15) &= 201.15482\,kJ/mole\\
g_{O_2}^\circ\,(298.15) &= -61.16531\,kJ/mole
\end{aligned} \tag{9.154}$$

and $R_uT = 2.47897\,kJ/mole$. The coefficients are

$$\begin{aligned}
B_1 &= Exp\left(-\frac{g^\circ_C}{R_uT}\right) = Exp\left(-\frac{669.54219}{2.47897}\right) = 5.03442\times10^{-118}\\
B_2 &= Exp\left(-\frac{g^\circ_{CO}}{R_uT}\right) = Exp\left(\frac{169.46747}{2.47897}\right) = 4.88930\times10^{29}\\
B_3 &= Exp\left(-\frac{g^\circ_{CO_2}}{R_uT}\right) = Exp\left(\frac{457.25071}{2.47897}\right) = 1.277622\times10^{80}\\
B_4 &= Exp\left(-\frac{g^\circ_{O}}{R_uT}\right) = Exp\left(-\frac{201.15482}{2.47897}\right) = 5.74645\times10^{-36}\\
B_5 &= Exp\left(-\frac{g^\circ_{O_2}}{R_uT}\right) = Exp\left(\frac{61.16531}{2.47897}\right) = 5.19563\times10^{10}.
\end{aligned} \tag{9.155}$$

At this relatively low temperature the coefficients range over 198 orders of magnitude! Despite this a good modern solver should be able to find the solution of (9.135), (9.136) and (9.137) for this difficult case even without the scaling used earlier. For example, Mathematica has a feature where the user can specify an arbitrary number of digits of precision for the calculation. The solution of (9.135), (9.136) and (9.137) at this temperature is

$$\begin{aligned}
y_1 &= 7.07098\times10^{-40}\\
\tilde{y}_2 &= 3.32704\times10^{-21}\\
n &= 1.0000.
\end{aligned} \tag{9.156}$$

The resulting mole fractions at $T = 298.15\,K$ are

$$\begin{aligned}
x_C &= B_1y_1 = 3.55983\times10^{-157}\\
x_{CO} &= B_2y_1y_2 = 1.15023\times10^{-30}\\
x_{CO_2} &= B_3y_1{y_2}^2 = 1.00000\\
x_O &= B_4y_2 = 1.91187\times10^{-56}\\
x_{O_2} &= B_5{y_2}^2 = 5.75116\times10^{-31}.
\end{aligned} \tag{9.157}$$

Only when the mixture is brought back to low temperature is the reaction model (9.125) valid. The enthalpy change for this last step is

$$h^\circ|_{mixture\,at\,298.15K} - h^\circ|_{mixture\,at\,2975.34K} = -8.94\times10^6 + 2.51\times10^6 = -6.43\times10^6\,J/kg. \tag{9.158}$$

This is the chemical energy released by the reaction (9.125) and is called the heat of reaction.

9.10.2 Adiabatic flame temperature

In the example in the previous section the products of combustion were evaluated at the adiabatic flame temperature. This can be defined at constant volume or constant pressure. For our purposes we will use the adiabatic flame temperature at constant pressure. Imagine the reactants brought together in a piston-cylinder combination permitting the volume to be adjusted to keep the pressure constant as the reaction proceeds. A source of ignition is used to start the reaction that evolves to the equilibrium state defined by the equilibrium species concentrations at the original pressure and at an elevated temperature called the adiabatic flame temperature. In the process the Gibbs function is minimized and since the process is adiabatic, the enthalpy before and after the reaction is the same.

The general enthalpy balance for a reaction is given in (9.67). Fully written out the balance is

$$\Delta h^{\circ}\left(T_{final}\right)=\sum_{i_{product}}^{I_{product}} n_{i_{product}}\left\{\Delta h^{\circ}_{fi_{product}}\left(298.15\right)+\left(h^{\circ}_{i_{product}}\left(T_{final}\right)-h^{\circ}_{i_{product}}\left(298.15\right)\right)\right\}- \sum_{i_{reactant}}^{I_{reactant}} n_{i_{reactant}}\left\{\Delta h^{\circ}_{fi_{reactant}}\left(298.15\right)+\left(h^{\circ}_{i_{reactant}}\left(T_{i_{reactant}}\right)-h^{\circ}_{i_{reactant}}\left(298.15\right)\right)\right\}. \tag{9.159}$$

If the reaction takes place adiabatically then $\Delta h^{\circ}\left(T_{final}\right)=0$ and

$$\sum_{i_{product}}^{I_{product}} n_{i_{product}}\left\{\Delta h^{\circ}_{fi_{product}}\left(298.15\right)+\left(h^{\circ}_{i_{product}}\left(T_{final}\right)-h^{\circ}_{i_{product}}\left(298.15\right)\right)\right\}= \sum_{i_{reactant}}^{I_{reactant}} n_{i_{reactant}}\left\{\Delta h^{\circ}_{fi_{reactant}}\left(298.15\right)+\left(h^{\circ}_{i_{reactant}}\left(T_{i_{reactant}}\right)-h^{\circ}_{i_{reactant}}\left(298.15\right)\right)\right\}. \tag{9.160}$$

Equation (9.160) can be solved along with (9.135), (9.136) and (9.137) to determine the final temperature of the mixture along with the mole fractions and total number of moles.

In the carbon monoxide combustion example of the previous section we would write

$$\begin{aligned}
&n_C\left\{\Delta h^\circ_{fC}\left(298.15\right)+\left(h^\circ_C\left(T_{final}\right)-h^\circ_C\left(298.15\right)\right)\right\}+\\
&n_{CO}\left\{\Delta h^\circ_{fCO}\left(298.15\right)+\left(h^\circ_{CO}\left(T_{final}\right)-h^\circ_{CO}\left(298.15\right)\right)\right\}+\\
&n_{CO_2}\left\{\Delta h^\circ_{fCO_2}\left(298.15\right)+\left(h^\circ_{CO_2}\left(T_{final}\right)-h^\circ_{CO_2}\left(298.15\right)\right)\right\}+\\
&n_O\left\{\Delta h^\circ_{fO}\left(298.15\right)+\left(h^\circ_O\left(T_{final}\right)-h^\circ_O\left(298.15\right)\right)\right\}+\\
&n_{O_2}\left\{\Delta h^\circ_{fO_2}\left(298.15\right)+\left(h^\circ_{O_2}\left(T_{final}\right)-h^\circ_{O_2}\left(298.15\right)\right)\right\}=\\
&n_{CO}\left\{\Delta h^\circ_{fCO}\left(298.15\right)\right\}+n_{O_2}\left\{\Delta h^\circ_{fO_2}\left(298.15\right)\right\}.
\end{aligned} \tag{9.161}$$

The enthalpy of the reactants is

$$\begin{aligned}
&n_{CO}\left\{\Delta h^\circ_{fCO}\left(298.15\right)\right\}+n_{O_2}\left\{\Delta h^\circ_{fO_2}\left(298.15\right)\right\}=\\
&1.0\,kgmole\left\{-110.527\times10^3\,kJ/kgmole\right\}+0.5\,kgmole\left\{0\,kJ/kgmole\right\}=\\
&-110.527\times10^3\,kJ.
\end{aligned} \tag{9.162}$$

On a per unit mass basis the enthalpy of the reactant mixture is

$$\frac{-110.527\times10^6\,J}{1\times28.014+0.5\times31.98}=-2.5117\times10^6\,J/kg. \tag{9.163}$$

The enthalpy per unit mass of the product mixture at various temperatures is plotted in Figure 9.7.

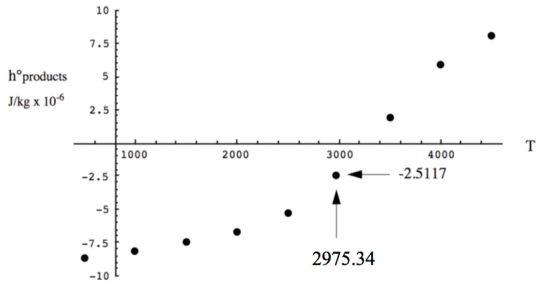

Figure 9.7: *Enthalpy of the product mixture as a function of temperature.*

As the products of combustion are cooled from 4000 K the enthalpy decreases monitonically. The only temperature where the enthalpy of the product mixture matches that of the original reactants is the adiabatic flame temperature, 2975.34 K.

9.10.3 Isentropic expansion

Now consider an isentropic expansion from a known initial state, $(T_{initial}, P_{initial})$ to a final state (T_{final}, P_{final}) with the final pressure known. The condition that determines the temperature of the final state is

$$S(T_{final}, P_{final}, n_{1_{final}}, n_{2_{final}}, n_{3_{final}}, ..., n_{I_{final}}) = S(T_{initial}, P_{initial}, n_{1_{initial}}, n_{2_{initial}}, n_{3_{initial}}, ..., n_{I_{initial}}) \tag{9.164}$$

or

$$\sum_{i=1}^{I} n_{i_{final}} s_i^{\circ}(T_{final}) - N_{final} R_u \sum_{i=1}^{I} x_{i_{final}} \ln\left(x_{i_{final}}\right) - N_{final} R_u \ln\left(\frac{P_{final}}{P^{\circ}}\right) = \sum_{i=1}^{I} n_{i_{initial}} s_i^{\circ}(T_{initial}) - N_{initial} R_u \sum_{i=1}^{I} x_{i_{initial}} \ln\left(x_{i_{initial}}\right) - N_{initial} R_u \ln\left(\frac{P_{initial}}{P^{\circ}}\right). \tag{9.165}$$

Equation (9.165) can be solved along with (9.135), (9.136) and (9.137) to determine the final temperature of the mixture after isentropic expansion along with the mole fractions and total number of moles.

For example, take the mixture from the previous section at the initial state, $T_{initial} = 2975.34\,K$ and $P_{initial} = 1\,bar$. The entropy of the system on a per unit mass basis is $8.7357 kJ/kg-K$ which is essentially equivalent to the extensive entropy. Now expand the mixture to $P_{final} = 0.1\,bar$. If we calculate the entropy of the system at this pressure and various temperatures, the result is the following plot.

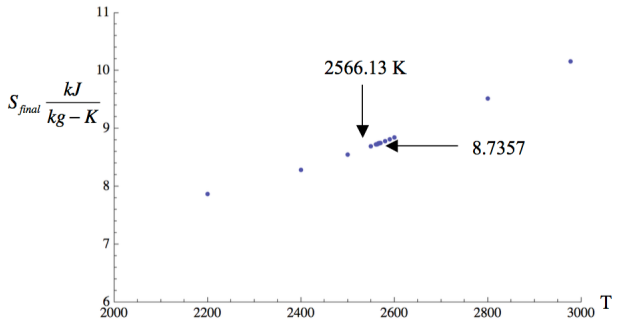

Figure 9.8: *Entropy of the product mixture as a function of temperature.*

The temperature at which the entropy of the final state is the same as the initial state is $T_{final} = 2566.13\,K$.

9.10.4 Nozzle expansion

If we interpret the expansion just described as an adiabatic, isentropic expansion in a nozzle we can use the conservation of stagnation enthalpy to determine the speed of the gas mixture at the end of the expansion.

$$H_{initial} = H_{final} + \frac{1}{2}U^2 \tag{9.166}$$

The initial enthalpy is taken to be the reservoir value. For this example the numbers are

$$U = \sqrt{2\left(H_{initial} - H_{final}\right)} = \sqrt{2\left(-2.51162 + 3.94733\right) \times 10^6\, J/kg} = 1694.53\, m/\sec\,. \tag{9.167}$$

Ordinarily we are given the geometric area ratio of the nozzle rather than the pressure ratio. Determining the exit velocity in this case is a little more involved. Here we need to carry out a series of calculations at constant entropy and varying final pressure. For each calculation we need to determine the density and velocity of the mixture and plot the product ρU as a function of the pressure ratio. Beginning with the mixture at the adiabatic flame temperature as the reservoir condition, the results are plotted below.

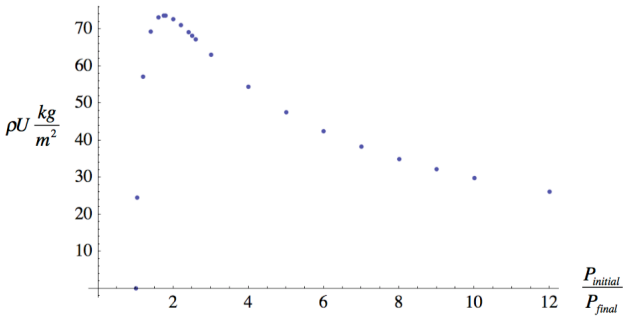

Figure 9.9: *Mass flux in a converging-diverging nozzle as a function of nozzle static pressure ratio.*

The maximum mass flux occurs at the nozzle throat. Equate the mass flow at the throat and the nozzle exit. For $P_{initial}/P_{final} = 10.0$ the nozzle area ratio is

$$\frac{A_e}{A_t} = \frac{\rho_t U_t}{\rho_e U_e} = \frac{73.6768}{29.8354} = 2.46944. \tag{9.168}$$

This completes the specification of the nozzle flow. The case we have considered here is called the shifting equilibrium case where the gas mixture is at equilibrium at every point in the nozzle. One can also consider the case of frozen flow where the composition of the gas mixture is held fixed at the reservoir condition.

9.10.5 Fuel-rich combustion, multiple phases

Suppose we choose a mixture of CO and O_2 that has an excess of CO. In this case the overall balance of carbon and oxygen can be satisfied in more than one way when the products of the reaction are brought back to low temperature. For example, if we mix 2 moles of CO with 0.5 moles of O_2 at a pressure of $10^5\ N/m^2$ we could end up with either of the following.

$$\begin{aligned} 2CO + \frac{1}{2}O_2 &\rightarrow CO_2 + CO \\ 2CO + \frac{1}{2}O_2 &\rightarrow \frac{3}{2}CO_2 + \frac{1}{2}C_{(gr)} \end{aligned} \tag{9.169}$$

Which balance actually occurs is of course determined by which one minimizes the Gibbs free energy at the given temperature. The set of species in the mixture is now

$$C, CO, CO_2, O, O_2, C_{(gr)} \tag{9.170}$$

where we have allowed for the possible condensation of solid carbon. The matrices of element coefficients A_{pij} for the two phases are shown in Figure 9.10.

The gas phase $p = 1$

	Atom	C	O
Molecule		$j = 1$	$j = 2$
C	$i = 1$	1	0
CO	$i = 2$	1	1
CO_2	$i = 3$	1	2
O	$i = 4$	0	1
O_2	$i = 5$	0	2

The solid phase $p = 2$

	Atom	C	O
Molecule		$j = 1$	$j = 2$
C	$i = 1$	1	0

Figure 9.10: *Matrix of element coefficients for the CO, O_2 system with condensed species (graphite).*

The governing equations (9.122) become the following.

$$2 = N_1 \left(B_{11} y_1 + B_{12} y_1 y_2 + B_{13} y_1 {y_2}^2 \right) + N_2 \left(B_{21} y_1 \right) \tag{9.171}$$

$$3 = N_1 \left(B_{12} y_1 y_2 + 2 B_{13} y_1 {y_2}^2 + B_{14} y_2 + 2 B_{15} {y_2}^2 \right) \tag{9.172}$$

$$1 = B_{11} y_1 + B_{12} y_1 y_2 + B_{13} y_1 {y_2}^2 + B_{14} y_2 + B_{15} {y_2}^2 \tag{9.173}$$

$$1 = B_{21} y_1 \tag{9.174}$$

$$N = N_1 + N_2 \tag{9.175}$$

The coefficients are

$$\begin{aligned} B_{11} &= e^{-\frac{g^\circ_C}{R_u T}} \\ B_{12} &= e^{-\frac{g^\circ_{CO}}{R_u T}} \\ B_{13} &= e^{-\frac{g^\circ_{CO_2}}{R_u T}} \\ B_{14} &= e^{-\frac{g^\circ_O}{R_u T}} \\ B_{15} &= e^{-\frac{g^\circ_{O_2}}{R_u T}} \end{aligned} \tag{9.176}$$

and

$$B_{21} = e^{-\frac{g^\circ_{C_{(gr)}}}{R_u T}}. \tag{9.177}$$

As an example, let's solve for the various mole fractions at a mixture temperature of $940\,K$. From tables, the standard Gibbs free energies at this temperature are

$$\begin{aligned} g^\circ_C\,(940) &= 558.95895\,kJ/mole \\ g^\circ_{CO}\,(940) &= -309.37696\,kJ/mole \\ g^\circ_{CO_2}\,(940) &= -613.34861\,kJ/mole \\ g^\circ_O\,(940) &= 88.41203\,kJ/mole \\ g^\circ_{O_2}\,(940) &= -206.32876\,kJ/mole \\ g^\circ_{C_{(gr)}}\,(940) &= -11.22955\,kJ/mole. \end{aligned} \tag{9.178}$$

The number of moles of each species in the mixture at $T = 940\,K$ are

$$\begin{aligned} n_C &= N_1 B_{11} y_1 = 4.11775 \times 10^{-32} \\ n_{CO} &= N_1 B_{12} y_1 y_2 = 0.977065 \\ n_{CO_2} &= N_1 B_{13} y_1 {y_2}^2 = 1.011467 \\ n_O &= N_1 B_{14} y_2 = 3.23469 \times 10^{-22} \\ n_{O_2} &= N_1 B_{15} {y_2}^2 = 1.027845 \times 10^{-22} \\ n_{C_{(gr)}} &= N_2 B_{21} y_1 = 0.011467. \end{aligned} \tag{9.179}$$

At this temperature, the mixture is predominately CO and CO_2 with some $C_{(gr)}$. Figure 9.11 shows the mole fraction of CO and $C_{(gr)}$ at a pressure of $10^5 N/m^2$ based on the total number of moles in the mixture for a variety of mixture temperatures.

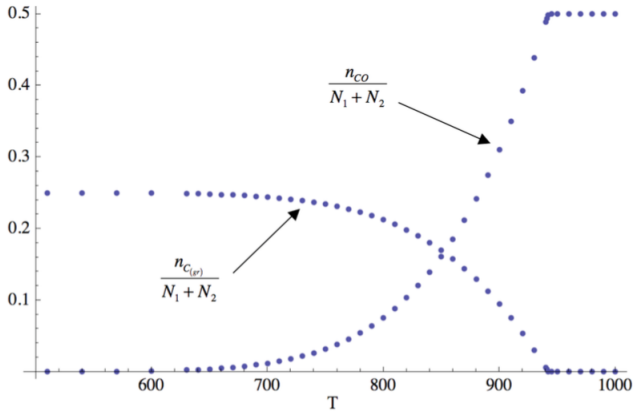

Figure 9.11: *Condensation of graphite in the CO, O_2 system.*

The excess CO begins to react and solid carbon begins to condense out at about $T = 942.2\,K$. Below $600\,K$ there is virtually no CO in the mixture.

9.11 Rocket performance using CEA

The equilibrium combustion package CEA (Chemical Equilibrium with Applications) from NASA Glenn can also be used to perform equilibrium chemistry calculations and has a capability similar to STANJAN but with a much wider range of chemicals with data based on the current standard pressure. Some typical performance parameters for several propellant combinations at two chamber pressures are shown in Figure 9.12. The propellants are taken to be at an equivalence ratio of one (complete consumption of fuel and oxidizer) and so the exhaust velocity is not optimized. The numbers correspond to the effective

exhaust velocity for the given chamber pressure and area ratio assuming vacuum ambient pressure. The maximum effective exhaust velocity generally occurs with a somewhat fuel rich mixture that produces more low molecular weight species in the exhaust stream.

Propellants	$P_{chamber}$ *bar*	$T_{chamber}$ *K*	C^* *M/Sec*	$C_e\|_{A_e/A_t = 100}$ *M/Sec*	$C_e\|_{A_e/A_t \to \infty}$ *M/Sec*
$H_2 + \frac{1}{2}O_2$	50	3626	2186	4541	5285
	100	3730	2203	4562	5287
$N_2H_4 + \frac{1}{2}N_2O_4$	50	3379	1818	3637	4030
	100	3451	1829	3643	4032
$(1.0)RP-1 + (3.4)O_2$ *by mass*	50	3676	1733	3631	4467
	100	3787	1749	3654	4469
$(0.1)Al + (0.835)NH_4ClO_4$ $+ (0.065)C_6H_6$ *by mass*	50	3434	1511	3160	3726
	100	3514	1520	3171	3728

Figure 9.12: *Some typical performance parameters for several propellant combinations at two chamber pressures.*

9.12 Problems

Problem 1 - A nuclear reactor is used to heat hydrogen gas in a rocket chamber to a temperature of $4000\,K$. The pressure in the chamber is $100\,atm$. At these conditions a significant fraction of the H_2 is dissociated to form atomic H. What are the mole fractions of H, H_2 in the mixture? Relevant thermochemical data is provided in Figure 9.13 . The reference temperature is $298.15\,K$.

species	molal mass gms/mole	$\Delta H^\circ_{fi}(T_{ref})$ *kJ/mole*	$h^\circ_i(4000) - h^\circ_i(T_{ref})$ *kJ/mole*	$s^\circ_i(4000)$ *J/mole-K*
H_2	2.016	0.00	126.874	213.848
H	1.00797	217.999	76.947	168.686

Figure 9.13: *Hydrogen dissociation at* $4000\,K$.

Work the problem by hand and compare with CEA.

Problem 2 - Hydrogen gas heated to $4000\,K$ is fed at a mass flow rate of $200\,kg/sec$ into

a rocket chamber with a throat area of $0.2\,m^2$. The gas is exhausted adiabatically and isentropically through a nozzle with an area ratio of 40. Determine the exhaust velocity for the following cases.

i) Expansion of undissociated H_2.

ii) Frozen flow expansion of dissociated H_2 at the rocket chamber composition of H and H_2.

(III) Shifting equilibrium expansion.

Problem 3 - An exotic concept for chemical rocket propulsion is to try to harness the energy released when two atoms of hydrogen combine to form H_2. The idea is to store the hydrogen atoms in solid helium at extremely low temperatures. Suppose a space engine is designed with a very large area ratio nozzle. Let a 50-50 mixture by mass of atomic hydrogen and helium be introduced into the combustion chamber at low temperature. The propellant vaporizes and the hydrogen atoms react releasing heat. The gas exhausts through the nozzle to the vacuum of space. Estimate the exhaust velocity of this rocket.

Problem 4 - I would like you to consider the Space Shuttle Main Engine (SSME). Use the thermochemical calculator CEA or an equivalent application to help solve the problem. The specifications of the SSME are

$$\begin{aligned} P_{t2} &= 3000\,psia \\ T_{t2} &= 3250\,K \\ A_e/A_t &= 77.5 \end{aligned} \tag{9.180}$$

and

$$\begin{aligned} \dot{m}_{H_2} &= 69\,kg/\sec \\ \dot{m}_{O_2} &= 400\,kg/\sec\,. \end{aligned} \tag{9.181}$$

i) Determine the adiabatic flame temperature and equilibrium mass fractions of the system $(H, H_2, HO, H_2O, O, O_2)$ at the given chamber pressure.

ii) You will find that the temperature in (1) is higher than the specified chamber temperature. Bring your mixture to the specified chamber pressure and temperature (in effect accounting for some heat loss from the engine).

Determine the exhaust velocity and sea level thrust assuming that the mixture remains at equilibrium during the expansion process. Suppose the mass flow rates are changed to the

stoichiometric ratio

$$\begin{aligned} \dot{m}_{H_2} &= 52.5\, kg/\sec \\ \dot{m}_{O_2} &= 416.5\, kg/\sec. \end{aligned} \tag{9.182}$$

How much does the exhaust velocity change?

Problem 5 - A monopropellant thruster for space applications uses nitrous oxide N_2O at a low initial temperature as a monopropellant. The gas is passed through a catalyst bed where it is decomposed releasing heat. The hot gas is expelled through a large area ratio nozzle to the vacuum of space. The exhaust gas is composed of O_2 and N_2. The enthalpy of formation of N_2O at the initial temperature is $1.86 \times 10^6\, J/kg$. Estimate the exhaust velocity of this rocket.

Problem 6 - Element number three in the periodic table is Lithium which is a soft, silvery white, highly reactive metal at room temperature. Because of its low atomic weight it has been considered as a propellant for propulsion applications. Above $1615\, K$ it is a monatomic gas. At high temperatures and pressures the diatomic gas begins to form. At the super extreme conditions of $7000\, K$ and $10^5\, bar$ almost 92% of the mixture is Li_2 and only 8% is Li. By the way, at these conditions the density of the mixture is $2.3 \times 10^4\, kg/m^3$, greater than Uranium. Perhaps this is the di-Lithium crystal propellant that, according to Gene Roddenberry, will in the future power generations of starships. Suppose this mixture at an enthalpy $h_{initial} = 38.4 \times 10^6\, J/kg$ expands isentropically from a rocket chamber to a nozzle exit where the enthalpy is $h_{final} = 9.3 \times 10^6\, J/kg$. What is the nozzle exit velocity? What is the composition of the mixture at the nozzle exit?

Problem 7 - One mole per second of methane CH_4 reacts with 2 moles per second of O_2 in a rocket chamber. The reaction produces products at $3000\, K$ and $100\, bar$. Assume the mixture contains $(CO, CO_2, H, H_2, H_2O, O, OH, O_2)$. Set up the system of equations (9.115) for this problem. Use data from Appendix 2 to evaluate the coefficients in these equations and solve for the mole fractions. Compare your results with CEA. The gas exhausts isentropically to the vacuum of space through a nozzle with an area ratio of 80. Determine the thrust.

Problem 8 - Ozone (O_3) releases energy when it decomposes and can be used as a monopropellant for a space thruster. Let ozone be decomposed across a manganese oxide catalyst bed and introduced into a thrust chamber. The pressure and temperature in the chamber are $10^5\, N/m^2$ and $2688\, K$. At these conditions the mixture is composed of only two constituents, O_2 and O. Relevant thermo-chemical data is given in Figure 9.14.

In the units used in this table the ideal gas constant is $R_u = 0.00831451\, kJ/\,(mole - K)$.

a) Determine the mole fractions of O_2 and O in the mixture.

Species	Molar mass (grams/mole	$\Delta h_f^\circ(298.15)$ kJ/mole	$h^\circ(2688)-h^\circ(298.15)$ kJ/mole	$s^\circ(2688)$ kJ/(mole-K)
O_2	31.9988	0.0	85.7423	0.28017
O	15.9994	249.175	50.0515	0.20741

Figure 9.14: *Ozone decomposition at* $2688\,K$.

b) Determine the total number of moles in the mixture.

c) Determine the enthalpy per unit mass of the mixture.

d) If the gas is exhausted to the vacuum of space what is the maximum gas speed that could be reached.

Chapter 10

Solid Rockets

10.1 Introduction

Figure 10.1 shows a section view of a typical solid propellant rocket.

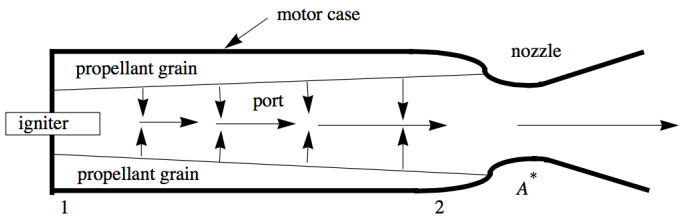

Figure 10.1: *Solid rocket cross-section.*

There are basically two types of propellant grains.

1) Homogeneous or double base propellants - Here fuel and oxidizer are contained within the same molecule which decomposes during combustion. Typical examples are Nitroglycerine and Nitrocellulose.

2) Composite propellants - heterogeneous mixtures of oxidizing crystals in an organic plastic- like fuel binder typically synthetic rubber.

Sometimes metal powders such as Aluminum are added to the propellant to increase the energy of the combustion process as well as fuel density. Typically these may be 12 to 22 % of propellant mass although in the space shuttle booster Aluminum is the primary fuel.

10.2 Combustion chamber pressure

The combustion proceeds from the surface of the propellant grain. The rate at which combustion gases are generated is expressed in terms of the regression speed of the grain as indicated in Figure 10.2.

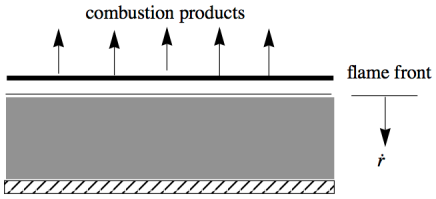

Figure 10.2: *Surface regression and gas generation.*

The gas generation rate integrated over the port surface area is

$$\dot{m}_g = \rho_p A_b \dot{r} \tag{10.1}$$

where

$$\begin{aligned} &\rho_p = solid\ propellant\ density \\ &A_b = area\ of\ the\ burning\ surface \\ &\dot{r} = surface\ regression\ speed \\ &\dot{m}_g = rate\ of\ gas\ generation\ at\ the\ propellant\ surface. \end{aligned} \tag{10.2}$$

The phase transition and combustion physics underlying the surface regression speed is extremely complex. In general $\dot{r}$ depends on the propellant initial temperature and the chamber pressure.

$$\dot{r} = \frac{K}{T_1 - T_p}(P_{t2})^n \tag{10.3}$$

The variables in (10.3) are as follows.

$$\begin{aligned} &P_{t2} = combustion\ chamber\ pressure \\ &K = impirical\ constant\ for\ a\ given\ propellant \\ &T_1 = impirical\ detonation\ temperature \\ &T_p = propellant\ temperature \\ &n = impirical\ exponent,\ approximately\ independent\ of\ temperature \end{aligned} \tag{10.4}$$

In general $0.4 < n < 0.7$ and T_1 is considerably larger than T_p by several hundred degrees.

Let M_g be the mass of gas in the combustion chamber at a given instant, ρ_g is the gas density and V is the chamber volume.

$$\frac{dM_g}{dt} = \frac{d}{dt}\left(\rho_g V\right) = \rho_g \frac{dV}{dt} + V\frac{d\rho_g}{dt} \tag{10.5}$$

The chamber volume changes as the propellant is converted from solid to gas.

$$\frac{dV}{dt} = \dot{r} A_b \tag{10.6}$$

To a good approximation, the chamber stagnation temperature, T_{t2}, is determined by the propellant energy density and tends to be independent of P_{t2}. From the ideal gas law, $P_{t2} = \rho_g R T_{t2}$ and

$$\frac{d\rho_g}{dt} = \frac{1}{RT_{t2}}\frac{dP_{t2}}{dt}. \tag{10.7}$$

The mass flow out of the nozzle is

$$\dot{m}_n = \frac{\gamma}{\left(\frac{\gamma+1}{2}\right)^{\frac{\gamma+1}{2(\gamma-1)}}} \frac{P_{t2}A^*}{\sqrt{\gamma R T_{t2}}}. \tag{10.8}$$

The mass generated at the propellant surface is divided between the mass flow exiting the nozzle and the time dependent mass accumulation in the combustion chamber volume.

$$\dot{m}_g = \frac{dM_g}{dt} + \dot{m}_n \tag{10.9}$$

Fill in the various terms in (10.9)

$$\rho_p \dot{r} A_b = \rho_g \dot{r} A_b + V\frac{d\rho_g}{dt} + \frac{\gamma}{\left(\frac{\gamma+1}{2}\right)^{\frac{\gamma+1}{2(\gamma-1)}}} \frac{P_{t2}A^*}{\sqrt{\gamma R T_{t2}}} \tag{10.10}$$

or

$$\frac{K\left(\rho_p-\rho_g\right)A_b}{T_1-T_p}(P_{t2})^n=\frac{V}{RT_{t2}}\frac{dP_{t2}}{dt}+\frac{\gamma}{\left(\frac{\gamma+1}{2}\right)^{\frac{\gamma+1}{2(\gamma-1)}}}\frac{P_{t2}A^*}{\sqrt{\gamma RT_{t2}}}. \tag{10.11}$$

Rearrange (10.11) to read

$$\frac{V}{RT_{t2}}\frac{dP_{t2}}{dt}+\frac{\gamma}{\left(\frac{\gamma+1}{2}\right)^{\frac{\gamma+1}{2(\gamma-1)}}}\frac{P_{t2}A^*}{\sqrt{\gamma RT_{t2}}}-\frac{K\left(\rho_p-\rho_g\right)A_b}{T_1-T_p}(P_{t2})^n=0. \tag{10.12}$$

After a startup transient, during which P_{t2} changes rapidly with time, the pressure reaches a quasi-steady state where the time derivative term in (10.12) can be regarded as small compared to the other terms. To a good approximation

$$\frac{\gamma}{\left(\frac{\gamma+1}{2}\right)^{\frac{\gamma+1}{2(\gamma-1)}}}\frac{P_{t2}A^*}{\sqrt{\gamma RT_{t2}}}=\frac{K\left(\rho_p-\rho_g\right)A_b}{T_1-T_p}(P_{t2})^n. \tag{10.13}$$

Solve for the chamber pressure

$$P_{t2}=\left(\left(\frac{\gamma+1}{2}\right)^{\frac{\gamma+1}{2(\gamma-1)}}\frac{K\left(\rho_p-\rho_g\right)}{\gamma\left(T_1-T_p\right)}\left(\frac{A_b}{A^*}\right)\sqrt{\gamma RT_{t2}}\right)^{\frac{1}{1-n}}. \tag{10.14}$$

This formula can be used as long as $A_b(t)$ is a slow function of time. All the quantities in (10.14) are apriori data with the exception of T_{t2} which must be estimated or calculated from a propellant chemistry model. Note that there is a tendency for the chamber pressure to increase as the burning area increases.

10.3 Dynamic analysis

Rearrange (10.12) to read

$$\frac{dP_{t2}}{dt}+\left(\frac{(\gamma RT_{t2})^{1/2}}{\left(\frac{\gamma+1}{2}\right)^{\frac{\gamma+1}{2(\gamma-1)}}}\left(\frac{A^*}{V}\right)\right)P_{t2}-\left(\frac{K\left(\rho_p-\rho_g\right)A_b}{T_1-T_p}\left(\frac{RT_{t2}}{V}\right)\right)(P_{t2})^n=0. \tag{10.15}$$

This is a nonlinear first order ordinary differential equation for the chamber pressure of the form

$$\frac{dP_{t2}}{dt} + \left(\frac{1}{\tau}\right) P_{t2} - \beta (P_{t2})^n = 0 \tag{10.16}$$

where the characteristic time is

$$\tau = \frac{\left(\frac{\gamma+1}{2}\right)^{\frac{\gamma+1}{2(\gamma-1)}}}{(\gamma R T_{t2})^{1/2}} \left(\frac{V}{A^*}\right). \tag{10.17}$$

This time is proportional to the time required for an acoustic wave to travel the length of the combustion chamber multiplied by the internal area ratio of the nozzle. The system has the character of a Helmholtz resonator and the inverse of (10.17) is the natural "Coke bottle" frequency of the rocket motor.

The constant in the nonlinear term is

$$\beta = \left(\frac{K\left(\rho_p - \rho_g\right) A_b}{T_1 - T_p} \left(\frac{R T_{t2}}{V}\right)\right). \tag{10.18}$$

Let's look at the linearized behavior of (10.16) near a steady state operating point. Let

$$P_{t2}(t) = \overline{P_{t2}} + p_{t2}(t) \tag{10.19}$$

where p_{t2} is a small deviation in the pressure from the steady state. Substitute into (10.16) and expand the nonlinear term in a binomial series. With higher order terms in the series neglected, the result is

$$\frac{dp_{t2}}{dt} + \left(\frac{1}{\tau}\right) \overline{P_{t2}} + \left(\frac{1}{\tau}\right) p_{t2} - \beta \left(\overline{P_{t2}}\right)^n - \beta n \left(\overline{P_{t2}}\right)^{n-1} p_{t2} = 0. \tag{10.20}$$

The steady state terms satisfy

$$\left(\frac{1}{\tau}\right) \overline{P_{t2}} - \beta \left(\overline{P_{t2}}\right)^n = 0 \tag{10.21}$$

and the dynamical equation becomes

$$\frac{dp_{t2}}{dt} + \left(\frac{1}{\tau} - \beta n\left(\overline{P_{t2}}\right)^{n-1}\right) p_{t2} = 0. \tag{10.22}$$

Note that from (10.21)

$$\frac{1}{\tau} = \beta n\left(\overline{P_{t2}}\right)^{n-1} \tag{10.23}$$

and so

$$\frac{dp_{t2}}{dt} + \left(\frac{1-n}{\tau}\right) p_{t2} = 0. \tag{10.24}$$

The solution of (10.24) is

$$\frac{p_{t2}}{p_{t2}\left(0\right)} = e^{-\left(\frac{1-n}{\tau}\right)t}. \tag{10.25}$$

If $n < 1$ a small deviation in pressure will be restored to the equilibrium value (the extra nozzle flow exceeds the extra gas generation from the propellant surface). But if $n > 1$ the gas generation rate exceeds the nozzle exhaust mass flow and the chamber pressure will increase exponentially; The vehicle will explode!

If the fluid velocity over the surface becomes very large, enhanced heat transfer can lead to a situation called erosive burning. In this case the burning rate can vary considerably along the port and excessive gas generation can lead to a failure.

In the case of very low chamber pressure, the combustion process can become unsteady or cease altogether this defines the combustion limit of a particular propellant. There is also an upper pressure limit above which combustion again becomes erratic or unpredictable. For most propellants this is above $5000\,psi$.

10.3.1 Exact solution

The chamber pressure is governed by the equation

$$\frac{dP_{t2}}{dt} + \left(\frac{1}{\tau}\right) P_{t2} - \beta(P_{t2})^n = 0. \tag{10.26}$$

Let's determine the exact integral of this equation and compare the behavior of the system with the linearized solution for both $n < 1$ and $n > 1$. It is virtually always best to work in terms of dimensionless variables. The steady state solution of (10.26) for which the time derivative term is zero is

$$\overline{P_{t2}} = (\tau\beta)^{\frac{1}{1-n}}. \tag{10.27}$$

Let

$$\begin{aligned} H &= \frac{P_{t2}}{\overline{P_{t2}}} \\ \eta &= \frac{t - t_0}{\tau}. \end{aligned} \tag{10.28}$$

In terms of new variables (10.26) becomes

$$\frac{dH}{d\eta} = H^n - H. \tag{10.29}$$

Equation (10.29) is rearranged as

$$\frac{dH}{H^n - H} = d\eta \tag{10.30}$$

which integrates to

$$\frac{1 - H^{1-n}}{1 - {H_0}^{1-n}} = e^{-(1-n)\eta} \tag{10.31}$$

where H_0 is the initial value of $P_{t2}/\overline{P_{t2}}$ and the initial value of η is taken to be zero. Now solve for H.

$$H = \left(1 - \left(1 - {H_0}^{1-n}\right) e^{-(1-n)\eta}\right)^{\frac{1}{1-n}} \tag{10.32}$$

Several cases are shown in Figure 10.3.

The exact solution is consistent with the linear analysis and shows that if $n > 1$ there is no actual steady state, the chamber pressure either decays to zero or blows up. If $n < 1$ then the chamber pressure will return to the steady state value even in the face

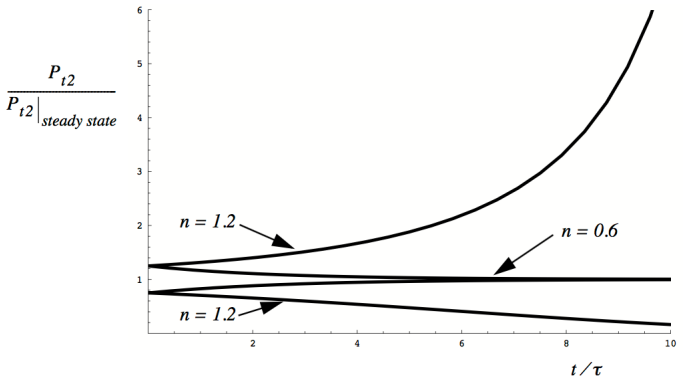

Figure 10.3: *Chamber pressure response of a solid rocket.*

of a large deviation away from steady state. The motor is stable in the face of finite disturbances.

10.3.2 Chamber pressure history

The analysis in the last section is useful for determining the behavior of the motor during transients such as start-up and shut down where the chamber pressure responds on a very short time scale measured by τ. As the burning area of a circular port increases over the course of the burn the chamber pressure changes on a much longer time scale and we can use the steady state balance (10.14) together with the regression rate law (10.3) to determine the port radius as a function of time. Rewrite (10.14) as

$$P_{t2} = \left(\alpha \left(\frac{r}{r_i}\right)\right)^{\frac{1}{1-n}} \tag{10.33}$$

where

$$\alpha = \left(\frac{\gamma+1}{2}\right)^{\frac{\gamma+1}{2(\gamma-1)}} \frac{K\left(\rho_p - \rho_g\right)}{\gamma\left(T_1 - T_p\right)} \sqrt{\gamma R T_{t2}} \left(\frac{2\pi r_i L}{A^*}\right) \tag{10.34}$$

and L is the length of the port assumed to be constant. Now solve

$$\frac{dr}{dt} = \frac{K}{T_1 - T_p} \left(\alpha \left(\frac{r}{r_i}\right)\right)^{\frac{n}{1-n}} \tag{10.35}$$

for the radius of the port as a function of time.

$$\frac{d\left(\frac{r}{r_i}\right)}{\left(\frac{r}{r_i}\right)^{\frac{n}{1-n}}} = \left(\frac{K}{(T_1 - T_p)\, r_i}(\alpha)^{\frac{n}{1-n}}\right) dt \tag{10.36}$$

Integrating (10.36) leads to

$$\begin{aligned} \frac{r}{r_i} &= \left(1 + \left(\frac{1-2n}{1-n}\right)\frac{K\alpha^{\left(\frac{n}{1-n}\right)}t}{(T_1 - T_p)\, r_i}\right)^{\frac{1-n}{1-2n}} \qquad \text{n} \neq 0.5 \\ \frac{r}{r_i} &= e^{\frac{K\alpha^{\left(\frac{n}{1-n}\right)}t}{(T_1 - T_p) r_i}} \qquad \text{n} = 0.5. \end{aligned} \tag{10.37}$$

This defines a much longer time scale

$$\tau_{burn} = \frac{(T_1 - T_p)\, r_i}{K\alpha^{\left(\frac{n}{1-n}\right)}} \tag{10.38}$$

This time scale characterizes the change in chamber pressure during the burn. The burn time is determined by the outer radius of the motor.

$$\begin{aligned} t_{burnout} &= \left(\left(\frac{r_f}{r_i}\right)^{\frac{1-2n}{1-n}} - 1\right)\left(\frac{1-n}{1-2n}\right)\tau_{burn} \qquad \text{n} \neq 0.5 \\ t_{burnout} &= Ln\left(\frac{r_f}{r_i}\right)\tau_{burn} \qquad \text{n} = 0.5 \end{aligned} \tag{10.39}$$

10.4 Problems

Problem 1 - It is a beautiful summer day at the Cape and a space shuttle astronaut on her second mission finds that the g forces during launch are noticeably larger than during her first mission that previous December. Can you offer a plausible explanation for this?

Problem 2 - A solid propellant rocket operates in a vacuum with a 10 cm diameter nozzle throat and a nozzle area ratio of 100. The motor has a cylindrical port 300 cm long. At the beginning of the burn the port is 20 cm in diameter and the propellant recession velocity

is $1\,cm/sec$. The port diameter at the end of the burn is $80\,cm$. The regression rate law is

$$\dot{r} = a{P_{t2}}^{0.5}. \tag{10.40}$$

The solid propellant density is $2\,grams/cm^3$ and the combustion gas has $\gamma = 1.2$ and molecular weight equal to 20. The combustion chamber temperature is $2500\,K$. Determine the thrust versus time history of the motor.

Problem 3 - One of the simplest types of solid rocket designs utilizes an end burning propellant grain as shown in Figure 10.4.

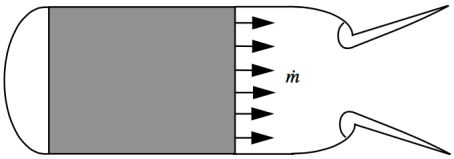

Figure 10.4: *Solid rocket with end burning grain.*

The motor diameter is $100\,cm$ and the grain length at the beginning of the burn is $200\,cm$. The solid propellant density is $2\,grams/cm^3$. The combustion gas has $\gamma = 1.2$ and molecular weight equal to 20. The combustion chamber temperature is $2500\,K$ and, at the beginning of the burn, the pressure is $P_{t2} = 5 \times 10^5\,N/m^2$. The motor exhausts to vacuum through a $30\,cm$ diameter nozzle throat and a nozzle area ratio of 10. Sketch the thrust-time history of the motor and determine the total impulse

$$I = \int_0^{t_b} (Thrust)dt \tag{10.41}$$

in units of $kg - m/sec$.

Problem 4 - The thrust versus time history of a solid rocket with a circular port is shown in Figure 10.5.

The regression rate of the propellant surface follows a law of the form

$$\dot{r} = \alpha {P_{t2}}^n \tag{10.42}$$

where the exponent n is in the range of 0.4 to 07. Briefly show why the thrust tends to increase over the course of the burn.

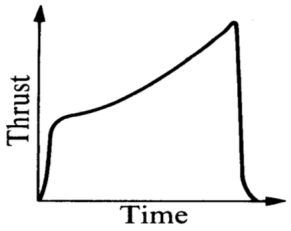

Figure 10.5: *Typical thrust time history of a solid rocket with a circular port.*

Problem 5 - A solid propellant upper stage rocket operates in space. The motor has a $0.2\,m$ diameter nozzle throat and a cylindrical port $4.2\,m$ long. At the end of the burn the port is $0.8\,m$ in diameter. The regression rate law is

$$\dot{r} = 3.8 \times 10^{-6} {P_{t2}}^{0.5} \tag{10.43}$$

where the pressure is expressed in N/m^2. The solid propellant density is $2000\,kg/m^3$ and the combustion gas has $\gamma = 1.2$ and molecular weight equal to 32. The combustion chamber temperature is $3000\,K$. The quasi-equilibrium chamber pressure at the end of the startup transient is $P_{t2} = 3.0 \times 10^6\,N/m^2$.

1)Determine the characteristic time τ for the start-up transient.

2)Determine the propellant mass expended during the startup transient. Take the start-up time to be 8τ.

3) Determine the mass flow and quasi-equilibrium chamber pressure P_{t2} at the end of the burn.

4) Once the propellant is all burned the remaining gas in the chamber is expelled through the nozzle and the pressure in the chamber drops to zero. Calculate the time required for the pressure to drop to 10% of its value at the end of the burn.

5) Sketch the pressure-time history of the motor.

Chapter 11

Hybrid Rockets

11.1 Conventional bi-propellant systems

A liquid bi-propellant chemical rocket system is shown schematically in Figure 11.1. Oxidizer and fuel from separate tanks are pressure-fed or pump-fed into a combustion chamber where atomization, mixing, ignition and combustion takes place. Despite the apparent simplicity of the diagram, liquid rockets are extremely complex. The complexity comes from the fact that the chamber pressure is usually quite high and one or both of the propellants may be cryogenic. In addition, the liquids are usually fed into the combustion chamber at very high mass flow rates requiring high performance turbo-pumps usually powered by a small flow of the propellants through a separate burner and turbine. Many of the most spectacular rocket failures have involved liquid bi-propellant systems.

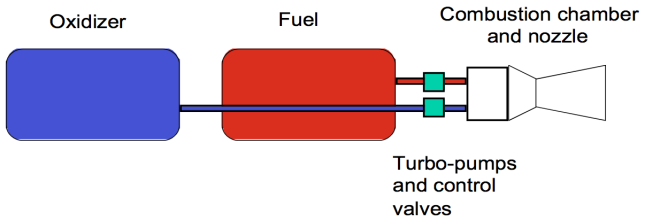

Figure 11.1: *Schematic of a liquid bi-propellant rocket system.*

Perhaps the most widely recognizable liquid engines are the space shuttle main engines that burn hydrogen and oxygen. These engines also make use of a pre-burner where most of the oxygen is burned with a small amount of hydrogen to raise the temperature of the gases that are injected into the main combustion chamber along with the rest of the hydrogen. The hydrogen is also used to regeneratively cool the rocket chamber and nozzle prior to mixing

with the oxygen. Many different oxidizers are used in bi-propellant systems. The two most popular are LOx (liquid oxygen) and N_2O_4. These are both very energetic oxidizers and burn readily with hydrocarbon fuels such as kerosene and alcohol as well as hydrazine (N_2H_4). The ideal specific impulse of kerosene burning with LOx is approximately 360 seconds depending on the chamber pressure and nozzle area ratio.

Liquid rockets can be throttled by controlling the flow of fuel and oxidizer while keeping the ratio of oxidizer to fuel flow the same. Wide throttle ratios are somewhat difficult to achieve because of the reduced mixing that can occur at low liquid flow rates. Liquid rockets are subject to a variety of instabilities and the design and development of a new injector and combustion chamber is an expensive multi-year process.

Figure 11.2 depicts a solid rocket system. Though mechanically much simpler than liquids, the solid rocket is complicated by the use of an explosive mixture of fuel and oxidizer that involves a very complex and expensive manufacturing process. In addition solid rockets require stringent safety precautions in manufacture, handling and launch.

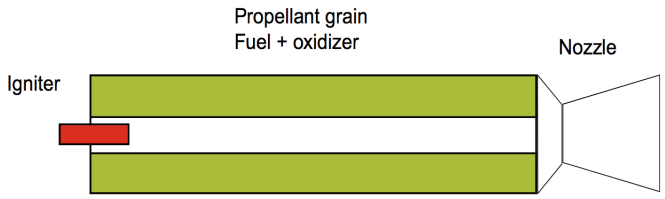

Figure 11.2: *Schematic of a solid rocket motor.*

The propellant regression rate for a solid rocket is proportional to the chamber pressure according to a relation of the form

$$\dot{r} = \alpha {P_{t2}}^n \tag{11.1}$$

where $n < 1$. Probably the most well known solids are the large re-usable space shuttle boosters. Each uses approximately a million pounds of propellant and produces roughly three million pounds of thrust at launch. The fuel is mainly aluminum in a polymer binder (Hydroxyl Terminated Poly-butadiene, HTPB) and the oxidizer is ammonium perchlorate (AP) which is the most widely used solid oxidizer. In general solid rockets use somewhat less energetic oxidizers than liquids and the specific impulse of solids is generally lower. The ideal specific impulse of the shuttle booster propellant is approximately 280 seconds depending on the nozzle area ratio. Recently ammonium perchlorate has been found in the groundwater near many of the rocket propellant processing plants across the US and concerns have been raised about the possible environmental impact of this chlorinated compound.

The hazardous operation of the two basic types of chemical rocket propulsion comes mainly from the oxidizer and fuel that must be mixed to release energy in the rocket combustion chamber. In liquid bi-propellant rockets, a pump leak or tank rupture that brings these chemicals together in an uncontrolled way can result in a large explosion. In solid propellant rockets, the fuel and oxidizer are pre-mixed and held together in a polymer binder. Cracks or imperfections in the propellant can cause uncontrolled combustion and explosion.

11.2 The hybrid rocket idea

Figure 11.3 shows a hybrid rocket. The hybrid is inherently safer than other rocket designs. The idea is to store the oxidizer as a liquid and the fuel as a solid, producing a design that is less susceptible to chemical explosion than conventional solid and bi-propellant liquid designs. The fuel is contained within the rocket combustion chamber in the form of a cylinder with a circular channel called a port hollowed out along its axis. Upon ignition, a diffusion flame forms over the fuel surface along the length of the port. The combustion is sustained by heat transfer from the flame to the solid fuel causing continuous fuel vaporization until the oxidizer flow is turned off. In the event of a structural failure, oxidizer and fuel cannot mix intimately leading to a catastrophic explosion that might endanger personnel or destroy a launch pad.

The idea of the hybrid rocket has been known since the first flight in 1933 by Soviet researchers, but wasn't given serious attention until the 1960's. The primary motivation was the non-explosive character of the fuel, which led to safety in both operation and manufacture. The fuel could be fabricated at any conventional commercial site and even at the launch complex with no danger of explosion. Thus a large cost saving could be realized both in manufacture and launch operation. Additional advantages over the solid rocket are: greatly reduced sensitivity to cracks and de-bonds in the propellant, better specific impulse, throttle-ability to optimize the trajectory during atmospheric launch and orbit injection and the ability to thrust terminate on demand. The products of combustion are environmentally benign unlike conventional solids that produce acid forming gases such as hydrogen chloride.

The hybrid rocket requires one rather than two liquid containment and delivery systems. The complexity is further reduced by omission of a regenerative cooling system for both the chamber and nozzle. Throttling control in a hybrid is simpler because it alleviates the requirement to match the momenta of the dual propellant streams during the mixing process. Throttle ratios up to 10 have been common in hybrid motors. The fact that the fuel is in the solid phase makes it very easy to add performance enhancing materials to the fuel such as aluminum powder. In principle, this could enable the hybrid to gain an I_{sp} advantage over a comparable hydrocarbon fueled liquid system.

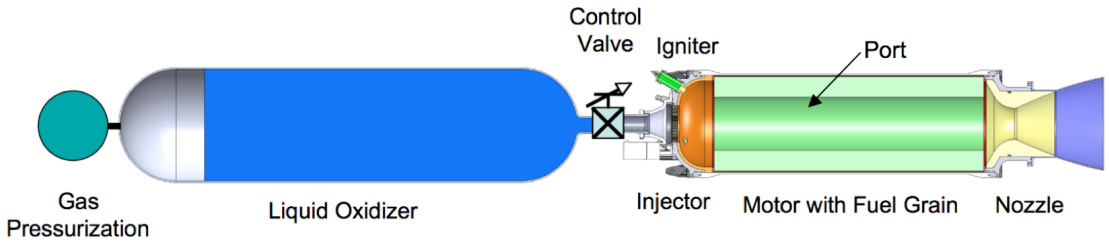

Figure 11.3: *Schematic of a hybrid rocket motor.*

Boundary layer combustion is the primary mechanism of hot gas generation in hybrid rockets. The idealized sketch in Figure 11.4 illustrates the flow configuration. The hybrid normally uses a liquid oxidizer that burns with a solid fuel although reverse hybrids such as liquid hydrogen burning with solid oxygen have been studied. The flame thickness and location in the boundary layer are shown roughly to scale. The flame zone is relatively deep in the boundary layer and the flame tends to be fuel rich based on the observed flame position and relatively low flame temperatures measured in the boundary layer. The hybrid enjoys many safety and environmental advantages over conventional systems, however large hybrids have not been commercially successful. The reason is that traditional systems use polymeric fuels that evaporate too slowly making it difficult to produce the high thrust needed for most applications.

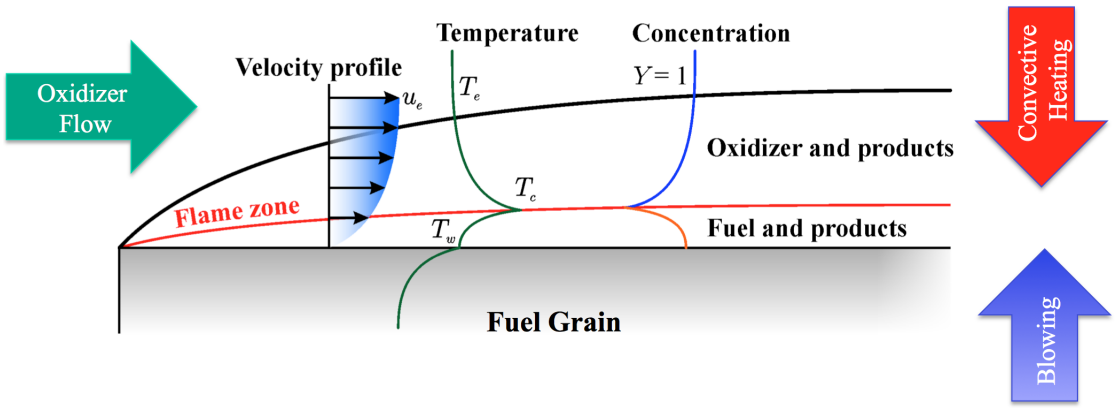

Figure 11.4: *Boundary layer combustion.*

11.2.1 The fuel regression rate law

Theory shows that the fuel mass transfer rate is proportional to the mass flux averaged

across the port. The mass flow rate increases with axial distance along the port leading to coupling between the local fuel regression rate and the local mass flux. For proper design, accurate expressions are needed for both the time dependent oxidizer-to-fuel ratio at the end of the port, and the time at which all the fuel is consumed. As the fuel is depleted the flame approaches the motor case at which point the burn must be terminated. The coupling between the local regression rate and the local mass flow rate means that both variables depend on time and space. This complicates the analysis of the thrust time behavior of the hybrid compared to a solid rocket. The problem is governed by two coupled first-order partial differential equations, the regression rate equation

$$\frac{\partial r\left(x,t\right)}{\partial t}=\frac{a}{x^{m}}\left(\frac{\dot{m}_{port}}{\pi r^{2}}\right)^{n} \tag{11.2}$$

and the mass flow growth equation

$$\frac{\partial \dot{m}_{port}\left(x,t\right)}{\partial x}=\rho_{f}\left(2\pi r\right)\frac{a}{x^{m}}\left(\frac{\dot{m}_{port}}{\pi r^{2}}\right)^{n}. \tag{11.3}$$

The local mass flux in the port is generally denoted G where

$$G=\frac{\dot{m}_{port}}{\pi r^{2}}=\frac{\dot{m}_{ox}+\dot{m}_{f}}{\pi r^{2}}. \tag{11.4}$$

The local port mass flow rate, $\dot{m}_{port}$, is the sum of the oxidizer mass flow rate, $\dot{m}_{ox}$, injected at the entrance to the port and the accumulated fuel mass flow rate, $\dot{m}_{f}$, transferred from the fuel grain upstream of a location x. The coefficient a is an empirical constant determined by the choice of fuel and oxidizer. The units of the regression rate constant are

$$\left[a\right]=\frac{Length^{2n+m+1}}{Mass^{n}Time^{1-n}}. \tag{11.5}$$

The dependence of regression rate on mass flux G and stream-wise coordinate x arises from the dependence of the skin friction and heat transfer rate on Reynolds number based on distance along the port. Values of the exponents suggested by theory are $m=0.2$ and $n=0.8$. Measured values of n tend to be in the range 0.3 to 0.8 depending on the choice of fuel and oxidizer. Values of n greater than 0.8 or less than about 0.3 are generally not observed. The length exponent turns out to be very difficult to measure since it is relatively small and would require a large number of motor tests at a wide range of scales to be determined accurately. As nearly as one can tell at this point m is considerably smaller than the prediction of classical theory.

A widely used approximation to (11.2) and (11.3) is the single equation

$$\frac{dr}{dt} = a_o G_{ox}^n. \tag{11.6}$$

where the port length effect is neglected and the fuel regression rate is assumed to only depend on the oxidizer mass flux,which is constant along the port. In general, equation (11.6) underestimates the fuel mass generation rate. However, (11.6) can be a reasonably accurate approximation in situations where the design O/F ratio is relatively large, more than 5 or so.

A greater problem is that the vast majority of values of the regression rate constant reported in the literature correspond to a_o based on data measured against (11.6). The problem with this is that every change in the value of O/F for a given test motor requires the determination of a new value of a_o. In point of fact the O/F generally varies during the course of a burn and so the reported value of a_o also depends on how the mean O/F is determined. Consider

$$\begin{aligned} &\frac{\partial r\left(x,t\right)}{\partial t} = \frac{a}{x^m}\left(\frac{\dot{m}_{port}}{\pi r^2}\right)^n = \\ &\frac{a}{x^m}\left(\frac{\dot{m}_{ox}\left(1+1/\left(\dot{m}_{ox}/\dot{m}_f\left(x,t\right)\right)\right)}{\pi r^2}\right)^n = \frac{a(1+1/\left(OF\left(x,t\right)\right))^n}{x^m}\left(\frac{\dot{m}_{ox}}{\pi r^2}\right)^n. \end{aligned} \tag{11.7}$$

If the basic regression rate equations (11.3) and (11.4) are to be believed then

$$a_o = a(1+1/\left(OF\left(x,t\right)\right))^n. \tag{11.8}$$

In principle a_o is a function of space and time. It can only be treated as a constant if some scheme of space time averaging of the O/F ratio is used for a given run and, even then, a_o will have a new value every time the O/F is changed. Unfortunately, when a_o is reported in the literature, the corresponding O/F is often not reported. A consequence is that today we often do not have good, solid empirical values of the regression rate constants for many propellant combinations.

In marked contrast to solid rockets, the regression rate of a hybrid is insensitive to the chamber pressure except at very low fluxes where radiation effects become important and at very high fluxes where chemical kinetics effects are important. This important characteristic enables the chamber pressure to be a free variable in the motor design enabling the designer to optimize the chamber pressure for a given mission. Although the hybrid seems to lie somewhere between a liquid and a solid system it has advantages that are unique and not enjoyed by liquids or solids.

11.2.2 Specific impulse

The theoretical specific impulse of a hybrid rocket is more appropriately compared to a bi-propellant liquid than a solid. The oxidizer can be any of the oxidizers used with liquid bi-propellant engines. Typically, the solid fuel is a polymeric hydrocarbon such as hydroxyl-terminated-poly-butadiene (HTPB), a common solid propellant binder with an energy density comparable to kerosene. But, hybrid solid fuel mass densities are typically 15-20 % greater than the density of liquid kerosene. Figure 11.5 (left) depicts the theoretical specific impulse versus oxidizer to fuel O/F ratio of liquid oxygen (LOx) burning with paraffin and HTPB. A plot of LOx burning with liquid kerosene would look very similar.

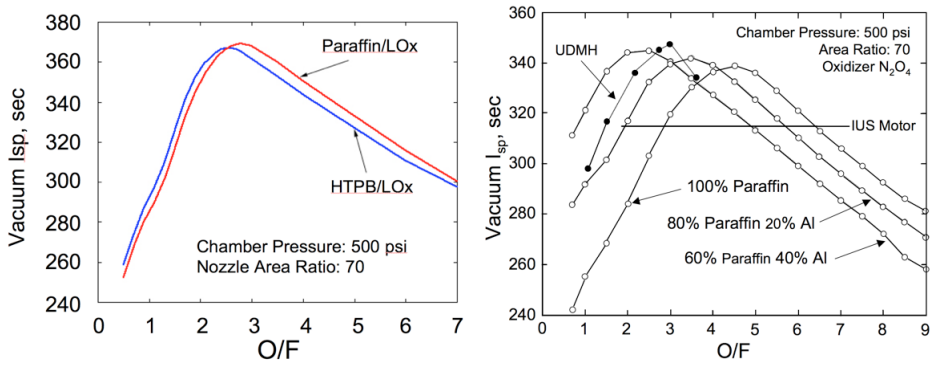

Figure 11.5: *Left figure, ideal specific impulse for paraffin and HTPB burning with LOx. Right figure paraffin-aluminum mixtures burning with nitrogen tetroxide. The IUS (Inertial Upper Stage) motor was a solid rocket built by the Chemical Systems Division of United Technologies and used as an upper stage in Boeing satellite launches for many years.*

The plot on the right of Figure 11.5 shows the specific impulse of paraffin burning with N_2O_4 with varying percentages of aluminum added to the fuel by mass. Aluminum addition tends to increase the specific impulse slightly while reducing the optimal O/F allowing the designer to use a smaller liquid storage and feed system. These figures give a pretty good illustration of the range of O/F ratios used in typical systems. Generally, the oxidizer mass flow rate tends to be two or more times the fuel mass flow rate at the end of the port.

11.2.3 The problem of low regression rate

The main drawback of the hybrid is that the combustion process relies on a relatively slow mechanism of fuel melting, evaporation and diffusive mixing as depicted in Figure 11.4. In a solid rocket, the flame is much closer to the fuel surface and the regression rate is typically an order of magnitude larger. As a rough comparison, the regression rate in a solid rocket

at a typical rocket combustion chamber pressure may be on the order of 1.0 cm/sec whereas a typical hybrid using a classical polymeric fuel such as HTPB may have a regression rate on the order of 0.1 cm/sec. To compensate for the low regression rate, the surface area for burning must be increased. This is accomplished through the use of a multi-port fuel grain such as that depicted in Figure 11.6. Most attempts to increase the regression rate involve some method for increasing the heat transfer rate to the fuel surface. This can be done, for example, by increasing turbulence levels in the port or by adding roughness to the fuel grain. The problem is that as the heat transfer rate is increased, the radial velocity of the evaporating fuel toward the center of the port increases. This so-called "blocking effect" tends to decrease the temperature gradient at the fuel surface leading to a reduction in the amount of heat transfer increase that can be achieved. A regression rate increase on the order of 25-30 % or so can be obtained using this approach - not the factor of 2 or 3 that is needed for a single port design.

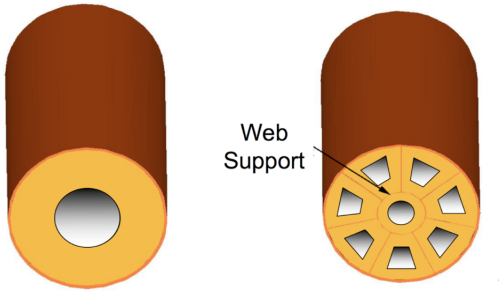

Figure 11.6: *Single versus multi-port (wagon wheel) grain design.*

The most obvious problem with the multi-port design is that the amount of fuel that can be loaded into a given volume is reduced, leading to an increase in the vehicle diameter for a given total fuel mass. There are other problems. The grain may need to be produced in segments and each segment must be supported structurally, adding weight and complexity. In addition it is very difficult to get each port to burn at the same rate. If one burns slightly faster than another, then the oxidizer will tend to follow the path of least resistance leading to further disparity in the oxidizer flow rate variation from port to port. Toward the end of burning, the port that reaches the liner first forces the motor to be shut down prematurely leading to an inordinately large sliver fraction of unburned fuel. Small pressure differences from port to port can lead to grain structural failure and loss of fuel fragments through the nozzle. Aside from possible damage to the nozzle, the resulting increase in the overall O/F ratio leads to a reduction of the specific impulse and an increase in the nozzle throat erosion rate. Due to the high erosion, the nozzle area ratio decreases excessively leading to an additional loss of specific impulse.

11.3 Historical perspective

Early hybrid rocket development and flight test programs were initiated both in Europe and the U.S. in the 1960's. The European programs in France and Sweden involved small sounding rockets, whereas the American flight programs were target drones (Sandpiper, HAST, and Firebolt) which required supersonic flight in the upper atmosphere for up to 5 minutes. These latter applications were suitable for the conventional hybrid because its very low burning rate was ideal for a long duration sustainer operation.

Despite the very low regression rate of the fuel, in the late 1960's Chemical Systems Division of United Technologies (CSD/UTC) investigated motor designs of larger diameters that could produce high thrust suitable for space launch vehicles. They experimented with a $38\,inch$ diameter motor delivering $40,000\,lbs$ of thrust. In order to achieve a high mass flow rate, a motor with 12 ports in the fuel grain was required. Although the motor was successfully fired several times, it was recognized that the poor volumetric fuel loading efficiency would lead to a deficit in vehicle performance.

Interest in the hybrid was revived again in the late 1970's when concern was expressed for the storage and handling of the large solid propellant segments of the Shuttle booster. The storage of potentially explosive grains is costly in terms of requirements for reinforced structures and interline distance separation. The same safety concern arose again after the Space Shuttle Challenger disaster, where it was recognized that a thrust termination option might have avoided the failure. This concern was heightened when, a few months later, there was a Titan failure, caused by an explosion of one of the solid boosters.

Several hybrid propulsion programs were initiated in the late 80's and early 90's. The Joint Government/Industry Research and Development (JIRAD) program involved the testing of 11 and 24 inch diameter hybrid motors at the Marshall Space Flight Center. Another hybrid program initiated during the early 90s was DARPA's Hybrid Technology Options Project (HyTOP). The goal of this program was to develop the HyFlyer launch vehicle and demonstrate the feasibility of hybrid boosters for space applications. The members of the HyTOP team were AMROC, Martin Marietta and CSD/UTC.

In the 1990s, two significant hybrid efforts occurred. One was the formation of the American Rocket Company (AMROC), an entrepreneurial industrial company devoted entirely to the development of large hybrid boosters. The second, with encouragement from NASA, was the formation of the Hybrid Propulsion Industry Action Group (HPIAG) composed of both system and propulsion companies devoted to exploring the possible use of hybrids for the Shuttle booster and other launch booster applications. Both efforts ran into technical stumbling blocks, basically caused by the low regression rate fuels, which resulted in large diameter motors with many ports to satisfy thrust requirements. The resulting configuration not only compromised potential retrofit for the Shuttle and Titan boosters

but also raised questions about the internal ballistic performance of a thin web multi-port motor, especially toward the end of burning when the web approaches structural failure. Although AMROC had many successful tests in 51 inch diameter motors, they ran into difficulties when the motor was scaled to 6 foot diameter and 250,000 pounds of thrust. The low regression rate of the fuel dictated a 15 port grain design and problems of poor grain integrity were the result. In 1995 AMROC filed for bankruptcy.

The Hybrid Propulsion Demonstration Program (HPDP) began in March 1995. The goal of the HPDP was to enhance and demonstrate several critical technologies that are essential for the full scale development of hybrid rocket boosters for space launch applications. The government and industry participants in the program were NASA, DARPA, Lockheed Martin, CSD/UTC, Thiokol, Rocketdyne, Allied Signal and Environmental Aeroscience Corporation. Even though the tasks of the HPDP program included systems studies and sub-scale testing, the main objective of the program was the design and fabrication of a 250,000 pound thrust test-bed. The design of the motor was guided by the sub-scale motor tests performed under the JIRAD program. The wagon wheel 7+1 multi-port fuel grain was made of conventional hydroxyl-terminated-polybutadiene (HTPB)/ Escorez fuel. The motor was fired for short times in July 1999. The motor exhibited large pressure oscillations and unequal burning rates in the various ports. Later the motor was stabilized by substantially increasing the heat input at the fore end of the motor. Problems related to low regression rate inherent in conventional hybrids fuels were not solved.

The most recent advance in hybrid rockets occurred in the Fall of 2004 when SpaceShipOne carried a pilot to over 328,000 feet to win the Ansari X-prize. This privately funded, sub-orbital flight seemed to usher in a new era in space tourism although the follow-on SpaceShipTwo has experienced lengthy delays in development.

Figure 11.7: *Space Ship One carried aloft by the White Knight carrier aircraft.*

The propulsion system for Space Ship One used a four port motor fueled by HTPB with nitrous oxide (N_2O) as the oxidizer. Although the flight of Space Ship One was a great success, it was not exactly a walk in the park for the pilot. The description in Figure 11.9

Figure 11.8: *Various systems of Space Ship One. Note the hybrid rocket on the left.*

reveals a pretty sobering picture of the flight.

Neither SpaceDev or eAc met Scaled's wishes. The SpaceDev design, which has four longitudinal ports in the rubber fuel for enough burning area for high thrust, comes on with a bang, producing maximum thrust at the start—not the smooth ramp-up envisioned to turn the corner. The peak thrust is only about 85% of the desired plateau, and declines steadily from there, according to the Sept. 18 SETP presentation. Despite the early start, this still means that to get enough total impulse to loft SpaceShipOne above 100 km., the motor has to run longer than desired, in the very thin atmosphere where control is tenuous.

The webs of rubber between the four SpaceDev ports thin out and come apart toward the end of the run. The chunks extrude through the nozzle, causing frightening shaking and explosion noises in the cockpit. It happened at least three times on one flight and Melvill thought the tail had blown off. After minutes by himself in zero-g and entry, he was relieved when chase aircraft said the spaceship appeared alright.

The eAc motor didn't ignite until five sec. after the switch was thrown, and then also came on with a bang, but the initial combustion instabilities were less. It has a single port and compensates for the lower burning area with fuel additives to increase burning rate. But not enough, because it only made about 65% of the desired thrust. That required the burn time to be even longer for sufficient total impulse, extending the engine run farther out of the atmosphere.

Longer burn time of the eAc motor was considered the more serious problem, and the contract went to SpaceDev.

Mike Dornheim - Aviation Week
October 18, 2004 page 36

Figure 11.9: *Space Ship One hybrid motor operation as described in Aviation Week.*

The conclusion from this history is that if a significantly higher burning rate fuel can be developed for the hybrid motor, the multi-port difficulties just described can be alleviated and a smaller, safer more efficient motor can be designed. Although this deficiency of conventional hybrid fuels was recognized more than forty years ago, attempts to increase the burning rate by more than 50-100 %, without compromising the safety and low-cost features of the hybrid design, have been largely unsuccessful until recently.

11.4 High regression rate fuels

In the late 1990s, the U.S. Air Force studied some exotic cryogenic designs for hybrid rockets. One scheme would have swapped the roles of the fuel and oxidizer. The fuel was liquid hydrogen and the oxidizer was solid oxygen. While investigating this unusual configuration, the Air Force also studied a different combination of cryogenic propellants: liquid oxygen and pentane, a hydrocarbon that is liquid at room temperature, but in this application was frozen solid using a bath of liquid nitrogen. The Air Force researchers found that solid pentane burns 3 to 4 times faster than normal fuels. The Air Force researchers kindly shared their data with us and after some careful analysis it appeared that mass transfer from the surface of this fuel involved more than simple evaporation.

Pentane produces a very thin, low viscosity, low surface tension, liquid layer on the fuel surface when it burns. The instability of this layer driven by the shearing effect of the oxidizer gas flow in the port leads to the lift-off and entrainment of droplets into the gas stream greatly increasing the overall fuel mass transfer rate. The multitude of entrained droplets offers an enormous amount of surface area for evaporation and burning without the usual reduction caused by the blocking effect. The basic mechanism is sketched in Figure 11.10.

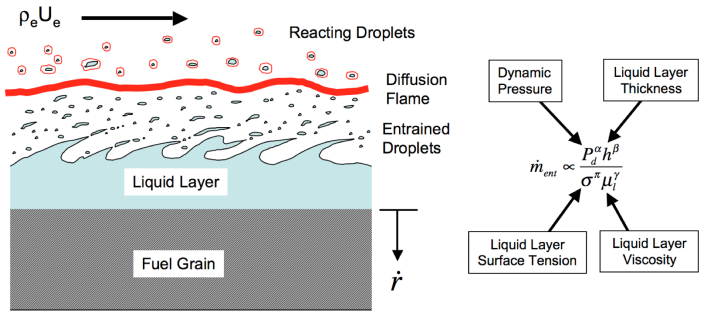

Figure 11.10: *Liquid layer entrainment mechanism.*

In effect, this mechanism acts like a continuous spray injection system distributed along the port with most of the fuel vaporization occurring around droplets convecting between the melt layer and the flame front. Since droplet entrainment is not limited by diffusive heat transfer to the fuel from the combustion zone, this mechanism can lead to much higher surface regression rates than can be achieved with conventional polymeric fuels that rely solely on evaporation. Equation (11.9) shows how the entrainment mass transfer component of the regression rate illustrated in Figure 11.10 depends on the parameters of the flow: the chamber pressure, P, liquid layer thickness, h, surface tension, σ and viscosity,

μ. The exponents in (11.9) are determined empirically and are of order one.

$$\dot{m}_{entrainment} \sim \frac{P_d^{\alpha} h^{\beta}}{\sigma^{\pi} \mu_l^{\gamma}} \tag{11.9}$$

The key fuel properties are in the denominator of (11.9) - low surface tension and low viscosity of the melt layer, evaluated at the characteristic temperature of the layer. This forms the basis of a fundamental criterion that can be used to identify high regression rate fuels. Not all fuels that form a melt layer at the fuel surface will entrain. For example, high-density-polyethelene (HDPE), which is a conventional hybrid fuel, does form a melt layer but the viscosity of the liquid is four orders of magnitude larger than pentane - too viscous to permit significant droplet entrainment. But frozen pentane itself is not a particularly promising fuel. It is not practical to have to soak the rocket motor in a liquid nitrogen bath before launch. This led to a search for a fuel that would be solid at room temperature, that would produce a low-viscosity liquid when it melted, and would be strong enough to withstand the high-temperature, high-pressure, high-vibration environment of a rocket motor's combustion chamber. To achieve this goal it was necessary to solve a puzzle.

Figure 11.11 shows the effect of molecular weight on the melt temperature and boiling temperature for the normal alkanes. The middle curve is an estimate of the mean melt layer temperature. The normal alkanes are linear, fully saturated hydrocarbons with the formula C_nH_{2n+2}. Familiar examples include methane (one carbon atom per molecule), ethane (two carbons), and propane (three carbons). As the number of carbon atoms in the molecule increases, the normal alkanes become room-temperature liquids, such as pentane (five carbons), and eventually solids such as waxes and polyethelene.

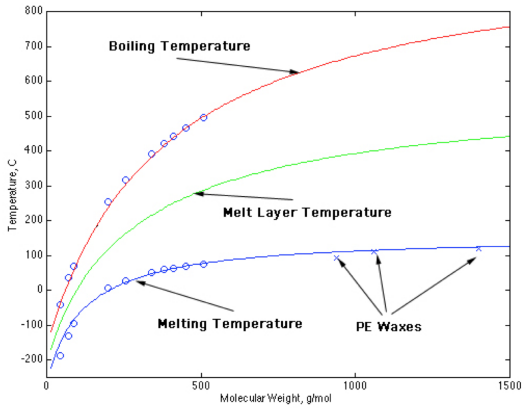

Figure 11.11: *Effect of molecular weight on key temperatures for the normal alkanes.*

The crucial point of Figure 11.11 is this. The melt layer temperature rises quickly at low

molecular weights but much more slowly at high molecular weights. In general, the viscosity of a liquid tends to increase with molecular weight. But, the viscosity of most liquids tends to decrease exponentially fast with temperature. These facts can be applied to the melt layer of the normal alkanes. At high molecular weight, where the melt layer temperature increases only slowly, the viscosity increases through the dominance of the molecular weight effect. But at lower molecular weight, where the melt layer temperature increases rapidly, the tendency for the viscosity to increase with molecular weight is strongly offset by the tendency for viscosity to decrease with temperature.

The design goal is to find a hydrocarbon with the right molecular weight. At high molecular weights, the viscosity of the liquid form of the alkane is too large for droplets to form readily. At low molecular weights, the alkanes are either gaseous or liquid or soft solids, much too weak to withstand the rigors of a rocket combustion chamber. In between is a sweet spot; Fuels with roughly 25 to 50 carbon atoms per molecule that are structurally robust and produce low-viscosity liquids when they melt. Figure 11.12 indicates schematically the range of carbon numbers that are likely to produce significant entrainment mass transfer.

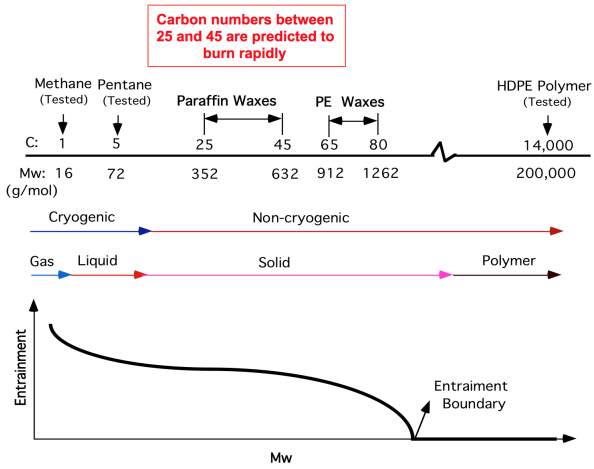

Figure 11.12: *Schematic diagram indicating the normal alkanes that are expected to exhibit high regression rate.*

These fuels, which include the paraffin waxes and polyethylene waxes, are predicted to have high regression rates at oxidizer mass fluxes covering a wide range of hybrid rocket applications. In fact, the viscosity of the melt layer in paraffin is comparable to pentane and so the regression rate is also similar despite the disparity in molecular weight. The kind of paraffin wax we use is a relatively high carbon number, fully refined, wax sometimes called sculptor's wax or hurricane wax. Fabricating, handling, and transporting traditional solid-rocket propellants is usually very costly, but a paraffin-based fuel is easy to deal with in all

those regards. It is nontoxic, and indeed not hazardous at all. What's more, the complete combustion of this fuel with oxygen produces no hazardous gases. The products are simply carbon dioxide and water. In contrast, the by-products of burning conventional solid rocket propellant often include carbon monoxide as well as acid forming gases such as hydrogen chloride. A more benign, easier to use, rocket fuel could hardly be imagined!

Regression rates 3 to 4 times the predicted classical rate have been observed in a laboratory scale motor using gaseous oxygen and an industrial grade paraffin wax. The specific impulse of a paraffin-based hybrid motor is slightly higher than that of a kerosene-based liquid motor and solid paraffin is approximately 20% more dense than liquid kerosene. Figure 11.4 shows the ideal specific impulse of paraffin wax and HTPB burning with liquid oxygen. The waxes comprise a wide range of molecular weight, surface tension and viscosity and therefore can be used to create mixtures whose regression rate characteristics are tailored for a given mission.

11.5 The O/F shift

Over the course of a burn at a fixed oxidizer mass flow rate there is a tendency for the oxidizer to fuel (O/F) ratio to shift to higher values as the port opens up. This can be seen from the following. For a single circular port a rough estimate of the O/F ratio at the end of the port is, using (11.6)

$$O/F = \frac{\dot{m}_o}{\dot{m}_f} = \frac{\dot{m}_o}{\rho_f \pi D L \alpha \left(\frac{\dot{m}_o}{\pi r^2}\right)^n} = \frac{\dot{m}_o^{1-n} D^{2n-1}}{4^n \pi^{1-n} \alpha \rho_f L} \tag{11.10}$$

where L is the port length and r is the port radius. Recall that the exponent is generally in the range $0.6 < n < 0.8$. As the port diameter increases the burning area increases and the oxidizer mass flux goes down. For $n > 0.5$ the decrease in mass flux dominates the increase in burning area and the overall generation rate of fuel mass goes down. The net effect is to cause the chamber pressure and hence the thrust to decrease naturally over the course of the burn as the vehicle mass decreases. This feature is desirable for a launch system where the payload is subject to a maximum acceleration constraint. Compare this to a solid rocket where the thrust tends to increase during the burn and a throttling option is not available.

Note the relatively strong sensitivity in Figure 11.4 of the specific impulse to the O/F ratio. The change of O/F implies a change in specific impulse and a possible reduction in vehicle performance. This is a factor that must be taken into account by the designer seeking to get maximum total delivered impulse from the motor. In practice the maximum payload acceleration limit leads to a requirement that the oxidizer mass flow be throttled

back while the port opens up and the two effects tend to offset one another. A typical case might be a factor of two decrease in the oxidizer mass flow rate and a factor of three increase in the port diameter. For $n = 0.62$ the net effect is less than a one percent change in O/F.

11.6 Scale-up tests

To demonstrate the feasibility of high regression rate fuels, a series of tests were carried out on intermediate scale motors at pressures and mass fluxes representative of commercial applications. A hybrid test facility designed to study these fuels was developed by NASA and Stanford researchers at NASA Ames Research Center. An image from one of these tests is shown in Figure 11.13.

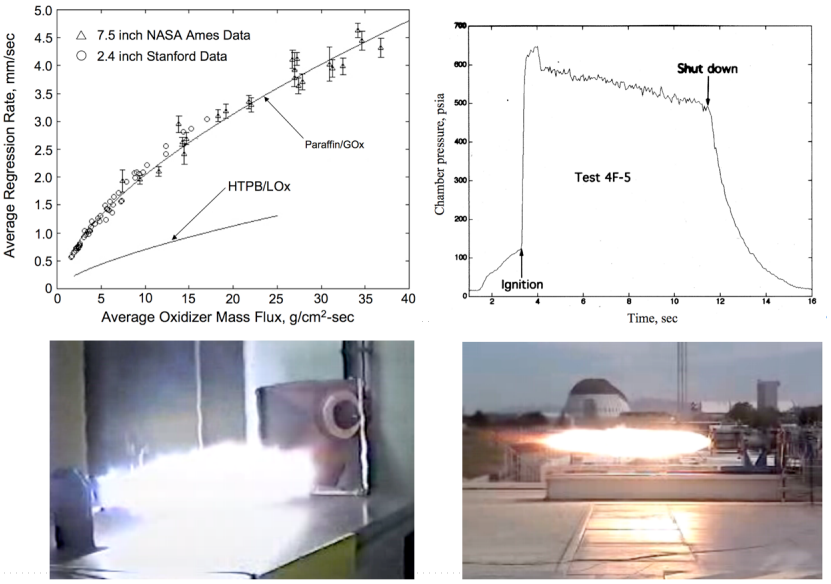

Figure 11.13: *Hybrid motor tests at Stanford and NASA Ames showing a typical pressure time history of the Ames tests. Thrust in the image shown is approximately 10000 Newtons with a simple convergent nozzle.*

Figure 11.14 shows the main results of these tests as well as earlier results of testing on a laboratory scale motor at Stanford. The results are compared with HTPB.

The main conclusions from these tests are the following.

1) The regression rate behavior observed in the small scale tests at Stanford prevails when the motor is scaled up to chamber pressures and mass fluxes characteristic of operational

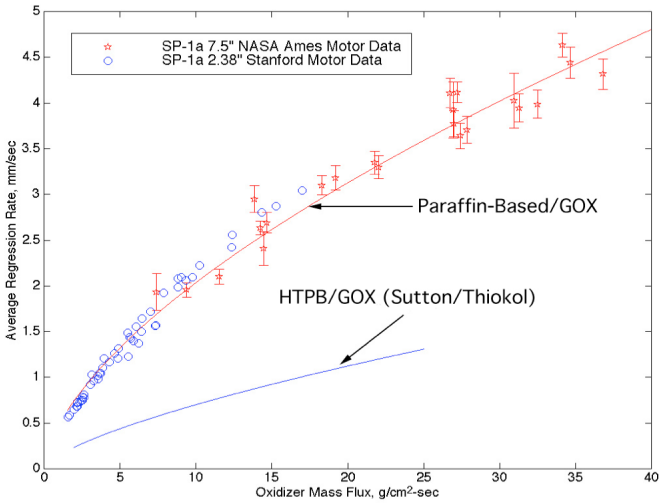

Figure 11.14: *Regression rate versus oxidizer mass flux for paraffin and HTPB.*

systems. Moreover the regression rate data from large and small motors matches quite well indicating that small scale tests can be used to infer the behavior of larger motors. This is extremely useful when it comes to developing the right fuel formulation for a given mission.

2) Paraffin-based fuels provide reliable ignition and stable combustion over the entire range of mass fluxes encountered $(50 - 600\, kg/m^2 - sec)$.

3) The fuel exhibited excellent structural integrity over the range of chamber pressures used $(10 - 65\, bar)$.

11.7 Regression rate analysis

11.7.1 Regression rate with the effect of fuel mass flow neglected.

The simplest approach to determining how the port radius varies with time is to neglect the effect of accumulated fuel mass flow on the regression rate and assume the length exponent $m = 0$ so the port radius is independent of x. This utilizes the fact that m is known to be small allowing the singularity at $x = 0$ to be removed. Moreover the optimal O/F is often three or more so the oxidizer usually comprises most of the mass flow. Recall (11.6) and

express the mass flux in terms of the radius and oxidizer mass flow.

$$\frac{dr\left(t\right)}{dt} = a_o\left(\frac{\dot{m}_{ox}\left(t\right)}{\pi r^2}\right)^n \tag{11.11}$$

Integrate (11.11) with respect to time.

$$r\left(t\right) = \left(r(0)^{2n+1} + \left(2n+1\right)\frac{a_o}{\pi^n}\int_0^t \dot{m}_{ox}\left(t'\right)^n dt'\right)^{\frac{1}{2n+1}} \tag{11.12}$$

Under the assumed regression rate (11.11) law the mass flow increases linearly along the port.

$$\frac{\dot{m}_{port}}{\dot{m}_{ox}} = \frac{\dot{m}_f + \dot{m}_{ox}}{\dot{m}_{ox}} = 1 + \left(\frac{2\pi^{1-n}a_o\rho_f}{\dot{m}_{ox}^{1-n}\left(r(0)^{2n+1} + \left(2n+1\right)\frac{a_{ox}}{\pi^n}\int_0^t \dot{m}_{ox}(t')^n dt'\right)^{\frac{2n-1}{2n+1}}}\right)x \tag{11.13}$$

11.7.2 Exact solution of the coupled space-time problem for $n = 1/2$.

In reality the regression rate is dependent on the local total mass flux including the fuel mass accumulated along the port and, in turn, the local mass flux depends on the local radius. The problem is governed by two coupled first-order partial differential equations, (11.2) and (11.3). For $n = 1/2$ the equations simplify to

$$\frac{\partial}{\partial t}\left(r^2\right) = 2\pi^{-1/2}a\frac{\dot{m}_{port}^{1/2}}{x^m} \tag{11.14}$$

and

$$\frac{\partial \dot{m}_{port}}{\partial x} = 2\pi^{1/2}a\rho_f\frac{\dot{m}_{port}^{1/2}}{x^m} \tag{11.15}$$

The solution of (11.14) and (11.15) is

$$r\left(x,t\right) = \left(r(x,0)^2 + \frac{2a}{x^m\pi^{1/2}}\left(\int_0^t \dot{m}_{ox}\left(t'\right)^{1/2}dt' + \frac{\pi^{1/2}a\rho_f x^{1-m}t}{1-m}\right)\right)^{1/2} \tag{11.16}$$

and

$$\dot{m}_{port}\left(x,t\right)=\left(\dot{m}_{ox}(t)^{1/2}+\frac{\pi^{1/2}a\rho_f x^{1-m}}{1-m}\right)^2 \tag{11.17}$$

For $n=1/2$, the increased fuel mass generation due to the increase in port surface area is exactly compensated by the decrease in mass flux due to the growth in port cross-sectional area. As a result the total mass flow rate (11.17) at any point in the port is independent of time if $\dot{m}_{ox}$ is constant. For $n>1/2$ the effect of decreasing mass flux dominates the increase in port surface area and the mass flow rate at a given coordinate along the port x decreases with time as the port opens up. If $n<1/2$ the mass flow rate increases with time. Note that according to (11.16), shortly after the oxidizer flow is initiated the radius of the fore end of the port is infinite if the length exponent, $m>0$. Figure 11.15 shows a typical shape of the port after some period of time has elapsed after ignition. There is typically a minimum radius point near the fore end of the port downstream of which the port opens up slightly.

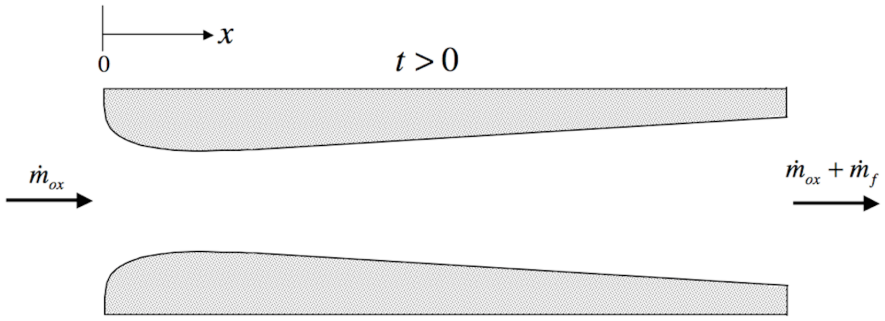

Figure 11.15: *Typical port shape at the end of a burn for* $m>0$.

11.7.3 Similarity solution of the coupled space-time problem for general n and m.

For general values of n and m the coupled equations (11.2) and (11.3) can be solved numerically given the initial port geometry and oxidizer mass flow rate, $\dot{m}_{ox}\left(t\right)$. Reference [1] discusses the coupled problem and includes an example of a numerical solution. As it turns out, (11.2) and (11.3) admit a similarity solution for constant $\dot{m}_{ox}$. This allows the

equations to be reduced to a pair of ODEs in the similarity variable

$$\theta = \left(\frac{(\pi^{-n} a)^2 (2\pi\rho_f)^{(2n+1)}}{\dot{m}_{ox}} \right)^{\frac{1}{2n-2m+1}} \frac{x}{t^{\left(\frac{2n-1}{2n-2m+1}\right)}}. \tag{11.18}$$

The similarity solution is derived in reference [2]. It can be used to generate accurate solutions for the port radius and O/F ratio. The similarity solution can even be applied to the case where $\dot{m}_{ox}$ does change with time by using a staircase function to approximate $\dot{m}_{ox}$.

11.7.4 Numerical solution for the coupled space-time problem, for general n and m and variable oxidizer flow rate.

The coupled equations (11.2) and (11.3) can be solved for a general initial port radius distribution and variable oxidizer mass flow rate using a first order forward difference scheme. First, the equations are non-dimensionalized using the initial oxidizer mass flow rate, $\dot{m}_{ox}(0)$, the initial port radius at the fore end, $r(0,0)$ and the burn time, $t_{burntime}$.

Dimensionless variables as follows.

$$\chi = \frac{x}{r\left(0,0\right)}$$

$$\tau = \frac{t}{t_{burntime}}$$

$$R = \frac{r\left(x,t\right)}{r\left(0,0\right)}$$

$$\tilde{J}\left(x,t\right) = \frac{\dot{m}_{port}}{\dot{m}_{ox}\left(0\right)} = \frac{\dot{m}_{ox}\left(t\right) + \dot{m}_{f}\left(x,t\right)}{\dot{m}_{ox}\left(0\right)} = \tag{11.19}$$

$$\frac{\dot{m}_{ox}\left(0\right) + \dot{m}_{f}\left(x,t\right)}{\dot{m}_{ox}\left(0\right)} + \left(\frac{\dot{m}_{ox}\left(t\right) - \dot{m}_{ox}\left(0\right)}{\dot{m}_{ox}\left(0\right)}\right)$$

$$J\left(x,t\right) = \frac{\dot{m}_{ox}\left(0\right) + \dot{m}_{f}\left(x,t\right)}{\dot{m}_{ox}\left(0\right)}$$

$$\lambda\left(t\right) = \frac{\dot{m}_{ox}\left(t\right) - \dot{m}_{ox}\left(0\right)}{\dot{m}_{ox}\left(0\right)}$$

In dimensionless form, the coupled equations are

$$\frac{\partial R}{\partial \tau} = C_R \frac{1}{\chi^m}\left(\frac{J+\lambda}{\pi R^2}\right)^n \tag{11.20}$$

and

$$\frac{\partial J}{\partial \tau} = C_J \frac{(2\pi R)}{\chi^m}\left(\frac{J+\lambda}{\pi R^2}\right)^n \tag{11.21}$$

where

$$C_R = \frac{a t_{burntime} \dot{m}_{ox}(0)^n}{r(0,0)^{2n+m+1}} \tag{11.22}$$

and

$$C_J = \frac{a\rho_f \dot{m}_{ox}(0)^{n-1}}{r(0,0)^{2n+m-2}}. \tag{11.23}$$

are dimensionless constants. The variable ranges are

$$\begin{aligned} 0 < \chi < \frac{L_{port}}{r\,(0,0)} \\ 0 < \tau < 1 \end{aligned} \tag{11.24}$$

where L_{port} is the port length.

Equations (11.20) and (11.21) can be integrated using a simple first order forward difference scheme.

Step 1 - Specify $r\,(0,0)$, L_{port}, $t_{burntime}$, and the regression rate constants, a, n, and m. Calculate C_R and C_J. If the initial port radius is not constant along the port, specify $R\,(\chi,0)$. If the oxidizer mass flow rate varies with time, specify $\lambda\,(\tau)$.

Step 2 - Choose a grid of χ and τ coordinates.

$$\begin{aligned} \chi_i &= (i/i_{\max})\,(L_{port}/r\,(0,0))\,, \quad i = 1,\ldots,i_{\max} \\ \tau_j &= (j/j_{\max})\,, \quad \mathrm{j} = 1,\ldots,j_{\max} \end{aligned} \tag{11.25}$$

Step 3 - Create tables defining the initial port geometry, $R\,(\chi_i,0)\,,\ i = 1,\ldots,i_{\max}$, and oxidizer mass flow rate values, $\lambda\,(\tau_j)\,,\ j = 1,\ldots,j_{\max}$.

Step 4 - Create tables defining the initial values of the radius and mass flow functions.

$$\begin{aligned} R\,(\chi_i,\tau_j) &= R\,(\chi_i,0)\,, \quad i = 1,\ldots,i_{\max}, \quad j = 1,\ldots,j_{\max} \\ J\,(\chi_i,\tau_j) &= 1, \quad i = 1,\ldots,i_{\max}, \quad j = 1,\ldots,j_{\max} \end{aligned} \tag{11.26}$$

Step 5 - Update the R and J tables over the length of the port and for the length of the

burn using the following first-order iterative scheme.

$$
\begin{aligned}
R\left(\chi_i, \tau_{j+1}\right) &= R\left(\chi_i, \tau_j\right) + \Delta\tau \frac{C_R}{{\chi_i}^m} \left(\frac{J\left(\chi_i, \tau_j\right) + \lambda\left(\tau_j\right)}{\pi R(\chi_i, \tau_j)^2} \right)^n \\
J\left(\chi_{i+1}, \tau_j\right) &= J\left(\chi_i, \tau_j\right) + \Delta\chi \frac{C_J\left(2\pi R\left(\chi_i, \tau_j\right)\right)}{{\chi_i}^m} \left(\frac{J\left(\chi_i, \tau_j\right) + \lambda\left(\tau_j\right)}{\pi R(\chi_i, \tau_j)^2} \right)^n \\
i &= 1, \ldots, i_{\max} - 1 \\
j &= 1, \ldots, j_{\max} - 1
\end{aligned}
\tag{11.27}
$$

where the differences in time and space are

$$
\begin{aligned}
\Delta\tau &= 1/j_{\max} \\
\Delta\chi &= \left(1/i_{\max}\right)\left(L_{port}/r\left(0,0\right)\right).
\end{aligned}
\tag{11.28}
$$

The resulting tables of $R\left(\chi_i, \tau_j\right)$ and $J\left(\chi_i, \tau_j\right)$ can be used to generate all of the information needed to characterize the burn.

11.7.5 Example - Numerical solution of the coupled problem for a long burning, midsize motor as presented in reference [1].

Regression rate data in Figure 11.14 from the tests described above of a 10,000 Newton class hybrid rocket motor at NASA Ames led to the following exponents for Liquid Oxygen burning with Paraffin, $n = 0.62$, $m = 0.015$. The multiplier was found to be $a = 9.27 \times 10^{-5} m^{(2n+m+1)} kg^{-n} \text{sec}^{n-1} = 9.27 \times 10^{-5} m^{2.39} kg^{-0.62} \text{sec}^{-0.38}$. Generally the motor ran for about 8 seconds during which time the port radius increased by a factor of a little less than 2. The port length is $L_{port} = 1.143\, m$. Initially, the port radius is $r\left(0,0\right) = 0.0508\, m$ and is constant along the port. The fuel density is $\rho_f = 920.0\, kg/m^3$. In the numerical results shown in Figures 11.16 and 11.17, the burn is continued for up to 100 seconds.

The computations in Figures 11.16 and 11.17 were carried out on an $i_{\max} = 2000$ by $j_{\max} = 2000$ grid with uniform increments in the x and t directions. I used *Mathematica* for the computation which took 62 seconds on my 3.4 GHz Intel Core i7 imac. In the 2007 JPP paper, reference [1], a higher order scheme was used on a much coarser grid.

A couple of features in Figure 11.16 (a) should be mentioned. Due to the singularity in x in the denominator of the coupled equations, the radius and regression rate are infinite at

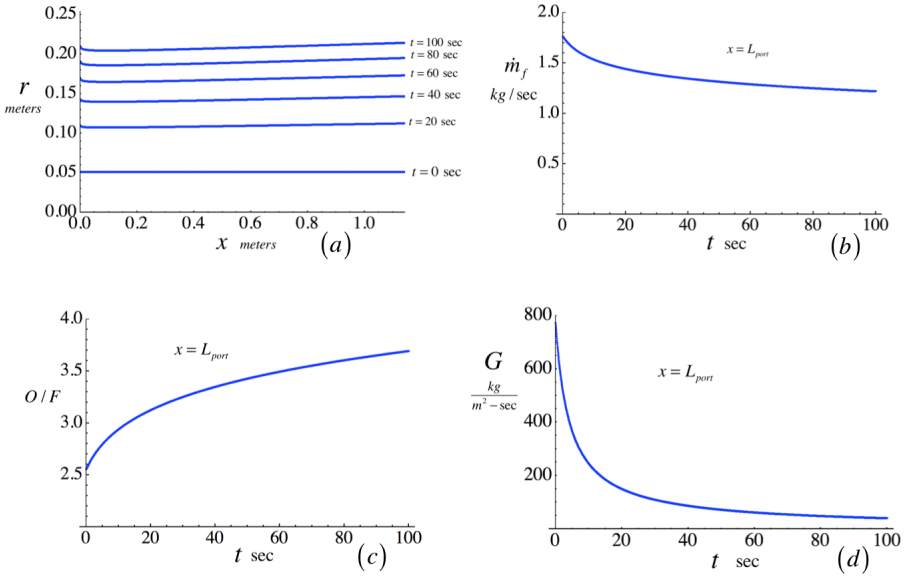

Figure 11.16: *Port functions during a 100 sec burn; (a) Port radius as a function of x at several times during the burn; (b) Fuel mass flow as a function of time at the downstream end of the port; (a) Oxidizer to fuel ratio as a function of time at the downstream end of the port; (b) Mass flux as a function of time at the downstream end of the port.*

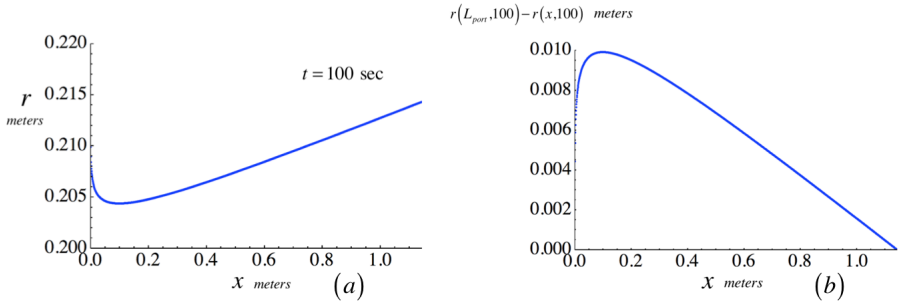

Figure 11.17: *Port functions during a 100 sec burn; (a) Close-up of the port radius function of x at the end of the burn; (b) Unburned fuel sliver at the end of the burn.*

$x = 0$. To avoid the singularity, the first numerical evaluation in x is at $x = L_{port}/i_{\max}$. The similarity solution described in the previous section can accurately resolve the solution near $x = 0$. There is a minimum in the port radius near the fore end of the port, the location of which depends on m. Beyond the minimum the port opens up slightly with the maximum radius occurring at the end of the port, a feature called "coning". Another important aspect of Figure 11.16 (a) is the slowing rate of increase in port radius with time as the burn progresses. This is reflected in Figure 11.16 (b) which depicts the decreasing rate of fuel generation as the port opens up, and in Figure 11.16 (c) which shows the corresponding increase in O/F ratio. For $n > 0.5$ the decrease in mass flux depicted in Figure 11.16 (d) dominates the increase in port surface area leading to a decrease in the fuel mass flow rate with time. A consequence of the increase in port radius with x is that when the burn ends, there is a sliver of fuel that remains unburned. This is shown in Figure 11.17 (a) and (b). One way to alleviate this in practice is to fabricate the initial port with a slight decrease in radius with x and a computation of this case is included in reference [1]. The required amount of decrease depends on the planned burn time.

11.7.6 Sensitivity of the coupled space-time problem to small changes in a, n, and m.

There is quite a bit of scatter in the data reported in the literature for the values of the regression rate parameters even for the same propellant combinations. It is of interest therefore to see how sensitive the regression rate is to small changes in the parameters a, n, and m. Let the parameters be changed by small amounts.

$$\begin{aligned} a &\rightarrow aa' \\ n &\rightarrow n + n' \\ m &\rightarrow m + m' \end{aligned} \tag{11.29}$$

The regression rate equations become

$$\begin{aligned} \frac{\partial r\left(x,t\right)}{\partial t} &= \frac{aa'}{x^{m+m'}}\left(\frac{\dot{m}_{port}\left(x,t\right) + \Delta\dot{m}_{ox}\left(t\right)}{\pi r^2}\right)^{n+n'} \\ \frac{\partial \dot{m}_{port}\left(x,t\right)}{\partial x} &= \rho_f\left(2\pi r\right)\frac{\left(aa'\right)}{x^{m+m'}}\left(\frac{\dot{m}_{port}\left(x,t\right) + \Delta\dot{m}_{ox}\left(t\right)}{\pi r^2}\right)^{n+n'}. \end{aligned} \tag{11.30}$$

The ratio of the disturbed to undisturbed regression rate and mass flow rate is

$$\frac{\frac{\partial R}{\partial \tau}}{\frac{\partial R}{\partial \tau}\Big|_{(n',m')=(0,0)}} = \frac{\frac{\partial J}{\partial \chi}}{\frac{\partial J}{\partial \chi}\Big|_{(n',m')=(0,0)}} = \left(\frac{a'\pi^{n'}}{r(0,0)^{m'}}\left(\frac{\dot{m}_{ox}(0)}{\pi r(0,0)^2}\right)^{n'}\right)\frac{1}{(\chi)^{m'}}\left(\frac{J+\lambda}{\pi R^2}\right)^{n'} \tag{11.31}$$

The relative error in both rates is the same. Notice that a and a' do not have the same units and that a' is a number close to one.

$$\begin{aligned}[a] &= \frac{L^{2n+m+1}T^{n-1}}{M^n} \\ [a'] &= \frac{L^{2n'+m'}T^{n'}}{M^{n'}}\end{aligned} \tag{11.32}$$

For small changes in n and m, and values of a' very close to one we can approximate Equation (11.31) as

$$\begin{aligned}&\frac{\frac{\partial R}{\partial \tau}}{\frac{\partial R}{\partial \tau}\Big|_{(n',m')=(0,0)}} = \frac{\frac{\partial J}{\partial \chi}}{\frac{\partial J}{\partial \chi}\Big|_{(n',m')=(0,0)}} \cong \\ &1 + n'\left\{Ln\left(\frac{(a')^{1/n'}\pi}{r(0,0)^{m'/n'}}\left(\frac{\dot{m}_{ox}(0)}{\pi r(0,0)^2}\right)\right) + Ln\left(\frac{J+\lambda}{(\chi)^{m'/n'}\pi R^2}\right)\right\}\end{aligned} \tag{11.33}$$

The first term in (11.33) in brackets is a fixed number and, to a good approximation, is the logarithm of π times the initial flux in the port, typically a number in the range 5 to 8. The second term in brackets is approximately the logarithm of the dimensionless flux in the port and depends on space and time. The dimensionless flux is generally less than one so this factor tends to be negative except near the port entrance. For $m = 0$ the second factor is approximately $Ln(1/\pi) = -1.14$. In general, small changes in n change the rates substantially more than comparable changes in a or m. Figure 11.18 shows the sensitivity to small changes in n for the 100 second run considered in the last section.

References

1) Karabeyoglu, M. A., B. J. Cantwell, and G. Zilliac 2005. Development of Scalable Space-time Averaged Regression Rate Expressions for Hybrid Rockets, AIAA 2005-3544, 41st Joint Propulsion Conference, p.1-21 also Journal of Propulsion and Power, Vol. 23, No. 4 (2007), pp. 737-747. doi: 10.2514/1.19226

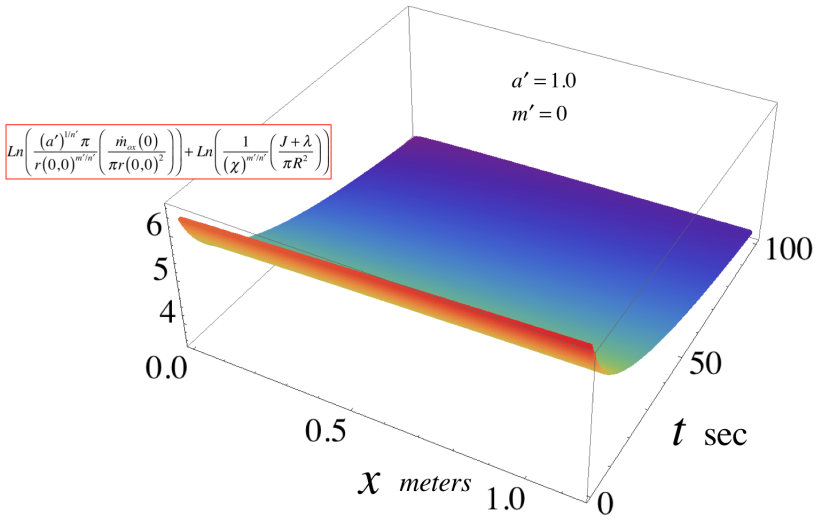

Figure 11.18: *For the example considered in the previous section, sensitivity of the regression rate and mass flow rate to small changes in the exponent n for $a' = 1$ and $m' = 0$.*

2) Cantwell, B. J., 2014 Similarity solution of fuel mass transfer, port mass flux coupling in hybrid propulsion, *Journal of Engineering Mathematics* (ISSN 0022 - 0833) (2014) 84:19-40. *J. Eng Math* (ISSN 1573 - 2703) DOI 10.1007/s10665-013-9624-y.This paper can also be found on my website.

11.8 Problems

Problem 1 - The thrust versus time history of a hybrid rocket with a circular port is shown in Figure 11.19. The oxidizer mass flow rate is constant during the burn. The regression rate of the fuel surface follows a law of the form

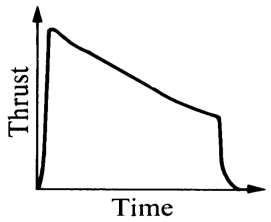

Figure 11.19: *Typical thrust time history of a single circular port hybrid rocket.*

$$\dot{r} = \alpha G^n \tag{11.34}$$

where the exponent n is in the range of 0.6 to 0.8 and G is the mass flux in the port. Briefly discuss why the thrust tends to decrease over the course of the burn. How would the thrust vary if the exponent was less than 0.5?

Problem 2 - A research project at NASA Ames called Peregrine has the goal of launching a fairly large sounding rocket to an altitude of 100 km from NASA Wallops. The current design uses a paraffin - N_2O hybrid rocket motor that operates with a nozzle throat diameter of 10 cm and a nozzle exit diameter of 30 cm. The motor has a cylindrical port and the fuel grain is 143 cm long. At the beginning of the burn the N_2O mass flow is 24.0 kg/sec, and the port diameter is 23.3 cm. The diameter at the end of the port and the end of the burn is 38 cm. Assume that the mass flow rate of the N_2O is constant over the burn. The regression rate law in mks units is

$$\dot{r} = 14.84 \times 10^{-5} G^{0.5} \, m/\sec . \tag{11.35}$$

The paraffin density is 924.5 kg/m^3. The chemical formula of the paraffin used is $C_{32}H_{66}$ and the heat of formation is 698.52 $kJ/mole$.

1) Determine port diameter as a function of x at the end of the burn. How long is the burn? Assume the outer diameter of the fuel grain is constant and matches the port diameter at the end of the port at the end of the burn. What is the mass of unburned fuel?

2) Determine the mass flow rate and O/F ratio at the end of the port.

3) Determine the chamber pressure.

4) Plot the sea level thrust-time history of the motor and estimate the total delivered impulse (the integral of the thrust time curve). Use CEA to determine the specific impulse, C^* and the nozzle exit pressure.

Problem 3 - A paraffin-oxygen hybrid rocket operates in a vacuum with a 10 cm diameter nozzle throat and a nozzle area ratio of 70. The motor has a cylindrical port 300 cm long. At the beginning of the burn the port is 20 cm in diameter and $O/F = 2.3$. The port diameter at the end of the burn is 60 cm. The regression rate law is

$$\dot{r} = 9.27 \times 10^{-5} G^{0.62} \, m/\sec . \tag{11.36}$$

The fuel density is 924.5 kg/m^3 and the combustion gas has $\gamma = 1.15$ and average molecular weight equal to 30. Assume the oxidizer flow rate is constant and the combustion cham-

ber temperature remains constant over the course of the burn. Approximate the specific impulse by a mean value of 360 sec over the course of the burn.

1) Estimate the chamber pressure at the beginning of the burn.

2) Plot the diameter of the port as a function of time.

3) Plot the thrust-time history of the burn and estimate the total delivered impulse (the integral of the thrust time curve).

4) Use Figure 11.4 to estimate the specific impulse at the end of the burn.

Problem 4 - A hybrid rocket with an initial mass of $m_{initial} = 900\,kg$ operates in space. The fuel is paraffin with a density $0.93\,gm/cm^3$ and the oxidizer is nitrous oxide. The oxidizer mass flow rate is held fixed at $2.4 \times 10^4\,gm/sec$. The motor has a $10\,cm$ diameter nozzle throat, $30\,cm$ diameter exit, and a cylindrical port $143\,cm$ long. The initial port radius is $8.75\,cm$. At the end of the burn the port radius is $15.5\,cm$. The regression rate law is $\dot{r} = 0.035 G_o^{0.6}\,cm/\sec$. A calculation using CEA shows that $c^* = 1.64 \times 10^5\,cm/\sec$ where C^* is defined by $\dot{m} = P_{t2}A^*/C^*$ and the effective nozzle exit velocity is $C = 2.8 \times 10^5\,cm/sec$.

1) When the fuel is all burned the oxidizer flow is turned off. Determine the time when this occurs.

2) Determine the total mass flow rate and motor thrust at the beginning and end of the burn.

3) Determine the chamber pressure at the beginning and end of the burn.

4) Determine the velocity change of the vehicle.

Appendix A

Thermochemistry

A.1 Thermochemical tables

In Chapter 9 we developed the theory for determining the equilibrium composition of a mixture of reacting gases. The procedure requires knowledge of the standard Gibbs free energy for each molecule in the mixture

$$g_i^\circ(T) = \Delta h_{fi}^\circ(T_{ref}) + \{h_i^\circ(T) - h_i^\circ(T_{ref})\} - Ts_i^\circ(T) \tag{A.1}$$

where $\Delta h_{fi}^\circ(T_{ref})$ is the standard heat of formation of the ith chemical species at some reference temperature, $\{h_i^\circ(T) - h_i^\circ(T_{ref})\}$ is the change in the standard enthalpy from the reference temperature and $s_i^\circ(T)$ is the standard entropy. Data for these variables for a given chemical species can be found in tabulations of thermochemical properties that have been developed from experimental measurements of heat capacity over many decades. The purpose of this appendix is to describe the tables, explain the data and connect thermodynamic properties of gases to the chemical bonds between the atoms that make up the gas. Perhaps the most widely used thermochemical data is from the compilation produced by the JANAF (Joint Army, Navy, Air Force) Committee. Parts of the JANAF tables for monatomic and diatomic hydrogen are shown in Figure A.1.

All quantities are quoted on a per mole basis and in units of Joules and degrees Kelvin. One mole is an Avagadros number, 6.0221415×10^{23}, of molecules. In the table headings in Figure A.1 properties are symbolized using capital letters, whereas, we have adopted the convention that all intensive (per unit mass or per unit mole) variables are denoted with lower case letters as in (A.1) and we will stick to that convention. Full tables for a variety of chemical species are provided in Appendix B.

Hydrogen (H_2), ideal gas-reference state, mol. wt. = 2.01588

Enthalpy Reference Temperature = T_r = 298.15 K — Standard State Pressure = p^0 = 0.1 MPa

T/K	C_p^0	S^0	$-(G^0-H^0(T_r))/T$	$H^0-H^0(T_r)$	$\Delta_f H^0$	$\Delta_f G^0$	Log K_f
	J K^{-1}mol^{-1}			kJ mol^{-1}			
0	0.	0.	INFINITE	-8.467	0.	0.	0.
100	28.154	100.727	155.408	-5.468	0.	0.	0.
200	27.447	119.412	133.284	-2.774	0.	0.	0.
250	28.344	125.640	131.152	-1.378	0.	0.	0.
298.15	28.836	130.680	130.680	0.	0.	0.	0.
300	28.849	130.858	130.680	0.053	0.	0.	0.
350	29.081	135.325	131.032	1.502	0.	0.	0.
400	29.181	139.216	131.817	2.959	0.	0.	0.
450	29.229	142.656	132.834	4.420	0.	0.	0.
500	29.260	145.737	133.973	5.882	0.	0.	0.
600	29.327	151.077	136.392	8.811	0.	0.	0.
700	29.441	155.606	138.822	11.749	0.	0.	0.
800	29.624	159.548	141.171	14.702	0.	0.	0.
900	29.881	163.051	143.411	17.676	0.	0.	0.
1000	30.205	166.216	145.536	20.680	0.	0.	0.
1100	30.581	169.112	147.549	23.719	0.	0.	0.
1200	30.992	171.790	149.459	26.797	0.	0.	0.
1300	31.423	174.288	151.274	29.918	0.	0.	0.
1400	31.861	176.633	153.003	33.082	0.	0.	0.
1500	32.298	178.846	154.652	36.290	0.	0.	0.
1600	32.725	180.944	156.231	39.541	0.	0.	0.
1700	33.139	182.940	157.743	42.835	0.	0.	0.
1800	33.537	184.846	159.197	46.169	0.	0.	0.
1900	33.917	186.669	160.595	49.541	0.	0.	0.
2000	34.280	188.418	161.943	52.951	0.	0.	0.

Hydrogen, Monatomic (H), ideal gas, mol. wt. = 1.00794

Enthalpy Reference Temperature = T_r = 298.15 K — Standard State Pressure = p^0 = 0.1 MPa

T/K	C_p^0	S^0	$-(G^0-H^0(T_r))/T$	$H^0-H^0(T_r)$	$\Delta_f H^0$	$\Delta_f G^0$	Log K_f
	J K^{-1}mol^{-1}			kJ mol^{-1}			
0	0.	0.	INFINITE	-6.197	216.035	216.035	INFINITE
100	20.786	92.009	133.197	-4.119	216.614	212.450	-110.972
200	20.786	106.417	116.618	-2.040	217.346	208.004	-54.325
250	20.786	111.055	115.059	-1.001	217.687	205.829	-42.964
298.15	20.786	114.716	114.716	0.	217.999	203.278	-35.613
300	20.786	114.845	114.717	0.038	218.011	203.186	-35.378
350	20.786	118.049	114.970	1.078	218.326	200.690	-29.951
400	20.786	120.925	115.532	2.117	218.637	198.150	-25.876
450	20.786	123.273	116.259	3.156	218.946	195.570	-22.701
500	20.786	125.463	117.072	4.196	219.254	192.957	-20.158
600	20.786	129.253	118.796	6.274	219.868	187.640	-16.335
700	20.786	132.457	120.524	8.353	220.478	182.220	-13.597
800	20.786	135.232	122.193	10.431	221.080	176.713	-11.536
900	20.786	137.681	123.781	12.510	221.671	171.132	-9.932
1000	20.786	139.871	125.282	14.589	222.248	165.485	-8.644
1100	20.786	141.852	126.700	16.667	222.807	159.782	-7.587
1200	20.786	143.660	128.039	18.746	223.346	154.028	-6.705
1300	20.786	145.324	129.305	20.824	223.865	148.230	-5.956
1400	20.786	146.865	130.505	22.903	224.361	142.394	-5.313
1500	20.786	148.299	131.644	24.982	224.836	136.522	-4.754
1600	20.786	149.640	132.728	27.060	225.289	130.620	-4.264
1700	20.786	150.900	133.760	29.139	225.721	124.689	-3.831
1800	20.786	152.088	134.745	31.217	226.132	118.734	-3.446
1900	20.786	153.212	135.686	33.296	226.523	112.757	-3.100
2000	20.786	154.278	136.591	35.375	226.898	106.760	-2.788

Figure A.1: *JANAF data for diatomic and monatomic hydrogen in the temperature range from* $0K$ *to* $2000K$*. The full tabulation runs to* $6000K$*.*

A.2 Standard pressure

Conservation of energy for a system containing some substance is expressed as the First Law of thermodynamics.

$$\delta q = de + PdV \tag{A.2}$$

The enthalpy is defined as

$$h = e + PV. \tag{A.3}$$

If we use (A.3) to replace the internal energy in (A.2) the result is an equivalent form of the first law expressed in terms of the enthalpy

$$\delta q = dh - VdP. \tag{A.4}$$

The internal energy e and enthalpy h are related to the temperature, pressure and volume of the system through the definitions of the specific heats.

$$\begin{aligned} C_V &= \left.\frac{\partial e}{\partial T}\right|_{Volume} \\ C_P &= \left.\frac{\partial e}{\partial T}\right|_{Pressure} \end{aligned} \tag{A.5}$$

For a process that takes place at constant pressure, the heat added or removed from the system is given by the change of enthalpy.

$$\delta q|_{P=constant} = dh|_{P=constant} = C_P dT \tag{A.6}$$

It is probably fair to say that the use of the tables of thermochemical properties is dominated by applications to mixtures of reacting gases typical of combustion at elevated temperatures. As long as the pressure is not extreme, and the system is not near a phase boundary, the equation of state for each gas in the mixture is the ideal gas law

$$P_i V = n_i R_u T \tag{A.7}$$

where n_i is the number of moles of the ith component of the mixture, P_i is the partial pressure and V is the volume of the mixture. The universal gas constant is

$$R_u = 8.314510\, J/mole - K. \tag{A.8}$$

For a general substance the heat capacity, enthalpy, entropy and Gibbs potential are functions of temperature and pressure.

$$\begin{array}{l} C_P\,(T,P) \\ h\,(T,P) \\ s\,(T,P) \\ g\,(T,P) \end{array} \tag{A.9}$$

For any substance that follows the ideal gas law equation of state, the heat capacities, internal energy and enthalpy are independent of pressure and the entropy and Gibbs free energy depend in a known way on the logarithm of the pressure. It therefore makes sense to standardize all thermochemical data at a standard pressure rather than, say, at standard volume.

The thermodynamic properties of a substance, whether it is an ideal gas or not, are always tabulated as a function of temperature at standard pressure. That the data is tabulated this way is indicated by the "$^\circ$" superscript that appears with each symbol in the tables. In various units, the standard pressure we will use in this course is

$$P^\circ = 10^5\, N/m^2 = 10^5\, Pascals = 100\, kPa = 1 bar. \tag{A.10}$$

The various thermodynamic variables for any species at standard pressure are denoted by

$$\begin{array}{l} C_P\left(T,100\right)=C_P^{\circ}\left(T\right) \\ h\left(T,P\right)=h^{\circ}\left(T\right) \\ s\left(T,P\right)=s^{\circ}\left(T\right) \\ g\left(T,P\right)=g^{\circ}\left(T\right). \end{array} \tag{A.11}$$

The standard pressure is very close to one atmosphere $1atm = 1.01325 \times 10^5\, Pa$ and indeed before 1982 the standard was atmospheric pressure at sea level. In 1982 the International Union of Pure and Applied Chemistry (IUPAC) recommended that for the purposes of specifying the physical properties of substances the standard pressure should be defined as precisely $100\, kPa$. This had the immediate effect of simplifying thermochemical calculations and the practical effect of specifying the standard pressure to be closer to the actual average altitude above sea level where most people around the world live.

A.2.1 What about pressures other than standard?

For substances in their gaseous state at elevated temperatures where the ideal gas law applies and the heat capacities, energy and enthalpy are independent of pressure the enthalpy is simply

$$h\left(T,P\right)=h^{\circ}\left(T\right)=\Delta h_f\left(298.15\right)+\int_{T_{ref}}^{T}C_P^{\circ}\left(T\right)dT. \tag{A.12}$$

The entropy is

$$s\left(T,P\right)=\int_{T_{ref}}^{T}C_P^{\circ}\left(T\right)\frac{dT}{T}-R_uLn\left(\frac{P}{100}\right)=s^{\circ}\left(T\right)-R_uLn\left(\frac{P}{100}\right) \tag{A.13}$$

and the Gibbs free energy is determined from the definition

$$g\left(T,P\right)=h-Ts=h^{\circ}\left(T\right)-Ts^{\circ}\left(T\right)+\left(R_uT\right)Ln\left(\frac{P}{100}\right)=g^{\circ}\left(T\right)+\left(R_uT\right)Ln\left(\frac{P}{100}\right). \tag{A.14}$$

In principle, the standard entropy requires an integration of the heat capacity from absolute zero.

A.2.2 Equilibrium between phases

For a liquid in equilibrium with its vapor the Gibbs free energy of the liquid is equal to the Gibbs free energy of the vapor.

$$g_{liquid}(T,P) = g_{gas}(T,P) \tag{A.15}$$

In terms of the definition of the Gibbs free energy

$$h_{liquid}(T,P) - Ts_{liquid}(T,P) = h_{gas}(T,P) - Ts_{gas}(T,P). \tag{A.16}$$

Differentiate (A.16).

$$dh_{liquid}(T,P) - Tds_{liquid}(T,P) - s_{liquid}(T,P)\,dT = dh_{gas}(T,P) - Tds_{gas}(T,P) - s_{gas}(T,P)\,dT \tag{A.17}$$

The Gibbs equation is

$$\begin{aligned} Tds_{liquid}(T,P) &= dh_{liquid}(T,P) - v_{liquid}dP \\ Tds_{gas}(T,P) &= dh_{gas}(T,P) - v_{gas}dP \end{aligned} \tag{A.18}$$

where $v = V/n$ is the molar density of the substance. Substitute (A.18) into (A.17). The result is

$$v_{liquid}dP - s_{liquid}dT = v_{gas}dP - s_{gas}dT. \tag{A.19}$$

With a little bit of rearrangement (A.19) becomes

$$\frac{dP}{dT} = \frac{s_{gas} - s_{liquid}}{v_{gas} - v_{liquid}}. \tag{A.20}$$

The heat required to convert a mole of liquid to gas at constant temperature is called the latent heat of vaporization. From (A.16)

$$\Delta h_{vap} = h_{gas} - h_{liquid} = T(s_{gas} - s_{liquid}). \tag{A.21}$$

If we substitute (A.21) into (A.20) the result is the famous Clausius-Clapeyron equation

$$\frac{dP}{dT} = \frac{\Delta h_{vap}}{T\left(v_{gas} - v_{liquid}\right)} \tag{A.22}$$

that relates the vapor pressure of a gas-liquid system to the temperature. Generally the temperature of the system is specified and the vapor pressure is to be determined. In some cases the condensed phase is a solid such as the graphite form of carbon or solid iodine sublimating directly from the solid to the vapor phase.

In the case of a solid in equilibrium with its liquid such as water and ice, the Gibbs free energies of the solid and liquid phases are equal and a similar relation governs the transition between phases. The enthalpy change is called the latent heat of fusion. In a solid-liquid system, usually the pressure is the specified condition and the temperature of melting is the property to be determined.

The heat of vaporization depends on the temperature according to

$$\begin{array}{l} h_{gas}\left(T\right) = h_{gas}\left(T_{ref}\right) + C_{P_{gas}}\left(T - T_{ref}\right) \\ h_{liquid}\left(T\right) = h_{liquid}\left(T_{ref}\right) + C_{P_{liquid}}\left(T - T_{ref}\right) \\ \Delta h_{vap}\left(T\right) = \Delta h_{vap}\left(T_{ref}\right) + \left(C_{P_{gas}} - C_{P_{liquid}}\right)\left(T - T_{ref}\right). \end{array} \tag{A.23}$$

Generally speaking the heat capacity term is relatively small for modest changes in temperature. For example, for water between its freezing and boiling point

$$\begin{array}{l} \Delta h_{vap}\left(273.15\,K\right) = \Delta h_{vap}\left(373.15\,K\right) + \left(33 - 75\right)\left(-100\right) \\ = 40.65\,kJ/mole + 4.20\,kJ/mole = 44.85\,kJ/mole. \end{array} \tag{A.24}$$

If the effect of heat capacity differences on the latent heat of vaporization is neglected, and the liquid molar volume is much smaller than the gas, and the gas follows the ideal gas law, then (A.22) can be integrated to give

$$\frac{P}{P_{ref}} = e^{-\frac{\Delta h_{vap}\left(T_{ref}\right)}{Ru}\left(\frac{1}{T} - \frac{1}{T_{ref}}\right)}. \tag{A.25}$$

The reference temperature and pressure are generally taken at the boiling point where the vapor pressure equals the gas pressure.

The Clausius -Clapeyron equation provides a direct connection between the temperature of a mixture of gases and the partial pressure of any constituent that is in equilibrium with its condensed phase.

In order to determine the heat capacity and enthalpy of a substance at conditions where pressure effects do apply, either in its condensed state or in a gaseous state close to the vaporization temperature at some given pressure, an equation of state is needed in order to evaluate $h(T,P) = e(T,P) + PV$. The heat capacities are determined using the definitions in (A.5). Generally the effect of pressure on the heat capacities of most liquids and solids is well understood and relatively small.

A.2.3 Reference temperature

The standard enthalpy of a species is usually tabulated as the difference between the standard enthalpy at a given temperature and the standard enthalpy at a reference temperature. In this course, and in most combustion applications, the reference temperature is taken to be $298.15\,K$ and this temperature is indicated in the headings of the tables shown in Figure A.1. The enthalpy of a species is expressed as

$$h^\circ(T) = h^\circ(298.15) + \{h^\circ(T) - h^\circ(298.15)\}. \tag{A.26}$$

This seemingly trivial representation of the enthalpy in (A.26) is explained in the next two sections.

A.3 Reference reaction and reference state for elements

The thermochemical tables are designed to enable one to analyze systems of reacting gases and condensed materials. To facilitate this, the enthalpy of a substance is defined to include the energy contained in the chemical bonds that hold together the various atoms that compose the substance. This leads to the concept of a *reference reaction* for a substance, the corresponding reference state for the elements that make up the substance, and the heat of formation for the substance.

The *reference reaction* for a given substance is the reaction in which the substance is created from its elements when those elements are in their reference state. The reference state for elements is always taken to be the thermodynamically stable state of the element at the standard temperature $298.15\,K$. For elements that are gases at $298.15\,K$ and $100\,kPa$ the reference state is taken by convention to be gaseous over the entire range of temperatures from $0\,K$ up to the highest temperature tabulated (typically $6000\,K$). For elements that are condensed at $298.15\,K$ such as metals like aluminum or titanium, the reference state is taken to be the element in its condensed state over the entire temperature range.

The great advantage of using a reference temperature of $25\,C$ close to room temperature is that, for applications at elevated temperature the enthalpy can be determined by integrating the heat capacity from the reference temperature without having to address the complexities of a given substance at low temperature. A choice of, say, $0\,K$ for the reference temperature would not offer this same convenience. For the analysis of systems at low temperature such as the cryogenic liquids used in rocket propulsion applications the tables are not very useful since the heat capacity data and enthalpy are often not provided below $100\,K$. Often the best source of data in this range is from the commercial suppliers of the liquid.

A.4 The heat of formation

The enthalpy (heat) of formation of a substance is defined as the enthalpy change that occurs when the substance is formed from its elements in their reference state at temperature T and standard pressure P° and is denoted

$$\Delta h_f^\circ(T) \tag{A.27}$$

A consequence of this definition is that the heat of formation of a pure element in its reference state at any temperature is always zero. For example, the enthalpy of formation of any of the diatomic gases is zero at all temperatures. This is clear when we write the (trivial) reaction to form H_2 from its elements in their reference state as

$$H_2 \rightarrow H_2. \tag{A.28}$$

The enthalpy change is clearly zero. In fact the change in any thermodynamic variable for any element in its reference state is zero at all temperatures. This is the reason for all the zeros in the last three columns in the left data set in Figure A.1. A similar reference reaction applies to any of the other diatomic species O_2, N_2, F_2, Cl_2, Br_2, I_2, etc and the heat of formation of these elements is zero at all temperatures.

The most stable form of carbon is solid carbon or graphite and the reference reaction is

$$C_{solid} \rightarrow C_{solid} \tag{A.29}$$

with zero heat of formation at all temperatures. The heat of formation of crystalline aluminum is zero at temperatures below the melting point, and the heat of formation of

liquid aluminum is zero at temperatures above the melting point. The same applies to Boron, Magnesium, Sulfur, Titanium, and other metals.

The enthalpy of a substance is tied to its heat of formation by the equality

$$h^\circ\left(298.15\right) = \Delta h_f^\circ\left(298.15\right). \tag{A.30}$$

Using (A.30) in (A.26), the standard enthalpy of a substance is expressed as

$$h^\circ\left(T\right) = \Delta h_f^\circ\left(298.15\right) + \left\{h^\circ\left(T\right) - h^\circ\left(298.15\right)\right\}. \tag{A.31}$$

The two terms in (A.31) are the quantities that are tabulated.

A.4.1 Example - heat of formation of monatomic hydrogen at 298.15 K and at 1000 K.

The heat of formation of atomic hydrogen at $298.15\,K$ is by definition the enthalpy change of the reference reaction.

$$\left.\frac{1}{2}H_2\right|_{gas\,@\,298.15\,K} \rightarrow \left.H\right|_{gas\,@\,298.15\,K} \tag{A.32}$$

Using the data in Figure A.1, the enthalpy change for (A.32) is

$$\begin{aligned}
&\Delta h_f^\circ\left(298.15\right)\big|_H = \\
&\Delta h_f^\circ\left(298.15\right)\big|_H - \frac{1}{2}\Delta h_f^\circ\left(298.15\right)\big|_{H_2\ in\ its\ reference\ state} = \\
&217.999 - \frac{1}{2}\left(0\right) = \\
&217.999\,kJ/mole\ of\ H\ formed.
\end{aligned} \tag{A.33}$$

The positive heat of formation of (A.33) indicates that the heat is absorbed in the process and the reaction is said to be endothermic. The conceptual physical process that is invisioned by these calculations is illustrated in Figure A.2. The emphasis here is on the word conceptual. This is not an experiment that actually could be performed since the reactivity of monatomic hydrogen is so strong that it would be impossible to stabilize the gas depicted in state 2 at room temperature. However that does not stop us from analyzing the energetics of such a reaction.

The appearance of the term $\Delta h^{\circ}_{f_H}(298.15)$ on both sides of (A.33) should not cause too much concern. It is just a reminder of the fact that for any reference reaction the heats of formation of the reactants are always zero by definition.

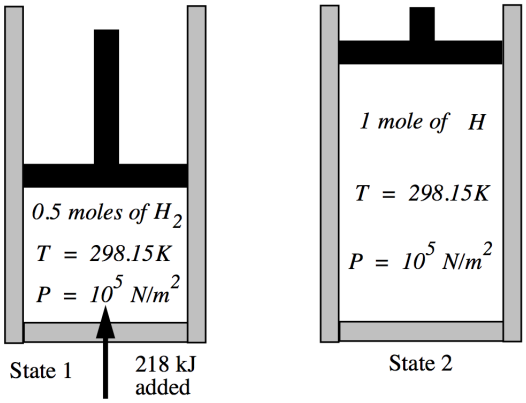

Figure A.2: *Dissociation of diatomic hydrogen to produce monatomic hydrogen by the addition of heat.*

Now lets use the heat capacity data in Figure A.1 to determine the heat of formation of atomic hydrogen at $1000\,K$. We need the data from the tables in Figure A.1 for the enthalpy change from the reference temperature to carry out the calculation at the new temperature. The reference reaction is still

$$\frac{1}{2}H_2\Big|_{gas@1000\,K} \rightarrow H|_{gas@1000\,K} \tag{A.34}$$

and the enthalpy balance is

$$\begin{aligned}
&\Delta h^{\circ}_f(1000)\big|_H = \\
&\left(\Delta h^{\circ}_f(298.15)\big|_H + \{h^{\circ}(1000) - h^{\circ}(298.15)\}|_H\right) - \\
&\frac{1}{2}\left(\Delta h^{\circ}_f(298.15)\big|_{H_2} + \{h^{\circ}(1000) - h^{\circ}(298.15)\}|_{H_2}\right) = \\
&(217.999 + 14.589) - \frac{1}{2}(0 + 20.680) = \\
&222.248\,kJ/mole\,of\,H\,formed.
\end{aligned} \tag{A.35}$$

The somewhat higher value than that calculated in (A.33) comes from the larger volume change that occurs when the number of moles is doubled at $1000\,K$ versus doubling the number of moles at $298.15\,K$.

A.4.2 Example - heat of formation of gaseous and liquid water

In this case the reference reaction is

$$H_2 + \frac{1}{2}O_2 \rightarrow H_2O|_{gas}. \tag{A.36}$$

Using the data for gaseous water in Appendix B, the enthalpy balance is

$$\begin{aligned}
&\Delta h_f^\circ\,(298.15)\big|_{H_2O} = \\
&\Delta h_f^\circ\,(298.15)\big|_{H_2O} - \\
&\left(\frac{1}{2}\,\Delta h_f^\circ\,(298.15)\big|_{O_2 in\ its\ reference\ state} + \Delta h_f^\circ\,(298.15)\big|_{H_2\ in\ its\ reference\ state}\right) = \\
&-241.826 - \frac{1}{2}\,(0) - (0) = \\
&-241.826\,kJ/moles\,of\,H_2O\,formed.
\end{aligned} \tag{A.37}$$

Figure A.3 below depicts one possible experiment that would be used to measure this heat of formation.

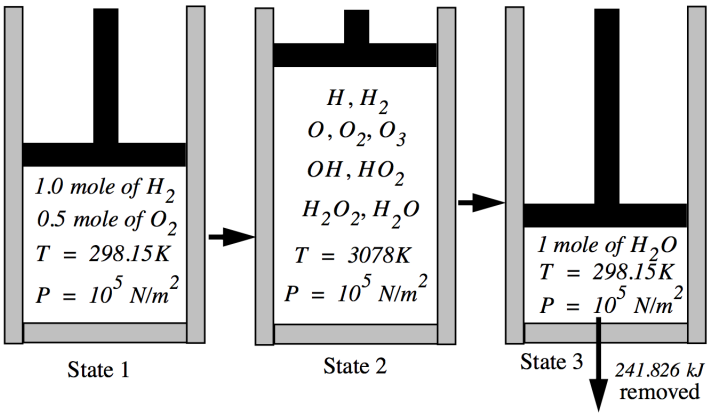

Figure A.3: *Reference reaction for (gaseous) water.*

Half a mole of diatomic oxygen and one mole of diatomic hydrogen are placed in an adiabatic piston-cylinder combination. The two will not react spontaneously and so a small source of ignition is needed to exceed the threshold energy to start the reaction. Once the reaction proceeds, the chemical energy contained in the chemical bonds of the reactants is released and a mixture of gases at a temperature of 3078 K results. The piston is withdrawn to keep the pressure constant during the reaction. The mixture contains atoms

and molecules that essentially represent all the reasonable combinations of H and O that one could conceive although more complex molecules such as H_2O_2 and O_3 would only be present in extremely low concentrations. More complex molecules, though possible in principle, are too unlikely to be worth considering.

Sufficient heat is removed and the piston is compressed to bring the mixture back to the original temperature and pressure. In the process the various molecules and atoms in the mixture combine to form gaseous water which is the most stable molecule with the lowest Gibbs free energy. State 3 in Figure A.3 is assumed to be pure water vapor. The water vapor in state 3 is not stable but will tend to condense to form liquid water in equilibrium with its vapor. This is really the lowest Gibbs free energy state of the system.

The last step in the process is illustrated in Figure A.4. The water vapor condenses to liquid water. At a temperature of $298.15\,K$ the vapor pressure of the liquid is much lower than the pressure of the system and since the system is closed with no possible mixing of outside gas with the vapor virtually all the water vapor must condense to form liquid.

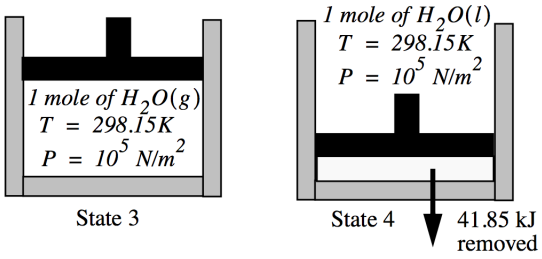

Figure A.4: *Condensation of water vapor to liquid at constant pressure.*

The reference reaction to form liquid water at the same temperature and pressure as the vapor is

$$H_2 + \frac{1}{2}O_2 \rightarrow H_2O|_{liquid} \qquad \Delta h_f^\circ\,(298.15) = -283.666\,kJ/mole. \tag{A.38}$$

Subtraction of (A.36) and (A.38) gives the heat released when steam condenses to form liquid water at the reference temperature.

$$\begin{aligned} &H_2 + \frac{1}{2}O_2 \rightarrow H_2O|_{liquid} \quad \Delta h_f^\circ\,(298.15) = -283.666\,kJ/mole \\ &minus \\ &H_2 + \frac{1}{2}O_2 \rightarrow H_2O|_{gas} \quad \Delta h_f^\circ\,(298.15) = -241.826\,kJ/mole \\ &equals \\ &H_2O|_{gas} \rightarrow H_2O|_{liquid} \quad \Delta h_f^\circ\,(298.15) = -41.840\,kJ/mole \end{aligned} \tag{A.39}$$

In practice the experimental measurement of the heat of formation would probably not be carried out in such a complex apparatus as a piston and cylinder but would be carried out at constant volume in a device called a bomb calorimeter. The amount of heat removed in the experiment would then be used to work out the heat that would have been released if the process were at constant pressure.

A.4.3 Example - combustion of hydrogen and oxygen diluted by nitrogen

Now lets look at an example where liquid water is produced in equilibrium with its vapor. We start with a mixture in state 1 of diatomic hydrogen, oxygen and nitrogen. A source of ignition is used to initiate the reaction and the mixture comes to state 2 at equilibrium at $2709\,K$. A fair amount of the nitrogen reacts to form NO and NO_2. As the mixture temperature is lowered these gases react leaving only trace amounts in the final mixture which is composed of approximately one mole of N_2 and one mole of water. The partial pressure of water vapor in the gas mixture is determined by the vapor pressure equation (A.40) repeated here for convenience.

$$\frac{P}{P_{ref}} = e^{-\frac{\Delta h_{vap}\left(T_{ref}\right)}{R_u}\left(\frac{1}{T}-\frac{1}{T_{ref}}\right)} \tag{A.40}$$

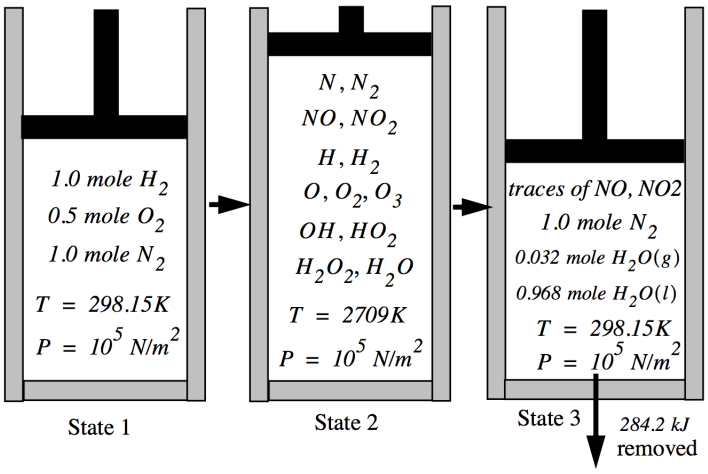

Figure A.5: *Hydrogen-oxygen combustion in the presence of nitrogen diluent.*

The heat of vaporization at the pressure and temperature of interest is, from (A.39), $\Delta h^{\circ}_{f_{H_2O}}\left(T_{ref}\right) = 41.84\,kJ/mole$. The reference temperature is the boiling temperature

$T_{ref} = 373.15\,K$ at the reference pressure of one atmosphere, $P^\circ = 1.0132 \times 10^5\,Pa$. The simplified solution of the Clausius-Clapeyron, Equation (A.40) gives the vapor pressure as

$$\frac{P}{1.0132 \times 10^5} = e^{-\frac{41.840 \times 10^3}{8.314510}\left(\frac{1}{298.15} - \frac{1}{373.15}\right)} = 0.03363 \tag{A.41}$$

corresponding to $n_{H_2O|_{gas}} = 0.035\,moles$ which is reasonably close to the more precise value of $0.032\,moles$ shown in Figure A.5 derived from the tables.

A.4.4 Example - combustion of methane

The heats of formation of various species can be used to evaluate the enthalpy released or absorbed during a reaction involving those species. From the data in Appendix B, the reference reactions to produce carbon dioxide and methane are

$$C|_{solid} + O_2 \rightarrow CO_2 \qquad \Delta h_f^\circ\,(298.15) = -393.510\,kJ/mole \tag{A.42}$$

and

$$C|_{solid} + 2H_2 \rightarrow CH_4 \qquad \Delta h_f^\circ\,(298.15) = -74.600\,kJ/mole \tag{A.43}$$

This data together with (A.36) and (A.38) can be used to evaluate the heat released by the combustion of methane with oxygen to form carbon dioxide and liquid water at $298.15\,K$. The reaction is

$$CH_4 + 2O_2 \rightarrow CO_2 + 2\,H_2O|_{liquid} \tag{A.44}$$

To produce (A.44) the algebra for the various reactions can be viewed as

$$\begin{array}{l} C|_{solid} + O_2 \rightarrow CO_2 \\ plus \\ 2 \times \left(H_2 + \frac{1}{2} O_2 \rightarrow H_2O|_{liquid} \right) \\ minus \\ C|_{solid} + 2H_2 \rightarrow CH_4 \\ minus \\ 2 \times (O_2 \rightarrow O_2) \\ equals \\ CH_4 + 2O_2 \rightarrow CO_2 + H_2O|_{liquid} \end{array} \tag{A.45}$$

and the algebra for the heats of formation is

$$\begin{array}{l} \Delta h^\circ (298.15)|_{reaction} = \\ \left(\Delta h_f^\circ (298.15)\big|_{CO_2} + 2 \times \Delta h_f^\circ (298.15)\big|_{H_2O|_{liquid}} \right) - \\ \left(\Delta h_f^\circ (298.15)\big|_{CH_4} + 2 \times \Delta h_f^\circ (298.15)\big|_{O_2} \right) = \\ -393.510 + 2(-283.666) - (-74.600) - 2(0) = \\ -886.242\, kJ/mole\, of\, CH_4\, burned. \end{array} \tag{A.46}$$

In general the reactants can be at different temperatures. Note that the reaction (A.45) is somewhat artificial in that, at equilibrium, there would actually be a small amount of water vapor mixed with the carbon dioxide and in equilibrium with the liquid water.

The general enthalpy balance for a reaction at standard pressure is

$$\Delta h^\circ (T_{final}) = \left(\sum_{i=1}^{I} n_i h_i^\circ (T_{final}) \right)_{products} - \left(\sum_{j=1}^{J} n_j h_j^\circ (T_j) \right)_{reactants} \tag{A.47}$$

where it is recognized that the products are mixed at the final temperature of the reaction. Equation (A.47) fully written out is

$$\begin{array}{l} \Delta h^\circ (T_{final}) = \\ \sum_{i=1}^{I} n_i \left(\Delta h_{f_i}^\circ (298.15) + \{ h_i^\circ (T_{final}) - h_i^\circ (298.15) \} \right) - \\ \sum_{j=1}^{J} n_j \left(\Delta h_{f_j}^\circ (298.15) + \left\{ h_j^\circ (T_j) - h_j^\circ (298.15) \right\} \right). \end{array} \tag{A.48}$$

For example, suppose in the methane-oxygen combustion problem above, the methane is initially at $600\,K$ and the oxygen is at $800\,K$ while the products are assumed to be at $1500\,K$. The heat of reaction is determined from

$$\begin{array}{l}\Delta h^{\circ}\left(1500\right) = \\ \left(\Delta h^{\circ}_{f_{CO_2}}\left(298.15\right) + \left\{h^{\circ}_{CO_2}\left(1500\right) - h^{\circ}_{CO_2}\left(298.15\right)\right\}\right) + \\ 2\left(\Delta h^{\circ}_{f_{H_2O|_{gas}}}\left(298.15\right) + \left\{h^{\circ}_{H_2O|_{gas}}\left(1500\right) - h^{\circ}_{H_2O|_{gas}}\left(298.15\right)\right\}\right) - \\ \left(\Delta h^{\circ}_{f_{CH_4}}\left(298.15\right) + \left\{h^{\circ}_{CH_4}\left(600\right) - h^{\circ}_{CH_4}\left(298.15\right)\right\}\right) - \\ 2\left(\Delta h^{\circ}_{f_{O_2}}\left(298.15\right) + \left\{h^{\circ}_{O_2}\left(800\right) - h^{\circ}_{O_2}\left(298.15\right)\right\}\right).\end{array} \tag{A.49}$$

The data is

$$\begin{array}{l}\Delta h^{\circ}\left(1500\right) = \\ \left(-393.510 + 61.705\right) + 2\left(-241.826 + 48.151\right) - \\ \left(-74.600 + 13.130\right) - 2\left(0 + 15.835\right) = \\ -689.355\,kJ/mole\,of\,CH_4\,burned.\end{array} \tag{A.50}$$

Somewhat less enthalpy is evolved compared to the enthalpy change at the reference temperature.

A.4.5 Example - the heating value of JP-4

In Chapter 2 a typical value of the fuel enthalpy for JP-4 jet fuel was given as

$$h_f|_{JP-4\,@\,298.15\,K} = 4.28 \times 10^7\,J/kg \tag{A.51}$$

although we never stated explicitly that this refers to the fuel and its products of combustion at a temperature of $298.15\,K$. Where does this number come from and how does it relate to the heat of formation of JP-4? According to CEA the effective molecular formula and heat of formation of JP-4 are

$$CH_{1.94} \qquad \Delta \mathrm{h}^{\circ}_{f}\left(298.15\right) = -22.723\,kJ/mole. \tag{A.52}$$

The reaction of this fuel with oxygen is

$$CH_{1.94} + 1.485O_2 \rightarrow CO_2 + 0.97H_2O \tag{A.53}$$

and the enthalpy released by the reaction is

$$\begin{array}{l}\Delta h^{\circ}\left(298.15\right) = \\ \left(\Delta h_f^{\circ}\left(298.15\right)\big|_{CO_2} + 0.97 \times \Delta h_f^{\circ}\left(298.15\right)\big|_{H_2O|_{gas}}\right) - \\ \left(\Delta h_f^{\circ}\left(298.15\right)\big|_{CH_{1.94}} + 1.485 \times \Delta h_f^{\circ}\left(298.15\right)\big|_{O_2}\right) = \\ -393.510 + 0.97\left(-241.826\right) - \left(-22.723\right) - 1.485\left(0\right) = \\ -605.358\, kJ/mole\ of\ CH_{1.94}\ burned.\end{array} \tag{A.54}$$

On a per mass basis the heating value is

$$h_f|_{JP-4\,@\,298.15\,K} = \frac{-605.358\, kJ/mole}{13.9664 \times 10^{-3}\, kg/mole} = -4.33 \times 10^7\, J/kg \tag{A.55}$$

which agrees closely with the accepted value (A.51). Notice the relatively small contribution of the actual enthalpy of formation of JP-4 to the calculation of the heat of reaction (A.54). Note also that the water formed in the reaction is taken to be in the gas phase and the values given in (A.51) and (A.55) are what would be called the *lower heating value* of JP-4. If the water is assumed to condense to its liquid phase in equilibrium with its vapor at $298.15K$ (see Figure A.5) , which of course it does, the enthalpy change is

$$\begin{array}{l}h_f|_{JP-4@298.15K} = \dfrac{-605.358 - 0.97 \times 0.968 \times 41.85}{13.9664 \times 10^{-3}} = \\ \dfrac{-644.653 kJ/mole}{13.9664 \times 10^{-3} kg/mole} = -4.62 \times 10^7 J/kg\end{array} \tag{A.56}$$

which would be called the *higher heating value*.

A.5 Heat capacity

The key piece of data needed for any species is its heat capacity. One of the most complete collections of such data can be found in the well known reference *NASA/TP - 2002-211556 - NASA Glenn Coefficients for Calculating Thermodynamic Properties of Individual Species* by Bonnie J. McBride, Michael J. Zehe, and Sanford Gordon, Glenn Research Center, Cleveland, Ohio. These authors provide accurate curve fits for the standard heat capacities, enthalpies and entropies of a vast range of species over the temperature range $200\,K$ to $6000\,K$.

The enthalpy change terms in (A.35) are

$$\begin{aligned} h_H^\circ(1000) - h_H^\circ(298.15) &= \int_{298.15}^{1000} C_{P_H}^\circ(T)\, dT \\ h_{H_2}^\circ(1000) - h_{H_2}^\circ(298.15) &= \int_{298.15}^{1000} C_{P_{H_2}}^\circ(T)\, dT. \end{aligned} \tag{A.57}$$

The molar heat gas capacities of both monatomic hydrogen and gaseous diatomic hydrogen are consistent with the classic formula from kinetic theory

$$C_P = \left(\frac{\beta+2}{2}\right) R_u \tag{A.58}$$

where β is the number of degrees of freedom of the gas molecular model. Atomic hydrogen is a gas at all temperatures with three translational degrees of freedom, $\beta = 3$ and one can expect that

$$C_{P_H}^\circ = \frac{5}{2} R_u = 20.786 J/(mole - K) \tag{A.59}$$

over a wide temperature range. That this is the case is clear from the right-hand table in Figure A.1. In fact, by convention, this value of the heat capacity of monatomic hydrogen is assumed valid up to $6000\,K$ which is the temperature at which the tables stop. Somewhat below this temperature the actual heat capacity of a gas of hydrogen atoms would begin to increase slightly as electronic degrees of freedom begin to be excited. The enthalpy change for monatomic hydrogen is

$$h_H^\circ(T) - h_H^\circ(298.15) = \frac{5}{2} R_u (T - 298.15) \tag{A.60}$$

which reproduces the tabulated data very well.

The number of degrees of freedom for diatomic hydrogen at room temperature is nominally $\beta = 5$ with three translational degrees of freedom and two rotational degrees. Kinetic theory (A.58) predicts

$$C_{P_{H_2}}^\circ = \frac{7}{2} R_u = 29.101 J/(mole - K)\,. \tag{A.61}$$

Actually the tabulated heat capacity is slightly less than this since the rotational degrees are not absolutely fully excited at room temperature.

As the gas is heated, vibrational degrees of freedom begin to come into play and the number increases to $\beta = 7$ at high combustion temperatures. Quantum statistical mechanics can be used to develop a theory for the onset of vibrational excitation. According to this theory, the specific heat of a diatomic gas from room temperature up to high combustion temperatures is accurately predicted by

$$\frac{C_P^\circ}{R_u} = \frac{7}{2} + \left\{ \frac{\theta_v/2T}{Sinh\left(\theta_v/2T\right)} \right\}^2 \tag{A.62}$$

where θ_v is the vibrational transition temperature for a given gas. Values of the vibrational transition temperature for several common diatomic species are presented in Figure A.6.

	θ_v K
H_2	6297
N_2	3354
O_2	2238
CO	3087

Figure A.6: *Vibrational transition temperature for several gases.*

The vibrational transition temperatures for common diatomic molecules are all at high combustion temperatures. Using the results of this theory, the standard enthalpy change of a diatomic gas heated to temperatures above room temperature can be expressed as

$$\begin{aligned} h^\circ\left(T\right) - h_H^\circ\left(298.15\right) = \int_{298.15}^{T} C_P^\circ\left(T\right) dT = \\ R_u \int_{298.15}^{T} \left(\frac{7}{2} + \left\{ \frac{\theta_v/2T}{Sinh\left(\theta_v/2T\right)} \right\}^2 \right) dT \end{aligned} \tag{A.63}$$

which integrates to

$$\begin{aligned} \frac{h^\circ\left(T\right) - h_H^\circ\left(298.15\right)}{R_u\left(T - 298.15\right)} = \\ \frac{7}{2} + \frac{\theta_v}{2\left(T - 298.15\right)} \left\{ Coth\left(\frac{\theta_v}{2T}\right) - Coth\left(\frac{\theta_v}{2\left(298.15\right)}\right) \right\}^2 \end{aligned} \tag{A.64}$$

plotted in Figure A.7 for diatomic hydrogen. This equation produces good approximate results for the enthalpy changes in hydrogen and other diatomic molecules. For hydrogen

(A.64) gives $h^{\circ}_{H_2}(2000) - h^{\circ}_{H_2}(298.15) = 51872.5\, J/mole$ which compares well with the value $52951\, J/mole$ given in the left table in Figure A.1.

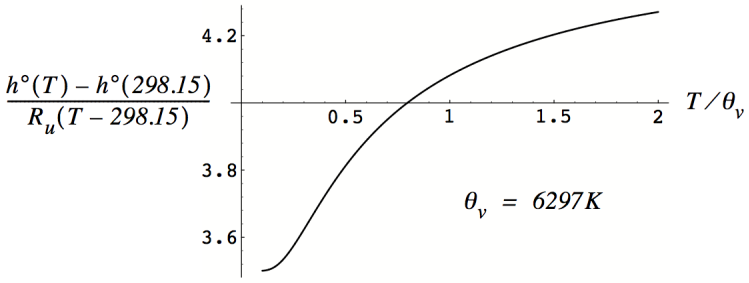

Figure A.7: *Enthalpy change for diatomic hydrogen at elevated temperature.*

A.6 Chemical bonds and the heat of formation

A.6.1 Potential energy of two hydrogen atoms

Figure A.8 below depicts the variation in potential energy as two hydrogen atoms at zero energy are brought together from infinity.

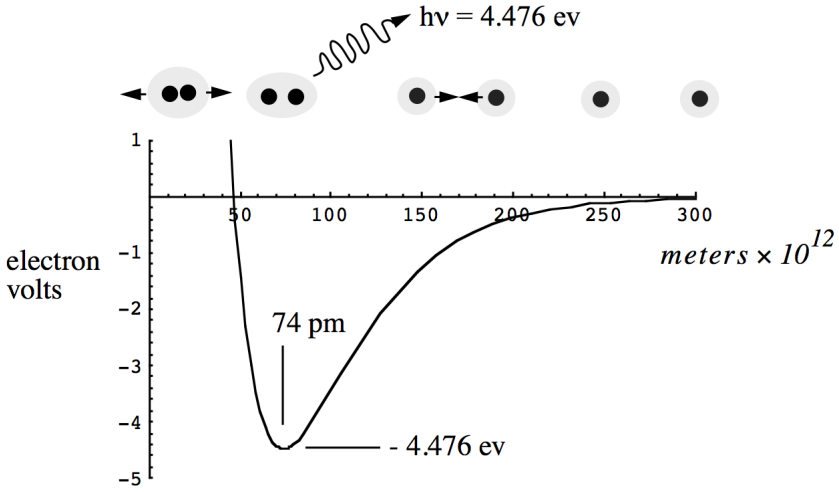

Figure A.8: *Potential energy of two hydrogen atoms as a function of bond distance.*

The molecule is stable at a bond length of 74 *picometers*. Noting the existence of minimum energy quantum vibrations, this distance can be viewed as an approximate measure of the

bond length between the two nuclei.

The potential energy of the system at this spacing is $-4.476\,electron\,volts$ where $1\,ev = 1.60217646 \times 10^{19}\,Joules$. This is the bond energy that is radiated away when the two atoms are allowed to approach each other through mutual attraction and react to form the chemical bond that holds them together in a stable molecule. It is also the energy that would have to be added to the molecule in order to dissociate the two atoms and return them to their zero energy state at infinity. The hydrogen molecule is a classic example of a covalent bond where the mutual attraction of the two nuclei arises from the attraction of each nucleus to the electron pair that is concentrated in the space between them. Some other bond lengths and zero Kelvin bond energies are given in Figure A.9.

Molecule	Bond length	Bond energy at 0K
	$\times 10^8 cm$	electron volts
H_2	0.7415	4.476
O_2	1.20739	5.080
N_2	1.0976	9.756
F_2	1.442	1.59
Cl_2	1.988	2.475
Br_2	2.283	1.971
I_2	2.666	1.5417
OH	0.9706	4.35
CH	1.1198	3.47
CO	1.1281	11.11

Figure A.9: *Bond lengths and bond energies for several diatomic molecules at* $0K$. *Reference: Moelwyn-Hughes, Physical Chemistry, page 427.*

Covalent bonds are the strongest chemical bonds found in nature and are always formed from the sharing of one or more pairs of electrons. Typical covalent bond energies range from $-1.5417ev$ for the single bond in diatomic iodine to $-6.364ev$ for the double bond between two carbon atoms to $-9.756ev$ for the triple bond that occurs between two atoms of nitrogen. For comparison the thermal energy per molecule of air at $298.15\,K$ is only about $0.064\,ev$. This is the reason why covalently bonded molecules tend be so difficult to break by heating.

Although, in principle, it is possible to analyze the energetics of all chemical reactions as a process of breaking down reactants and assembling products to and from their constituent atoms at zero Kelvin it is not particularly convenient to do so. The reason is that virtually all chemical reactions of interest take place in a surrounding gas at some pressure above vacuum and, in accounting for all the energy changes, it is necessary to include the work associated with the changes in volume that occur during the reaction. Consider the reaction depicted in Figure A.10 which is the opposite of the reaction shown in Figure A.2.

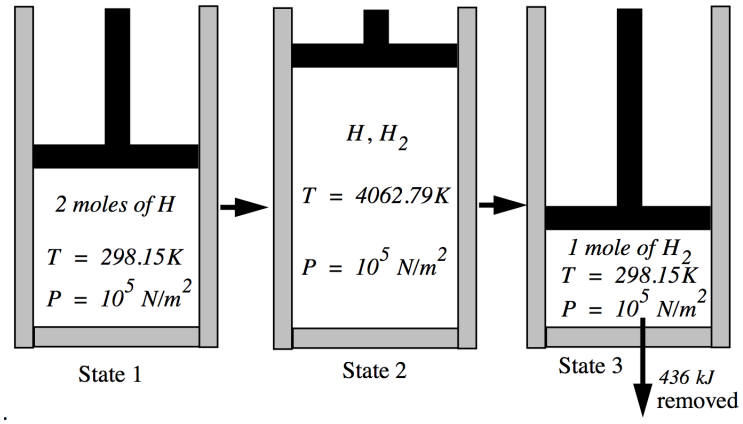

Figure A.10: *Reaction of atomic hydrogen to form diatomic hydrogen at standard pressure and temperature.*

Two moles of hydrogen atoms are placed in an adiabatic piston-cylinder combination at a temperature $T = 298.15\,K$ and pressure $P = 10^5\,N/m^2$. The atoms in state 1 are allowed to react and the piston is withdrawn to produce a mixture of H and H_2 in state 2 at very high temperature and at the original pressure. Heat is removed and the piston is compressed to bring the gas back to the original temperature and pressure at state 3. At the relatively low final temperature of $298.15\,K$ virtually all of the atomic hydrogen has reacted to produce one mole of diatomic hydrogen.

A.6.2 Atomic hydrogen

Taking the reference energy of the hydrogen atoms to be zero at absolute zero, the atomic hydrogen is brought to state 1 through the addition of heat and the production of work as the collection of atoms expands from essentially zero volume against the surrounding constant pressure.

Any phase changes that may occur in atomic hydrogen are ignored and it seems that little is known about the nature or even the existence of a stable solid or liquid state of

atomic hydrogen in the neighborhood of absolute zero. There are papers on the subject that describe theoretical models of atomic hydrogen in a face-centered cubic crystal but there is no definitive experimental evidence of solid hydrogen near absolute zero. If such a condensed state does exist, the temperature of any phase change would be extremely low and would make only a very small contribution to the enthalpy.

The total enthalpy change needed to bring the two moles of atomic hydrogen from zero energy at $0K$ to state 1 at $298.15\,K$ is therefore determined from the gas phase heat capacity.

$$\begin{aligned} &n\left(h_H^\circ\left(298.15\right)-h_H^\circ\left(0\right)\right)= \\ &n\int_0^{298.15} C_{P_H}\left(T\right)dT = 2\times 20.785\times 298.15 = 12394\,J \end{aligned} \tag{A.65}$$

The enthalpy required per mole of H is

$$h_H^\circ\left(298.15\right)-h_H^\circ\left(0\right)=\frac{12394}{2}=6197\,J/mole\,of\,H \tag{A.66}$$

This is the enthalpy change given in the tables in Figure A.1 but with the opposite sign.

A.6.3 Diatomic hydrogen

An accurate determination of the enthalpy of state 3 requires a knowledge of the heat capacity of diatomic hydrogen at very low temperatures as well as data for the heat of fusion and vaporization. The number of degrees of freedom for diatomic hydrogen is $\beta = 5$ at room temperature and drops to $\beta = 3$ near the vaporization point as rotational degrees of freedom freeze out. Hydrogen is somewhat unusual in this respect. Because of the strong bond reflected in the short bond length between the two hydrogen atoms and the correspondingly low vaporization point, the freezing out of the rotational degrees of freedom is evident in the gas heat capacity with a transition temperature at about $87\,K$. For other diatomic gases the theoretical transition temperature tends to be far below the vaporization point and is therefore less evident in the heat capacity function.

The heats of fusion and vaporization of diatomic hydrogen are well known. Equation (A.67)

shows some data at $P = P^\circ = 10^2 kPa$.

$$\begin{array}{l} Heat\ capacity, C_P\,@\,0.0\,K = 0.0\,J/\,(mole - K) \\ Heat\ capacity, C_P\,@\,13.15\,K = 5.729\,J/\,(mole - K) \\ Enthalpy\ of\ fusion = 117.25\,J/mole\,@\,13.15\,K \\ Heat\ capacity, C_P\,@\,20.0\,K = 19.4895\,J/\,(mole - K) \\ Enthalpy\ of\ vaporization = 912.0\,J/mole\,@\,20.28\,K \\ Heat\ capacity, C_P\,@\,175.0\,K = 26.4499\,J/\,(mole - K) \\ Heat\ capacity, C_P\,@\,250.0\,K = 28.3248\,J/\,(mole - K) \\ Heat\ capacity, C_P\,@\,298.15\,K = 28.836\,J/\,(mole - K)\,. \end{array} \tag{A.67}$$

The heat capacity of all materials is zero at absolute zero. An approximation to the heat capacity of gaseous H_2 that works reasonably well between the temperatures of $20.28\,K$ and $298.15\,K$ is

$$\begin{array}{l} C_{P_{H_2}}(T) = \\ 18.834 + 1.30487 \times 10^3 T^2 - 1.14829 \times 10^5 T^3 + 3.98205 \times 10^{-8} T^4 - 4.9369 \times 10^{-11} T^5. \end{array} \tag{A.68}$$

This model for the heat capacity is plotted in Figure A.11. For simplicity we assume the heat capacities of the solid and liquid states vary linearly between the values given in (A.67). Actually this model of the heat capacity of diatomic hydrogen is over simplified. Any sample of hydrogen contains both the ortho and para forms of hydrogen and each has a somewhat different heat capacity. As a result there is a range of temperatures around $100\,K$ where the heat capacity of the mixture actually decreases with increasing temperature.

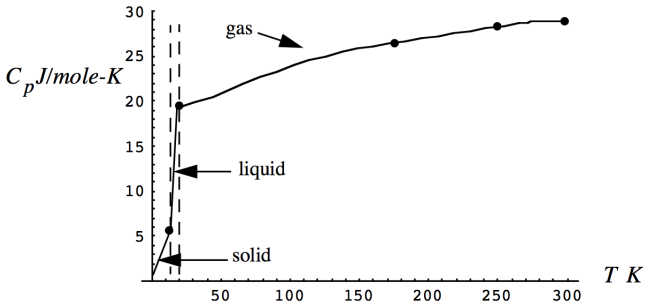

Figure A.11: *Approximation to the heat capacity of gaseous H_2 at low temperatures and $P = 100kPa$.*

The enthalpy of a species including the absolute zero energy of the chemical bond is

$$\begin{aligned} & h\left(T,P\right)= \\ & E_{chemical\ bond\ energy/mole}\left(0,P\right)+ \\ & \int_{0}^{T_{melting}(P)}C_{P}\left(T,P\right)dT+\Delta h_{fusion}\left(T_{melting}\left(P\right),P\right)+ \\ & \int_{T_{melting}(P)}^{T_{vaporization}(P)}C_{P}\left(T,P\right)dT+\Delta h_{vaporization}\left(T_{vaporization}\left(P\right),P\right)+ \\ & \int_{T_{vaporization}(P)}^{T}C_{P}\left(T,P\right)dT. \end{aligned} \tag{A.69}$$

The pressure dependence comes primarily from the effect of pressure on the heat of vaporization and to a lesser extent on the heat of fusion as well as the possible pressure dependence of the heat capacities of the condensed phases particularly near phase transition points. The gas phase heat capacity becomes independent of pressure as the gas approaches ideal gas behavior at increasing temperatures above the vaporization temperature.

On a per unit mole basis the chemical bond energy of H_2 at zero Kelvin is

$$\begin{aligned} & E_{chemical\,bond\,energy/mole}\left(0,P^{\circ}\right)= \\ & -4.476\frac{electron\,volts}{molecule}\times 6.0221415\times 10^{23}\frac{molecules}{mole}\times 1.60217646\times 10^{-19}\frac{J}{electron\,volts}= \\ & -431.87\times 10^{3}\,J/mole \end{aligned} \tag{A.70}$$

Using the data in (A.67), the enthalpy at $T=298.15\,K$ and $P=100\,kPa$ including the chemical bond energy is

$$\begin{aligned} & h_{H_2}^{\circ}\left(298.15,100\right)=-431.87\times 10^{3}+\int_{0}^{13.95}\left(\frac{5.729}{13.95}\right)TdT+117.25+ \\ & \int_{13.95}^{20.28}\left(5.729+\left(\frac{19.49-5.729}{20.28-13.95}\right)\left(T-13.95\right)\right)dT+912+\int_{20.28}^{298.15}C_{P}^{\circ}\left(T\right)dT \end{aligned} \tag{A.71}$$

Use (A.68) to carry out the last integral in (A.71) giving

$$h^{\circ}_{H_2}(298.15, 100) = -431.87 \times 10^3 + \left(\frac{5.729 \times 13.95}{2}\right) + 117.25 + \left(\frac{19.49 + 5.729}{2}\right)(20.28 - 13.95) + 912 + 7057 = -431.87 \times 10^3 + 8206 \tag{A.72}$$

The heat released by the reaction to form diatomic hydrogen from its atoms at $298.15\,K$ and $1\,atmosphere$ is

$$\begin{array}{l} \Delta h^{\circ} = h^{\circ}_{H_2}(298.15, 100) - 2h^{\circ}_{H}(298.15, 100) = \\ \left(-431.87 \times 10^3 + 8206\right) - 2 \times 6197.35 = \\ -436.059 \times 10^3\, J/moles\, of\, H_2\, formed \end{array} \tag{A.73}$$

The result (A.73) is the enthalpy released during the reaction of atomic hydrogen to form diatomic hydrogen at a temperature of $298.15\,K$ and pressure $10^5\,N/m^2$. This result can be found in the right table in Figure A.1 as twice the heat of formation of one mole of monatomic hydrogen. We worked this out in equation (A.33).

Note that, because the heat input and work needed to bring two moles of atomic hydrogen to the initial temperature of $298.15\,K$ is greater that that needed to bring one mole of diatomic hydrogen to the same temperature, the reaction releases four more kilo-Joules of enthalpy than it would if the reaction was carried out at zero Kelvin.

A.7 Heats of formation computed from bond energies

We began this appendix by discussing tabulations of the heats of formation of various species from their elements in their reference state. In this last section we will describe how heats of formation can be determined from bond energies. The enthalpy changes involved in chemical reactions come from the breaking and making of chemical bonds to decompose the reactants and then compose the products.

Figure A.12 gives average bond energies for a variety of diatomic molecules.

Consider the reference reaction for water

$$H_2 + \frac{1}{2}O_2 \rightarrow H_2O|_{gas} \qquad \Delta h^{\circ}_{f_{H_2O|_{gas}}}(298.15) = -241.826 kJ/mole \tag{A.74}$$

Molecule	Bond energy at 298.15K	Molecule	Bond energy at 298.15K
	kJoules per mole		kJoules per mole
$H-H$	436	$C=C$	615
$O-O$	145	$N=N$	418
$N-N$	170	$O=O$	498
$F-F$	158	$C=N$	615
$Cl-Cl$	243	$C=O$	725
$Br-Br$	193	$C=S$	477
$I-I$	151	$C\equiv C$	812
$O-H$	463	$N\equiv N$	946
$C-H$	416	$C\equiv N$	890
$C-O$	350	$C-N$	308

Figure A.12: *Average single, and multiple bond energies for several diatomic molecules at 298.15K.*

To break down the reactants we have to break the 0.5 mole of O_2 double bonds as well as one mole of H_2 single bonds. When we compose the products we will make two OH single bonds. All the bond changes are evaluated at $298.15\,K$. The heat of the reaction is

$$\Delta h^\circ \cong \sum \Delta h^\circ|_{bonds\,broken} - \sum \Delta h^\circ|_{bonds\,made}. \tag{A.75}$$

Using the data in Figure A.12 we get

$$\Delta h^\circ = 436 + \frac{1}{2}(498) - 2(463) = -241\,kJ/moles\,of\,H_2O\,formed. \tag{A.76}$$

which is very close to the tabulated heat of formation.

A certain amount of caution is always required when computing heats of formation from bond energies. The energy of a chemical bond always depends on the particular atomic configuration of the molecule where the bond appears. For example to remove one of the hydrogens from a molecule of water requires $502\,kJ/mole$ whereas the energy required to break the remaining OH bond is only $424\,kJ/mole$. Therefore the average bond energy is $463\,kJ/mole$.

For methane $435\,kJ/mole$ is required to break a single CH whereas it takes $1662\,kJ/mole$ to break all four bonds therefore the average bond energy is $416\,kJ/mole$ not $435\,kJ/mole$.

A.8 References

1) Linus Pauling, *General Chemistry*, Dover 1970.

2) Irvin Glassman, *Combustion*, Third Edition, Academic Press 1996.

3) NASA/TP - 2002-211556 - *NASA Glenn Coefficients for Calculating Thermo- dynamic Properties of Individual Species* by Bonnie J. McBride, Michael J. Zehe, and Sanford Gordon, Glenn Research Center, Cleveland, Ohio.

In addition to providing curve fits for the heat capacity, enthalpy and entropy for a wide range of species, a number of variables are also tabulated in this reference including $\Delta h_f^\circ\,(298.15)$, $h^\circ\,(0)$ and $\Delta h_f^\circ\,(0)$.

Appendix B

Selected JANAF data

Carbon (C), ideal gas, mol. wt. = 12.011

Enthalpy Reference Temperature = T_r = 298.15 K				Standard State Pressure = p^o = 0.1 MPa			
	J K^{-1}mol^{-1}			kJ mol^{-1}			
T/K	C_p^o	S^o	$-[G^o-H^o(T_r)]/T$	$H^o-H^o(T_r)$	$\Delta_f H^o$	$\Delta_f G^o$	Log K_f
0	0.	0.	INFINITE	-6.536	711.185	711.185	INFINITE
100	21.271	135.180	176.684	-4.150	713.511	700.088	-365.689
200	20.904	149.768	160.007	-2.048	715.287	685.950	-179.152
250	20.861	154.427	158.443	-1.004	716.035	678.527	-141.770
298.15	20.838	158.100	158.100	0.	716.670	671.244	-117.599
300	20.838	158.228	158.100	0.039	716.693	670.962	-116.825
350	20.824	161.439	158.354	1.080	717.263	663.294	-98.991
400	20.815	164.219	158.917	2.121	717.752	655.550	-85.606
450	20.809	166.671	159.645	3.162	718.165	647.749	-75.189
500	20.804	168.863	160.459	4.202	718.507	639.906	-66.851
600	20.799	172.655	162.185	6.282	719.009	624.135	-54.336
700	20.795	175.861	163.916	8.362	719.315	608.296	-45.392
800	20.793	178.638	165.587	10.441	719.474	592.424	-38.681
900	20.792	181.087	167.175	12.520	719.519	576.539	-33.461
1000	20.791	183.278	168.678	14.600	719.475	560.654	-29.286
1100	20.791	185.259	170.097	16.679	719.360	544.777	-25.869
1200	20.793	187.068	171.437	18.758	719.188	528.913	-23.023
1300	20.796	188.733	172.704	20.837	718.968	513.066	-20.615
1400	20.803	190.274	173.905	22.917	718.709	497.237	-18.552
1500	20.814	191.710	175.044	24.998	718.415	481.427	-16.765
1600	20.829	193.053	176.128	27.080	718.092	465.639	-15.202
1700	20.850	194.317	177.162	29.164	717.744	449.871	-13.823
1800	20.878	195.509	178.148	31.250	717.373	434.124	-12.598
1900	20.912	196.639	179.092	33.340	716.984	418.399	-11.503
2000	20.952	197.713	179.996	35.433	716.577	402.694	-10.517
2100	20.999	198.736	180.864	37.530	716.156	387.010	-9.626
2200	21.052	199.714	181.699	39.633	715.722	371.347	-8.817
2300	21.110	200.651	182.503	41.741	715.277	355.703	-8.078
2400	21.174	201.551	183.278	43.855	714.821	340.079	-7.402
2500	21.241	202.417	184.026	45.976	714.357	324.474	-6.780
2600	21.313	203.251	184.750	48.103	713.884	308.888	-6.206
2700	21.387	204.057	185.450	50.238	713.405	293.321	-5.675
2800	21.464	204.836	186.129	52.381	712.920	277.771	-5.182
2900	21.542	205.591	186.787	54.531	712.429	262.239	-4.723
3000	21.621	206.322	187.426	56.689	711.932	246.723	-4.296
3100	21.701	207.032	188.047	58.856	711.431	231.224	-3.896
3200	21.780	207.723	188.651	61.030	710.925	215.742	-3.522
3300	21.859	208.394	189.239	63.212	710.414	200.275	-3.170
3400	21.936	209.048	189.812	65.401	709.899	184.824	-2.839
3500	22.012	209.685	190.371	67.599	709.380	169.389	-2.528
3600	22.087	210.306	190.916	69.804	708.857	153.968	-2.234
3700	22.159	210.912	191.448	72.016	708.329	138.561	-1.956
3800	22.230	211.504	191.968	74.235	707.797	123.169	-1.693
3900	22.298	212.082	192.477	76.462	707.260	107.791	-1.444
4000	22.363	212.648	192.974	78.695	706.719	92.427	-1.207
4100	22.426	213.201	193.461	80.934	706.173	77.077	-0.982
4200	22.487	213.742	193.937	83.180	705.621	61.740	-0.768
4300	22.544	214.272	194.404	85.432	705.065	46.416	-0.564
4400	22.600	214.791	194.861	87.689	704.503	31.105	-0.369
4500	22.652	215.299	195.310	89.951	703.936	15.807	-0.183
4600	22.702	215.797	195.750	92.219	703.363	0.521	-0.006
4700	22.750	216.286	196.182	94.492	702.784	-14.752	0.164
4800	22.795	216.766	196.605	96.769	702.199	-30.012	0.327
4900	22.838	217.236	197.022	99.051	701.607	-45.261	0.482
5000	22.878	217.698	197.431	101.337	701.009	-60.497	0.632
5100	22.917	218.151	197.832	103.626	700.404	-75.721	0.776
5200	22.953	218.597	198.227	105.920	699.793	-90.933	0.913
5300	22.987	219.034	198.616	108.217	699.174	-106.133	1.046
5400	23.020	219.464	196.998	110.517	698.548	-121.322	1.174
5500	23.051	219.887	199.374	112.821	697.914	-136.499	1.296
5600	23.080	220.302	199.744	115.127	697.273	-151.664	1.415
5700	23.107	220.711	200.108	117.437	696.625	-166.818	1.529
5800	23.133	221.113	200.467	119.749	695.968	-181.961	1.639
5900	23.157	221.509	200.820	122.063	695.304	-197.092	1.745
6000	23.181	221.898	201.168	124.380	694.631	-212.211	1.847

Figure B.1: *JANAF data for monatomic carbon gas.*

Carbon (C), reference state-graphite, mol. wt. = 12.011

Enthalpy Reference Temperature = T_r = 298.15 K — Standard State Pressure = p° = 0.1 MPa

T/K	C_p°	S°	$-[G^\circ-H^\circ(T_r)]/T$	$H^\circ-H^\circ(T_r)$	$\Delta_f H^\circ$	$\Delta_f G^\circ$	Log K_f
	J K^{-1}mol^{-1}			kJ mol^{-1}			
0	0.	0.	INFINITE	-1.051	0.	0.	0.
100	1.674	0.952	10.867	-0.991	0.	0.	0.
200	5.006	3.082	6.407	-0.665	0.	0.	0.
250	6.816	4.394	5.871	-0.369	0.	0.	0.
298.15	8.517	5.740	5.740	0.	0.	0.	0.
300	8.581	5.793	5.741	0.016	0.	0.	0.
350	10.241	7.242	5.851	0.487	0.	0.	0.
400	11.817	8.713	6.117	1.039	0.	0.	0.
450	13.289	10.191	6.487	1.667	0.	0.	0.
500	14.623	11.662	6.932	2.365	0.	0.	0.
600	16.844	14.533	7.961	3.943	0.	0.	0.
700	18.537	17.263	9.097	5.716	0.	0.	0.
800	19.827	19.826	10.279	7.637	0.	0.	0.
900	20.824	22.221	11.475	9.672	0.	0.	0.
1000	21.610	24.457	12.662	11.795	0.	0.	0.
1100	22.244	26.548	13.831	13.989	0.	0.	0.
1200	22.766	28.506	14.973	16.240	0.	0.	0.
1300	23.204	30.346	16.085	18.539	0.	0.	0.
1400	23.578	32.080	17.167	20.879	0.	0.	0.
1500	23.904	33.718	18.216	23.253	0.	0.	0.
1600	24.191	35.270	19.234	25.658	0.	0.	0.
1700	24.448	36.744	20.221	28.090	0.	0.	0.
1800	24.681	38.149	21.178	30.547	0.	0.	0.
1900	24.895	39.489	22.107	33.026	0.	0.	0.
2000	25.094	40.771	23.008	35.525	0.	0.	0.
2100	25.278	42.000	23.883	38.044	0.	0.	0.
2200	25.453	43.180	24.734	40.581	0.	0.	0.
2300	25.618	44.315	25.561	43.134	0.	0.	0.
2400	25.775	45.408	26.365	45.704	0.	0.	0.
2500	25.926	46.464	27.148	48.289	0.	0.	0.
2600	26.071	47.483	27.911	50.889	0.	0.	0.
2700	26.212	48.470	28.654	53.503	0.	0.	0.
2800	26.348	49.426	29.379	56.131	0.	0.	0.
2900	26.481	50.353	30.086	58.773	0.	0.	0.
3000	26.611	51.253	30.777	61.427	0.	0.	0.
3100	26.738	52.127	31.451	64.095	0.	0.	0.
3200	26.863	52.978	32.111	66.775	0.	0.	0.
3300	26.986	53.807	32.756	69.467	0.	0.	0.
3400	27.106	54.614	33.387	72.172	0.	0.	0.
3500	27.225	55.401	34.005	74.889	0.	0.	0.
3600	27.342	56.170	34.610	77.617	0.	0.	0.
3700	27.459	56.921	35.203	80.357	0.	0.	0.
3800	27.574	57.655	35.784	83.109	0.	0.	0.
3900	27.688	58.372	36.354	85.872	0.	0.	0.
4000	27.801	59.075	38.913	88.646	0.	0.	0.
4100	27.913	59.763	37.462	91.432	0.	0.	0.
4200	28.024	60.437	38.001	94.229	0.	0.	0.
4300	28.134	61.097	38.531	97.037	0.	0.	0.
4400	28.245	61.745	39.051	99.856	0.	0.	0.
4500	28.354	62.381	39.562	102.685	0.	0.	0.
4600	28.462	63.006	40.065	105.526	0.	0.	0.
4700	28.570	63.619	40.560	108.378	0.	0.	0.
4800	28.678	64.222	41.047	111.240	0.	0.	0.
4900	28.785	64.814	41.526	114.114	0.	0.	0.
5000	28.893	65.397	41.997	116.997	0.	0.	0.
5100	28.999	65.970	42.462	119.892	0.	0.	0.
5200	29.106	66.534	42.919	122.797	0.	0.	0.
5300	29.211	67.089	43.370	125.713	0.	0.	0.
5400	29.317	67.636	43.814	128.640	0.	0.	0.
5500	29.422	68.175	44.252	131.577	0.	0.	0.
5600	29.528	68.706	44.684	134.524	0.	0.	0.
5700	29.632	69.230	45.110	137.482	0.	0.	0.
5800	29.737	69.746	45.531	140.451	0.	0.	0.
5900	29.842	70.255	45.945	143.429	0.	0.	0.
6000	29.946	70.758	46.355	146.419	0.	0.	0.

Figure B.2: *JANAF data for solid carbon in the form of graphite.*

Acetylene (C_2H_2), ideal gas, mol. wt. = 26.03788

Enthalpy Reference Temperature = T_r = 298.15 K				Standard State Pressure = p^o = 0.1 MPa			
	J $K^{-1}mol^{-1}$			kJ mol^{-1}			
T/K	C_p^o	S^o	$-(G^o-H^o(T_r))/T$	$H^o-H^o(T_r)$	$\Delta_f H^o$	$\Delta_f G^o$	Log K_f
0	0.	0.	INFINITE	-10.012	235.755	235.755	INFINITE
100	29.347	163.294	234.338	-7.104	232.546	236.552	-123.562
200	35.585	185.097	204.720	-3.925	229.685	241.663	-63.116
298.15	44.095	200.958	200.958	0.	226.731	248.163	-43.477
300	44.229	201.231	200.959	0.082	226.674	248.296	-43.232
400	50.480	214.856	202.774	4.833	223.568	255.969	-33.426
500	54.869	226.610	206.393	10.108	220.345	264.439	-27.626
600	58.287	236.924	210.640	15.771	216.993	273.571	-23.816
700	61.149	246.127	215.064	21.745	213.545	283.272	-21.138
800	63.760	254.466	219.476	27.992	210.046	293.471	-19.162
900	66.111	262.113	223.794	34.487	206.522	304.111	-17.650
1000	68.275	269.192	227.984	41.208	202.989	315.144	-16.461
1100	70.245	275.793	232.034	48.136	199.451	326.530	-15.506
1200	72.053	281.984	235.941	55.252	195.908	338.239	-14.723
1300	73.693	287.817	239.709	62.540	192.357	350.244	-14.073
1400	75.178	293.334	243.344	69.985	188.795	362.523	-13.526
1500	76.530	298.567	246.853	77.572	185.216	375.057	-13.061
1600	77.747	303.546	250.242	85.286	181.619	387.830	-12.661
1700	78.847	308.293	253.518	93.117	177.998	400.829	-12.316
1800	79.852	312.829	256.688	101.053	174.353	414.041	-12.015
1900	80.760	317.171	259.758	109.084	170.680	427.457	-11.752
2000	81.605	321.335	262.733	117.203	166.980	441.068	-11.520
2100	82.362	325.335	265.620	125.401	163.250	454.864	-11.314
2200	83.065	329.183	268.422	133.673	159.491	468.838	-11.132
2300	83.712	332.890	271.145	142.012	155.701	482.984	-10.969
2400	84.312	336.465	273.793	150.414	151.881	497.295	-10.823
2500	84.858	339.918	276.369	158.873	148.029	511.767	-10.693
2600	85.370	343.256	278.878	167.384	144.146	526.393	-10.575
2700	85.846	346.487	281.322	175.945	140.230	541.169	-10.470
2800	86.295	349.618	283 706	184.553	136.282	556.090	-10.374
2900	86.713	352.653	286 031	193.203	132.302	571.154	-10.288
3000	87.111	355.600	288.301	201.895	128.290	586.355	-10.209
3100	87.474	358.462	290.519	210.624	124.245	601.690	-10.138
3200	87.825	361.245	292.686	219.389	120.166	617.157	-10.074
3300	88.164	363.952	294.804	228.189	116.053	632.751	-10.016
3400	88.491	366.589	296.877	237.022	111.908	648.471	-9.963
3500	88.805	369.159	298.906	245.886	107.731	664.313	-9.914
3600	89.101	371.665	300.892	254.782	103.519	680.275	-9.871
3700	89.388	374.110	302.838	263.706	99.274	696.354	-9.831
3800	89.666	376.498	304.745	272.659	94.996	712.549	-9.795
3900	89.935	378.830	306.615	281.639	90.683	728.856	-9.762
4000	90.194	381.110	308.449	290.646	86.336	745.275	-9.732
4100	90.439	383.341	310.248	299.678	81.955	761.803	-9.705
4200	90.678	385.523	312.015	308.733	77.538	778.438	-9.681
4300	90.910	387.659	313.749	317.813	73.087	795.178	-9.660
4400	91.137	389.752	315.453	326.915	68.601	812.023	-9.640
4500	91.358	391.802	317.127	336.040	64.080	828.969	-9.622
4600	91.563	393.813	318.772	345.186	59.524	846.017	-9.607
4700	91.768	395.784	320.390	354.353	54.933	863.164	-9.593
4800	91.970	397.718	321.981	363.540	50.307	880.410	-9.581
4900	92.171	399.617	323.546	372.747	45.648	897.751	-9.570
5000	92.370	401.481	325.086	381.974	40.957	915.189	-9.561
5100	92.571	403.312	326.602	391.221	36.234	932.720	-9.553
5200	92.768	405.111	328.094	400.488	31.481	950.345	-9.546
5300	92.963	406.880	329.564	409.774	26.699	968.061	-9.541
5400	93.153	408.620	331.012	419.080	21.889	985.868	-9.536
5500	93.341	410.331	332.439	428.405	17.052	1003.763	-9.533
5600	93.525	412.014	333.845	437.748	12.189	1021.748	-9.530
5700	93.706	413.671	335.231	447.110	7.303	1039.819	-9.529
5800	93.883	415.302	336.597	456.489	2.393	1057.976	-9.528
5900	94.057	416.909	337.945	465.886	-2.537	1076.217	-9.528
6000	94.228	418.491	339.274	475.301	-7.488	1094.543	-9.529

Figure B.3: *JANAF data for acetylene gas.*

Ethene (C_2H_4), ideal gas, mol. wt. = 28.05376

Enthalpy Reference Temperature = T_r = 298.15 K				Standard State Pressure = p^o = 0.1 MPa			
	J $K^{-1}mol^{-1}$			kJ mol^{-1}			
T/K	C_p^o	S^o	$-[G^o-H^o(T_r)]/T$	$H^o-H^o(T_r)$	$\Delta_f H^o$	$\Delta_f G^o$	Log K_f
0	0.	0.	INFINITE	-10.518	60.986	60.986	INFINITE
100	33.270	180.542	252.466	-7.192	58.194	60.476	-31.589
200	35.359	203.955	222.975	-3.804	55.542	63.749	-16.649
250	38.645	212.172	220.011	-1.960	54.002	65.976	-13.785
298.15	42.886	219.330	219.330	0.	52.467	68.421	-11.987
300	43.063	219.596	219.331	0.079	52.408	68.521	-11.930
350	48.013	226.602	219.873	2.355	50.844	71.330	-10.645
400	53.048	233.343	221.138	4.882	49.354	74.360	-9.710
450	57.907	239.874	222.858	7.657	47.951	77.571	-9.004
500	62.477	246.215	224.879	10.668	46.641	80.933	-8.455
600	70.663	258.348	229.456	17.335	44.294	88.017	-7.663
700	77.714	269.783	234.408	24.763	42.300	95.467	-7.124
800	83.840	280.570	239.511	32.847	40.637	103.180	-6.737
900	89.200	290.761	244.644	41.505	39.277	111.082	-6.447
1000	93.899	300.408	249.742	50.665	38.183	119.122	-6.222
1100	98.018	309.555	254.768	60.266	37.318	127.259	-6.043
1200	101.626	318.242	259.698	70.252	36.645	135.467	-5.897
1300	104.784	326.504	264.522	80.576	36.129	143.724	-5.775
1400	107.550	334.372	269.233	91.196	35.742	152.016	-5.672
1500	109.974	341.877	273.827	102.074	35.456	160.331	-5.583
1600	112.103	349.044	278.306	113.181	35.249	168.663	-5.506
1700	113.976	355.898	282.670	124.486	35.104	177.007	-5.439
1800	115.628	362.460	286.922	135.968	35.005	185.357	-5.379
1900	117.089	368.752	291.064	147.606	34.938	193.712	-5.326
2000	118.386	374.791	295.101	159.381	34.894	202.070	-5.278
2100	119.540	380.596	299.035	171.278	34.864	210.429	-5.234
2200	120.569	386.181	302.870	183.284	34.839	218.790	-5.195
2300	121.491	391.561	306.610	195.388	34.814	227.152	-5.159
2400	122.319	396.750	310.258	207.580	34.783	235.515	-5.126
2500	123.064	401.758	313.818	219.849	34.743	243.880	-5.096
2600	123.738	406.596	317.294	232.190	34.688	252.246	-5.068
2700	124.347	411.280	320.689	244.595	34.616	260.615	-5.042
2800	124.901	415.812	324.006	257.058	34.524	268.987	-5.018
2900	125.404	420.204	327.248	269.573	34.409	277.363	-4.996
3000	125.864	424.463	330.418	282.137	34.269	285.743	-4.975
3100	126.284	428.597	333.518	294.745	34.102	294.128	-4.956
3200	126.670	432.613	336.553	307.393	33.906	302.518	-4.938
3300	127.024	436.516	339.523	320.078	33.679	310.916	-4.921
3400	127.350	440.313	342.432	332.797	33.420	319.321	-4.906
3500	127.650	444.009	345.281	345.547	33.127	327.734	-4.891
3600	127.928	447.609	348.074	358.326	32.800	336.156	-4.877
3700	128.186	451.118	350.812	371.132	32.436	344.588	-4.865
3800	128.424	454.539	353.497	383.962	32.035	353.030	-4.853
3900	128.646	457.878	356.130	396.816	31.596	361.482	-4.842
4000	128.852	461.138	358.715	409.691	31.118	369.947	-4.831
4100	129.045	464.322	361.252	422.586	30.600	378.424	-4.821
4200	129.224	467.434	363.743	435.500	30.041	388.915	-4.812
4300	129.392	470.476	366.190	448.430	29.441	395.418	-4.803
4400	129.549	473.453	368.594	461.378	28.799	403.937	-4.795
4500	129.696	476.366	370.957	474.340	28.116	412.470	-4.788
4600	129.835	479.218	373.280	487.317	27.390	421.019	-4.781
4700	129.965	482.012	375.563	500.307	26.623	429.584	-4.774
4800	130.087	484.749	377.810	513.309	25.813	438.167	-4.768
4900	130.202	487.433	380.020	526.324	24.962	446.766	-4.763
5000	130.311	490.064	382.194	539.349	24.069	455.384	-4.757
5100	130.413	492.646	384.335	552.386	23.136	464.019	-4.753
5200	130.510	495.179	386.442	565.432	22.162	472.673	-4.748
5300	130.602	497.666	388.517	578.488	21.149	481.346	-4.744
5400	130.689	500.108	390.561	591.552	20.097	490.040	-4.740
5500	130.771	502.507	392.575	604.625	19.008	498.751	-4.737
5600	130.849	504.864	394.559	617.706	17.884	507.485	-4.734
5700	130.923	507.180	396.515	630.795	16.724	516.238	-4.731
5800	130.993	509.458	398.442	643.891	15.531	525.012	-4.728
5900	131.060	511.698	400.343	656.993	14.306	533.806	-4.726
6000	131.124	513.901	402.217	670.103	13.051	542.621	-4.724

Figure B.4: *JANAF data for ethene gas.*

Methane (CH_4), ideal gas, mol. wt. = 16.04276

Enthalpy Reference Temperature = T_r = 298.15 K — Standard State Pressure = p^o = 0.1 MPa

T/K	C_p^o	S^o	$-[G^o-H^o(T_r)]/T$	$H^o-H^o(T_r)$	$\Delta_f H^o$	$\Delta_f G^o$	Log K_f
	J K^{-1}mol^{-1}			kJ mol^{-1}			
0	0.	0.	INFINITE	-10.024	-66.911	-66.911	INFINITE
100	33.258	149.500	216.485	-6.698	-69.644	-64.353	33.615
200	33.473	172.577	189.418	-3.368	-72.027	-58.161	15.190
250	34.216	180.113	186.829	-1.679	-73.426	-54.536	11.395
298.15	35.639	186.251	186.251	0.	- 74.873	-50.768	8.894
300	35.708	186.472	186.252	0.066	-74.929	-50.618	8.813
350	37.874	192.131	186.694	1.903	-76.461	-46.445	6.932
400	40.500	197.356	187.704	3.861	-77.969	-42.054	5.492
450	43.374	202.291	189.053	5.957	-79.422	-37.476	4.350
500	46.342	207.014	190.614	8.200	-80.802	-32.741	3.420
600	52.227	215.987	194.103	13.130	-83.308	-22.887	1.993
700	57.794	224.461	197.840	18.635	-85.452	-12.643	0.943
800	62.932	232.518	201.675	24.675	-87.238	-2.115	0.138
900	67.601	240.205	205.532	31.205	-88.692	8.616	-0.500
1000	71.795	247.549	209.370	38.179	-89.849	19.492	-1.018
1100	75.529	254.570	213.162	45.549	-90.750	30.472	-1.447
1200	78.833	261.287	216.895	53.270	-91.437	41.524	-1.807
1300	81.744	267.714	220.558	61.302	-91.945	52.626	-2.115
1400	84.305	273.868	224.148	69.608	-92.308	63.761	-2.379
1500	86.556	279.763	227.660	78.153	-92.553	74.918	-2.609
1600	88.537	285.413	231.095	86.910	-92.703	86.088	-2.810
1700	90.283	290.834	234.450	95.853	-92.780	97.265	-2.989
1800	91.824	296.039	237.728	104.960	-92.797	108.445	-3.147
1900	93.188	301.041	240.930	114.212	-92.770	119.624	-3.289
2000	94.399	305.853	244.057	123.592	-92.709	130.802	-3.416
2100	95.477	310.485	247.110	133.087	-92.624	141.975	-3.531
2200	96.439	314.949	250.093	142.684	-92.521	153.144	-3.636
2300	97.301	319.255	253.007	152.371	-92.409	164.308	-3.732
2400	98.075	323.413	255.854	162.141	-92.291	175.467	-3.819
2500	98.772	327.431	258.638	171.984	-92.174	186.622	-3.899
2600	99.401	331.317	261.359	181.893	-92.060	197.771	-3.973
2700	99.971	335.080	264.020	191.862	-91.954	208.916	-4.042
2800	100.489	338.725	266.623	201.885	-91.857	220.058	-4.105
2900	100.960	342.260	269.171	211.958	-91.773	231.196	-4.164
3000	101.389	345.690	271.664	222.076	-91.705	242.332	-4.219
3100	101.782	349.021	274.106	232.235	-91.653	253.465	-4.271
3200	102.143	352.258	276.498	242.431	-91.621	264.598	-4.319
3300	102.474	355.406	278.842	252.662	-91.609	275.730	-4.364
3400	102.778	358.470	281.139	262.925	-91.619	286.861	-4.407
3500	103.060	361.453	283.391	273.217	-91.654	297.993	-4.447
3600	103.319	364.360	285.600	283.536	-91.713	309.127	-4.485
3700	103.560	367.194	287.767	293.881	-91.798	320.262	-4.521
3800	103.783	369.959	289.894	304.248	-91.911	331.401	-4.555
3900	103.990	372.658	291.982	314.637	-92.051	342.542	-4.588
4000	104.183	375.293	294.032	325.045	-92.222	353.687	-4.619
4100	104.363	377.868	296.045	335.473	-92.422	364.838	-4.648
4200	104.531	380.385	298.023	345.918	-92.652	375.993	-4.676
4300	104.688	382.846	299.967	356.379	-92.914	387.155	-4.703
4400	104.834	385.255	301.879	366.855	-93.208	398.322	-4.729
4500	104.972	387.612	303.758	377.345	-93.533	409.497	-4.753
4600	105.101	389.921	305.606	387.849	-93.891	420.679	-4.777
4700	105.223	392.182	307.424	398.365	-94.281	431.869	-4.800
4800	105.337	394.399	309.213	408.893	-94.702	443.069	-4.822
4900	105.445	396.572	310.973	419.432	-95.156	454.277	-4.843
5000	105.546	398.703	312.707	429.982	-95.641	465.495	-4.863
5100	105.642	400.794	314.414	440.541	-96.157	476.722	-4.883
5200	105.733	402.847	316.095	451.110	-96.703	487.961	-4.902
5300	105.818	404.861	317.750	461.688	-97.278	499.210	-4.920
5400	105.899	406.840	319.382	472.274	-97.882	510.470	-4.938
5500	105.976	408.784	320.990	482.867	-98.513	521.741	-4.955
5600	106.049	410.694	322.575	493.469	-99.170	533.025	-4.972
5700	106.118	412.572	324.137	504.077	-99.852	544.320	-4.988
5800	106.184	414.418	325.678	514.692	-100.557	555.628	-5.004
5900	106.247	416.234	327.197	525.314	-101.284	566.946	-5.019
6000	106.306	418.020	328.696	535.942	-102.032	578.279	-5.034

Figure B.5: *JANAF data for methane gas.*

Carbon Monoxide (CO), ideal gas, mol. wt. = 28.0104

Enthalpy Reference Temperature = T_r = 298.15 K		J K^{-1}mol^{-1}		Standard State Pressure = p^0 = 0.1 MPa kJ mol^{-1}			
T/K	C_p^o	S^o	$-[G^o-H^o(T_r)]/T$	$H^o-H^o(T_r)$	$\Delta_f H^o$	$\Delta_f G^o$	Log K_f
0	0.	0.	INFINITE	-8.671	-113.805	-113.805	INFINITE
100	29.104	165.850	223.539	-5.769	-112.415	-120.239	62.807
200	29.108	186.025	200.317	-2.858	-111.286	-128.526	33.568
298.15	29.142	197.653	197.653	0.	-110.527	-137.163	24.030
300	29.142	197.833	197.653	0.054	-110.516	-137.328	23.911
400	29.342	206.238	198.798	2.976	-110.102	-146.338	19.110
500	29.794	212.831	200.968	5.931	-110.003	-155.414	16.236
600	30.443	218.319	203.415	8.942	-110.150	-164.486	14.320
700	31.171	223.066	205.890	12.023	-110.469	-173.518	12.948
800	31.899	227.277	208.305	15.177	-110.905	-182.497	11.916
900	32.577	231.074	210.628	18.401	-111.418	-191.416	11.109
1000	33.183	234.538	212.848	21.690	-111.983	-200.275	10.461
1100	33.710	237.726	214.967	25.035	-112.586	-209.075	9.928
1200	34.175	240.679	216.988	28.430	-113.217	-217.819	9.481
1300	34.572	243.431	218.917	31.868	-113.870	-226.509	9.101
1400	34.920	246.006	220.761	35.343	-114.541	-235.149	8.774
1500	35.217	248.426	222.526	38.850	-115.229	-243.740	8.488
1600	35.480	250.707	224.216	42.385	-115.933	-252.284	8.236
1700	35.710	252.865	225.839	45.945	-116.651	-260.784	8.013
1800	35.911	254.912	227.398	49.526	-117.384	-269.242	7.813
1900	36.091	256.859	228.897	53.126	-118.133	-277.658	7.633
2000	36.250	258.714	230.342	56.744	-118.896	-286.034	7.470
2100	36.392	260.486	231.736	60.376	-119.675	-294.372	7.322
2200	36.518	262.182	233.081	64.021	-120.470	-302.672	7.186
2300	36.635	263.809	234.382	67.683	-121.278	-310.936	7.062
2400	36.321	265.359	235.641	71.324	-122.133	-319.164	6.946
2500	36.836	266.854	236.860	74.985	-122.994	-327.356	6.840
2600	36.924	268.300	238.041	78.673	-123.854	-335.514	6.741
2700	37.003	269.695	239.188	82.369	-124.731	-343.638	6.648
2800	37.083	271.042	240.302	86.074	-125.623	-351.729	6.562
2900	37.150	272.345	241.384	89.786	-126.532	-359.789	6.480
3000	37.217	273.605	242.437	93.504	-127.457	-367.816	6.404
3100	37.279	274.827	243.463	97.229	-128.397	-375.812	6.332
3200	37.338	276.011	244.461	100.960	-129.353	-383.778	6.265
3300	37.392	277.161	245.435	104.696	-130.325	-391.714	6.200
3400	37.443	278.278	246.385	108.438	-131.312	-399.620	6.139
3500	37.493	279.364	247.311	112.185	-132.313	-407.497	6.082
3600	37.543	280.421	248.216	115.937	-133.329	-415.345	6.027
3700	37.589	281.450	249.101	119.693	-134.360	-423.165	5.974
3800	37.631	282.453	249.965	123.454	-135.405	-430.956	5.924
3900	37.673	283.431	250.811	127.219	-136.464	-438.720	5.876
4000	37.715	284.386	251.638	130.989	-137.537	-446.457	5.830
4100	37.756	285.317	252.449	134.762	-138.623	-454.166	5.786
4200	37.794	286.228	253.242	138.540	-139.723	-461.849	5.744
4300	37.832	287.117	254.020	142.321	-140.836	-469.506	5.703
4400	37.869	287.988	254.782	146.106	-141.963	-477.136	5.664
4500	37.903	288.839	255.529	149.895	-143.103	-484.741	5.627
4600	37.941	289.673	256.262	153.687	-144.257	-492.321	5.590
4700	37.974	290.489	256.982	157.483	-145.424	-499.875	5.555
4800	38.007	291.289	257.688	161.282	-146.605	-507.404	5.522
4900	38.041	292.073	258.382	165.084	-147.800	-514.908	5.489
5000	38.074	292.842	259.064	168.890	-149.009	-522.387	5.457
5100	38.104	293.596	259.733	172.699	-150.231	-529.843	5.427
5200	38.137	294.336	260.392	176.511	-151.469	-537.275	5.397
5300	38.171	295.063	261.039	180.326	-152.721	-544.681	5.368
5400	38.200	295.777	261.676	184.146	-153.987	-552.065	5.340
5500	38.074	296.476	262.302	187.957	-155.279	-559.426	5.313
5600	38.263	297.164	262.919	191.775	-156.585	-566.762	5.287
5700	38.296	297.842	263.525	195.603	-157.899	-574.075	5.261
5800	38.325	298.508	264.123	199.434	-159.230	-581.364	5.236
5900	38.355	299.163	264.711	203.268	-160.579	-588.631	5.211
6000	38.388	299.808	265.291	207.106	-161.945	-595.875	5.188

Figure B.6: *JANAF data for carbon monoxide gas.*

Carbon Dioxide (CO_2), ideal gas, mol. wt. = 44.0098

Enthalpy Reference Temperature = T_r = 298.15 K; Standard State Pressure = p^o = 0.1 MPa

	J K^{-1}mol^{-1}			kJ mol^{-1}			
T/K	C_p^o	S^o	$-[G^o-H^o(T_r)]/T$	$H^o-H^o(T_r)$	$\Delta_f H^o$	$\Delta_f G^o$	Log K_f
0	0.	0.	INFINITE	-9.364	-393.151	-393.151	INFINITE
100	29.208	179.009	243.568	-6.456	-393.208	-393.683	205.639
200	32.359	199.975	217.046	-3.414	-393.404	-394.085	102.924
298.15	37.129	213.795	213.795	0.	-393.522	-394.389	69.095
300	37.221	214.025	213.795	0.069	-393.523	-394.394	68.670
400	41.325	225.314	215.307	4.003	-393.583	-394.675	51.539
500	44.627	234.901	218.290	8.305	-393.666	-394.939	41.259
600	47.321	243.283	221.772	12.907	-393.803	-395.182	34.404
700	49.564	250.750	225.388	17.754	-393.983	-395.398	29.505
800	51.434	257.494	228.986	22.806	-394.168	-395.586	25.829
900	52.999	263.645	232.500	28.030	-394.405	-395.748	22.969
1000	54.308	269.299	235.901	33.397	-394.623	-395.886	20.679
1100	55.409	274.528	239.178	38.884	-394.838	-396.001	18.805
1200	56.342	279.390	242.329	44.473	-395.050	-396.098	17.242
1300	57.137	283.932	245.356	50.148	-395.257	-396.177	15.919
1400	57.802	288.191	248.265	55.896	-395.462	-396.240	14.784
1500	58.379	292.199	251.062	61.705	-395.668	-396.288	13.800
1600	58.886	295.983	253.753	67.569	-395.876	-396.323	12.939
1700	59.317	299.566	256.343	73.480	-396.090	-396.344	12.178
1800	59.701	302.968	258.840	79.431	-396.311	-396.353	11.502
1900	60.049	306.205	261.248	85.419	-396.542	-396.349	10.896
2000	60.350	309.293	263.574	91.439	-396.784	-396.333	10.351
2100	60.622	312.244	265.822	97.488	-397.039	-396.304	9.858
2200	60.865	315.070	267.996	103.562	-397.309	-396.262	9.408
2300	61.086	317.781	270.102	109.660	-397.596	-396.209	8.998
2400	61.287	320.385	272.144	115.779	-397.900	-396.142	8.622
2500	61.471	322.890	274.124	121.917	-398.222	-396.062	8.275
2600	61.647	325.305	276.046	128.073	-398.562	-395.969	7.955
2700	61.802	327.634	277.914	134.246	-398.921	-395.862	7.658
2800	61.952	329.885	279.730	140.433	-399.299	-395.742	7.383
2900	62.095	332.061	281.497	146.636	-399.695	-395.609	7.126
3000	62.229	334.169	283.218	152.852	-400.111	-395.461	6.886
3100	62.347	336.211	284.895	159.081	-400.545	-395.298	6.661
3200	62.462	338.192	286.529	165.321	-400.998	-395.122	6.450
3300	62.573	340.116	288.124	171.573	-401.470	-394.932	6.251
3400	62.681	341.986	289.681	177.836	-401.960	-394.726	6.064
3500	62.785	343.804	291.202	184.109	-402.467	-394.506	5.888
3600	62.884	345.574	292.687	190.393	-402.991	-394.271	5.721
3700	62.980	347.299	294.140	196.686	-403.532	-394.022	5.563
3800	63.074	348.979	295.561	202.989	-404.089	-393.756	5.413
3900	63.166	350.619	296.952	209.301	-404.662	-393.477	5.270
4000	63.254	352.219	298.314	215.622	-405.251	-393.183	5.134
4100	63.341	353.782	299.648	221.951	-405.856	-392.874	5.005
4200	63.426	355.310	300.955	228.290	-406.475	-392.550	4.882
4300	63.509	356.803	302.236	234.637	-407.110	-392.210	4.764
4400	63.588	358.264	303.493	240.991	-407.760	-391.857	4.652
4500	63.667	359.694	304.726	247.354	-408.426	-391.488	4.544
4600	63.745	361.094	305.937	253.725	-409.106	-391.105	4.441
4700	63.823	362.466	307.125	260.103	-409.802	-390.706	4.342
4800	63.893	363.810	308.292	266.489	-410.514	-390.292	4.247
4900	63.968	365.126	309.438	272.882	-411.242	-389.892	4.156
5000	64.046	366.422	310.565	279.283	-411.986	-389.419	4.068
5100	64.128	367.691	311.673	285.691	-412.746	-388.959	3.984
5200	64.220	368.937	312.762	292.109	-413.522	-388.486	3.902
5300	64.312	370.161	313.833	298.535	-414.314	-387.996	3.824
5400	64.404	371.364	314.888	304.971	-415.123	-387.493	3.748
5500	64.496	372.547	315.925	311.416	-415.949	-386.974	3.675
5600	64.588	373.709	316.947	317.870	-416.794	-386.439	3.605
5700	64.680	374.853	317.953	324.334	-417.658	-385.890	3.536
5800	64.772	375.979	318.944	330.806	-418.541	-385.324	3.470
5900	64.865	377.087	319.920	337.288	-419.445	-384.745	3.406
6000	64.957	378.178	320.882	343.779	-420.372	-384.148	3.344

Figure B.7: *JANAF data for carbon dioxide gas.*

Hydrogen (H_2), ideal gas-reference state, mol. wt. = 2.01588

Enthalpy Reference Temperature = T_r = 298.15 K				Standard State Pressure = p^o = 0.1 MPa			
	J $K^{-1}mol^{-1}$			kJ mol^{-1}			
T/K	C_p^o	S^o	$-[G^o-H^o(T_r)]/T$	$H^o-H^o(T_r)$	$\Delta_f H^o$	$\Delta_f G^o$	Log K_f
0	0.	0.	INFINITE	-8.467	0.	0.	0.
100	28.154	100.727	155.408	-5.468	0.	0.	0.
200	27.447	119.412	133.284	-2.774	0.	0.	0.
250	28.344	125.640	131.152	-1.378	0.	0.	0.
298.15	28.836	130.680	130.680	0.	0.	0.	0.
300	28.849	130.858	130.680	0.053	0.	0.	0.
350	29.081	135.325	131.032	1.502	0.	0.	0.
400	29.181	139.216	131.817	2.959	0.	0.	0.
450	29.229	142.656	132.834	4.420	0.	0.	0.
500	29.260	145.737	133.973	5.882	0.	0.	0.
600	29.327	151.077	136.392	8.811	0.	0.	0.
700	29.441	155.606	138.822	11.749	0.	0.	0.
800	29.624	159.548	141.171	14.702	0.	0.	0.
900	29.881	163.051	143.411	17.676	0.	0.	0.
1000	30.205	166.216	145.536	20.680	0.	0.	0.
1100	30.581	169.112	147.549	23.719	0.	0.	0.
1200	30.992	171.790	149.459	26.797	0.	0.	0.
1300	31.423	174.288	151.274	29.918	0.	0.	0.
1400	31.861	176.633	153.003	33.082	0.	0.	0.
1500	32.298	178.846	154.652	36.290	0.	0.	0.
1600	32.725	180.944	156.231	39.541	0.	0.	0.
1700	33.139	182.940	157.743	42.835	0.	0.	0.
1800	33.537	184.846	159.197	46.169	0.	0.	0.
1900	33.917	186.669	160.595	49.541	0.	0.	0.
2000	34.280	188.418	161.943	52.951	0.	0.	0.
2100	34.624	190.099	163.244	56.397	0.	0.	0.
2200	34.952	191.718	164.501	59.876	0.	0.	0.
2300	35.263	193.278	165.719	63.387	0.	0.	0.
2400	35.559	194.785	166.899	66.928	0.	0.	0.
2500	35.842	196.243	168.044	70.498	0.	0.	0.
2600	36.111	197.654	169.155	74.096	0.	0.	0.
2700	36.370	199.021	170.236	77.720	0.	0.	0.
2800	36.618	200.349	171.288	81.369	0.	0.	0.
2900	36.856	201.638	172.313	85.043	0.	0.	0.
3000	37.087	202.891	173.311	88.740	0.	0.	0.
3100	37.311	204.111	174.285	92.460	0.	0.	0.
3200	37.528	205.299	175.236	96.202	0.	0.	0.
3300	37.740	206.457	176.164	99.966	0.	0.	0.
3400	37.946	207.587	177.072	103.750	0.	0.	0.
3500	38.149	208.690	177.960	107.555	0.	0.	0.
3600	38.348	209.767	178.828	111.380	0.	0.	0.
3700	38.544	210.821	179.679	115.224	0.	0.	0.
3800	38.738	211.851	180.512	119.089	0.	0.	0.
3900	38.928	212.860	181.328	122.972	0.	0.	0.
4000	39.116	213.848	182.129	126.874	0.	0.	0.
4100	39.301	214.816	182.915	130.795	0.	0.	0.
4200	39.484	215.765	183.686	134.734	0.	0.	0.
4300	39.665	216.696	184.442	138.692	0.	0.	0.
4400	39.842	217.610	185.186	142.667	0.	0.	0.
4500	40.017	218.508	185.916	146.660	0.	0.	0.
4600	40.188	219.389	186.635	150.670	0.	0.	0.
4700	40.355	220.255	187.341	154.698	0.	0.	0.
4800	40.518	221.106	188.035	158.741	0.	0.	0.
4900	40.676	221.943	188.719	162.801	0.	0.	0.
5000	40.829	222.767	189.392	166.876	0.	0.	0.
5100	40.976	223.577	190.054	170.967	0.	0.	0.
5200	41.117	224.374	190.706	175.071	0.	0.	0.
5300	41.252	225.158	191.349	179.190	0.	0.	0.
5400	41.379	225.931	191.982	183.322	0.	0.	0.
5500	41.498	226.691	192.606	187.465	0.	0.	0.
5600	41.609	227.440	193.222	191.621	0.	0.	0.
5700	41.712	228.177	193.829	195.787	0.	0.	0.
5800	41.806	228.903	194.427	199.963	0.	0.	0.
5900	41.890	229.619	195.017	204.148	0.	0.	0.
6000	41.965	230.323	195.600	208.341	0.	0.	0.

Figure B.8: *JANAF data for diatomic hydrogen gas.*

Hydrogen, Monatomic (H), ideal gas, mol. wt. = 1.00794

Enthalpy Reference Temperature = T_r = 298.15 K				Standard State Pressure = p^o = 0.1 MPa			
	J $K^{-1}mol^{-1}$			kJ mol^{-1}			
T/K	C_p^o	S^o	$-[G^o-H^o(T_r)]/T$	$H^o-H^o(T_r)$	$\Delta_f H^o$	$\Delta_f G^o$	Log K_f
0	0.	0.	INFINITE	-6.197	216.035	216.035	INFINITE
100	20.786	92.009	133.197	-4.119	216.614	212.450	-110.972
200	20.786	106.417	116.618	-2.040	217.346	208.004	-54.325
250	20.786	111.055	115.059	-1.001	217.687	205.629	-42.964
298.15	20.786	114.716	114.716	0.	217.999	203.278	-35.613
300	20.786	114.845	114.717	0.038	218.011	203.186	-35.378
350	20.786	118.049	114.970	1.078	218.326	200.690	-29.951
400	20.786	120.825	115.532	2.117	218.637	198.150	-25.876
450	20.786	123.273	116.259	3.156	218.946	195.570	-22.701
500	20.786	125.463	117.072	4.196	219.254	192.957	-20.158
600	20.786	129.253	118.796	6.274	219.868	187.640	-16.335
700	20.786	132.457	120.524	8.353	220.478	182.220	-13.597
800	20.788	135.232	122.193	10.431	221.080	176.713	-11.538
900	20.786	137.681	123.781	12.510	221.671	171.132	-9.932
1000	20.786	139.871	125.282	14.589	222.248	165.485	-8.644
1100	20.786	141.852	126.700	16.667	222.807	159.782	-7.587
1200	20.786	143.660	128.039	18.746	223.346	154.028	-6.705
1300	20.786	145.324	129.305	20.824	223.865	148.230	-5.956
1400	20.786	146.865	130.505	22.903	224.361	142.394	-5.313
1500	20.786	148.299	131.644	24.982	224.836	136.522	-4.754
1600	20.786	149.640	132.728	27.060	225.289	130.620	-4.264
1700	20.786	150.900	133.760	29.139	225.721	124.689	-3.831
1800	20.786	152.088	134.745	31.217	226.132	118.734	-3.446
1900	20.786	153.212	135.688	33.296	226.525	112.757	-3.100
2000	20.786	154.278	136.591	35.375	226.898	106.760	-2.788
2100	20.786	155.293	137.458	37.453	227.254	100.744	-2.506
2200	20.786	156.260	138.291	39.532	227.593	94.712	-2.249
2300	20.786	157.184	139.092	41.610	227.916	88.664	-2.014
2400	20.786	158.068	139.864	43.689	228.224	82.603	-1.798
2500	20.786	158.917	140.610	45.768	228.518	76.530	-1.599
2600	20.786	159.732	141.330	47.846	228.798	70.444	-1.415
2700	20.786	160.516	142.026	49.925	229.064	64.349	-1.245
2800	20.786	161.272	142.700	52.004	229.318	58.243	-1.087
2900	20.786	162.002	143.353	54.082	229.560	52.129	-0.939
3000	20.786	162.706	143.986	56.161	229.790	46.007	-0.801
3100	20.786	163.388	144.601	58.239	230.008	39.877	-0.672
3200	20.786	164.048	145.199	60.318	230.216	33.741	-0.551
3300	20.786	164.688	145.780	62.397	230.413	27.598	-0.437
3400	20.786	165.308	146.345	64.475	230.599	21.449	-0.330
3500	20.786	165.911	146.895	66.554	230.776	15.295	-0.228
3600	20.786	166.496	147.432	68.632	230.942	9.136	-0.133
3700	20.786	167.066	147.955	70.711	231.098	2.973	-0.042
3800	20.786	167.620	148.465	72.790	231.244	-3.195	0.044
3900	20.786	168.160	148.963	74.868	231.381	-9.366	0.125
4000	20.786	168.686	149.450	76.947	231.509	-15.541	0.203
4100	20.786	169.200	149.925	79.025	231.627	-21.718	0.277
4200	20.786	169.700	150.390	81.104	231.736	-27.899	0.347
4300	20.786	170.190	150.845	83.183	231.836	-34.082	0.414
4400	20.786	170.667	151.290	85.261	231.927	-40.267	0.478
4500	20.786	171.135	151.726	87.340	232.009	-46.454	0.539
4600	20.786	171.591	152.153	89.418	232.082	-52.643	0.598
4700	20.786	172.038	152.571	91.497	232.147	-58.834	0.654
4800	20.786	172.476	152.981	93.576	232.204	-65.025	0.708
4900	20.786	172.905	153.383	95.654	232.253	-71.218	0.759
5000	20.786	173.325	153.778	97.733	232.294	-77.412	0.809
5100	20.786	173.736	154.165	99.811	232.327	-83.606	0.856
5200	20.786	174.140	154.546	101.890	232.353	-89.801	0.902
5300	20.786	174.536	154.919	103.969	232.373	-95.997	0.946
5400	20.786	174.924	155.286	106.047	232.386	-102.192	0.989
5500	20.786	175.306	155.646	108.126	232.392	-108.389	1.029
5600	20.786	175.680	156.001	110.204	232.393	-114.584	1.069
5700	20.786	176.048	156.349	112.283	232.389	-120.780	1.107
5800	20.786	176.410	156.692	114.362	232.379	-126.976	1.144
5900	20.786	176.765	157.029	116.440	232.365	-133.172	1.179
6000	20.786	177.114	157.361	118.519	232.348	-139.368	1.213

Figure B.9: *JANAF data for monatomic hydrogen gas.*

Hydroperoxyl (HO_2), ideal gas, mol. wt. = 33.00674

Enthalpy Reference Temperature = T_r = 298.15 K				Standard State Pressure = p^o = 0.1 MPa			
	J K^{-1}mol^{-1}			kJ mol^{-1}			
T/K	C_p^o	S^o	$-[G^o-H^o(T_r)]/T$	$H^o-H^o(T_r)$	$\Delta_f H^o$	$\Delta_f G^o$	Log K_f
0	0.	0.	INFINITE	-10.003	5.006	5.006	INFINITE
100	33.258	192.430	259.201	-6.677	3.928	7.052	-3.683
200	33.491	215.515	232.243	-3.346	3.001	10.536	-2.752
250	34.044	223.040	229.676	-1.659	2.532	12.475	-2.606
298.15	34.905	229.106	229.106	0.	2.092	14.430	-2.528
300	34.943	229.322	229.107	0.065	2.076	14.506	-2.526
350	36.072	234.791	229.536	1.839	1.649	16.612	-2.479
400	37.296	239.688	230.504	3.673	1.260	18.777	-2.452
450	38.519	244.151	231.776	5.569	0.908	20.988	-2.436
500	39.687	248.271	233.222	7.524	0.591	23.236	-2.427
600	41.781	255.697	236.363	11.601	0.043	27.819	-2.422
700	43.558	262.275	239.603	15.870	-0.411	32.485	-2.424
800	45.084	268.193	242.813	20.304	-0.790	37.211	-2.430
900	46.418	273.582	245.937	24.880	-1.107	41.981	-2.436
1000	47.604	278.535	248.952	29.583	-1.368	46.783	-2.444
1100	48.672	283.123	251.853	34.397	-1.582	51.609	-2.451
1200	49.643	287.400	254.639	39.314	-1.754	56.452	-2.457
1300	50.535	291.410	257.315	44.323	-1.887	61.308	-2.463
1400	51.360	295.185	259.886	49.419	-1.988	66.173	-2.469
1500	52.128	298.755	262.360	54.593	-2.058	71.045	-2.474
1600	52.845	302.143	264.741	59.842	-2.102	75.920	-2.479
1700	53.518	305.367	267.037	65.161	-2.122	80.797	-2.483
1800	54.149	308.444	269.252	70.545	-2.121	85.674	-2.486
1900	54.742	311.388	271.393	75.989	-2.102	90.551	-2.489
2000	55.299	314.210	273.464	81.492	-2.067	95.427	-2.492
2100	55.820	316.921	275.469	87.048	-2.019	100.301	-2.495
2200	56.308	319.529	277.413	92.655	-1.960	105.172	-2.497
2300	56.763	322.042	279.299	98.309	-1.893	110.040	-2.499
2400	57.186	324.467	281.131	104.006	-1.818	114.905	-2.501
2500	57.578	326.809	282.911	109.745	-1.740	119.767	-2.502
2600	57.940	329.075	284.644	115.521	-1.659	124.625	-2.504
2700	58.274	331.268	286.330	121.332	-1.577	129.481	-2.505
2800	58.580	333.393	287.973	127.175	-1.497	134.334	-2.506
2900	58.860	335.453	289.575	133.047	-1.419	139.183	-2.507
3000	59.115	337.453	291.138	138.946	-1.346	144.030	-2.508
3100	59.347	339.395	292.663	144.869	-1.278	148.876	-2.509
3200	59.557	341.283	294.153	150.814	-1.218	153.718	-2.509
3300	59.745	343.118	295.609	156.780	-1.165	158.558	-2.510
3400	59.915	344.904	297.033	162.763	-1.122	163.398	-2.510
3500	60.066	346.643	298.426	168.762	-1.089	168.236	-2.511
3600	60.200	348.337	299.789	174.775	-1.067	173.074	-2.511
3700	60.318	349.989	301.123	180.801	-1.058	177.910	-2.512
3800	60.423	351.599	302.431	186.839	-1.061	182.748	-2.512
3900	60.513	353.169	303.711	192.886	-1.078	187.586	-2.512
4000	60.592	354.702	304.987	198.941	-1.109	192.423	-2.513
4100	60.659	356.199	306.199	205.004	-1.156	197.262	-2.513
4200	60.716	357.662	307.406	211.072	-1.217	202.102	-2.514
4300	60.764	359.091	308.592	217.146	-1.296	206.945	-2.514
4400	60.803	360.488	309.756	223.225	-1.391	211.788	-2.514
4500	60.834	361.855	310.898	229.307	-1.504	216.634	-2.515
4600	60.858	363.193	312.021	235.391	-1.634	221.482	-2.515
4700	60.876	364.502	313.123	241.478	-1.784	226.335	-2.515
4800	60.888	365.783	314.207	247.566	-1.952	231.190	-2.516
4900	60.895	367.039	315.272	253.656	-2.141	236.050	-2.516
5000	60.897	368.269	316.320	259.745	-2.350	240.913	-2.517
5100	60.894	369.475	317.351	265.835	-2.580	245.780	-2.517
5200	60.888	370.658	318.364	271.924	-2.831	250.652	-2.518
5300	60.879	371.817	319.362	278.012	-3.105	255.530	-2.518
5400	60.866	372.955	320.344	284.100	-3.402	260.412	-2.519
5500	60.851	374.072	321.311	290.185	-3.722	265.300	-2.520
5600	60.834	375.168	322.263	296.270	-4.067	270.195	-2.520
5700	60.814	376.245	323.200	302.352	-4.437	275.096	-2.521
5800	60.792	377.302	324.124	308.432	-4.832	280.004	-2.522
5900	60.769	378.341	325.034	314.511	-5.254	284.917	-2.522
6000	60.745	379.362	325.931	320.586	-5.702	289.839	-2.523

Figure B.10: *JANAF data for hydroperoxide gas.*

Hydroxyl (OH), ideal gas, mol. wt. = 17.0074

Enthalpy Reference Temperature = T_r = 298.15 K				Standard State Pressure = p^o = 0.1 MPa			
	J $K^{-1}mol^{-1}$			kJ mol^{-1}			
T/K	C_p^o	S^o	$-[G^o-H^o(T_r)]/T$	$H^o-H^o(T_r)$	$\Delta_f H^o$	$\Delta_f G^o$	Log K_f
0	0.	0.	INFINITE	-9.172	38.390	38.390	INFINITE
100	32.627	149.590	210.980	-6.139	38.471	37.214	-19.438
200	30.777	171.592	186.471	-2.976	38.832	35.803	-9.351
250	30.283	178.402	184.204	-1.450	38.930	35.033	-7.320
298.15	29.986	183.708	183.708	0.	38.987	34.277	-6.005
300	29.977	183.894	183.709	0.055	38.988	34.248	-5.963
350	29.780	188.499	184.073	1.549	39.019	33.455	-4.993
400	29.650	192.466	184.880	3.035	39.029	32.660	-4.265
450	29.567	195.954	185.921	4.515	39.020	31.864	-3.699
500	29.521	199.066	187.082	5.992	38.995	31.070	-3.246
600	29.527	204.447	189.542	8.943	38.902	29.493	-2.568
700	29.663	209.007	192.005	11.902	38.764	27.935	-2.085
800	29.917	212.983	194.384	14.880	38.598	26.399	-1.724
900	30.264	216.526	196.651	17.888	38.416	24.884	-1.444
1000	30.676	219.736	198.801	20.935	38.230	23.391	-1.222
1100	31.124	222.680	200.840	24.024	38.046	21.916	-1.041
1200	31.586	225.408	202.775	27.160	37.867	20.458	-0.891
1300	32.046	227.955	204.615	30.342	37.697	19.014	-0.764
1400	32.492	230.346	206.368	33.569	37.535	17.583	-0.656
1500	32.917	232.602	208.043	36.839	37.381	16.163	-0.563
1600	33.319	234.740	209.645	40.151	37.234	14.753	-0.482
1700	33.694	236.771	211.182	43.502	37.093	13.352	-0.410
1800	34.044	238.707	212.657	46.889	36.955	11.960	-0.347
1900	34.369	240.557	214.078	50.310	36.819	10.575	-0.291
2000	34.670	242.327	215.446	53.762	36.685	9.197	-0.240
2100	34.950	244.026	216.767	57.243	36.551	7.826	-0.195
2200	35.209	245.658	218.043	60.752	36.416	6.462	-0.153
2300	35.449	247.228	219.278	64.285	36.278	5.103	-0.116
2400	35.673	248.741	220.474	67.841	36.137	3.750	-0.082
2500	35.881	250.202	221.635	71.419	35.992	2.404	-0.050
2600	36.075	251.613	222.761	75.017	35.843	1.063	-0.021
2700	36.256	252.978	223.855	78.633	35.689	-0.271	0.005
2800	36.426	254.300	224.918	82.267	35.530	-1.600	0.030
2900	36.586	255.581	225.954	85.918	35.365	-2.924	0.053
3000	36.736	256.824	226.962	89.584	35.194	-4.241	0.074
3100	36.878	258.031	227.945	93.265	35.017	-5.552	0.094
3200	37.013	259.203	228.904	96.960	34.834	-6.858	0.112
3300	37.140	260.344	229.839	100.667	34.644	-8.158	0.129
3400	37.261	261.455	230.753	104.387	34.448	-9.452	0.145
3500	37.376	262.537	231.645	108.119	34.246	-10.741	0.160
3600	37.486	263.591	232.518	111.863	34.037	-12.023	0.174
3700	37.592	264.620	233.372	115.617	33.821	-13.300	0.188
3800	37.693	265.624	234.208	119.381	33.599	-14.570	0.200
3900	37.791	266.604	235.026	123.155	33.371	-15.834	0.212
4000	37.885	267.562	235.827	126.939	33.136	-17.093	0.223
4100	37.976	268.499	236.613	130.732	32.894	-18.346	0.234
4200	38.064	269.415	237.383	134.534	32.646	-19.593	0.244
4300	38.150	270.311	238.138	138.345	32.391	-20.833	0.253
4400	38.233	271.189	238.879	142.164	32.130	-22.068	0.262
4500	38.315	272.050	239.607	145.991	31.862	-23.297	0.270
4600	38.394	272.893	240.322	149.827	31.587	-24.520	0.278
4700	38.472	273.719	241.023	153.670	31.305	-25.737	0.286
4800	38.549	274.530	241.713	157.521	31.017	-26.947	0.293
4900	38.625	275.326	242.391	161.380	30.722	-28.152	0.300
5000	38.699	276.107	243.057	165.246	30.420	-29.350	0.307
5100	38.773	276.874	243.713	169.120	30.111	-30.542	0.313
5200	38.846	277.627	244.358	173.001	29.796	-31.729	0.319
5300	38.919	278.368	244.993	176.889	29.473	-32.909	0.324
5400	38.991	279.096	245.617	180.784	29.144	-34.083	0.330
5500	39.062	279.812	246.233	184.687	28.807	-35.251	0.335
5600	39.134	280.517	246.839	188.597	28.464	-36.412	0.340
5700	39.206	281.210	247.436	192.514	28.113	-37.568	0.344
5800	39.278	281.892	248.024	196.438	27.756	-38.716	0.349
5900	39.350	282.564	248.604	200.369	27.391	-39.860	0.353
6000	39.423	283.226	249.175	204.308	27.019	-40.997	0.357

Figure B.11: *JANAF data for hydroxyl gas.*

Water (H_2O), ideal gas, mol. wt. = 18.01528

Enthalpy Reference Temperature = T_r = 298.15 K				Standard State Pressure = p^o = 0.1 MPa			
	J $K^{-1}mol^{-1}$			kJ mol^{-1}			
T/K	C_p^o	S^o	$-[G^o-H^o(T_r)]/T$	$H^o-H^o(T_r)$	$\Delta_f H^o$	$\Delta_f G^o$	Log K_f
0	0.	0.	INFINITE	-9.904	-238.921	-238.921	INFINITE
100	33.299	152.388	218.534	-6.615	-240.083	-236.584	123.579
200	33.349	175.485	191.896	-3.282	-240.900	-232.766	60.792
298.15	33.590	188.834	188.834	0.	-241.826	-228.582	40.047
300	33.596	189.042	188.835	0.062	-241.844	-228.500	39.785
400	34.262	198.788	190.159	3.452	-242.846	-223.901	29.238
500	35.226	206.534	192.685	6.925	-243.826	-219.051	22.884
600	36.325	213.052	195.550	10.501	-244.758	-214.007	18.631
700	37.495	218.739	198.465	14.192	-245.632	-208.612	15.582
800	38.721	223.825	201.322	18.002	-246.443	-203.496	13.287
900	39.987	228.459	204.084	21.938	-247.185	-198.083	11.496
1000	41.268	232.738	206.738	26.000	-247.857	-192.590	10.060
1100	42.536	236.731	209.285	30.191	-248.460	-187.033	8.881
1200	43.768	240.485	211.730	34.506	-248.997	-181.425	7.897
1300	44.945	244.035	214.080	38.942	-249.473	-175.774	7.063
1400	46.054	247.407	216.341	43.493	-249.894	-170.089	6.346
1500	47.090	250.620	218.520	48.151	-250.265	-164.376	5.724
1600	48.050	253.690	220.623	52.908	-250.592	-158.639	5.179
1700	48.935	256.630	222.655	57.758	-250.881	-152.883	4.698
1800	49.749	259.451	224.621	62.693	-251.138	-147.111	4.269
1900	50.496	262.161	226.526	67.706	-251.368	-141.325	3.885
2000	51.180	264.769	228.374	72.790	-251.575	-135.528	3.540
2100	51.823	267.282	230.167	77.941	-251.762	-129.721	3.227
2200	52.408	269.706	231.909	83.153	-251.934	-123.905	2.942
2300	52.947	272.048	233.604	88.421	-252.092	-118.082	2.682
2400	53.444	274.312	235.253	93.741	-252.239	-112.252	2.443
2500	53.904	276.503	236.860	99.108	-252.379	-106.416	2.223
2600	54.329	278.625	238.425	104.520	-252.513	-100.575	2.021
2700	54.723	280.683	239.952	109.973	-252.643	-94.729	1.833
2800	55.089	282.680	241.443	115.464	-252.771	-88.878	1.658
2900	55.430	284.619	242.899	120.990	-252.897	-83.023	1.495
3000	55.748	286.504	244.321	126.549	-253.024	-77.163	1.344
3100	56.044	288.337	245.711	132.139	-253.152	-71.298	1.201
3200	56.323	290.120	247.071	137.757	-253.282	-65.430	1.068
3300	56.583	291.858	248.402	143.403	-253.416	-59.558	0.943
3400	56.828	293.550	249.705	149.073	-253.553	-53.681	0.825
3500	57.058	295.201	250.982	154.768	-253.696	-47.801	0.713
3600	57.276	296.812	252.233	160.485	-253.844	-41.916	0.608
3700	57.480	298.384	253.459	166.222	-253.997	-36.027	0.509
3800	57.675	299.919	254.661	171.980	-254.158	-30.133	0.414
3900	57.859	301.420	255.841	177.757	-254.326	-24.236	0.325
4000	58.033	302.887	256.999	183.552	-254.501	-18.334	0.239
4100	58.199	304.322	258.136	189.363	-254.684	-12.427	0.158
4200	58.357	305.726	259.252	195.191	-254.876	-6.516	0.081
4300	58.507	307.101	260.349	201.034	-255.078	-0.600	0.007
4400	58.650	308.448	261.427	206.892	-255.288	5.320	-0.063
4500	58.787	309.767	262.486	212.764	-255.508	11.245	-0.131
4600	58.918	311.061	263.528	218.650	-255.738	17.175	-0.195
4700	59.044	312.329	264.553	224.548	-255.978	23.111	-0.257
4800	59.164	313.574	265.562	230.458	-256.229	29.052	-0.316
4900	59.275	314.795	266.554	236.380	-256.491	34.998	-0.373
5000	59.390	315.993	267.531	242.313	-256.763	40.949	-0.428
5100	59.509	317.171	268.493	248.256	-257.046	46.906	-0.480
5200	59.628	318.327	269.440	254.215	-257.338	52.869	-0.531
5300	59.746	319.464	270.373	260.184	-257.639	58.838	-0.580
5400	59.864	320.582	271.293	266.164	-257.950	64.811	-0.627
5500	59.982	321.682	272.199	272.157	-258.268	70.791	-0.672
5600	60.100	322.764	273.092	278.161	-258.595	76.777	-0.716
5700	60.218	323.828	273.973	284.177	-258.930	82.769	-0.758
5800	60.335	324.877	274.841	290.204	-259.272	88.787	-0.799
5900	60.453	325.909	275.698	296.244	-259.621	94.770	-0.839
6000	60.571	326.926	276.544	302.295	-259.977	100.780	-0.877

Figure B.12: *JANAF data for water vapor.*

Nitrogen (N_2), ideal gas-reference state, mol. wt. = 28.0134

Enthalpy Reference Temperature = T_r = 298.15 K; Standard State Pressure = p^o = 0.1 MPa

T/K	C_p^o	S^o	$-[G^o-H^o(T_r)]/T$	$H^o-H^o(T_r)$	$\Delta_f H^o$	$\Delta_f G^o$	Log K_f
	J K^{-1}mol^{-1}			kJ mol^{-1}			
0	0.	0.	INFINITE	-8.670	0.	0.	0.
100	29.104	159.811	217.490	-5.768	0.	0.	0.
200	29.107	179.985	194.272	-2.857	0.	0.	0.
250	29.111	186.481	192.088	-1.402	0.	0.	0.
298.15	29.124	191.609	191.609	0.	0.	0.	0.
300	29.125	191.789	191.610	0.054	0.	0.	0.
350	29.165	196.281	191.964	1.511	0.	0.	0.
400	29.249	200.181	192.753	2.971	0.	0.	0.
450	29.387	203.633	193.774	4.437	0.	0.	0.
500	29.580	206.739	194.917	5.911	0.	0.	0.
600	30.110	212.176	197.353	8.894	0.	0.	0.
700	30.754	216.866	199.813	11.937	0.	0.	0.
800	31.433	221.017	202.209	15.046	0.	0.	0.
900	32.090	224.757	204.510	18.223	0.	0.	0.
1000	32.697	228.170	206.708	21.463	0.	0.	0.
1100	33.241	231.313	208.804	24.760	0.	0.	0.
1200	33.723	234.226	210.802	28.109	0.	0.	0.
1300	34.147	236.943	212.710	31.503	0.	0.	0.
1400	34.518	239.487	214.533	34.936	0.	0.	0.
1500	34.843	241.880	216.277	38.405	0.	0.	0.
1600	35.128	244.138	217.948	41.904	0.	0.	0.
1700	35.378	246.275	219.552	45.429	0.	0.	0.
1800	35.600	248.304	221.094	48.978	0.	0.	0.
1900	35.796	250.234	222.577	52.548	0.	0.	0.
2000	35.971	252.074	224.006	56.137	0.	0.	0.
2100	36.126	253.833	225.385	59.742	0.	0.	0.
2200	36.268	255.517	226.717	63.361	0.	0.	0.
2300	36.395	257.132	228.004	66.995	0.	0.	0.
2400	36.511	258.684	229.250	70.640	0.	0.	0.
2500	36.616	260.176	230.458	74.296	0.	0.	0.
2600	36.713	261.614	231.629	77.963	0.	0.	0.
2700	36.801	263.001	232.765	81.639	0.	0.	0.
2800	36.883	264.341	233.869	85.323	0.	0.	0.
2900	36.959	265.637	234.942	89.015	0.	0.	0.
3000	37.030	266.891	235.986	92.715	0.	0.	0.
3100	37.096	268.106	237.003	96.421	0.	0.	0.
3200	37.158	269.285	237.993	100.134	0.	0.	0.
3300	37.216	270.429	238.959	103.852	0.	0.	0.
3400	37.271	271.541	239.901	107.577	0.	0.	0.
3500	37.323	272.622	240.821	111.306	0.	0.	0.
3600	37.373	273.675	241.719	115.041	0.	0.	0.
3700	37.420	274.699	242.596	118.781	0.	0.	0.
3800	37.465	275.698	243.454	122.525	0.	0.	0.
3900	37.508	276.671	244.294	126.274	0.	0.	0.
4000	37.550	277.622	245.115	130.027	0.	0.	0.
4100	37.590	278.549	245.919	133.784	0.	0.	0.
4200	37.629	279.456	246.707	137.545	0.	0.	0.
4300	37.666	280.341	247.479	141.309	0.	0.	0.
4400	37.702	281.208	248.236	145.078	0.	0.	0.
4500	37.738	282.056	248.978	148.850	0.	0.	0.
4600	37.773	282.885	249.706	152.625	0.	0.	0.
4700	37.808	283.698	250.420	156.405	0.	0.	0.
4800	37.843	284.494	251.122	160.187	0.	0.	0.
4900	37.878	285.275	251.811	163.973	0.	0.	0.
5000	37.912	286.041	252.488	167.763	0.	0.	0.
5100	37.947	286.792	253.153	171.556	0.	0.	0.
5200	37.981	287.529	253.807	175.352	0.	0.	0.
5300	38.013	288.253	254.451	179.152	0.	0.	0.
5400	38.046	288.964	255.083	182.955	0.	0.	0.
5500	38.080	289.662	255.705	186.761	0.	0.	0.
5600	38.116	290.348	256.318	190.571	0.	0.	0.
5700	38.154	291.023	256.921	194.384	0.	0.	0.
5800	38.193	291.687	257.515	198.201	0.	0.	0.
5900	38.234	292.341	258.099	202.023	0.	0.	0.
6000	38.276	292.984	258.675	205.848	0.	0.	0.

Figure B.13: *JANAF data for diatomic nitrogen gas.*

Nitrogen, Monatomic (N), ideal gas, mol. wt. = 14.0067

Enthalpy Reference Temperature = T_r = 298.15 K				Standard State Pressure = p° = 0.1 MPa			
	J K^{-1}mol^{-1}			kJ mol^{-1}			
T/K	C_p°	S°	$-[G^\circ-H^\circ(T_r)]/T$	$H^\circ-H^\circ(T_r)$	$\Delta_f H^\circ$	$\Delta_f G^\circ$	Log K_f
0	0.	0.	INFINITE	-6.197	470.820	470.820	INFINITE
100	20.786	130.593	171.780	-4.119	471.448	466.379	-243.611
200	20.786	145.001	155.201	-2.040	472.071	461.070	-120.419
250	20.786	149.639	153.642	-1.001	472.383	458.283	-95.753
298.15	20.786	153.300	153.300	0.	472.683	455.540	-79.809
300	20.788	153.429	153.300	0.038	472.694	455.434	-79.298
350	20.786	156.633	153.554	1.078	473.005	452.533	-67.537
400	20.786	159.408	154.116	2.117	473.314	449.587	-58.710
450	20.786	161.857	154.843	3.156	473.621	446.603	-51.840
500	20.786	164.047	155.655	4.196	473.923	443.584	-46.341
600	20.766	167.836	157.379	6.274	474.510	437.461	-38.084
700	20.786	171.041	159.108	8.353	475.067	431.242	-32.180
800	20.786	173.816	160.777	10.431	475.591	424.945	-27.746
900	20.786	176.264	162.364	12.510	476.081	418.584	-24.294
1000	20.786	178.454	163.866	14.589	476.540	412.171	-21.530
1100	20.786	180.436	165.284	16.667	476.970	405.713	-19.266
1200	20.786	182.244	166.623	18.746	477.374	399.217	-17.377
1300	20.788	183.908	167.889	20.824	477.756	392.688	-15.778
1400	20.786	185.448	169.089	22.903	478.118	386.131	-14.407
1500	20.786	186.882	170.228	24.982	478.462	379.548	-13.217
1600	20.766	188.224	171.311	27.060	478.791	372.943	-12.175
1700	20.786	189.484	172.344	29.139	479.107	366.318	-11.256
1800	20.787	190.672	173.329	31.218	479.411	359.674	-10.437
1900	20.788	191.796	174.272	33.296	479.705	353.014	-9.705
2000	20.790	192.863	175.175	35.375	479.990	346.339	-9.045
2100	20.793	193.877	176.042	37.454	480.266	339.650	-8.448
2200	20.797	194.844	176.874	39.534	480.536	332.947	-7.905
2300	20.804	195.769	177.676	41.614	480.799	326.233	-7.409
2400	20.813	196.655	178.448	43.695	481.057	319.507	-6.954
2500	20.826	197.504	179.194	45.777	481.311	312.770	-6.535
2600	20.843	198.322	179.914	47.860	481.561	306.024	-6.148
2700	20.864	199.109	180.610	49.945	481.809	299.268	-5.790
2800	20.891	199.868	181.285	52.033	482.054	292.502	-5.457
2900	20.924	200.601	181.938	54.124	482.299	285.728	-5.147
3000	20.963	201.311	182.572	56.218	482.543	278.946	-4.857
3100	21.010	202.000	183.188	58.317	482.789	272.155	-4.586
3200	21.064	202.667	183.786	60.420	483.036	265.357	-4.332
3300	21.126	203.317	184.368	62.530	483.286	258.550	-4.093
3400	21.197	203.948	184.935	64.646	483.540	251.736	-3.867
3500	21.277	204.564	185.487	66.769	483.799	244.915	-3.655
3600	21.365	205.164	186.025	68.902	484.064	238.086	-3.455
3700	21.463	205.751	186.550	71.043	484.335	231.249	-3.265
3800	21.569	206.325	187.063	73.194	484.614	224.405	-3.085
3900	21.685	206.887	187.564	75.357	484.903	217.554	-2.914
4000	21.809	207.437	188.054	77.532	485.201	210.695	-2.751
4100	21.941	207.977	188.534	79.719	485.510	203.829	-2.597
4200	22.082	208.508	189.003	81.920	485.830	196.955	-2.449
4300	22.231	209.029	189.463	84.136	486.164	190.073	-2.309
4400	22.388	209.542	189.913	86.367	486.510	183.183	-2.175
4500	22.551	210.047	190.355	88.614	486.871	176.285	-2.046
4600	22.722	210.544	190.788	90.877	487.247	169.379	-1.923
4700	22.899	211.035	191.214	93.158	487.638	162.465	-1.806
4800	23.081	211.519	191.632	95.457	488.046	155.542	-1.693
4900	23.269	211.997	192.043	97.775	488.471	148.610	-1.584
5000	23.461	212.469	192.447	100.111	488.912	141.670	-1.480
5100	23.658	212.935	192.844	102.467	489.372	134.721	-1.380
5200	23.858	213.397	193.235	104.843	489.849	127.762	-1.283
5300	24.061	213.853	193.619	107.238	490.345	120.794	-1.190
5400	24.266	214.305	193.998	109.655	490.860	113.817	-1.101
5500	24.474	214.752	194.371	112.092	491.394	106.829	-1.015
5600	24.682	215.195	194.739	114.550	491.947	99.832	-0.931
5700	24.892	215.633	195.102	117.028	492.519	92.825	-0.851
5800	25.102	216.068	195.460	119.528	493.110	85.808	-0.773
5900	25.312	216.499	195.813	122.049	493.720	78.780	-0.697
6000	25.521	216.926	196.161	124.590	494.349	71.742	-0.625

Figure B.14: *JANAF data for monatomic nitrogen gas.*

Ammonia (NH_3), ideal gas, mol. wt. = 17.0352

Enthalpy Reference Temperature = T_r = 298.15 K — Standard State Pressure = p° = 0.1 MPa

T/K	C_p°	S°	$-[G^\circ-H^\circ(T_r)]/T$	$H^\circ-H^\circ(T_r)$	$\Delta_f H^\circ$	$\Delta_f G^\circ$	Log K_f
	J K^{-1} mol^{-1}			kJ mol^{-1}			
0	0.	0.	INFINITE	-10.045	-38.907	-38.907	INFINITE
100	33.284	155.840	223.211	-6.737	-41.550	-34.034	17.777
200	33.757	178.990	195.962	-3.394	-43.703	-25.679	6.707
298.15	35.652	192.774	192.774	0.	-45.898	-16.367	2.867
300	35.701	192.995	192.775	0.066	-45.939	-16.183	2.818
400	38.716	203.663	194.209	3.781	-48.041	-5.941	0.776
500	42.048	212.659	197.021	7.819	-49.857	4.800	-0.501
600	45.293	220.615	200.302	12.188	-51.374	15.879	-1.382
700	48.354	227.829	203.727	16.872	-52.618	27.190	-2.029
800	51.235	234.476	207.160	21.853	-53.621	38.662	-2.524
900	53.948	240.669	210.543	27.113	-54.411	50.247	-2.916
1000	56.491	246.486	213.849	32.637	-55.013	61.910	-3.234
1100	58.859	251.983	217.069	38.406	-55.451	73.625	-3.496
1200	61.048	257.199	220.197	44.402	-55.746	85.373	-3.716
1300	63.057	262.166	223.236	50.609	-55.917	97.141	-3.903
1400	64.893	266.907	226.187	57.008	-55.982	108.918	-4.064
1500	66.564	271.442	229.054	63.582	-55.954	120.696	-4.203
1600	68.079	275.788	231.840	70.315	-55.847	132.469	-4.325
1700	69.452	279.957	234.549	77.193	-55.672	144.234	-4.432
1800	70.695	283.962	237.184	84.201	-55.439	155.986	-4.527
1900	71.818	287.815	239.748	91.328	-55.157	167.725	-4.611
2000	72.833	291.525	242.244	98.561	-54.833	179.447	-4.687
2100	73.751	295.101	244.677	105.891	-54.473	191.152	-4.755
2200	74.581	298.552	247.048	113.309	-54.084	202.840	-4.816
2300	75.330	301.884	249.360	120.805	-53.671	214.509	-4.872
2400	76.009	305.104	251.616	128.372	-53.238	226.160	-4.922
2500	76.626	308.220	253.818	136.005	-52.789	237.792	-4.968
2600	77.174	311.236	255.969	143.695	-52.329	249.406	-5.011
2700	77.672	314.158	258.070	151.438	-51.860	261.003	-5.049
2800	78.132	316.991	260.124	159.228	-51.386	272.581	-5.085
2900	78.529	319.740	262.132	167.062	-50.909	284.143	-5.118
3000	78.902	322.409	264.097	174.933	-50.433	295.689	-5.148
3100	79.228	325.001	266.020	182.840	-49.959	307.218	-5.177
3200	79.521	327.521	267.903	190.778	-49.491	318.733	-5.203
3300	79.785	329.972	269.747	198.744	-49.030	330.233	-5.227
3400	80.011	332.358	271.554	206.734	-48.578	341.719	-5.250
3500	80.216	334.680	273.324	214.745	-48.139	353.191	-5.271
3600	80.400	336.942	275.060	222.776	-47.713	364.652	-5.291
3700	80.550	339.147	276.763	230.824	-47.302	376.101	-5.310
3800	80.684	341.297	278.433	238.886	-46.908	387.539	-5.327
3900	80.793	343.395	280.072	246.960	-46.534	398.967	-5.344
4000	80.881	345.441	281.680	255.043	-46.180	410.385	-5.359
4100	80.956	347.439	283.260	263.136	-45.847	421.795	-5.374
4200	81.006	349.391	284.811	271.234	-45.539	433.198	-5.388
4300	81.048	351.297	286.335	279.337	-45.254	444.593	-5.401
4400	81.065	353.161	287.833	287.442	-44.996	455.981	-5.413
4500	81.073	354.983	289.305	295.550	-44.764	467.364	-5.425
4600	81.057	356.765	290.752	303.656	-44.561	478.743	-5.436
4700	81.032	358.508	292.175	311.761	-44.387	490.117	-5.447
4800	80.990	360.213	293.575	319.862	-44.242	501.488	-5.457
4900	80.931	361.882	294.952	327.958	-44.129	512.856	-5.467
5000	80.856	363.517	296.307	336.048	-44.047	524.223	-5.477
5100	80.751	365.117	297.641	344.127	-43.999	535.587	-5.486
5200	80.751	366.685	298.954	352.202	-43.979	546.951	-5.494
5300	80.751	368.223	300.246	360.277	-43.982	558.315	-5.503
5400	80.751	369.732	301.519	368.352	-44.006	569.680	-5.511
5500	80.751	371.214	302.773	376.428	-44.049	581.044	-5.518
5600	80.751	372.669	304.008	384.503	-44.112	592.410	-5.526
5700	80.751	374.098	305.225	392.578	-44.193	603.778	-5.533
5800	80.751	375.503	306.425	400.653	-44.291	615.147	-5.540
5900	80.751	376.883	307.607	408.728	-44.404	626.516	-5.547
6000	80.751	378.240	308.773	416.803	-44.531	637.889	-5.553

Figure B.15: *JANAF data for ammonia gas.*

Nitrogen Dioxide (NO_2), ideal gas, mol. wt. = 46.0055

Enthalpy Reference Temperature = T_r = 298.15 K; Standard State Pressure = p^o = 0.1 MPa

T/K	C_p^o	S^o	$-[G^o-H^o(T_r)]/T$	$H^o-H^o(T_r)$	$\Delta_f H^o$	$\Delta_f G^o$	Log K_f
	J K^{-1}mol^{-1}			kJ mol^{-1}			
0	0.	0.	INFINITE	-10.186	35.927	35.927	INFINITE
100	33.276	202.563	271.168	-6.861	34.898	39.963	-20.874
200	34.385	225.852	243.325	-3.495	33.897	45.422	-11.863
250	35.593	233.649	240.634	-1.746	33.460	48.355	-10.103
298.15	36.974	240.034	240.034	0.	33.095	51.258	-8.980
300	37.029	240.262	240.034	0.068	33.083	51.371	-8.944
350	38.583	246.086	240.491	1.958	32.768	54.445	-8.125
400	40.171	251.342	241.524	3.927	32.512	57.560	-7.517
450	41.728	256.164	242.886	5.975	32.310	60.703	-7.046
500	43.206	260.638	244.440	8.099	32.154	63.867	-6.672
600	45.834	268.755	247.830	12.555	31.959	70.230	-6.114
700	47.986	275.988	251.345	17.250	31.878	76.616	-5.717
800	49.708	282.512	254.840	22.138	31.874	83.008	-5.420
900	51.076	288.449	258.250	27.179	31.923	89.397	-5.188
1000	52.166	293.889	261.545	32.344	32.005	95.779	-5.003
1100	53.041	298.903	264.717	37.605	32.109	102.152	-4.851
1200	53.748	303.550	267.761	42.946	32.226	108.514	-4.724
1300	54.326	307.876	270.683	48.351	32.351	114.867	-4.615
1400	54.803	311.920	273.485	53.808	32.478	121.209	-4.522
1500	55.200	315.715	276.175	59.309	32.603	127.543	-4.441
1600	55.533	319.288	278.759	64.846	32.724	133.868	-4.370
1700	55.815	322.663	281.244	70.414	32.837	140.186	-4.307
1800	56.055	325.861	283.634	76.007	32.940	146.497	-4.251
1900	56.262	328.897	285.937	81.624	33.032	152.804	-4.201
2000	56.441	331.788	288.158	87.259	33.111	159.106	-4.155
2100	56.596	334.545	290.302	92.911	33.175	165.404	-4.114
2200	56.732	337.181	292.373	98.577	33.223	171.700	-4.077
2300	56.852	339.706	294.377	104.257	33.255	177.993	-4.042
2400	56.958	342.128	296.316	109.947	33.270	184.285	-4.011
2500	57.052	344.455	298.196	115.648	33.268	190.577	-3.982
2600	57.136	346.694	300.018	121.357	33.248	196.870	-3.955
2700	57.211	348.852	301.787	127.075	33.210	203.164	-3.930
2800	57.278	350.934	303.505	132.799	33.155	209.460	-3.908
2900	57.339	352.945	305.176	138.530	33.082	215.757	-3.886
3000	57.394	354.889	306.800	144.267	32.992	222.058	-3.866
3100	57.444	356.772	308.382	150.009	32.885	228.363	-3.848
3200	57.490	358.597	309.923	155.756	32.761	234.670	-3.831
3300	57.531	360.366	311.425	161.507	32.622	240.981	-3.814
3400	57.569	362.084	312.890	167.262	32.467	247.298	-3.799
3500	57.604	363.754	314.319	173.020	32.297	253.618	-3.785
3600	57.636	365.377	315.715	178.783	32.113	259.945	-3.772
3700	57.666	366.957	317.079	184.548	31.914	266.276	-3.759
3800	57.693	368.495	318.412	190.316	31.701	272.613	-3.747
3900	57.719	369.994	319.715	196.086	31.475	278.956	-3.736
4000	57.742	371.455	320.991	201.859	31.236	285.305	-3.726
4100	57.764	372.881	322.239	207.635	30.985	291.659	-3.716
4200	57.784	374.274	323.461	213.412	30.720	298.020	-3.706
4300	57.803	375.634	324.659	219.191	30.444	304.388	-3.698
4400	57.821	376.963	325.833	224.973	30.155	310.762	-3.689
4500	57.837	378.262	326.983	230.756	29.854	317.142	-3.681
4600	57.853	379.534	328.112	236.540	29.540	323.530	-3.674
4700	57.867	380.778	329.219	242.326	29.214	329.925	-3.667
4800	57.881	381.996	330.306	248.114	28.875	336.326	-3.660
4900	57.894	383.190	331.373	253.902	28.523	342.736	-3.654
5000	57.906	384.360	332.421	259.692	28.158	349.152	-3.648
5100	57.917	385.507	333.451	265.483	27.778	355.576	-3.642
5200	57.928	386.631	334.463	271.276	27.384	362.006	-3.636
5300	57.938	387.735	335.458	277.069	26.974	368.446	-3.631
5400	57.948	388.818	336.436	282.863	26.548	374.892	-3.626
5500	57.957	389.881	337.398	288.658	26.106	381.347	-3.622
5600	57.965	390.926	338.344	294.455	25.646	387.811	-3.617
5700	57.973	391.952	339.276	300.251	25.167	394.281	-3.613
5800	57.981	392.960	340.193	306.049	24.669	400.762	-3.609
5900	57.988	393.951	341.096	311.848	24.150	407.249	-3.606
6000	57.995	394.926	341.985	317.647	23.608	413.748	-3.602

Figure B.16: *JANAF data for nitrogen dioxide gas.*

Nitrogen Oxide (NO), ideal gas, mol. wt. = 30.0061

Enthalpy Reference Temperature = T_r = 298.15 K				Standard State Pressure = p^o = 0.1 MPa			
	J $K^{-1}mol^{-1}$			kJ mol^{-1}			
T/K	C_p^o	S^o	$-(G^o-H^o(T_r))/T$	$H^o-H^o(T_r)$	$\Delta_f H^o$	$\Delta_f G^o$	Log K_f
0	0.	0.	INFINITE	-9.192	89.775	89.775	INFINITE
100	32.302	177.031	237.757	-6.073	89.991	88.944	-46.460
200	30.420	198.747	213.501	-2.951	90.202	87.800	-22.931
250	30.025	205.488	211.251	-1.441	90.256	87.193	-18.218
298.15	29.845	210.758	210.758	0.	90.291	86.600	-15.172
300	29.841	210.943	210.759	0.055	90.292	86.577	-15.074
350	29.823	215.540	211.122	1.546	90.316	85.955	-12.828
400	29.944	219.529	211.929	3.040	90.332	85.331	-11.143
450	30.175	223.068	212.974	4.542	90.343	84.705	-9.832
500	30.486	226.263	214.145	6.059	90.352	84.079	-8.784
600	31.238	231.886	216.646	9.144	90.366	82.822	-7.210
700	32.028	236.761	219.179	12.307	90.381	81.564	-6.086
800	32.767	241.087	221.652	15.548	90.398	80.303	-5.243
900	33.422	244.985	224.031	18.858	90.417	79.041	-4.587
1000	33.987	248.536	226.307	22.229	90.437	77.775	-4.063
1100	34.468	251.799	228.478	25.653	90.457	76.508	-3.633
1200	34.877	254.816	230.549	29.120	90.476	75.239	-3.275
1300	35.226	257.621	232.525	32.626	90.493	73.969	-2.972
1400	35.524	260.243	234.412	36.164	90.508	72.697	-2.712
1500	35.780	262.703	236.217	39.729	90.518	71.425	-2.487
1600	36.002	265.019	237.945	43.319	90.525	70.151	-2.290
1700	36.195	267.208	239.603	46.929	90.526	68.878	-2.116
1800	36.364	269.282	241.195	50.557	90.522	67.605	-1.962
1900	36.514	271.252	242.725	54.201	90.511	66.332	-1.824
2000	36.647	273.128	244.199	57.859	90.494	65.060	-1.699
2100	36.767	274.919	245.619	61.530	90.469	63.788	-1.587
2200	36.874	276.632	246.990	65.212	90.438	62.519	-1.484
2300	36.971	278.273	248.315	68.904	90.398	61.251	-1.391
2400	37.060	279.849	249.596	72.606	90.350	59.984	-1.306
2500	37.141	281.363	250.837	76.316	90.295	58.720	-1.227
2600	37.216	282.822	252.039	80.034	90.231	57.458	-1.154
2700	37.285	284.227	253.205	83.759	90.160	56.199	-1.087
2800	37.350	285.585	254.338	87.491	90.081	54.943	-1.025
2900	37.410	286.896	255.438.	91.229	89.994	53.689	-0.967
3000	37.466	288.165	256.508	94.973	89.899	52.439	-0.913
3100	37.519	289.395	257.549	98.722	89.798	51.192	-0.863
3200	37.570	290.587	258.563	102.477	89.689	49.948	-0.815
3300	37.617	291.744	259.551	106.236	89.574	48.708	-0.771
3400	37.663	292.867	260.514	110.000	89.451	47.472	-0.729
3500	37.706	293.960	261.454	113.768	89.323	46.239	-0.690
3600	37.747	295.022	262.372	117.541	89.189	45.010	-0.653
3700	37.787	296.057	263.269	121.318	89.049	43.784	-0.618
3800	37.825	297.065	264.145	125.098	88.903	42.563	-0.585
3900	37.862	298.048	265.902	128.883	88.752	41.346	-0.554
4000	37.898	299.008	265.840	132.671	88.596	40.132	-0.524
4100	37.933	299.944	266.660	136.462	88.434	38.922	-0.496
4200	37.966	300.858	267.464	140.257	88.268	37.717	-0.469
4300	37.999	301.752	268.251	144.056	88.097	36.515	-0.444
4400	38.031	302.626	269.022	147.857	87.922	35.318	-0.419
4500	38.062	303.481	269.778	151.662	87.741	34.124	-0.396
4600	38.092	304.318	270.520	155.469	87.556	32.934	-0.374
4700	38.122	305.137	271.248	159.280	87.366	31.749	-0.353
4800	38.151	305.940	271.962	163.094	87.171	30.568	-0.333
4900	38.180	306.727	272.664	166.910	86.970	29.391	-0.313
5000	38.208	307.499	273.353	170.730	86.765	28.218	-0.295
5100	38.235	308.256	274.030	174.552	86.553	27.049	-0.277
5200	38.262	308.998	274.695	178.377	86.336	25.884	-0.260
5300	38.289	309.728	275.349	182.204	86.112	24.724	-0.244
5400	38.316	310.443	275.993	186.034	85.881	23.568	-0.228
5500	38.342	311.147	276.625	189.867	85.644	22.416	-0.213
5600	38.367	311.838	277.248	193.703	85.399	21.269	-0.198
5700	38.393	312.517	277.861	197.541	85.146	20.125	-0.184
5800	38.418	313.185	278.464	201.381	84.884	18.987	-0.171
5900	38.443	313.842	279.058	205.224	84.613	17.853	-0.158
6000	38.468	314.488	279.643	209.070	84.331	16.724	-0.146

Figure B.17: *JANAF data for nitric oxide gas.*

Oxygen (O_2), ideal gas-reference state, mol. wt. = 31.9988

Enthalpy Reference Temperature = T_r = 298.15 K — Standard State Pressure = p^o = 0.1 MPa

	J K^{-1}mol^{-1}			kJ mol^{-1}			
T/K	C_p^o	S^o	$-[G^o-H^o(T_r)]/T$	$H^o-H^o(T_r)$	$\Delta_f H^o$	$\Delta_f G^o$	Log K_f
0	0.	0.	INFINITE	-8.683	0.	0.	0.
100	29.106	173.307	231.094	-5.779	0.	0.	0.
200	29.126	193.485	207.823	-2.868	0.	0.	0.
250	29.201	199.990	205.630	-1.410	0.	0.	0.
298.15	29.376	205.147	205.147	0.	0.	0.	0.
300	29.385	205.329	205.148	0.054	0.	0.	0.
350	29.694	209.880	205.506	1.531	0.	0.	0.
400	30.106	213.871	206.308	3.025	0.	0.	0.
450	30.584	217.445	207.350	4.543	0.	0.	0.
500	31.091	220.693	208.524	6.084	0.	0.	0.
600	32.090	226.451	211.044	9.244	0.	0.	0.
700	32.981	231.466	213.611	12.499	0.	0.	0.
800	33.733	235.921	216.126	15.835	0.	0.	0.
900	34.355	239.931	218.552	19.241	0.	0.	0.
1000	34.870	243.578	220.875	22.703	0.	0.	0.
1100	35.300	246.922	223.093	26.212	0.	0.	0.
1200	35.667	250.010	225.209	29.761	0.	0.	0.
1300	35.988	252.878	227.229	33.344	0.	0.	0.
1400	36.277	255.556	229.158	36.957	0.	0.	0.
1500	36.544	258.068	231.002	40.599	0.	0.	0.
1600	36.796	260.434	232.768	44.266	0.	0.	0.
1700	37.040	262.672	234.462	47.958	0.	0.	0.
1800	37.277	264.796	236.089	51.673	0.	0.	0.
1900	37.510	266.818	237.653	55.413	0.	0.	0.
2000	37.741	268.748	239.160	59.175	0.	0.	0.
2100	37.969	270.595	240.613	62.961	0.	0.	0.
2200	38.195	272.366	242.017	66.769	0.	0.	0.
2300	38.419	274.069	243.374	70.600	0.	0.	0.
2400	38.639	275.709	244.687	74.453	0.	0.	0.
2500	38.856	277.290	245.959	78.328	0.	0.	0.
2600	39.068	278.819	247.194	82.224	0.	0.	0.
2700	39.276	280.297	248.393	86.141	0.	0.	0.
2800	39.478	281.729	249.558	90.079	0.	0.	0.
2900	39.674	283.118	250.691	94.036	0.	0.	0.
3000	39.864	284.466	251.795	98.013	0.	0.	0.
3100	40.048	285.776	252.870	102.009	0.	0.	0.
3200	40.225	287.050	253.918	106.023	0.	0.	0.
3300	40.395	288.291	254.941	110.054	0.	0.	0.
3400	40.559	289.499	255.940	114.102	0.	0.	0.
3500	40.716	290.677	256.916	118.165	0.	0.	0.
3600	40.868	291.826	257.870	122.245	0.	0.	0.
3700	41.013	292.948	258.802	126.339	0.	0.	0.
3800	41.154	294.044	259.716	130.447	0.	0.	0.
3900	41.289	295.115	260.610	134.569	0.	0.	0.
4000	41.421	296.162	261.485	138.705	0.	0.	0.
4100	41.549	297.186	262.344	142.854	0.	0.	0.
4200	41.674	298.189	263.185	147.015	0.	0.	0.
4300	41.798	299.171	264.011	151.188	0.	0.	0.
4400	41.920	300.133	264.821	155.374	0.	0.	0.
4500	42.042	301.076	265.616	159.572	0.	0.	0.
4600	42.164	302.002	266.397	163.783	0.	0.	0.
4700	42.287	302.910	267.164	168.005	0.	0.	0.
4800	42.413	303.801	267.918	172.240	0.	0.	0.
4900	42.542	304.677	268.660	176.488	0.	0.	0.
5000	42.675	305.538	269.389	180.749	0.	0.	0.
5100	42.813	306.385	270.106	185.023	0.	0.	0.
5200	42.956	307.217	270.811	189.311	0.	0.	0.
5300	43.105	308.037	271.506	193.614	0.	0.	0.
5400	43.262	308.844	272.190	197.933	0.	0.	0.
5500	43.426	309.639	272.864	202.267	0.	0.	0.
5600	43.599	310.424	273.527	206.618	0.	0.	0.
5700	43.781	311.197	274.181	210.987	0.	0.	0.
5800	43.973	311.960	274.826	215.375	0.	0.	0.
5900	44.175	312.713	275.462	219.782	0.	0.	0.
6000	44.387	313.457	276.089	224.210	0.	0.	0.

Figure B.18: *JANAF data for diatomic oxygen gas.*

Oxygen, Monatomic (O), ideal gas, mol. wt. = 15.9994

Enthalpy Reference Temperature = T_r = 298.15 K — Standard State Pressure = p^o = 0.1 MPa

	J K^{-1}mol^{-1}			kJ mol^{-1}			
T/K	C_p^o	S^o	$-[G^o-H^o(T_r)]/T$	$H^o-H^o(T_r)$	$\Delta_f H^o$	$\Delta_f G^o$	Log K_f
0	0.	0.	INFINITE	-6.725	246.790	246.790	INFINITE
100	23.703	135.947	181.131	-4.518	247.544	242.615	-126.729
200	22.734	152.153	163.085	-2.186	248.421	237.339	-61.986
250	22.246	157.170	161.421	-1.063	248.816	234.522	-49.001
298.15	21.911	161.058	161.058	0.	249.173	231.736	-40.599
300	21.901	161.194	161.059	0.041	249.187	231.628	-40.330
350	21.657	164.551	161.324	1.129	249.537	228.673	-34.128
400	21.482	167.430	161.912	2.207	249.868	225.670	-29.469
450	21.354	169.953	162.668	3.278	250.180	222.626	-25.842
500	21.257	172.197	163.511	4.343	250.474	219.549	-22.936
600	21.124	176.060	165.291	6.462	251.013	213.312	-18.570
700	21.040	179.310	167.067	8.570	251.494	206.990	-15.446
800	20.984	182.116	168.777	10.671	251.926	200.602	-13.098
900	20.944	184.585	170.399	12.767	252.320	194.163	-11.269
1000	20.915	186.790	171.930	14.860	252.682	187.681	-9.803
1100	20.893	188.782	173.373	16.950	253.018	181.165	-8.603
1200	20.877	190.599	174.734	19.039	253.332	174.619	-7.601
1300	20.864	192.270	176.019	21.126	253.627	168.047	-6.752
1400	20.853	193.816	177.236	23.212	253.906	161.453	-6.024
1500	20.845	195.254	178.390	25.296	254.171	154.840	-5.392
1600	20.838	196.599	179.486	27.381	254.421	148.210	-4.839
1700	20.833	197.862	180.530	29.464	254.659	141.564	-4.350
1800	20.830	199.053	181.527	31.547	254.884	134.905	-3.915
1900	20.827	200.179	182.479	33.630	255.097	128.234	-3.525
2000	20.826	201.247	183.391	35.713	255.299	121.552	-3.175
2100	20.827	202.263	184.266	37.796	255.488	114.860	-2.857
2200	20.830	203.232	185.106	39.878	255.667	108.159	-2.568
2300	20.835	204.158	185.914	41.962	255.835	101.450	-2.304
2400	20.841	205.045	186.693	44.045	255.992	94.734	-2.062
2500	20.851	205.896	187.444	46.130	256.139	88.012	-1.839
2600	20.862	206.714	188.170	48.216	256.277	81.284	-1.633
2700	20.877	207.502	188.871	50.303	256.405	74.551	-1.442
2800	20.894	208.261	189.550	52.391	256.525	67.814	-1.265
2900	20.914	208.995	190.208	54.481	256.637	61.072	-1.100
3000	20.937	209.704	190.846	56.574	256.741	54.327	-0.946
3100	20.963	210.391	191.466	58.669	256.838	47.578	-0.802
3200	20.991	211.057	192.068	60.767	256.929	40.826	-0.666
3300	21.022	211.704	192.653	62.867	257.014	34.071	-0.539
3400	21.056	212.332	193.223	64.971	257.094	27.315	-0.420
3500	21.092	212.943	193.777	67.079	257.169	20.555	-0.307
3600	21.130	213.537	194.318	69.190	257.241	13.794	-0.200
3700	21.170	214.117	194.845	71.305	257.309	7.030	-0.099
3800	21.213	214.682	195.360	73.424	257.373	0.265	-0.004
3900	21.257	215.234	195.862	75.547	257.436	-6.501	0.087
4000	21.302	215.772	196.353	77.675	257.496	-13.270	0.173
4100	21.349	216.299	196.834	79.808	257.554	-20.010	0.255
4200	21.397	216.814	197.303	81.945	257.611	-26.811	0.333
4300	21.445	217.318	197.763	84.087	257.666	-33.583	0.408
4400	21.495	217.812	198.213	86.234	257.720	-40.358	0.479
4500	21.545	218.295	198.654	88.386	257.773	-47.133	0.547
4600	21.596	218.769	199.086	90.543	257.825	-53.909	0.612
4700	21.647	219.234	199.510	92.705	257.876	-60.687	0.674
4800	21.697	219.690	199.925	94.872	257.926	-67.465	0.734
4900	21.748	220.138	200.333	97.045	257.974	-74.244	0.791
5000	21.799	220.578	200.734	99.222	258.021	-81.025	0.846
5100	21.849	221.010	201.127	101.405	258.066	-87.806	0.899
5200	21.899	221.435	201.514	103.592	258.110	-94.589	0.950
5300	21.949	221.853	201.893	105.784	258.150	-101.371	0.999
5400	21.997	222.264	202.267	107.982	258.189	-108.155	1.046
5500	22.045	222.668	202.634	110.184	258.224	-114.940	1.092
5600	22.093	223.065	202.995	112.391	258.255	-121.725	1.135
5700	22.139	223.457	203.351	114.602	258.282	-128.510	1.178
5800	22.184	223.842	203.701	116.818	258.304	-135.296	1.218
5900	22.229	224.222	204.046	119.039	258.321	-142.083	1.258
6000	22.273	224.596	204.385	121.264	258.332	-148.869	1.296

Figure B.19: *JANAF data for monatomic oxygen gas.*

Ozone (O_3), ideal gas, mol. wt. = 47.9982

Enthalpy Reference Temperature = T_r = 298.15 K — Standard State Pressure = p^o = 0.1 MPa

T/K	C_p^o	S^o	$-[G^o-H^o(T_r)]/T$	$H^o-H^o(T_r)$	$\Delta_f H^o$	$\Delta_f G^o$	Log K_f
	J K^{-1}mol^{-1}			kJ mol^{-1}			
0	0.	0.	INFINITE	-10.351	145.348	145.348	INFINITE
100	33.292	200.791	271.040	-7.025	144.318	150.235	-78.474
200	35.058	224.221	242.401	-3.636	143.340	156.541	-40.884
298.15	39.238	238.932	238.932	0.000	142.674	163.184	-28.589
300	39.330	239.175	238.933	0.073	142.665	163.311	-28.435
400	43.744	251.116	240.531	4.234	142.370	170.247	-22.232
500	47.262	261.272	243.688	8.792	142.340	177.224	-18.514
600	49.857	270.129	247.373	13.654	142.462	184.191	-16.035
700	51.752	277.963	251.194	18.738	142.665	191.130	-14.262
800	53.154	284.969	254.986	23.986	142.907	198.037	-12.931
900	54.208	291.292	258.674	29.356	143.169	204.913	-11.893
1000	55.024	297.048	262.228	34.819	143.439	211.759	-11.061
1100	55.660	302.323	265.637	40.355	143.711	218.578	-10.379
1200	56.174	307.189	268.899	45.947	143.980	225.372	-9.810
1300	56.593	311.702	272.020	51.586	144.245	232.144	-9.328
1400	56.948	315.909	275.007	57.264	144.502	238.896	-8.913
1500	57.245	319.849	277.866	62.974	144.750	245.629	-8.554
1600	57.501	323.551	280.607	68.711	144.987	252.347	-8.238
1700	57.722	327.044	283.237	74.473	145.211	259.050	-7.960
1800	57.919	330.349	285.763	80.255	145.419	265.740	-7.712
1900	58.095	333.485	288.193	86.056	145.611	272.419	-7.489
2000	58.250	336.469	290.533	91.873	145.784	279.089	-7.289
2100	58.396	339.315	292.789	97.705	145.938	285.750	-7.108
2200	58.526	342.035	294.966	103.552	146.072	292.406	-6.943
2300	58.647	344.639	297.069	109.410	146.185	299.054	-6.792
2400	58.764	347.137	299.104	115.281	146.276	305.698	-6.653
2500	58.869	349.538	301.073	121.163	146.346	312.339	-6.526
2600	58.969	351.849	302.982	127.055	146.393	318.978	-6.408
2700	59.066	354.077	304.833	132.956	146.419	325.616	-6.299
2800	59.158	356.226	306.631	138.868	146.424	332.253	-6.198
2900	59.245	358.304	308.377	144.788	146.408	338.889	-6.104
3000	59.329	360.314	310.075	150.716	146.371	345.527	-6.016
3100	59.409	362.260	311.727	156.653	146.314	352.167	-5.934
3200	59.488	364.148	313.336	162.598	146.238	358.808	-5.857
3300	59.563	365.980	314.904	168.551	146.144	365.451	-5.785
3400	59.639	367.759	316.432	174.511	146.033	372.100	-5.717
3500	59.714	369.489	317.923	180.479	145.905	378.750	-5.653
3600	59.781	371.172	319.379	186.453	145.761	385.405	-5.592
3700	59.852	372.811	320.801	192.435	145.601	392.063	-5.535
3800	59.919	374.408	322.191	198.424	145.427	398.728	-5.481
3900	59.986	375.965	323.550	204.419	145.239	405.396	-5.430
4000	60.053	377.485	324.879	210.421	145.038	412.069	-5.381
4100	60.120	378.968	326.181	216.429	144.823	418.747	-5.335
4200	60.183	380.418	327.455	222.445	144.597	425.431	-5.291
4300	60.245	381.835	328.703	228.466	144.358	432.121	-5.249
4400	60.308	383.220	329.926	234.494	144.106	438.815	-5.209
4500	60.371	384.576	331.126	240.528	143.844	445.516	-5.171
4600	60.434	385.904	332.302	246.568	143.568	452.222	-5.135
4700	60.492	387.204	333.457	252.614	143.281	458.935	-5.100
4800	60.555	388.479	334.590	258.667	142.981	465.655	-5.067
4900	60.614	389.728	335.702	264.725	142.667	472.381	-5.036
5000	60.672	390.953	336.795	270.789	142.340	479.113	-5.005
5100	60.731	392.155	337.869	276.859	141.999	485.853	-4.976
5200	60.789	393.335	338.924	282.935	141.643	492.597	-4.948
5300	60.848	394.493	339.962	289.017	141.270	499.351	-4.921
5400	60.906	395.631	340.982	295.105	140.880	506.110	-4.896
5500	60.965	396.749	341.986	301.199	140.472	512.876	-4.871
5600	61.024	397.848	342.974	307.298	140.045	519.653	-4.847
5700	61.078	398.929	343.946	313.403	139.596	526.434	-4.824
5800	61.137	399.992	344.903	319.514	139.126	533.226	-4.802
5900	61.191	401.037	345.846	325.630	138.631	540.023	-4.781
6000	61.250	402.066	346.774	331.752	138.111	546.832	-4.761

Figure B.20: *JANAF data for ozone gas.*